

REINFORCEMENT SCHEMES FOR COLD-FORMED
STEEL JOISTS HAVING WEB OPENINGS

To my late grandfather, Udaya Raj Acharya
for his love.

REINFORCEMENT SCHEMES FOR COLD-FORMED
STEEL JOISTS HAVING WEB OPENINGS

By

SANDESH RAJ ACHARYA, B. ENG., M. ENG.

A Dissertation
Submitted to the School of Graduate Studies
in Partial Fulfilment of the Requirements
for the Degree of
Doctor of Philosophy

McMaster University
© Copyright by Sandesh Raj Acharya, August 2009

DOCTOR OF PHILOSOPHY (2009)
(Civil Engineering)

McMaster University
Hamilton, Ontario, Canada

TITLE: Reinforcement Schemes for Cold-Formed Steel Joists Having Web Openings

AUTHOR: Sandesh Raj Acharya, B. Eng. (Tribhuvan University, Kathmandu, Nepal)

M. Eng. (Asian Institute of Technology, Thailand)

SUPERVISOR: Dr. K. S. Sivakumaran

NUMBER OF PAGES: xxxvi, 332

Abstract

The use of cold-formed steel (CFS) structures has become increasingly popular in different fields of building technology. For example, small housing systems using cold-formed steel for wall structures, framing systems and roof structures, including trusses and shielding materials, have been developed during recent years. The reasons behind the growing popularity of these products include their ease of fabrication, high strength/weight ratio and suitability for a wide range of applications. These advantages can result in more cost-effective designs, as compared with hot-rolled steel, especially in short-span applications.

It has been common practice in cold-formed steel construction to cut openings in the web of beams for the passage of service ducts and piping. The provision of such openings reduces the story heights and consequently can result in saving of considerable amount of construction materials. On the other hand, the presence of a large web opening causes localized redistribution of stress around the opening region. The large opening causes loss of strength and changes the buckling characteristics of an entire member. It also affects the flexural stiffness, resulting in poor performance of member under serviceability.

It is common practice to reinforce the opening of hot-rolled steel members, but proper reinforcement schemes for CFS perforated members has not been established yet. Various reinforcement schemes for cold-formed steel sections were investigated during this study. Two types of reinforcement schemes (for flexural zones and shear

zones) were developed. Fifty-four flexural tests and 33 shear tests were conducted. Two types of sections (lipped channel joists with h/t ratio 180 and 118) were tested in flexure and one type of section (lipped channel joists with h/t ratio 180) was tested in shear. The study also included a finite element based numerical investigation, consisting of parametric studies on the size (web depth and thickness) of joists, size and shape of web openings, reinforcement and associated fastening schemes.

It was observed that a 75 percent of opening in the web of CFS channel joist causes up to 25 percent reduction in flexural strength and up to 60 percent reduction in shear strength. Such reduced flexural and shear strengths were re-captured by providing proper reinforcement schemes. The flexural reinforcement schemes recommended by the current AISI Standard were found to be ineffective for the sections having low w/t ratios. Bridging channel reinforcement scheme was also considered in this study. Bridging channel reinforcement scheme was capable of restoring the flexural strength of cold formed steel joist having w/t ratios 118 and 180.

Similarly, the reinforcement schemes recommended in AISI Standard were not adequate to restore the shear strength of joist sections. A newly developed Vierendeel type reinforcement system was capable of restoring the original shear strength of a cold-formed steel joist section.

Acknowledgments

First and foremost, I am deeply indebted to my parents and my brothers. Where I am today is in no small part due to their love and support. I owe a special thanks to my wife Dr. Sanjaya Sharma who provided me with inspiration and love to finish this work.

I would like to thank my supervisor, Dr. K. S. Sivakumaran. His willingness to support my work and his guidance throughout my studies has allowed me to develop my skills as a researcher within a supportive team environment. I thank him for that opportunity. Also, I would like to thank, Dr. Ghani Razaqpur. His advice and counsel over the years have been of equal importance. To Dr. Philip Koshi, I say thank you as well for the many technical—and sometimes not-so technical—discussions with regard to this research and life in general.

Within the Applied Dynamic Lab, I owe many thanks to both students and staff. Throughout my work, Dave Perrett, Maurice Forget and Peter Koudys, have routinely worked miracles, and for that they have my heart-felt admiration. Special thanks to Paul Heerema for his friendly and cooperative help through out the experimental work. To my fellow graduate students, I express my sincerest gratitude for the many conversations that have had a tremendous impact on my research and myself as a person. Pramalathan Arasaratnam, thank you so much.

The financial support through the Department of Civil Engineering, Center for Effective Design of Structures (CEDs), Ontario Graduate Scholarship (OGS) are

gratefully acknowledged. I would also like to thank Canadian Sheet Steel Building Institute (CSSBI) for providing the test specimens.

Last but not least, I thank our administrative secretary, Carol Robinson, Rebecca Woodworth and Tatiana Dobrovolska for their jovial smile and helpful nature that have always greeted any problem or deadline.

Contents

Abstract	iii
Acknowledgements	v
Contents	xiv
List of Tables	xvii
List of Figures	xxx
List of Symbols	xxxii
1 Introduction	1
1.1 Introduction	1
1.2 Problem Statement	2
1.3 Objectives and Scopes	4
1.4 Organization of the Dissertation	5
1.5 Stability of Thin Walled Structures	7
1.5.1 General	7
1.5.2 Buckling of Plates in Compression	7
2 Reinforcements for CFS Joists with Web Openings in Flexural Zone:	
Experimental Study	13
2.1 Introduction	13
2.2 Flexural Resistance of Cold-Formed Steel Joists	14

2.2.1	Flexural Resistance of Solid Joists	14
2.2.2	Flexural Resistance of the Joists with Web Openings	17
2.3	Flexural Reinforcements for Web Openings	20
2.3.1	Previous Studies	20
2.3.2	AISI Reinforcement Criteria	22
2.4	Experimental Program	24
2.4.1	Selection of the Test Joists	24
2.4.2	Test Specimens	25
2.4.3	Test Designations	26
2.4.4	Test Setup	26
2.4.5	Test Procedures	29
2.5	Flexural Resistance of Solid Joists	31
2.5.1	Joists having h/t ratio = 180 (203.2 mm deep)	31
2.5.2	Joists having h/t ratio = 118 (304.8 mm deep)	32
2.6	Flexural Resistance of Joists with Web Openings	33
2.6.1	Joists having h/t ratio = 180 (203.2 mm deep)	33
2.6.2	Joists having h/t ratio = 118 (304.8 mm deep)	34
2.7	Flexural Resistance of Joists with Reinforced Web Openings	35
2.7.1	Design of Flexural Reinforcement	36
2.7.2	Development of New Reinforcement Schemes	41
2.7.3	Reinforcement Schemes	44
2.7.4	Joists having h/t ratio = 180 (203.2 mm deep)	45
2.7.5	Joists having h/t ratio = 118 (304.8 mm deep)	47
2.8	Lateral Displacements, Strains and Initiation of Local Buckling	49
2.9	Conclusions	50

3 Reinforcements for CFS Joists with Web Openings in Shear Zone:

Experimental Study 83

3.1 Introduction 83

3.2 Shear Resistance of the Cold-Formed Steel Joists 84

 3.2.1 Shear Resistance of Solid Joists 84

 3.2.2 Shear Resistance of the Joists having Web Openings 87

3.3 Shear Reinforcements for Web Openings 93

 3.3.1 Previous Studies 93

 3.3.2 Shear Buckling and Vierendeel Action 95

3.4 Experimental Program 97

 3.4.1 Test Designation 97

 3.4.2 Test Setup 98

 3.4.3 Test Procedure 99

3.5 Solid Joists and Joists with Unreinforced Web Openings 101

3.6 Joists with Reinforced Web Openings 103

 3.6.1 Shear Reinforcement Schemes 103

 3.6.2 Test Results 105

 3.6.3 Strains on the Main Joists and Reinforcement Channels 106

 3.6.4 Lateral Displacements and Initiation of Shear Buckling 106

3.7 Conclusions 107

3.8 Recommendation for Flexural and Shear Reinforcement 107

 3.8.1 Flexural and Shear Zones 107

 3.8.2 Conclusion 110

4 Finite Element Models for Lap Connections in Thin Walled Mem-

bers 133

6 Reinforcement of Cold-Formed Steel Joists with Web Openings in Flexural Zone: Numerical Study	225
6.1 Introduction	225
6.2 Analysis Consideration for Cold-Formed Steel Joists	226
6.2.1 Buckling Analysis Techniques	226
6.2.2 Geometrical Imperfections	227
6.2.3 Mechanical Properties	227
6.2.4 Residual Stress	228
6.3 The Finite Element Model	230
6.3.1 Material Modeling	230
6.3.2 The Full Scale Model	230
6.3.3 The Reduced Model	233
6.3.4 Reinforcements	234
6.4 Finite Element Analysis Results	234
6.4.1 The Full Scale Model	234
6.4.2 The Reduced Finite Element Model	237
6.5 The Parametric Study: Results and Discussion	238
6.5.1 Comparative Study of Experimental, FEM and AISI Standard Results	238
6.5.2 Effects of Opening Size	239
6.5.3 Effects of h/t Ratio	241
6.5.4 Effects of Shape of Opening	242
6.5.5 Effects of Web Depth	243
6.5.6 Reinforcements	243
6.5.7 Effects of Reinforcement Size	244
6.6 Conclusion	244

7	Conclusions and Recommendations	265
7.1	Summary	265
7.2	Limitations	266
7.3	Conclusions	267
7.4	Recommendations for Future Research	270
	References	273
	Appendices	281
A	Mechanical Properties of the CFS Joists	283
A.1	General	283
A.2	Tensile Coupons	284
A.3	Test Procedure	284
A.4	Test Results	285
B	Cold-Formed Steel Joists with Large Web Openings Flexural Tests:	
	Section 800S162-43	297
B.1	General	297
B.2	Flexural Tests: Solid Sections, Circular Openings and Square Openings	297
B.3	Flexural Tests: Reinforced Circular Openings (Schemes-A, B and C) .	298
B.4	Flexural Tests: Reinforced Square Openings (Schemes- A, B and C) .	298
C	Cold-Formed Steel Joists with Large Web Openings Flexural Tests:	
	Section 1200S162-97	309
C.1	General	309
C.2	Flexural Tests: Solid Sections, Circular Openings and Square Openings	309
C.3	Flexural Tests: Reinforced Circular Openings (Schemes-A, B and C) .	310
C.4	Flexural Tests: Reinforced Square Openings (Schemes-A, B and C) .	310

D Cold-Formed Steel Joists with Large Web Openings Shear Tests:

Section 800S162-43	321
D.1 General	321
D.2 Shear Tests: Solid Sections, Circular Openings and Square Openings .	321
D.3 Shear Tests: Reinforced Circular Openings (Schemes- A, B and C) . .	322
D.4 Shear Tests: Reinforced Square Openings (Schemes- A, B and C) . .	322

List of Tables

2.1	h/t ratio for common CFS lipped channel sections	52
2.2	Section properties and the mechanical properties of the CFS joists (Ref: Appendix A)	53
2.3	Measured geometrical dimensions of the CFS steel sections - 800S162-43 (203.2 mm deep, h/t = 180)	54
2.4	Measured geometrical dimensions of the CFS steel sections - 1200S162-97 (308.8 mm deep, h/t = 118)	56
2.5	Flexural resistance of CFS joists (h/t = 180) with and without web opening in high moment regions (flexural zone)	58
2.6	Flexural resistance of CFS joists (h/t = 118) with and without web opening in high moment regions (flexural zone)	59
2.7	Flexural resistance of CFS joists (h/t = 180) with reinforced circular web opening in high moment regions (flexural zone)	60
2.8	Flexural resistance of CFS joists (h/t = 118) with reinforced circular web opening in high moment regions (flexural zone)	61
2.9	Flexural resistance of CFS joists (h/t = 180) with reinforced square web opening in high moment regions (flexural zone)	62
2.10	Flexural resistance of CFS joists (h/t = 118) with reinforced square web opening in high moment regions (flexural zone)	63

2.11	Alternative flexural reinforcement schemes for scheme -c	64
2.12	Trial stages to develop the reinforcement schemes for high moment regions	65
3.1	Maximum spans for CFS joists in meter (AISI, 007a)	111
3.2	Shear ratios (Shear Force / Shear Resistance)	112
3.3	Measured geometrical dimensions of the CFS joists tested in shear . .	113
3.4	Shear resistance of CFS joists ($h/t = 180$) with and without web openings in high shear zones	115
3.5	Trial stages to develop the reinforcement schemes for high shear zones	116
3.6	Shear resistance of CFS joists ($h/t = 180$) with reinforced circular web opening in high shear zones	117
3.7	Shear resistance of CFS joists ($h/t = 180$) with reinforced square web opening in high shear shear zones	118
4.1	Measured Dimensions of Screw Connection Specimen	153
4.2	Measured Dimensions of Bolted Connection Specimen	153
6.1	Moment capacity of CFS joists with large circular web openings: Opening size = ($h-76.2$ mm)	246
6.2	Moment capacity of CFS joists with large square web openings: Opening size = ($h-76.2$ mm)	247
A.1	Measured gauge width and thickness for tensile coupons from 203.2 mm (8 inch) deep joists	287
A.2	Measured gauge width and thickness for tensile coupons from 304.8 mm (12 inch) deep joists	287

A.3	Material properties based on tensile coupons from 203.2 mm (8 inch) deep joists	288
A.4	Material properties based on tensile coupons from 304.8mm (12 inch) deep joists	288

List of Figures

1.1	Building composed entirely of cold-formed steel sections	9
1.2	Cold-formed steel (CFS) joists used as floor joists	9
1.3	Light weight CFS framing members	10
1.4	Openings in the web of CFS joists	10
1.5	Application of web openings in cold-formed steel (CFS) joists	11
1.6	Buckling coefficients for flat rectangular plates	11
2.1	Stress distribution and effective width in a stiffened flange	66
2.2	Stress distribution and effective width of a web in flexure	66
2.3	Various reinforcement schemes recommended for hot-rolled steel beams (Segner, 1964)	67
2.4	Reinforcement schemes for CFS joists considered by Pennock, (2001)	68
2.5	Typical reinforcement schemes for CFS joists tested by Ng, (2004) (a) scheme A (b) scheme B	68
2.6	Reinforcement schemes for CFS joists suggested by AISI, (2001)	69
2.7	Flexural test setup-I	69
2.8	Cross sections at A and B	70
2.9	Photograph of flexural test setup-I	70
2.10	Test setup-II for flexural test	71

2.11	Test setup-II picture for flexure test	71
2.12	Typical comparative plot for two support reactions	72
2.13	Typical comparative plot for two mid-span deflections	72
2.14	Load deflection curve for solid joist ($h/t = 180$)	73
2.15	Typical flexural failure of solid joist ($h/t = 180$)	73
2.16	Typical flexural failure of joist having circular openings ($h/t = 180$)	74
2.17	Typical flexural failure of joist having square openings ($h/t = 118$)	74
2.18	Free body diagram of CFS joist at the opening region	75
2.19	Reinforcement for compression element	75
2.20	Flowchart to design flexural reinforcement	76
2.21	Local plate buckling because of inadequate screw spacing	77
2.22	Reinforcement scheme-A and B for flexural zone, (AISI, 2007a)	77
2.23	Reinforcement scheme-C for flexural zone, (Current study)	78
2.24	Typical failure of plate reinforcement (Scheme-A)	78
2.25	Typical failure of stud reinforcement (Scheme-B)	79
2.26	Matching bridging channel reinforcement (Scheme-C)	79
2.27	Typical comparative plot of solid, unreinforced and reinforced studs	80
2.28	Lateral deflection showing beginning of local buckling	80
2.29	Strain measurements showing beginning of local buckling	81
3.1	Nominal shear stress variation with slenderness (AISI, 2007)	119
3.2	Shear resistance reduction factor for the joists having circular web openings	119
3.3	Shear resistance reduction factor for the joists having square web openings	120

3.4	Web of CFS joists subjected in shear forming compression and tension band along the diagonals	120
3.5	Shear buckling of the web of CFS joists having opening	121
3.6	Shear reinforcement (a) Vierendeel truss (b) Vierendeel action	121
3.7	Test setup for shear test	122
3.8	Section at A and B	122
3.9	Test setup picture for shear test	123
3.10	Typical comparative plot for two support reactions	123
3.11	Typical comparative plot for two mid-span deflections	124
3.12	Load displacement curve for solid joists in shear ($a/h = 1.5$)	124
3.13	Typical failure of solid joists ($a/h = 1.5$)	125
3.14	Sample test result for the shear test of joists having circular web openings	125
3.15	Diagonal shear buckling failure for the joists having circular web opening	126
3.16	Typical diagonal shear failure of joists having square web openings	126
3.17	Shear reinforcement schemes "A" and "B" (AISI, 007a)	127
3.18	Shear reinforcement scheme "C" (Current study)	127
3.19	Typical shear failure of joists having reinforced (Scheme-A) web openings	128
3.20	Typical shear failure of joists having reinforced (Scheme-B) web openings	128
3.21	Typical shear failure of joists having reinforced (Scheme-C) web openings	129
3.22	Comparison of reinforced and unreinforced (circular openings) specimens with solid specimen in shear	129

3.23	Strain measurements on the joist having square web openings in shear test	130
3.24	Strain measurements on the reinforcements of joists having circular web openings in shear test	130
3.25	Typical lateral displacement measurements of joists having square web openings in shear test	131
3.26	Shear variations on floor joist	131
3.27	Moment variations on floor joist	132
3.28	Shear zone and flexural zone for a floor joist	132
4.1	Self-drilling screws and their designations	154
4.2	Nodal degrees of freedom for the shell elements	154
4.3	von Mises failure for two dimensional problem	155
4.4	Experimental stress-strain relations and idealized stress-strain relations used in FEM	155
4.5	Finite element model-I	156
4.6	Finite element model-II	156
4.7	Screw connection showing all the dimensions	157
4.8	Thin sheet steel coupons used for connection tests	157
4.9	Self drilling screw connection assembly before testing	158
4.10	Test setup for connection test	158
4.11	Screw/bolted connection picture after the test - experiment	159
4.12	Screw/bolted connection picture after test - FEM	159
4.13	Gauge extension of the screw connection	160
4.14	Screw tilting of the screw connection	160
4.15	Strain at the center of the screw connection	161

4.16	Gauge extension of the bolted connection	161
4.17	Screw tilting of the bolted connection	162
4.18	Strain at the center of the screw connection	162
4.19	Effect on curling on gauge extension	163
4.20	Effect on curling on screw tilting	163
5.1	Finite element boundary conditions for a quarter plate model	194
5.2	Load displacements curves for simply supported square plate subjected in compression (corresponding to quarter model)	194
5.3	Behavior of simply supported square plate subjected in compression .	195
5.4	Stresses variation along A-A on the outer surface (convex face)of the plate at peak load	195
5.5	Stresses variation along A-A on the inner surface (concave face)of the plate at the peak load level	196
5.6	Stresses variation along A-A on the mid-surface (mid-thickness)of the plate at the peak load level	196
5.7	Stresses through the thickness at the center of the plate	197
5.8	Stresses through the thickness at the side-edge of the plate ()	197
5.9	Finite element boundary conditions for the long plate in compression	198
5.10	Band plots of axial stress for the plate in compression (a) thick plate (b) thin plate	198
5.11	Deformed shape of thick plate in compression	199
5.12	Stresses along A-A of thick plate in compression	199
5.13	Deformed shape of thin plate in compression	200
5.14	Stresses along A-A of thin plate in compression	200
5.15	Deformed shape of thick plate having square openings in compression	201

5.16 Stresses along A-A of thick plate having square openings in compression 201

5.17 Deformed shape of thin plate having square openings in compression . 202

5.18 Stresses along A-A of thin plate having square openings in compression 202

5.19 Band plots of stress for the plate having square opening in compression
(a) thick plate (b) thin plate 203

5.20 Load deformation curves for the thick plate having square openings in
compression 203

5.21 Load deformation curves for the thin plate having square openings in
compression 204

5.22 Load reduction curves for the plates having square openings in com-
pression 204

5.23 Deformed shape of thick plate having circular openings in compression 205

5.24 Stresses along A-A of thick plate having circular opening in compression 205

5.25 Deformed shape of thin plate having circular openings in compression 206

5.26 Stresses along A-A of thin plate having circular openings in compression 206

5.27 Band plots of stress for the plate having circular openings in compres-
sion (a) thick plate (b) thin plate 207

5.28 Load deformation curves for the thick plate having circular openings
of various sizes in compression 207

5.29 Load deformation curves for the thin plate having circular openings of
various sizes in compression 208

5.30 Load reduction curves for the plates having circular openings in com-
pression 208

5.31 Finite element boundary conditions for the plate in in-plane bending 209

5.32 Band plot of stress for the plate in bending (a) thick plate (b) thin plate 209

5.33 Deformed shape of thick plate in bending 210

5.34	Stresses along A-A of thick plate in bending	210
5.35	Deformed shape of thin plate in bending	211
5.36	Stresses along A-A of thin plate in bending	211
5.37	Deformed shape of thick plate having square openings in bending . .	212
5.38	Stresses along A-A of thick plate having square openings in bending .	212
5.39	Deformed shape of thin plate having square openings in bending . . .	213
5.40	Stresses along A-A of thin plate having square openings in bending .	213
5.41	Band plots of stress for the plate having square openings in bending (a) thick plate (b) thin plate	214
5.42	Moment rotation curves for the thick plate having square openings in bending	214
5.43	Moment rotation curves for the thin plate having square openings in bending	215
5.44	Moment reduction curves for the plates having square openings in bending	215
5.45	Deformed shape of thick plate having circular openings in bending . .	216
5.46	Stresses along A-A of thick plate having circular openings in bending	216
5.47	Deformed shape of thin plate having circular openings in bending . .	217
5.48	Stresses along A-A of thin plate having circular openings in bending .	217
5.49	Band plots of stress for the plate having circular opening in bending (a) thick plate (b) thin plate	218
5.50	Moment rotation curves for the thick plate having circular openings in bending	218
5.51	Moment rotation curves for the thin plate having circular openings in bending	219

5.52	Moment reduction curves for the plates having circular openings in bending	219
5.53	Deformed shape of 1 mm thick plate having reinforced square openings in bending	220
5.54	Moment rotation curves for 1 mm thick plate having reinforced square openings in bending	220
5.55	Deformed shapes of 2 mm thick plate having reinforced square openings in bending	221
5.56	Moment rotation curves for 2 mm thick plate having reinforced square openings in bending	221
5.57	Deformed shapes of 4 mm thick plate having reinforced square openings in bending	222
5.58	Moment rotation curves for 4 mm thick plate having reinforced square openings in bending	222
5.59	Deformed shapes of 8 mm thick plate having reinforced square openings in bending	223
5.60	Moment rotation curves for 8 mm thick plate having reinforced square openings in bending	223
6.1	Geometrical imperfections	248
6.2	Idealized material properties	248
6.3	Boundary conditions for full scale finite element models	249
6.4	Full scale finite element models	249
6.5	Boundary conditions for reduced model	250
6.6	X-Displacements of the joist along the height at left loading point . .	250
6.7	Load displacement curve for solid joists	251

6.8	Deformed shape of full scale FE model of solid joists	251
6.9	Load displacement curve for joists having circular web openings . . .	252
6.10	Deformed shape of full scale FE model of joists having circular web openings	252
6.11	Load displacement curve for joists having square web openings	253
6.12	Deformed shape of full scale FE model of joists having square web openings	253
6.13	Moment rotation curves for solid joists	254
6.14	Comparison of deformed shapes: Solid joists	254
6.15	Moment rotation curves for joists having circular web openings	255
6.16	Comparison of deformed shapes: Joists having circular web openings	255
6.17	Moment rotation curves for joists having square web openings	256
6.18	Comparison of deformed shapes: Joists having square web openings .	256
6.19	Normalized moment rotation curves for the thin joists having circular web openings	257
6.20	Normalized moment rotation curves for the thick joists having circular web openings	257
6.21	Normalized moment rotation curves for the thin joists having square web openings	258
6.22	Normalized moment rotation curves for the thick joists having square web openings	258
6.23	Moment reduction curves for the 203.2 mm (8 inch) deep joists having circular web openings	259
6.24	Moment reduction curves for the 203.2 mm (8 inch) deep joists having square web openings	259
6.25	Typical failure mode of thin joists	260

6.26	Typical failure mode of thick joists	260
6.27	Moment reduction curves for the 304.8 mm (12 inch) deep joists having circular web openings	261
6.28	Moment reduction curves for the 304.8 mm (12 inch) deep joists having square web openings	261
6.29	Normalized moment rotation curves of reinforced 2.464 mm (97 mils) thick joist	262
6.30	Deformed shapes of reinforced 2.464 mm (97 mils) thick joist	262
6.31	Normalized moment rotation curves of reinforced 1.727 mm (68 mils) thick joist	263
6.32	Normalized moment rotation curves of reinforced 1.372 mm (54 mils) thick joist	263
6.33	Normalized moment rotation curves of reinforced 1.902 mm (43 mils) thick joist	264
6.34	Deformed shape of reinforced 1.092 mm (43 mils) thick joist	264
A.1	Locations and dimensions of tensile coupons	289
A.2	Tensile coupons testing on INSTRON-5566 machine	289
A.3	Tensile coupons before testing	290
A.4	Tensile coupons after testing	290
A.5	Stress-strain relationships of tensile coupons for 43-mils thick section-1	291
A.6	Stress-strain relationships of tensile coupons for 43-mils thick section-2	292
A.7	Stress-strain relationships of tensile coupons for 43-mils thick section-3	293
A.8	Stress-strain relationships of tensile coupons for 97-mils thick section-1	294
A.9	Stress-strain relationships of tensile coupons for 97-mils thick section-2	295
A.10	Stress-strain relationships of tensile coupons for 97-mils thick section-3	296

B.1	Test results for solid specimens	299
B.2	Test results for specimens having circular web openings	300
B.3	Test results for specimens having square web openings	301
B.4	Test results for specimens having reinforced (Scheme-A) circular web openings	302
B.5	Test results for specimens having reinforced (Scheme-B) circular web openings	303
B.6	Test results for specimens having reinforced (Scheme-C) circular web openings	304
B.7	Test results for specimens having reinforced (Scheme-A) square web openings	305
B.8	Test results for specimens having reinforced (Scheme-B) square web openings	306
B.9	Test results for specimens having reinforced (Scheme-C) square web openings	307
C.1	Test results for solid specimens	311
C.2	Test results for specimens having circular web openings	312
C.3	Test results for specimens having square web openings	313
C.4	Test results for specimens having reinforced (Scheme-A) circular web openings	*314
C.5	Test results for specimens having reinforced (Scheme-B) circular web openings	315
C.6	Test results for specimens having reinforced (Scheme-C) circular web openings	316

C.7	Test results for specimens having reinforced (Scheme-A) square web openings	317
C.8	Test results for specimens having reinforced (Scheme-B) square web openings	318
C.9	Test results for specimens having reinforced (Scheme-C) square web openings	319
D.1	Test results for solid specimens ($a/h = 1.0$)	323
D.2	Test results for solid specimens ($a/h = 1.5$)	324
D.3	Test results for specimens having circular web openings ($a/h = 1.5$)	325
D.4	Test results for specimens having square web openings ($a/h = 1.5$)	326
D.5	Test results for specimens having reinforced (Scheme-A) circular web openings ($a/h = 1.5$)	327
D.6	Test results for specimens having reinforced (Scheme-B) circular web openings ($a/h = 1.5$)	328
D.7	Test results for specimens having reinforced (Scheme-C) circular web openings ($a/h = 1.5$)	329
D.8	Test results for specimens having reinforced (Scheme-A) square web openings ($a/h = 1.5$)	330
D.9	Test results for specimens having reinforced (Scheme-B) square web openings ($a/h = 1.5$)	331
D.10	Test results for specimens having reinforced (Scheme-C) square web openings ($a/h = 1.5$)	332

List of Symbols

A	Gross cross sectional Area
A_c^e	Effective cross sectional area in compression
A_e	Effective cross sectional area
A_{flange}^e	Effective cross sectional area of flange
A_{lip}^e	Effective cross sectional area of lip
A_m, A_{mn}	Amplitude of out of plane displacements of plate
A_{net}	Net cross sectional Area *
A_o	Area of openings
A_w	Area of flat web
$A_{web+renf}^e$	Effective cross sectional area of web and reinforcement
a	Shear panel length
B, B_c, B_t	Out-to-out width of flange, compression flange and tension flange
B_{co}	Coefficient defined by Equation 6.2
C_{ijkl}	Material property tensor
b_1, b_2	Effective width defined by Figure 2.2
b_e	Effective width
b_{eo}	Effective width of plate having openings
b_h	Width of the opening
C	Coefficient corresponding to shear reduction factor

D	Out-to-out depth of the web
D_{ep}	Idealized elasto-plastic stress strain relationship
D_L	Dead load
d	Nominal diameter of the screw
d_{ct}	distance between compression and tension resultants
d_c, d_t	Out-to-out depth of lip in compression and tension
d_h	Depth or diameter of the opening
d_s	Diameter of the screws
dx	Derivative of x
E	Modulus of elasticity
F_{cr}	Critical buckling stress
F_p	Proportional limit of the material
F_v	Nominal shear strength
F_{vo}	Nominal shear strength for the sections having openings
F_{vp}	Proportional limit in shear
F_y	Yield strength of the material
F_u	Ultimate strength of the material
f	Stress distribution
f_1, f_2	Stresses at the top and bottom of the web defined by Figure 2.2
f_{max}	Maximum stress at the edge
f_x	Compression stress in X-direction
h	Flat height of the web
K_o, K_L, K_{NL}	Small displacement, initial displacement and Large displacement matrixes
K_B	Stiffness matrix for plane stress element
K_m	Stiffness matrix for membrane element

K_s	Stiffness matrix for shell element
k	Plate buckling coefficient in compression
k_v	Plate buckling coefficient in shear
k_{vo}	Plate buckling coefficient in shear for the sections having openings
I_{req}, I_{avi}	Required and available moment of inertia
I_{xx}, I_{yy}	Gross moment of inertia about X- and Y-axis
I_{xxe}, I_{yye}	Effective moment of inertia about X- and Y-axis
L_L	Live load
L_r	Length of the reinforcement
l	Length of the plate
l_a	Anchorage length of reinforcements
M_m	Moment in shear reinforcement
M_n	Nominal moment capacity for solid section
M_{no}	Nominal moment capacity for section having web openings
M_o	Moment capacity of the plate having openings
M_s	Moment capacity of solid plate
m	Number of sine wave along the length of the plate
m_{co}	Coefficient defined by Equation 6.3
n	Number of sine wave along the width of the plate
P	Applied load
P_c	Nominal compression load
P_m	Axial load in shear reinforcement
P_n	Nominal load capacity
P_{nov}	Pull-over load capacity
P_{not}	Pull-out load capacity

P_{ns}	Nominal shear strength of screw
P_r	Load at reinforcement
P_o	Compressive load capacity of the plate having openings
P_s	Compressive load capacity of solid plate
P_{ss}	Nominal shear capacity of screw specified by manufacturer
q_s	Shear reduction factor
R	External force
r	Inner radius of the corner of the section
S	Coefficient corresponding to Equation 2.15
S_e	Effective section modulus
S_{ij}	Second Piola-Kirchhoff stress tensor
t	Base metal thickness excluding galvanized layer
t_r	Thickness of the reinforcement
t	Overall thickness including galvanized layer
u_x, u_y, u_z	Displacements in X, Y and Z-directions
V_f	Factored shear force
V_m	Shear load in shear reinforcement
V_n	Nominal shear resistance
V_o	Shear resistance of joist with openings
V_r	Reduced shear resistance
V_s	Shear resistance of solid joist
W	External virtual work
w	Flat width of the plate
\bar{w}	Average width of the plate
w_f	Factored load intensity

w_r	Width of reinforcement
X, Y	Strength reduction coefficients. See Equation 5.8
α_c	Strength reduction coefficient for plate having circular openings
α_r	Strength reduction coefficient for plate having rectangular opening
δ	Out of plane imperfection
δ_o	Amplitude of out of plane imperfection
$\varepsilon_{ij}, \varepsilon_{kl}$	Green-Lagrange strain tensor
ε_u	Strain at rupture
ϕ_m	Function corresponding to the anchorage length of the reinforcements
λ	Slenderness factor defined by Equation 2.5
μ	Poissons ratio
η_{ij}	Non-linear incremental strain
$\theta_x, \theta_y, \theta_z$	Rotation about X- Y- and Z-axes
ρ	Local reduction factor defined by Equation 2.4
$\sigma_1, \sigma_2, \sigma_3$	Principle stresses
σ_{von}	Von Mises stress
$\sigma_{xx}, \sigma_{yy}, \sigma_{zz}$	Stresses in X- Y- and Z- directions
σ_y	Yield stress
ψ	Stress ratio defined by Equation 2.8
ω	Out of plane deflection of plate

Chapter 1

Introduction

1.1 Introduction

The use of cold-formed steel (CFS) structures has become increasingly popular in building constructions. For example, houses, low rise offices and retail buildings can be constructed using cold-formed steel. The CFS structures can be used as wall structures, framing systems and roof structures including trusses and shielding materials. Figure 1.1 shows a typical example of buildings composed of cold-formed steel. The reasons behind the growing popularity of cold-formed steel products include their ease of fabrication, high strength/weight ratio and suitability for a wide range of applications. These advantages can result in more cost-effective designs, as compared with hot-rolled steel, especially in low-rise short-span applications. Cold-formed steel also offers very flexible design using different cross-sectional shapes.

Cold-formed steel (CFS) members can be classified into two major categories: panels or decks and individual structural framing member. The first category such as panels and decks are generally used for roof decks, floor decks, wall panels, siding material, and bridge forms. The second category such as structural framing members is commonly used as load carrying primary or secondary structural framing members. Structural strength and the stiffness are the main consideration in the design of such

members. These members are available in various shapes such as C-sections, lipped channel sections, Z-sections, angles, hat sections etc.

The CFS structural framing members are commonly used as floor joists for the residential homes and low-rise buildings. A typical use of CFS member as a floor joists is shown in Figure 1.2. Common types of CFS framing members are: stud or joist sections, track sections, channel sections and furring channel sections. Shapes of these sections are shown in Figure 1.3. The stud or joist sections are widely used as floor joists due to their good performance under flexural loads. This study considers the flexural and shear strength of lipped channel cold-formed steel joist sections.

Cold-formed steel floor joists are subjected to failure modes quite different than those of hot-rolled steel beams. In general, CFS floor joists are susceptible to the following five failure modes: (a) lateral torsional buckling (b) web crippling (c) cross sectional failure governed by local buckling (d) distortional buckling and (e) shear buckling of webs. Usually, floor deck is constructed over the CFS members when they are used as floor joists. The floor deck provides lateral bracing to CFS floor joists and prevents them from failure by lateral torsional buckling. The web crippling of the CFS floor joists can be prevented by providing web stiffeners at the supports. Therefore, local buckling, distortional buckling and shear buckling of webs are the expected failure modes for CFS floor joists.

1.2 Problem Statement

It is a common practice in cold-formed steel construction to cut openings in the web of floor joists to facilitate passage of service ducts, heating ducts and piping. Such web openings provide the necessary space for ductwork and piping systems. Figure 1.4 shows such construction practices where openings have been made in the web of

cold-formed steel (CFS) joists. The web openings shown in Figure 1.4 are made in the fabrication plant. Figure 1.5 shows the application of web openings, where drainage pipes, heating ducts and electric wires have been passed through the web of the CFS floor joists. If the openings are not made in the web of floor joists, then the ducts and piping would have to pass below the floor joists resulting in a reduction of clear story height. In other word, the overall story height would have to be increased in order to maintain the desirable story height. Thus the provision of such web openings reduces the story height and consequently can result in considerable reduction in the project cost.

Web openings in CFS joists cause localized redistribution of stresses in the opening regions. The web openings can result in reduction of flexural and shear strengths due to the removal of materials. Furthermore, the web openings change the buckling characteristics of the members around the openings because of change in boundary conditions at the opening regions. Web openings also affect the flexural stiffness resulting in inferior serviceability performance of the member.

A cost effective way to alleviate the detrimental effects of large web openings may be to apply appropriate reinforcements around the opening regions. The web reinforcement of CFS joists has not been studied extensively. Some experimental studies (Pennock, 2001; Ng et al., 2005) were conducted to establish reinforcement schemes for cold-formed steel joists having large web openings in the flexural zone. So far no studies have been made to develop criteria for shear reinforcement of CFS joists having large web openings. This study deals with the reinforcement schemes for CFS joists having large web openings subjected on flexural and shear loads.

1.3 Objectives and Scopes

The overall objective of this research is to develop reinforcement schemes for lipped channel shaped cold-formed steel (CFS) joists having large web openings. The goal is to develop reinforcement schemes that would restore the original strength of the joists, so that the original design of the member need not be changed. The study has the following scopes.

- Experimental Investigation
 - Establishment of the flexural strength of laterally braced lipped channel shaped CFS solid joists.
 - Establishment of the flexural strength of laterally braced lipped channel shaped CFS joists having web openings.
 - Development of reinforcement schemes for lipped channel shaped CFS joists having web openings predominantly in the flexural zone.
 - Establishment of the shear strength of lipped channel shaped CFS solid joists.
 - Establishment of the shear strength of lipped channel shaped CFS joists having web openings.
 - Development of reinforcement schemes for lipped channel shaped cold-formed steel joists having web openings predominantly in the shear zone.
- Numerical (Finite Element Method) Investigation
 - Development of a simplified finite element connection models for thin-walled structures, such as connections between cold-formed steel joists and reinforcements.

- Examinations of the effect of openings on the behavior of thin plates subjected to compression and in-plane bending.
- Design of reinforcement schemes for thin plates having openings and subjected to in-plane bending.
- Examinations of the effect of web openings on lipped channel shaped CFS joists subjected to bending.
- Development of flexural reinforcement schemes for lipped channel shaped cold-formed steel joists having web openings.

1.4 Organization of the Dissertation

This dissertation has seven chapters and four appendices. The main research work is presented in five major chapters (Chapter 2 to Chapter 6). Each of these chapters contains literature review, research work and results. All the tables and figures are presented at the end of each chapter. Chapter 7 contains conclusions of the dissertation.

Chapter 2: This chapter presents the details of an experimental program conducted to determine the flexural strength of cold-formed steel (CFS) joists with and without web openings. Openings of up to 75 percent of the web depth were considered. The web openings were reinforced with three different reinforcement schemes. The results associated with the flexural tests of CFS joists with no openings, with unreinforced web openings and with reinforced web openings are presented.

Chapter 3: This chapter presents an experimental investigation of the shear strength of cold-formed steel (CFS) joists with and without web openings. About 65 percent of the webs of the cold-formed steel joists were cut out in the form of circular

and square openings and the web openings were reinforced using three different shear reinforcement schemes.

Chapter 4: This chapter presents the details associated with two simplified finite element models suitable for the analysis of screw connections and bolt connections as used in with thin walled members. Two types of finite element models were investigated. The finite element models were calibrated against experimental results.

Chapter 5: This chapter presents the finite element analysis of the compressive strength and in-plane flexural strength of simply supported thin plates with and without openings. The study considers various thicknesses of plates ranging from one millimetre to eight millimetres. Opening sizes of zero to eighty percent of the plate width were considered. The openings were reinforced using plates having various thicknesses.

Chapter 6: This chapter presents the finite element investigation of the flexural strength of cold-formed steel joists. The finite element model was validated against experimental results. The validated model was used for the parametric study. The parameters considered were: joist size, joist thickness, opening size and reinforcement size.

Chapter 7: This chapter summarizes the findings of the study. The chapter also suggests future research topics that have evolved from the work presented in this dissertation.

1.5 Stability of Thin Walled Structures

1.5.1 General

Thin-walled structures, such as, cold-formed steel structures consist of a wide and growing field of engineering applications which seek efficiency in strength and cost by minimizing material. The result is a structure in which the stability of the components, controls behavior and design.

The structural stability for thin walled structures can be divided into two types: limit load buckling and bifurcation buckling. In the limit load buckling, the members deform in the direction of the load from beginning until the maximum load is reached. However, the deflection shape experiences a sudden change. Buckling of shallow arches and spherical caps are the examples of limit load buckling.

In the bifurcation buckling, initially the member deforms in the direction of the load and at some particular load, called buckling load, the deformation suddenly takes up a pattern which is different from the load direction. Buckling of cylindrical shells and plates are examples of bifurcation buckling.

1.5.2 Buckling of Plates in Compression

Considering a simply supported rectangular plate subjected to a uniform compression stress in one direction, it will buckle in a multiple curvature along the length and a single curvature across the length. The critical buckling stress of such plate can be determined by solving Bryan's differential equation as follows:

$$\frac{\partial^4 \omega}{\partial x^4} + 2 \frac{\partial^4 \omega}{\partial x^2 \partial y^2} + \frac{\partial^4 \omega}{\partial y^4} + \frac{f_x t}{D} \frac{\partial^2 \omega}{\partial x^2} = 0 \quad (1.1)$$

where,

$$D = \frac{Et^3}{12(1 - \mu^2)} \quad (1.2)$$

and E = modulus of elasticity of steel, t = thickness of plate, μ = Poisson's ratio = 0.3, ω = deflection of plate perpendicular to the surface and f_x = compression stress.

If m and n are the numbers of half sine waves in the X- and Y-directions, respectively, the deflected shape of the rectangular plate may be represented by a double series:

$$\omega = \sum_{m=1}^{\infty} \sum_{n=1}^{\infty} A_{mn} \sin \frac{m\pi x}{l} \sin \frac{n\pi y}{w} \quad (1.3)$$

Where, l and w are length and width of the plate.

Solving Equation 1.1 by using Equation 1.3 one can obtain the following equation for which is the elastic buckling stress:

$$F_{cr} = f_x = \frac{k\pi^2 E}{12(1 - \mu^2)(w/t)^2} \quad (1.4)$$

where

$$k = \left[m \left(\frac{w}{l} \right) + \frac{1}{m} \left(\frac{l}{w} \right) \right]^2 \quad (1.5)$$

The plot of Equation 1.5 is shown in Figure 1.6. The figure shows that when the l/w ratio is an integer, the value of k equals 4. The value of k equal to 4 is also applicable for relatively large l/w ratios.

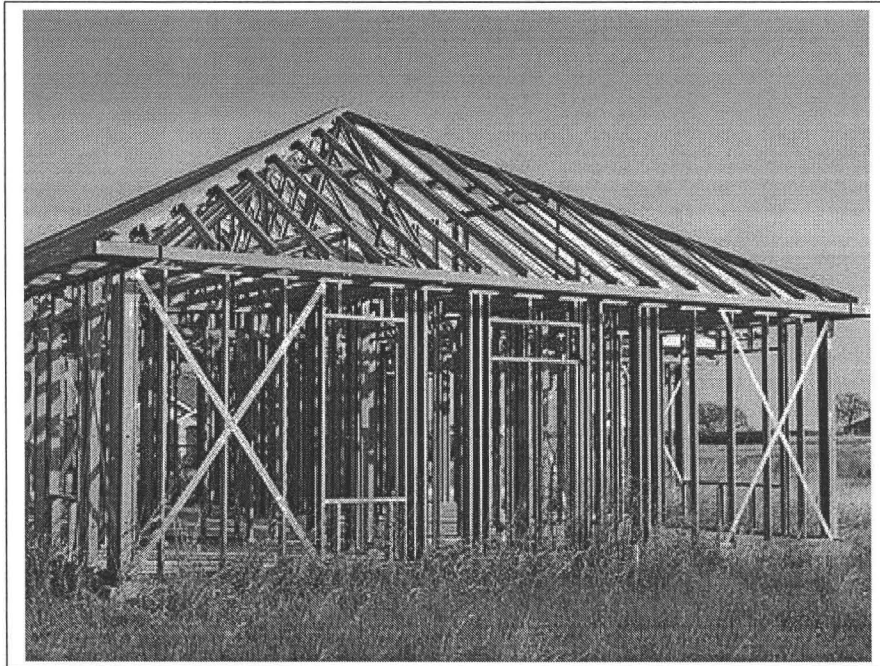


Figure 1.1: Building composed entirely of cold-formed steel sections (<http://yourenergysavinghome.com>)

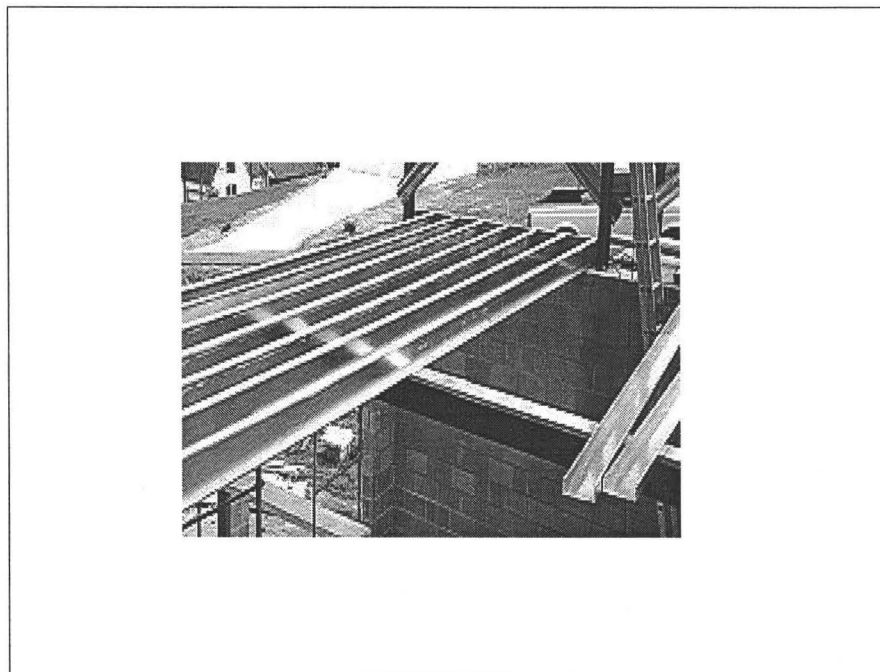


Figure 1.2: Cold-formed steel (CFS) joists used as floor joists (<http://www.superior-truss.com>)

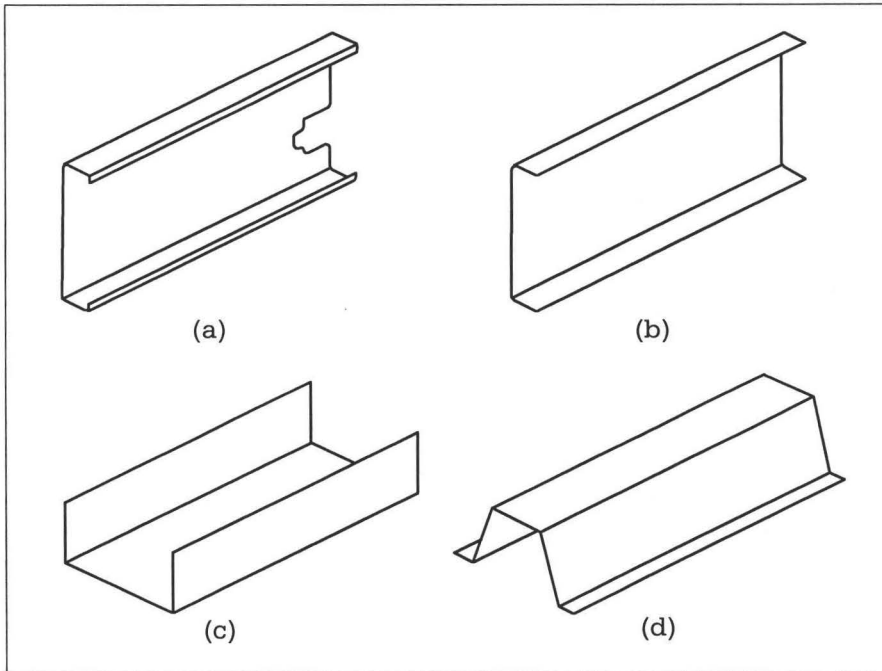


Figure 1.3: Light weight CFS framing members: (a) stud or joist section (b) track section (c) channel section (d) furring channel section

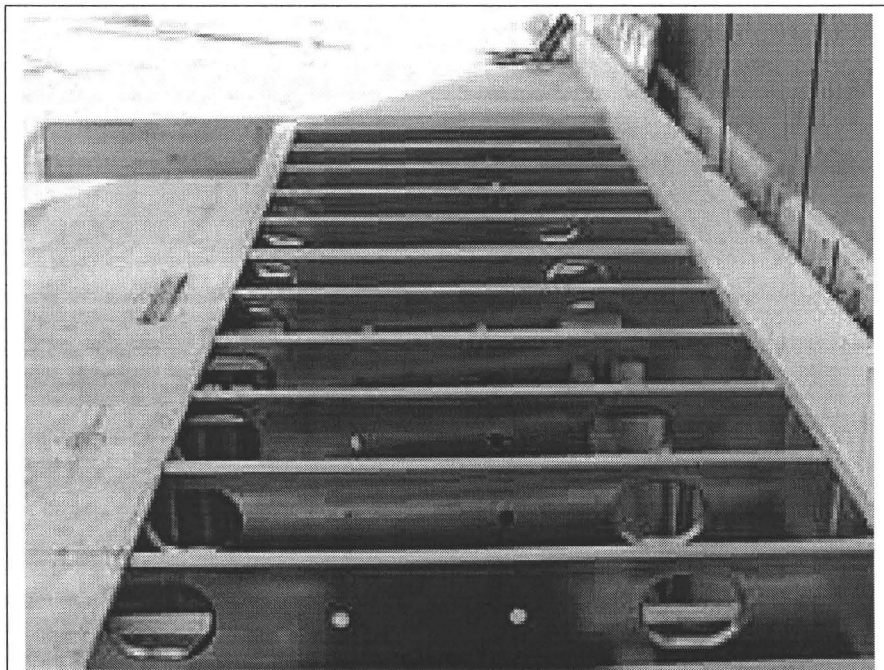


Figure 1.4: Openings in the web of CFS joists (<http://www.superior-truss.com>)



Figure 1.5: Application of web openings in cold-formed steel (CFS) joists (<http://www.aegismetalframing.com>)

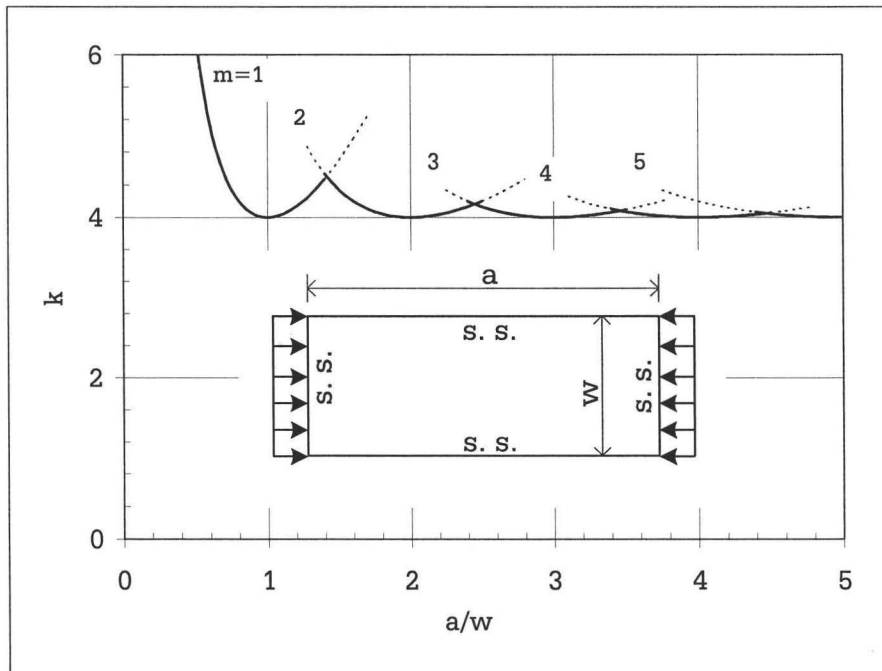


Figure 1.6: Buckling coefficients for flat rectangular plates

Chapter 2

Reinforcements for CFS Joists with Web Openings in Flexural Zone: Experimental Study

2.1 Introduction

This chapter discusses the flexural resistance of cold-formed steel (CFS) joists having web openings. The web openings were reinforced using various reinforcement schemes. A total of 108 cold-formed steel joists were subjected to flexural tests. Tests were carried out using two types of loading arrangements: uniformly distributed loads and two point loads. These tests included sections with no openings, sections with unreinforced web openings and sections with reinforced web openings. Circular and square web openings were investigated in this study. The objective of this part of the experimental study was to assess the effectiveness of three different reinforcement schemes.

2.2 Flexural Resistance of Cold-Formed Steel Joists

2.2.1 Flexural Resistance of Solid Joists

Lipped channel cold-formed steel joists can be considered as a combination of thin plate elements (web, flanges and lip stiffeners). The flexural strength of a fully braced cold-formed steel joist is fundamentally governed by local buckling of such thin plate elements. The North American Specification for the Design of Cold-Formed Steel Structural Members published by American Iron and Steel Institute (AISI) and Canadian Standard Association (CSA, 2007) hereafter referred as “AISI Standard (AISI, 2007)” employs the concept of an effective width to account for the strength of thin plate elements in compression. According to the AISI Standard (AISI, 2007), the nominal moment capacity M_n of CFS joists is determined by the product of effective section modulus S_e and yield strength of the material, F_y , as follows:

$$M_n = S_e F_y \quad (2.1)$$

The effective section modulus S_e is calculated based on the effective width of the compression flange and compression web of the joists. The flanges of the CFS joist experience uniform stresses. The flanges of the CFS joist are supported by a web and a lip stiffener along the two long edges. Therefore, the compression flange of a CFS joist can be considered as a uniformly compressed stiffened element. At ultimate load level, the actual stress distribution over the entire width of thin plate subjected to the uniform compression load would be non-uniform because of the plate local buckling. Figure 2.1 shows such a stress distribution. However, for practical design, the effective width concept was introduced by von Karman et al. in 1932. In this approach, instead of considering the non-uniform distribution of stress over the entire

width of the plate w , it is assumed that the total load is carried by a fictitious effective width b_e , subjected to a uniformly distributed stress equal to the edge stress f_{max} , as shown in Figure 2.1. The width b_e is selected so that the area under the curve of the actual non-uniform stress distribution is equal to the sum of the two parts of the equivalent rectangular shaded area with a width b_e and an intensity of stress equal to the edge stress f_{max} . That is,

$$\int_0^w f dx = b_e f_{max} \quad (2.2)$$

Currently, the effective width of the compression flanges, b_e , is determined in accordance with Section B2.1 of AISI Standard (AISI, 2007) as follows:

$$b_e = \begin{cases} w, & \text{when } \lambda \leq 0.673 \\ \rho w, & \text{when } \lambda > 0.673 \end{cases} \quad (2.3)$$

where, w = flat width of compression flange and ρ = local reduction factor calculated as,

$$\rho = \frac{1 - 0.22/\lambda}{\lambda} \quad (2.4)$$

λ is a slenderness factor determined as follows:

$$\lambda = \sqrt{\frac{f}{F_{cr}}} \quad (2.5)$$

$$F_{cr} = k \frac{\pi^2 E}{12(1 - \mu^2)} \left(\frac{t}{w}\right)^2 \quad (2.6)$$

where

E = modulus of elasticity of steel, usually taken as 203,000 MPa for cold-formed steel

t = thickness of compression element

μ = Poissons ratio of steel = 0.3

k = plate buckling coefficient, calculated from Table B4-1 of AISI Standard (AISI, 2007)

$$f = \begin{cases} F_y, & \text{When the initial yielding is in compression flange} \\ f_{max}, & \text{Maximum stress on compression element to be determined on the} \\ & \text{basis of effective section when the initial yielding is in tension flange} \end{cases}$$

The web of the joist is considered to be subjected to linearly varying stress. Section B2.3 of AISI Standard (AISI, 2007) has a provision to calculate the effective width of the web. According to the provision, the plate buckling coefficient and effective widths b_1 and b_2 for webs under stress gradient shall be calculated as follows:

$$k = 4 + 2(1 + \psi)^3 + 2(1 + \psi) \quad (2.7)$$

where,

$$\psi = |f_2/f_1| \quad (2.8)$$

See Figure 2.2 for b_1 , b_2 , f_1 and f_2 ;

For $D/B \leq 4$, where B and D are out-to-out width of compression flange and web respectively,

$$b_1 = b_e/(3 + \psi) \quad (2.9)$$

$$b_2 = \begin{cases} b_e/2, & \text{when } \psi > 0.236 \\ b_e - b_1, & \text{when } \psi \leq 0.236 \end{cases} \quad (2.10)$$

In addition, $b_1 + b_2$ shall not exceed the compression portion of the web calculated on the basis of effective section.

For $D/B > 4$

$$b_1 = b_e/(3 + \psi) \quad (2.11)$$

$$b_2 = b_e/(1 + \psi) - b_1 \quad (2.12)$$

where, b_e = effective width determined in accordance with Equations 2.3 to 2.6 with f_1 substituted with f and with k determined using Equation 2.7.

2.2.2 Flexural Resistance of the Joists with Web Openings

Various studies (Hoglund, 1971; Yu and Davis, 1973; Redwood and Uenoya 1979; Chow and Narayan 1984; Sivakumaran, 1987; Shan and LaBoube, 1994; Shan et al., 1996; LaBoube et al. 1997; Davies et al., 1997; Shanmugam, 1997; Pu et al., 1999, Pennok, 2001; Ng 2004) have been carried out about the effects of web openings on the strength of thin-walled members. The paper by Hoglund (1971) was the first attempt of relevance to thin perforated webs (Shanmugam, 1997). Hoglund's paper reported the results on statically loaded plate girders containing circular and rectangular openings and subjected to transverse loading. The web plates of these girders were slender having h/t values ranging from 200 to 300, they would, therefore, buckle before failure. In these experiments, the girders with openings which were in

the high shear zone failed at significantly lower loads than those in the zone of high bending and low shear.

The study of Yu and Davis (1973) and Sivakumaran (1987) were focused on shear and compressive strength of web-perforated CFS members. Redwood and Uenoya (1979) and Chow and Narayan (1984) studied hot-rolled steel plate girders with web openings.

A study on the flexural resistance of CFS joists having web opening was performed by Shan and Laboube (1994). These authors conducted an experimental study was carried out in order to develop a model for determining the load carrying capacity of the cold-formed steel flexural members. A total of 108 fully braced CFS joists with web openings subjected to flexure were tested under simply supported conditions. The tests were carried out for the following range of CFS joists: web depth-to-thickness ratio: 33-210, web depth: 63.5-304.8 mm, yield strength: 228-560 MPa, ultimate strength: 380-690 MPa, width of web openings: 51-102 mm, depth of web openings: 19-38 mm and opening depth-to-web depth ratio: 0.25-0.75. The study showed that the buckling behavior of web perforated members differs from the original solid members. The failure of the specimens was mainly due to the local buckling at the opening region mixed with distortional buckling. Various simplified approaches were applied to evaluate the flexural resistance of CFS joists having web openings. These approaches were developed based on the governing failure modes.

Based on the Shan and Laboube's (1994) study, Shan et al. (1996) and LaBoube et al. (1997) concluded that, within the limit of tested joists, the flexural capacity can be calculated based on the effective section concept given by Equation 2.1. When computing the effective section modulus, the effective width of the compression portion of the web above the web opening is to be treated as an unstiffened compression element with the buckling coefficient, k , taken as 0.43.

Davies et al. (1997) and Pu et al. (1999) investigated CFS columns having perforated web subjected to compression. Shanmugam (1997) studied the shear strength of web of a plate girder. Pennok (2001) tested CFS joists having openings subjected to bending and shear. Circular and square web openings, which reduced the web area by 75 percent, were investigated. The study showed that web openings in areas of high moment and low shear are significantly less detrimental to the member strength than are similar openings in regions of high shear and low moment.

In a study made by Ng (2004), CFS joists having small central punch-out and having circular, square and rectangular (opening-to-web depth ratio 0.66 and aspect ratio equal to 2) web openings were subjected to flexure. The tested joists had web depth of 203.2 mm and web thickness of 1.89 mm ($h/t = 100$). The reduction of flexural resistance due to the presence of openings was up to 13 percent. This reduction in flexural resistance was due to the weakness caused by unstiffened edges of the opening, which lead to premature local buckling at the opening locations.

The AISI Standard (AISI, 2007) Clause B.2.4.(a) has suggested that the effective width of a web element can be taken as the actual depth of the web when the depth of opening is less than 38 percent of the web depth. Such perforated members can be treated as members with no opening. It explains that small size of web openings may not cause significant reduction in strength and serviceability of the entire member. When the depth of the openings is higher than 38 percent of the flat web depth, The AISI Standard (AISI, 2007) recommends the following procedure for calculating the flexural resistance of C-sections having web openings. These provisions are limited to,

- $d_h/h \leq 0.7$
- $h/t \leq 200$

- Holes centered at mid-depth of web
- Clear distance between holes $\geq 457mm$
- Non-circular holes: corner radii $\geq 2t$
- Non-circular holes: $d_h \leq 64mm$ and $b_h \leq 114mm$
- Circular holes: $14mm \leq d_h \leq 152mm$

The moment capacity, M_n , is determined based on the effective cross section as shown in Equation 2.1. The effective width of web shall be determined by assuming the compression portion of the web consists of an unstiffened element adjacent to the hole. The effective width of the compressive element of the web, exclusive of the openings, shall be determined from Equations 2.3 to 2.6, where the k value has to be taken as 0.43.

2.3 Flexural Reinforcements for Web Openings

2.3.1 Previous Studies

Segner (1964), Cogdon and Redwood (1968), Copper and Snell (1972), Wang et al. (1975) and Larson and Shah (1976) addressed the behavior of hot-rolled steel beams with reinforced web openings. Various reinforcement schemes tested by Segner (1964) are shown in Figure 2.3. The reinforcement schemes tested by all the researchers mentioned above consisted of horizontal, vertical and inclined bars welded to the web around the openings. These reinforcement techniques are widely used in hot-rolled steel construction because of their economy and easy of fabrication. These investigations emphasized the ultimate (plastic) strength analysis of hot-rolled steel

beams with web openings. These studies primarily focused on square and rectangular openings, having a particular form of web reinforcement. Shrivastava (1979) presented design recommendations for W-shaped hot-rolled beams with and without reinforced openings. Both square and rectangular openings having the height of the openings between 30-70 percent of the beam depth were studied.

Pennock (2001) and Ng (2004) conducted tests on reinforcement schemes in the CFS joists having web openings. The flexural reinforcement schemes for CFS joists tested by Pennock (2001) is shown in Figure 2.4. Similarly, Figure 2.5 shows the flexural reinforcement schemes for CFS joists tested by Ng (2004). The Standard for Cold-Formed Steel Framing- Prescriptive Method for One and Two Family Dwellings published by American Iron and Steel Institute (AISI), hereafter referred as “AISI Standard (AISI, 2007a)” has a provision of hole patching of cold formed-steel joists. The flexural reinforcement schemes for CFS joists recommended by AISI Standard (AISI, 2007a) is shown in Figure 2.6. Pennock (2001) conducted an experimental investigation on the strength of CFS joists with web openings. Fifty six specimens were tested under eight different loading configurations. The purpose of this investigation was not only to determine the effects of circular openings on the strength of CFS joists, but also to investigate various reinforcement schemes. The test specimens were subjected to bending and combined effects of shear and bending under simply supported conditions. The CFS steel joists with web openings were tested under four point loading. Circular and square openings which reduced the web area by 75 percent were investigated. Load and opening locations were varied so that the effect of different levels of moment and shear could be evaluated. In the investigation by Pennock (2001), the web openings of the CFS joists were reinforced with joist having web opening of the same shape and size. The reinforcement schemes tested by Pennock (2001) are shown in Figure 2.4. It was observed that the use of CFS joist

as reinforcements for the joists having web openings was ineffective in restoring their flexural capacity.

Ng (2004) attempted to find an effective reinforcement scheme for CFS flexural joists with web openings. The experimental study involved eleven sets of three identical test specimens. The tests consisted of specimens with no web openings, specimens with knock-out openings, specimens with web openings, and specimens with two different reinforcement schemes. The CFS joists having circular, square and rectangular openings with opening depth of 66 percent of the flat width of the web were tested under flexure. Reinforcement was provided by bridging channels having 38.1 mm (1-1/2 inch) web depth and 1.09 mm (43 mils) thickness. Such reinforcements were screw fastened on the top and bottom of the openings. The reinforcement schemes tested by Ng (2004) are shown in Figure 2.5. These reinforcements were not only capable of regaining the original flexural resistance of the section, but are also simple, economical and could be applied to joists already in place. Overall, the study by Ng (2005) showed that it is possible to establish reinforcement schemes for cold-formed steel joists having web openings.

2.3.2 AISI Reinforcement Criteria

According to the AISI Standard (AISI, 2007a), hole patching is required when any of the following requirements is violated.

- Web holes shall have center-to-center spacing of not less than 610 mm (24 inches).
- Web hole width for floor and ceiling joists shall not be greater than 0.5 times the member depth D or 64.5 mm (2-1/2 inches).

- Web hole width for studs and other structural members shall not be greater than 0.5 times the member depth D or 38.1 mm (1-1/2 inches).
- Web hole length shall not exceed 114 mm (4-1/2 inches).
- Minimum distance between the end of the member or edge of bearing and the near edge of the web hole shall be 254 mm (10 inches).

Web holes violating the above requirements shall be patched if the depth of the hole does not exceed 70 percent of the flat width of the web and the length of the hole measured along the web does not exceed 254 mm (10 inches) or the depth of the web, whichever is greater. The patch should be a solid steel plate, stud section, or track section. The steel plate shall be of a minimum thickness as the receiving member and shall extend at least 25.4 mm (1 inch) beyond all edges of the hole. The steel patch shall be fastened to the web of the receiving member with No. 8 screws spaced no greater than 25.4 mm (1 inch) center-to-center along the edges of the patch with minimum edge distance of 12.7 mm (1/2 inch). Resulting reinforcement arrangement is shown in Figure 2.6.

Furthermore, AISI Standard (AISI, 007a) suggests that structural members shall be replaced or designed in accordance with accepted engineering practices when web holes exceed the following size limits.

- The depth of the hole, measured across the web, exceeds 70 percent of the flat width of the web, and/or,
- The length of the hole measured along the web, exceeds 254 mm (10 inches) or the depth of the web, whichever is greater.

2.4 Experimental Program

2.4.1 Selection of the Test Joists

An effective experimental study requires appropriate selection of types and sizes of the test specimens. Cold-formed steel (CFS) joists are available in various sizes and thicknesses. Table 2.1 summarizes the h/t ratios for various lipped channel sections that are common in practice, where h is the flat width of the web and t is the thickness of the web. For thin walled structures such as CFS joists, the initiation of local buckling has a governing effect on compression, shear and bending strengths. The buckling load of thin walled elements is sensitive to plate width-to-thickness (h/t) ratio. Hence, web depth-to-thickness ratio was one of the major criteria for the proper selection of joist size for the test. Moreover, AISI Standard (AISI, 2007) Sec. B1.2 limits the h/t ratio to 200, when there are no bearing and intermediate stiffeners on the web.

In Cold-formed steel (CFS) building construction practice, lipped channel sections having web depth 203.2 mm (8 inch) is one of the most commonly used floor joist size. Therefore, this section can be a good representative floor joist for this experimental study. However, joists having greater depths are also used in practice. AISI Standard (AISI, 2007a) provides information on web depths as high as 304.8 mm (12 inch) for the design of cold-formed steel framing for one and two family dwellings. In Canadian cold-formed steel construction practice, joists having web depth of 355.6 mm (14 inch) are in use. Hence, a section with web depth of 304.8 mm (12 inch) was also selected for the experimental study to represent higher web-depth sections.

Two different joist thicknesses were selected to represent a wide range of h/t ratios and available thicknesses. Considering all of the above criteria, finally, joists having thickness 1.092 mm (43 mils), web depth 203.2 mm (8 inch) and joists having

thickness 2.464 mm (97 mils), web depth 304.8 mm (12 inch) were selected for this experimental programme. The mechanical properties of the selected joists were established by tensile coupon tests according to ASTM Standard. Detail test procedures for the tensile coupon test are presented in Appendix A. The average mechanical and sectional properties of the selected CFS sections are presented in Table 2.2. The Table 2.2 is a summary of the tensile coupon test results presented in Appendix A.

2.4.2 Test Specimens

Figure 2.7 illustrates the assembled test specimen mounted on the test set-up. The cross-section of the test specimen assembly at locations A and B is as shown in Figure 2.8. These locations have been identified in Figure 2.7. The cold-formed steel (CFS) joists of open sections generally possess a low torsional rigidity. This is due to the fact that the shear center of CFS joists does not coincide with the centroid of the joist and that they are open sections. It is not practical to apply the load through the shear center of a single joist as the shear center lies outside the web of the joist. The test specimens consisted of two 3.048 m (10 feet) long CFS joists assembled front-to-front. The specimens were assembled using steel brackets at the locations where higher concentrated loads were expected (e.g., supports, loading points). Such steel brackets primarily helped to transfer the high concentrated loads to the web of the joists, thereby preventing web crippling of the sections. The steel brackets also helped to maintain the joists vertically and face-to-face together. The inner width of these brackets was 152.4 mm (6 inch). The test joists were attached to the steel brackets using two lines (four screws in each line) of No. 10 self-drilling screws. In order to provide a fully braced condition, the test sections were also connected together using 130 mm x 20 mm x 6.4 mm steel strips, which were located at every 305 mm (1 foot)

along the compression flanges and at every 686 mm (2.25 feet) along the tension flanges of the test specimen. Spacing of these steel strips represents the spacing of connections of floor decks and floor joists in cold-formed steel housing construction. The steel strips were fastened using No. 8 self-drilling screws.

2.4.3 Test Designations

For the convenience of identification of the tests, each test was assigned a specific designation. The coding represents the size of the joist, type of the test, opening type, sequences of the test and the position of the section on the specimen assembly. For example, the test “**8F-SRC-2-L**” indicates the following:

8 : 203.2 mm (8-inch) deep joist

F : Flexural test

SRC : “S” for square hole, “R” for reinforced and “C” for reinforcement scheme “C” (see Section 2.7.3 for various reinforcement schemes)

2 : Second set of test, and

L : Left section of the test specimen assembly

The measured geometric properties of test specimens are presented in Tables 2.3 and 2.4.

2.4.4 Test Setup

Flexural tests were carried out using two different loading arrangements: uniformly distributed loads and two point loads. The 203.2 mm (8 inch) deep joists were tested under uniformly distributed load setup and the 304.8 (12 inch) deep joists were tested under four point loads setup.

Test Setup-I: Uniformly Distributed Load: The flexural tests were carried out on 2743 mm (9 feet) long simply supported span. Pinned and roller supports were used at the ends of the test specimen. Since most of the CFS floor joists in practice are expected to be subjected to uniformly distributed loads that are transferred from the floor deck, this test setup was designed to reproduce such a loading on the test specimen. Such a uniformly distributed load was assumed to have been created by using a series of six identical hydraulic jacks of maximum capacity of 10 ton each, connected to a single hydraulic pump. This arrangement results in equal loads on all jacks at all times. Figure 2.7 and Figure 2.8 shows the sketch of the flexural test setup-I, whereas Figure 2.9 gives the photograph of the test setup-I. Each load was transmitted to the test specimen through a 280 mm x 254 mm x 20 mm oriented strand board (OSB). Such loading arrangement would impart even distribution of loads on the specimen thereby minimizing the possibility of web crippling. The applied loads on the hydraulic jacks were monitored through a pressure gauge connected to the hydraulic pump. The reactions at the end supports were also measured using two load cells, which were located on a hot-rolled steel cross-beam at each support. Both cross beams were anchored to the rigid floor below, using two 38.1 mm (1-1/2 inch) diameter hot-rolled steel rods. Since the loads were applied vertically upwards, the supports were anchored downwards through the 610 mm (2 feet) thick reinforced concrete test floor. The ends of the test specimen were laterally supported by angles having smooth vertical face to prevent lateral movement of the ends. Furthermore, in order to prevent lateral-torsional buckling of the test specimens, lateral braces were also provided at one third span locations. Two vertical linear variable displacement transducers (LVDTs) mounted on the top of two sections measured the central vertical displacements of the specimen. Two lateral LVDTs were set to measure the lateral displacements of the web at central region. Lateral displacements were measured

at 38.1 mm (1-1/2 inch) below the top flange and 38.1 mm (1-1/2 inch) above the bottom flange. In one of three identical tests, four strain gauges were attached to measure the longitudinal strain on the top flange, bottom flange, the web at 38.1 mm (1-1/2 inch) below the top flange and at 38.1 mm (1-1/2 inch) above the bottom flange.

Test Setup-II: Two-Point Load: Figure 2.10 shows the sketch of the test setup used for the 304.8 mm (12 inch) deep joists. Figure 2.11 shows a photographic image of the test setup, including the test specimen during a typical test. The test specimens were simply supported at their ends, and were subjected to two equal point loads acting at equal distances from the supports. One end of the test specimens was pin-supported, whereas the other end was roller-supported in order to allow for any horizontal movements. The ends of the test specimen were laterally supported by smooth vertical rods to prevent lateral movement of the ends. Furthermore, in order to prevent lateral torsional buckling of the test specimens, lateral braces were provided at one-third span locations. End supports were welded to concrete blocks, which were resting on the test floor. A hydraulic jack having 152.4 mm (6 inch) stroke was used to apply a vertical downward load. A load cell having 200 kN load capacity was attached at the end of the jack to measure the total applied load. However, as shown in Figure 2.10 and Figure 2.11, a transfer beam was used to subdivide the applied load into two equal point loads. Two identical load cells were used at the supports in order to verify the load transfer. Since the test specimen, the transfer beam, and the load cells were arranged symmetrically with respect to the hydraulic jack, the specimen was expected to experience equal point loads and equal support reactions. The load measurements based on calibrated 50 kN load cells placed at the supports in fact confirmed this hypothesis. Clear span-to-shear span ratio determines the relations between the applied shear force and the bending moments. For flexural

tests such as this a clear span-to-shear span ratio within a range of 2.5 to 3.0 is recommended (Li, 2002). A clear span of 2743mm (9 feet), and a shear span of 1016 mm (3 feet 4 inch) used in the investigation give such a ratio of 2.7. The test arrangement described above, and shown in Figure 2.10 and Figure 2.11, results in a uniform bending moment and zero shear region between the two point loads.

When the central load is 'P', each point load would be 'P/2'. For a shear span of 'a', this loading arrangement produces a uniform moment of '(P/2).a'. In the above test setup, however, load 'P/2' are applied to the specimens at the load locations, as well as at the support locations. These concentrated loads may cause a web-crippling failure, prior to the anticipated flexural failure in the mid span region. In this investigation, as shown in Figure 2.10 and Figure 2.11, steel brackets were used to prevent premature web crippling of the test specimen. At the support locations at the ends, instead of directly supporting the test specimens on the rollers, the test channels were supported on these steel brackets, which acted as bearing plates thereby distributing the concentrated support reactions. At the load locations, the bearing plates were between the load cells and the test specimen. Further, the vertical planes of the steel brackets were fastened to the webs of the test specimens using self-drilling screws. These connections were expected to help transfer the concentrated loads and reactions effectively into the web. The support and loading arrangements performed as expected and prevented premature web crippling during the whole test program.

2.4.5 Test Procedures

Once a test specimen was placed within the test setup, the longitudinal and lateral levels of the specimen were checked. The span length and the positions of vertical loads were measured and recorded. The tightness of lateral supports and verticality

of lateral supporting plates were checked. The load cells, LVDTs and strain gauges readings were initialized to zero. Then, the load was gradually applied using a hydraulic pump. The loading rate was controlled such that the support shear increased at approximately 1.0 kN per minute. The loading rate was selected such that: (a) sufficient load increments can be recorded for graphing the load-displacement relations (60 readings per kN of support shear) and (b) stress increase at any point of the section does not exceed the stress rate specified by ASTM Specification (ASTM, 2003) for tensile coupon test (690 MPa/min). Frequently, the loading was stopped for few minutes in order for the specimens and the loads to reach equilibrium positions. The load cells, LVDTs and the strain gauge readings were recorded using a computer controlled data acquisition system. The loading was continued until the load dropped back to approximately 70 percent of the failure load.

The support reactions at both supports were observed to be almost identical at every load step. Figure 2.12 shows a typical plot of two support reactions with respect to each other for a solid joist. The result shows that the deviations of the reactions are within the 10 percent of the average load. Figure 2.13 shows typical plots for the mid-span deflection of two solid joists. It can be seen from the figure that the displacements were close (within the 10 percent of the average value) to each other. Therefore the average support reactions and average mid-span displacements were plotted for all tests. Detail results associated with these tests are presented in Appendices B and C. Only sample plots and peak values from the test plots are presented in this chapter (Table 2.5 to Table 2.12). Flexural strengths were established based on the average value of three tests.

2.5 Flexural Resistance of Solid Joists

This section considers the flexural resistance of joists with no openings. Three identical tests were performed for each specimen type, thus, this part included six tests. The results are compared to the flexural resistance given by AISI Standard (AISI, 2007).

2.5.1 Joists having h/t ratio = 180 (203.2 mm deep)

Joists having $h/t = 180$ ratio were tested using Test Setup-I as described in section 2.4.4. These joists had 203.2 mm (8 inch) deep web. Table 2.5 summarizes the flexural strength of cold-formed steel solid joists ($h/t = 180$). Test designation 8F-N indicates the flexural resistance of joists having h/t ratio 180 (8 inch deep) with no openings. A typical plot for the average support reaction and the average mid-span deflection for solid joist tests is shown in Figure 2.14. Based on the average of two support reactions, the peak support reactions for three tests were established as 11.72 kN, 11.46 kN and 11.46 kN. The moment capacity of the joist was established based on these load readings and based on the distance measurements. Based on three identical tests, the load displacement relations were consistent. The average moment capacity of a single joist, based on these tests was 4.40 kN-m. The calculated moment capacity (based on measured mechanical properties) of the section according to AISI Standard (AISI, 2007a) design provisions is 4.35 kN-m. It was observed that failure was initiated with the distortion of the flange. However, in the end, the specimen failed due to local buckling of the compression flange and web. All three specimens failed at the central region (maximum moment region). A typical failure pattern of solid joists in flexure is shown in Figure 2.15. The figure was flipped such that the top side would show compression region and the bottom side would show tension region.

The test results and photographs of the failed specimens are also given in Appendix B.

2.5.2 Joists having h/t ratio = 118 (304.8 mm deep)

The cold-formed joists having 304.8 mm (12 inch) deep web ($h/t = 118$) were tested using Test Setup-II. The detail of test setup is shown and described in Section 2.4.4. The flexural strength and failure mode of cold-formed steel joists ($h/t = 118$) without a web opening in the flexural zone are presented in Table 2.6. Based on the average values of the two support reactions, the peak support reactions for three identical tests were established as 45.14 kN, 46.50 kN and 45.22 kN. These peak values were derived from the test results presented in Appendix C. The moment capacity of the joist was established based on these load readings and based on the distance measurements. The average moment capacity of a single joist based on these tests was 23.18 kN-m. The calculated moment capacity (based on measured mechanical properties) of the section according to AISI Standard (AISI, 2007) design provisions was 21.41 kN-m. Thus, the experimental flexural resistance was higher than the calculated flexural resistance by 8 percent. It was observed during testing that the failure was initiated with the distortion of the flange. However, at the end, the specimen failed due to local buckling of the compression flange and the web. All three specimens failed at the mid region (maximum moment region).

2.6 Flexural Resistance of Joists with Web Openings

This section considers the flexural resistance of (a) joists with circular openings, and (b) joists with square openings. Water-jet cutting was used to make these web openings. Three identical tests were performed for each case, thus this part considered 12 tests. Table 2.5 summarizes the flexural resistance of cold-formed steel joists ($h/t = 180$) with a web openings in the flexural zone. The maximum size of the openings for test was determined on the basis of space requirements for reinforcement arrangement. A bridging channel section having 38.1 mm (1-1/2 inch) depth was considered as potential element to be used as reinforcement. These bridging channels are easily available in cold-formed steel construction. Therefore, spaces of 38.1 mm (1-1/2 inch) were left on the top and bottom of the openings.

2.6.1 Joists having h/t ratio = 180 (203.2 mm deep)

Circular and square openings with 127 mm (5 inch) diameter and side, respectively, were considered for the study. The opening depth considered herein is 65 percent of the flat width of the web and these openings were located at the mid-span of the test specimens.

Specimens with Circular Web Openings: The Table 2.5 presents the flexural capacity of joists with circular openings and pictures of associated failure. All three identical specimens exhibited consistent load displacement relations and failure modes which are given in Appendix B. Figure 2.16 shows a typical flexural failure of joists having circular web openings. The peak support reactions associated with three specimens tested were 11.08 kN, 11.06 kN and 10.42 kN. The average moment capacity

of a single section based on these support reactions was established as 4.13 kN-m. A circular web opening reduced the moment capacity by 6.13 percent. According to the AISI Standard (AISI, 2007) the nominal moment capacity of a section with such openings would be 4.06 kN-m. Thus, the experimental value was 1.72 percent higher than the value predicted by AISI Standard (AISI, 2007).

Specimens with Square Web Openings: The test results for specimens with square web openings presented in Table 2.5 are based on three identical tests. The average moment capacity of cold formed sections with square web opening was determined to be 3.78 kN-m, which is 14 percent less compared to the moment capacity of a solid section. The theoretical moment capacity according to AISI Standard (AISI, 2007) for 65 percent square web opening is 4.04 kN-m, which is the same as for circular web openings. However, the test results showed that the square openings were more severe than the circular openings. This can be explained by the fact that the square openings have longer unsupported edge around the openings compared to the circular openings. The associated detailed results are given in Appendix B.

2.6.2 Joists having h/t ratio = 118 (304.8 mm deep)

Circular and square openings with 229 mm (9 inch) diameter and side, respectively, were considered for the study which would leave the sufficient space to place the 38.1 mm (1-1/2 inch) wide bridging channel reinforcement. The opening depth considered herein was 75 percent of the flat width of the web. A summary of the flexural resistance of cold-formed steel joists ($h/t = 118$) with and without a web opening in the flexural zone are presented in Table 2.6. The detailed test results are presented in Appendix C.

Specimens with Circular Web Openings: These specimens failed due to local buckling of the web and the flange at the opening region. Three identical specimens exhibited consistent load displacement behaviors. The results are given in Appendix C. The peak support reactions associated with these specimens were 39.17 kN, 38.27 kN and 38.97 kN. The average moment capacity of single section based on these support reactions was established as 19.71 kN-m. A circular web opening reduced the moment capacity by 15 percent. The AISI nominal moment capacity (based on measured mechanical properties) for such openings is 17.93 kN-m, which is 10 percent less than the experimental value.

Specimens with Square Web Openings: The test results for specimens with square web openings are presented in Table 2.6. The compression element of the CFS sections having square web openings acted as a column. All three specimens appeared to have failed by buckling of the compression element at the opening region as shown in Figure 2.17. The peak support reactions associated with three specimens were 34.03 kN, 34.78 kN and 36.14 kN. The average moment capacity of cold formed sections with 75 percent square web opening was determined to be 17.77 kN-m, which is 23.34 percent less compared to a solid section and 0.9 percent less than theoretical (AISI, 2007) value (17.93 kN-m). The associated detail results are given in Appendix C.

2.7 Flexural Resistance of Joists with Reinforced Web Openings

This section considers the flexural resistance of reinforced circular and square web openings. Three different reinforcement schemes were considered in this investigation. A total of 33 tests were carried out. The results are summarized in Tables 2.7 to 2.11.

2.7.1 Design of Flexural Reinforcement

Figure 2.18 shows a CFS joist with web opening subjected to bending moment, M_n . Assuming that sagging moment is applied, the portion of web and flange above the opening would experience compressive load. Similarly, the portion of web and flange below the opening would experience tensile load. Such compressive and tensile loads may be assumed to act at the center of gravity of the corresponding element. Figure 2.18 also shows a free body diagram at section A-A. Reinforcement of opening may restore the capacity of the section. However, the load carrying capacity of compression element should be checked with two major considerations: stability consideration and strength consideration. The following assumptions were made in order to check the considerations for flexural reinforcements.

- Neutral axis of CFS joist passes through the center of gravity of gross cross sectional area.
- Fully effective compressive elements (lip, flange and web) above the opening experience uniform compressive stress.

Stability Consideration: Experimental results showed that the failure of CFS joists having web openings subjected to flexural load was primarily due to local buckling of the compression element. Therefore, to ensure that the failure does not occur within the opening region, consideration should be given to this failure mode. Local buckling of the web element above the opening can be prevented either by increasing the thickness (decreasing w/t ratio) of the web by means of additional reinforcement or by providing stiffeners along the free edge. Use of bridging channel as reinforcement would in fact provide both additional thickness and edge stiffeners (see Figure 2.19). Assuming that there is no edge stiffener, the width-to-thickness ratio (w/t) of web

reinforcement to prevent the web from local buckling is limited by (CISC Handbook, 2007):

$$\frac{w}{t} \leq \frac{200}{\sqrt{F_y}} \quad (2.13)$$

in which w is projecting flat width of the web plate, t is the thickness of the web and the reinforcement and F_y is the yield strength in MPa.

An edge stiffener would provide a continuous support along the edge of the opening and would increase the critical buckling stress of the compression element. In order to provide necessary stiffener for the compression element such edge stiffeners must possess sufficient rigidity. According to AISI Standard (AISI, 2007), the required moment of inertia of edge stiffener is given by:

$$I_{req} = 399t^4 \left[\frac{w/t}{S} - 0.328 \right]^3 \leq t^4 \left[\frac{115w/t}{S} + 5 \right] \quad (2.14)$$

where, w is the flat width of the compression element, t is the thickness of the compression element and S is given by (AISI, 2007):

$$S = 1.28\sqrt{E/f_{max}} \quad (2.15)$$

Where E is modulus of elasticity and f_{max} is maximum compressive stress. The width-to-thickness ratio (w/t) of web with edge stiffener (stiffened compressive element) to prevent the web from local buckling is given by (CISC Handbook, 2007):

$$\frac{w}{t} \leq \frac{670}{\sqrt{F_y}} \quad (2.16)$$

Strength Consideration: The compressive load that needs to be carried by the compression elements (web and flange above the opening including reinforcement) to resist the nominal moment resistance of the section can be given as:

$$P_c = \frac{M_n}{d_{ct}} \quad (2.17)$$

where, M_n is nominal moment capacity of solid joist and d_{ct} is distance between compression and tension resultants acting above and below the openings. The minimum required effective cross sectional area, A_c^e , of the compression element to carry the moment M_n is given as:

$$A_c^e = \frac{P_c}{F_y} = \frac{M_n}{F_y d_{ct}} \quad (2.18)$$

where, F_y is yield strength. Available effective cross sectional area is given by the summation of effective cross sectional areas of lip, flange, the portion of the web and reinforcement as follows:

$$A_c^e = A_{lip}^e + A_{flange}^e + A_{web+renf}^e \quad (2.19)$$

Where, A_{lip}^e is effective area of lip, A_{flange}^e is effective area of flange and $A_{web+renf}^e$ is effective area of combined web and reinforcement. Combined web and reinforcement can be considered as composite element.

Figure 2.20 shows a complete flow chart to design flexural reinforcement.

Sample Problem: Design a flexural reinforcement for the following CFS joist: Joist section size: 203.2 (8 inches) deep and 1.11 mm (43 mils) thick, Nominal moment capacity of solid joist = 4.35 kN-m, Opening size: 127 mm (5 inches), Internal radius of curve = $2^* t$, = 345 MPa. Effective cross sectional area of compression elements

above the opening = 64.51 ($A_{lip}^e = 10.40$, $A_{flange}^e = 37.51$, $A_{web+renf}^e = 16.60$)mm²,
 $d_{ct} = 182.22$ mm.

Solution: *Stability Consideration:* Check for local buckling of web element in compression: Total width of remaining web in compression = $\frac{203.2-127}{2} = 38.1$ mm

Flat width of remaining web in compression = $38.1-3*t = 38.1-3*1.11 = 34.77$ mm

Now, using Equation 2.13

$$\frac{w}{t} \leq \frac{200}{\sqrt{F_y}}$$

$$\frac{34.77}{1.11} \leq \frac{200}{\sqrt{345}}$$

$$31.32 \leq 10.56$$

FALSE. This shows that web will fail in local buckling at the opening region.

Flexural reinforcement: Let's consider a bridging channel having a thickness equal to the joist thickness (1.11 mm) , 38.1 mm (1.5 inches) deep , 12.7 mm (0.5 inch) flange width and $F_y = 345$ MPa. The thickness of the web would be doubled by the reinforcement. Therefore, Equation 2.13 would give,

$$\frac{w}{t} \leq \frac{200}{\sqrt{F_y}}$$

$$\frac{34.77}{2*1.11} \leq \frac{200}{\sqrt{345}}$$

$$15.66 \leq 10.56$$

FALSE. This shows that combined web and reinforcement will fail in local buckling at the opening region.

However, if adequate edge stiffener is provided along the free edge of the web, local buckling at the free edge can be prevented. Flange of bridging channel would act as edge stiffener. Adequacy of such edge stiffener would be given by Equation 2.14 and 2.15.

Here,

$$S = 1.28\sqrt{\frac{E}{f_{max}}}$$

where, $f_{max} = F_y = 345$ MPa

$$S = 1.28 \sqrt{\frac{200000}{345}}$$

30.82

Required moment of inertia of edge stiffener to make the plate stiffened is given by the Equation 2.14,

$$I_{req} = 399t^4 \left[\frac{w/t}{S} - 0.328 \right]^3 \leq t^4 \left[\frac{115w/t}{S} + 5 \right]$$

$$I_{req} = 399 * 2.22^4 \left[\frac{15.66}{30.82} - 0.328 \right]^3 \leq 2.22^4 \left[\frac{115 * 15.66}{30.82} + 5 \right]$$

$$I_{req} = 60.30 \leq 1551.40$$

Available moment of inertia of edge stiffener = $I_{avi} = \frac{tw^3}{12}$

$$I_{avi} = \frac{1.11 * (12.5 - 3 * 1.11)^3}{12}$$

$$I_{avi} = 76.10 mm^4$$

Therefore, plate is fully stiffened.

Now the w/t ratio for stiffened plate is limited by Equation 2.16:

$$\frac{w}{t} \leq \frac{670}{\sqrt{F_y}}$$

$$\frac{34.77}{2 * 1.11} \leq \frac{670}{\sqrt{345}}$$

$$15.66 \leq 36.07$$

Local buckling is prevented.

Strength Consideration: From Equation 2.18, minimum required cross sectional area of compression element is given by,

$$A_c^e = \frac{P_c}{F_y} = \frac{M_n}{F_y d_{ct}}$$

$$A_c^e = \frac{4.35 * 10^6}{345 * 182.22}$$

$$69.19 mm^2$$

Given,

Effective area of lip (A_{lip}^e) = $10.40 mm^2$; Effective area of flange (A_{flange}^e) = $16.60 mm^2$. Providing reinforcement to the web would change the effective area of web. Since the web is prevented from local buckling, the web element, including the

reinforcement, would be fully effective. Therefore, Effective area of web and reinforcement ($A_{web+renf}^e$) = $34.77 * (2 * 1.11) = 77.20mm^2$. Now , available effective area of compression element is given by,

$$A_c^e = 10.40 + 16.60 + 77.20$$

$$A_c^e = 104.2mm^2 > 64.51mm^2$$

Effective cross sectional area is enough.

Therefore, a bridging channel reinforcement having equal thickness to the joist thickness (1.11 mm), 38.1 mm (1.5 inches) deep and 12.7 mm (0.5 inch) flange width is recommended for the given joist. This reinforcement was also verified by the experiment.

2.7.2 Development of New Reinforcement Schemes

AISI Standard (AISI, 007a) provides provisions for patching openings that violates the opening limitations. However, no related experimental work was found in the published literature to support the provisions. This study showed that the AISI Standard (AISI, 007a) hole patching requirements are not adequate to restore the flexural capacity of all type of joists having web openings (see Tables 2.8 and 2.10). Furthermore, plate or stud patching is not possible if the joists are already in place and drainage, pipe and wires are already passing through the openings. One of the objective in this study was to develop simple and effective reinforcement schemes which can be used even if the joist is already in place.

Reinforcements: A 38.1 mm (1-1/2 inches) deep bridging channel was selected as reinforcement. Such bridging channels are easily available in the steel construction. They are light weight and easy to handle.

Thickness of the Reinforcement: The initial idea was to use same bridging channel as reinforcement for all sizes of joists. Therefore, a bridging channel with thickness 1.37 mm (54 Mils), which is easily available, was selected for reinforcement. However, experiments showed that the total thickness of the reinforcements should be not less than the thickness of the main joists (see Table 2.12). Therefore, bridging channels with matching thickness with joist were selected for all subsequent reinforcements.

Length and Position of the Reinforcement: Two bridging channels were placed above and below (compression and tension region) the openings. Such arrangement would enhance the flexural strength of the joists at the opening region. It was also found, from the previous studies (Ng et al., 2005; Sivakumaran et al., 2006), that the reinforcement should be placed close to the openings to prevent the local buckling triggered by the unstiffened element adjacent to the opening edge. The length of the reinforcement was chosen to support the whole length of the opening. The reinforcement was also extended by half of the depth of the openings on either side of the openings to support the high stress regions. An edge distance of 10 mm was maintained beyond the end screws. Thus, the length of the reinforcement has the width of the openings plus one half of the depth of the openings on either side plus a minimum edge distance for screws (10 mm).

Screw Spacings: When compression elements are joined to other sections by connections, the connectors must be spaced close enough to provide structural integrity to the built-up section. According to (Yu, 2000), in the design of connections in compression elements, consideration should be given to:

- The required shear strength,
- buckling of compression elements between connections, and,

- possible buckling of unstiffened elements between the center of the connection lines and the free edge.

Section D1.3 of the AISI Standard (AISI, 2007) suggests the spacing, s , in the line of stress, of welds, rivets, or bolts connecting a cover plate, sheet, or a non-integral stiffener in compression to another element shall not exceed:

- That which is required to transmit the shear between the connected parts on the basis of the design strength (factored resistance) per connection specified; nor
- $1.16t\sqrt{E/f}$, where t is the thickness of the cover plate or sheet, and f is the stress at nominal load (specified load) in the cover plate or sheet; nor
- Three times the flat width, w , of the narrowest unstiffened compression element tributary to the connection, but need not be less than $1.11t\sqrt{E/F_y}$ if $h/t < 0.50\sqrt{E/F_y}$, or $1.33t\sqrt{E/F_y}$ if $h/t \geq 0.50\sqrt{E/F_y}$, unless closer spacing is required above two criteria.

The theoretical values for the screw spacing based on above criteria were 32.90 mm and 69.24 mm for 203.2 mm deep ($t = 1.11$ mm, $w = 196.54$ mm, $E = 203$ GPa, $f = F_y = 311$ MPa) and 304.8 mm deep ($t = 2.45$ mm, $w = 290.1$ mm, $E = 203$ GPa, $f = F_y = 342$ MPa) sections, respectively. Initially, the screw spacing was selected as $d_h/4$ as per the previous studies (Ng et al., 2005; Sivakumaran et al., 2006), where d_h is depth of the openings. Therefore, the screw spacings were selected as 31.75 mm (1.25 inches) and 57.15 mm (2.25 inches) for 203.2 mm deep (opening size, $d_h = 127$ mm) and 304.8 mm deep (opening size, $d_h = 228.6$ mm) sections, respectively. These spacings were within the limits specified in the AISI Standard (AISI, 2007). However, the experimental results shown in Table 2.12 indicates that the screw spacing for 304.8

mm deep section was not sufficient to prevent the compression element from failing by local buckling. It was observed that the failure was triggered by local buckling of the compression element between the screws.

The remaining portions of the web above the openings can be treated as unstiffened compression elements. Such elements can be considered as plates with one edge fixed (connected to the flange) and the other edge free (free edge along the openings). The failure mode of such plates can be described by the simple plate buckling theory, as shown in Figure 2.21. This figure shows that a long plate would buckle making a wavelength of two times the unsupported plate width. Therefore, to prevent the plate from buckling, it was necessary to reinforce the plate with another plate providing screw spacing not greater than half of the wavelength (that is equal to the width of the plate). Considering the above facts, the screw spacing was decided to be not greater than the flat width of the compression elements.

2.7.3 Reinforcement Schemes

Three different types of reinforcement schemes were considered during this investigation.

Reinforcement Scheme - A (AISI, 2007a): The web opening was reinforced with a steel plate having the same size and shape as the primary opening. The thickness of the steel plate was equal to the thickness of the section being considered and extended 25.4 mm (1 inch) beyond all edges of the hole. The steel plate was fastened to the web of the section with No. 8 screws spaced 25.4 mm (1 inch) center-to-center along the edges of the patch with an edge distance of 12.7 mm (1/2 inch). A sketch of reinforcement Scheme-A is shown in Figure 2.22.

Reinforcement Scheme - B (AISI, 2007a): The web opening was reinforced with CFS stud sections having the same size and shape as the primary openings. The thickness of the reinforcement was equal to the thickness of the section being considered and extended 25.4 mm (1 inch) beyond all edges of the hole. The stud reinforcement was fastened to the web of the section with No. 8 screws spaced 25.4 mm (1 inch) center-to-center along the edges of the patch with edge distance of 12.7 mm (1/2 inch). Figure 2.22 also shows the detail of reinforcement Scheme-B.

Reinforcement Scheme - C (Present Study): The reinforcement Scheme-C involved screw fastening of bridging channels (depth 38.1 mm, and a bridging channel with matching thickness of the joist or two bridging channels inside and outside of the openings in such a way that the total thickness of the reinforcements would be not less than the thickness of the joists). In this reinforcement scheme, it was decided to use bridging channels of length determined by the width of the openings plus one half of the depth of the openings on either side plus a minimum edge distance for screws (10 mm). The reinforcement Scheme-C for the flexural zone consisted of two sets of bridging channels, one along the top edge of the openings, and the other along the bottom edge of the openings. The screws were fastened at a spacing of 31.75 mm (1.25 inch) close to the opening edges within the opening region, starting from the central screw. Figure 2.23 depicts the detail associated with reinforcement Scheme-C.

2.7.4 Joists having h/t ratio = 180 (203.2 mm deep)

Single tests were carried out for each of Scheme-A and B reinforcements for circular web openings. The detailed test results including the load-displacement relations and the photographs of the failures are given in Appendix B. However, the Tables 2.7 and 2.9 summarize the moment capacity of the cold-formed steel sections ($h/t = 180$)

with reinforced web openings. Eight tests were carried out using the AISI, (AISI, 2007a) reinforcement (hole patching) requirements. Plate reinforcements (Scheme-A) and the stud reinforcements (Scheme-B) were considered for both circular and square openings. However, since the square openings present a worse case situation, only single tests were conducted for the cases of plate and stud reinforcements on circular openings. As shown in Tables 2.7 and 2.9, three identical tests were considered for all other cases. Detail results are given in Appendix B. All the specimens containing reinforcement Scheme-A failed at locations other than the opening locations. Furthermore, the reinforced sections carried about 5 percent higher moments at the reinforced opening locations. This indicates that the reinforcement Scheme-A is capable of restoring the flexural strengths of 203.2 mm (8 inch) deep joist sections ($h/t = 180$) with web opening. Based on the test results associated with Scheme-A, similar observations can be made on the reinforcement Scheme-B.

Tables 2.7 and 2.9 give the moment capacity of Scheme-C reinforced sections having circular and square openings. Once again, the specimens with reinforcement Scheme-C failed at locations outside the openings and reinforced zone. The failure mode can be described as local buckling of the flange and the web. The reinforcement Scheme-C in a circular opening produced peak moments 5 percent higher than the moments observed in the solid joist sections. Similarly, reinforcement Scheme-C in a square opening resisted moments of 3 percent more than the peak moments observed in solid joist sections. Thus, it can be stated that the reinforcement Scheme-C is also capable of restoring the original flexural resistance of a cold-formed steel joist section.

Moreover, three sets of tests were carried out with compression reinforcements only. Bridging channels were placed on the top of the openings (compression), but no reinforcements were there on the bottom of the openings. The tests showed that

no tension reinforcements are required for joists having circular web openings. Test results are shown in Table 2.11.

2.7.5 Joists having h/t ratio = 118 (304.8 mm deep)

Only single tests were carried out for each of Scheme-A and B reinforcements for circular and square web openings. The detailed test results including the load displacement relations and the photographs of the failures are given in Appendix D. Tables 2.8 and 2.10 summarize the moment capacities of the cold-formed steel sections ($h/t = 118$) with reinforced web openings.

Four tests were carried out following the AISI Standard (AISI, 2007a) reinforcement (hole patching) requirements. Plate reinforcement (Scheme-A) and the stud reinforcements (Scheme-B) were considered for both circular and square openings. Neither A nor the B scheme seemed to work for circular and square openings. Therefore, these tests were not repeated. As shown in Tables 2.8 and 2.10, three identical tests were considered for reinforcement Scheme C. Detail results are given in Appendix C. All specimens containing reinforcement Scheme A and B failed at the opening locations. Typical failure patterns for the reinforcement Scheme-A, B and C are shown in Figures 2.24, 2.25 and 2.26, respectively. These figures indicates that the reinforcement Schemes-A and B are ineffective in restoring the flexural strength of joist sections ($h/t = 118$) with openings.

A series of trial tests were carried out to establish the reinforcement Scheme-C. Results of all trial tests are summarized in Table 2.12. The trial tests began with a 1.37 mm (54 mils) thick bridging channel as reinforcement and course screw spacing (spacing equal to $d_h/4$). The test results show that the spacing of the screws must be close enough to prevent local buckling between the screws. Such local buckling can

be prevented by providing a screw spacing less than the half of minimum wavelength of the buckling. In plate type structures, the width of the plate gives the half of minimum wavelength of buckling. Therefore, the screw spacings should not be higher than the flat width of the remaining web width above/below the openings (flat width = 1-1/4" for this study).

The second trial test consisted of 1.37 mm (54 mils) bridging channel reinforcements on square openings with 31.75 mm (1-1/4 inch) screw spacing. The failure was again at the opening region. The compression element acted as a short column and buckled out of the web plane. This behavior indicated that the reinforcement does not have enough bending stiffness to carry the compression load above the openings. The third trial test was carried out on the specimen having circular openings and 1.37 mm (54 mils) bridging channel reinforcements with 31.75 mm (1-1/4 inch) screw spacing. The failure was again within the opening region because of inadequate bending stiffness of the reinforcements. Finally, it was decided to use the bridging channel having matching thickness with the joists. Tables 2.8 and 2.10 give the moment capacities of Scheme-C reinforced sections having circular and square openings. The specimens with reinforcement Scheme-C failed at locations outside the opening and reinforced zone. Thus, the reinforcement Scheme-C was capable of restoring the original flexural resistance of a cold-formed steel joist. A typical comparison of load displacement curves for solid joist, joist with square web openings and joist with reinforced (Scheme-C) square web openings is presented in Figure 2.27.

An alternative reinforcement scheme (Scheme-C') was also tested. The basic idea of this alternative reinforcement was to use readily available bridging channels. The bridging channels having matching thickness with the joists may not always be available in construction site. The most available bridging channels are 1.09 mm (43 mils) and 1.37 mm (54 mils). Reinforcement Scheme-C' consisted of two bridging channel

screwed together on inner and outer faces of the joists. The total thickness of the bridging channel reinforcements should not be less than the thickness of the joists. Therefore, 2.44 mm (97 mils) thick joists can also be reinforced using two 1.37 mm (54 mils) bridging channels placed together on the inner and outer faces of the joist. The test results of reinforcement Scheme-C' are shown in Table 2.11. Reinforcement Scheme-C' was tested for the circular openings only. The reinforcements were placed only on the compression zone. The failure was outside of the opening regions.

2.8 Lateral Displacements, Strains and Initiation of Local Buckling

Two LVDTs were placed to measure lateral displacements of the compression and tension elements above and below the openings. The locations of the lateral displacement measurements (A and B) are shown in Figure 2.17. Point A refers to the compression zone and point B refers to the tension zone. No significant lateral displacements were observed before local buckling initiated around the openings. A sudden lateral displacement on the compression zone, A, was observed after a certain load level. Such sudden lateral displacement was due to the local buckling at the edge of the compression element. Figure 2.28 shows the plots for support reaction versus lateral displacement of the point A. Since the point B is in tension zone, no significant lateral movement was observed. Therefore Figure 2.28 shows only the plot for the lateral displacement at point A. The initiation of local buckling can be clearly seen in the Figure 2.28.

Longitudinal strains were measured at four different locations. Strains were measured using electric resistance strain gauge having 3 percent strain measurement capacity. The location of the strain gauges is shown in Figure 2.17 . Figure 2.29 shows the strains from all four strain gauges that were placed across the section. The figure clearly depicts that the top two strain gauges (1 and 2) read compression strains and the bottom two strain gauges (3 and 4) read tension strains. The compression and tension strain readings increases symmetrically until local buckling begins. Strain gauge 2 (experiencing compression strain) was placed at the outer face of the web above the opening (compression element). Once the compression element started buckling outwards, the outer face of the compression element was experiencing tensile stress resulting in reduction of the overall compression strain as recorded by strain gauge 2. Figure 2.29 clearly shows the beginning of local buckling. The load at which local buckling took place, as observed from strain measurements (Figure 2.29), was same as the load at which local buckling was observed from the lateral displacement measurements (Figure 2.28).

2.9 Conclusions

The flexural strength of solid cold-formed steel joists calculated according to current AISI Standard (AISI, 2007) was 8 percent lower than the strength obtained through the testing. Failure of the solid section was triggered by local buckling of the compression flange and accompanied by distortional buckling. The reduction in flexural strength of CFS joists due to web openings (up to 75 percent of web height) was less than 25 percent. The square openings were more severe than the circular openings. The failure of 203.2 mm (8 inch) deep section with circular and square openings was

initiated by local buckling of the web at the opening region and mixed with distortional and local buckling of flanges. Similar failure mode was observed for the 304.8 mm (12 inch) deep sections with circular openings. However, local column buckling of the compression element was the governing failure mode for the 304.8 mm (12 inch) sections having square web openings. The reinforcement schemes (Scheme-A and B) recommended by current AISI Standard (AISI, 2007a) is ineffective for sections having low h/t ratios. Reinforcement Scheme-C, proposed in this study, can restore the flexural resistance of steel joist sections having web openings. The total thickness of the reinforcement should not be less than the thickness of the joists. No tension reinforcement was necessary for joists having circular web openings. The screw spacing for the connection specified by the AISI Standard (AISI, 2007) were not adequate to fasten the reinforcements to the main joists. The test results showed that the screw spacing should not be greater than the width of the connected compression elements to prevent local buckling of the element between screws.

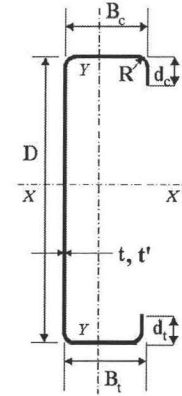
Table 2.1: h/t ratio for common CFS lipped channel sections

Thickness, t (mm)	Web Height, h, (mm)				
	152.4 (6 inch)	203.2 (8 inch)	254 (10 inch)	304.8 (12 inch)	355.6 (14 inch)
1.092 (43 mils)	134	180#	-	-	-
1.372 (54 mils)	105	142	179	-	-
1.727 (68 mils)	82	112	141	170	200
2.464 (97 mils)	56	76	97	118#	138

#Selected h/t ratios for this experimental program

Table 2.2: Section properties and the mechanical properties of the CFS joists (See Appendix A)

Section Designation	800S162-43		1200S162-97	
	Specified	Measured	Specified	Measured
Web Height - $D(mm)$	203.20	201.45	304.80	303.94
Flange Width - $B(mm)$	41.15	40.65	41.15	40.98
Lip Depth - $d_c(mm)$	12.70	11.76	12.70	12.06
Base Metal Thickness - $t(mm)$	1.09	1.12	2.46	2.46
Effective Cross Sectional Area - $A_e(mm^2)$	177	176	558	551
Effective Moment of Inertia - $I_{xxe} * 10^6(mm^4)$	1.71	1.68	10.36	10.16
Effective Moment of Inertia - $I_{yye} * 10^6(mm^4)$	0.07	0.07	0.12	0.12
Proportional Limit - $F_p(MPa)$	-	288	-	340
Yield Strength - $F_y(MPa)$	345	311	345	343
Ultimate Strength - $F_u(MPa)$	450	401	450	469
F_u/F_y	-	1.29	-	1.37
Strain at Rupture - ϵ_u	-	21%	-	33%



Note: Measured values are average values.

1 inch = 25.4 mm, 50ksi = 345 MPa

Table 2.3: Measured geometrical dimensions of the CFS steel sections - 800S162-43 (203.2 mm deep, $h/t = 180$)

S.N.	Specimen	D	B_c	B_t	d_c	d_t	t'	t
1	8F-N-1-L	201.30	41.14	40.54	10.75	12.92	1.17	1.12
2	8F-N-1-R	201.22	40.54	40.50	12.80	10.88	1.14	1.12
3	8F-N-2-L	201.08	40.54	40.72	12.90	10.66	1.16	1.12
4	8F-N-2-R	201.10	40.93	40.63	10.87	12.87	1.14	1.10
5	8F-N-3-L	201.62	41.11	40.55	10.89	12.84	1.16	1.12
6	8F-N-3-R	200.94	40.67	40.48	12.89	10.62	1.14	1.10
7	8F-C-1-L	201.20	40.97	40.29	10.88	12.79	1.13	1.09
8	8F-C-1-R	201.96	40.53	40.46	12.88	10.90	1.14	1.10
9	8F-C-2-L	201.16	40.53	40.35	12.90	10.87	1.14	1.10
10	8F-C-2-R	201.18	40.65	40.53	12.86	10.78	1.17	1.13
11	8F-C-3-L	201.32	40.69	40.55	12.82	10.85	1.17	1.12
12	8F-C-3-R	200.90	41.89	40.63	10.52	12.96	1.16	1.12
13	8F-S-1-L	201.22	40.51	40.26	12.78	10.91	1.19	1.08
14	8F-S-1-R	201.16	40.63	40.23	12.81	10.67	1.13	1.09
15	8F-S-2-L	201.26	40.55	40.19	13.11	10.76	1.17	1.12
16	8F-S-2-R	201.38	41.14	40.50	10.90	12.80	1.16	1.12
17	8F-S-3-L	201.06	41.17	40.39	10.54	12.87	1.14	1.13
18	8F-S-3-R	202.04	40.71	40.58	12.90	10.86	1.14	1.10
19	8F-CRA-1-L	200.86	40.73	40.34	12.92	10.80	1.14	1.10
20	8F-CRA-1-R	201.90	41.20	40.65	10.91	12.86	1.17	1.13
21	8F-CRB-1-L	201.00	41.23	40.24	10.77	12.85	1.14	1.12
22	8F-CRB-1-R	202.10	40.67	40.50	12.86	10.83	1.16	1.12
23	8F-CRC-1-L	202.00	41.25	40.62	10.99	12.88	1.13	1.09
24	8F-CRC-1-R	201.42	40.61	40.30	12.92	10.84	1.17	1.12
25	8F-CRC-2-L	201.28	41.10	40.73	10.55	12.82	1.16	1.12
26	8F-CRC-2-R	201.34	40.63	40.41	12.90	10.74	1.17	1.12
27	8F-CRC-3-L	201.38	40.74	40.32	12.83	10.91	1.17	1.12
28	8F-CRC-3-R	201.56	40.80	40.40	13.02	10.73	1.14	1.12
29	8F-CRC'-1-L	201.22	40.76	40.65	12.57	10.45	1.15	1.11

Continued on Next Page...

Table 2.3 – Continued

S.N.	Specimen	D	B_c	B_t	d_c	d_t	t'	t
30	8F-CRC ¹ -1-R	201.49	40.56	40.20	12.32	10.34	1.14	1.12
31	8F-CRC ¹ -2-L	201.55	40.82	40.33	10.91	12.54	1.16	1.12
32	8F-CRC ¹ -2-R	202.21	40.65	40.04	10.22	12.34	1.14	1.11
33	8F-CRC ¹ -3-L	201.90	40.92	40.85	10.75	12.87	1.13	1.10
34	8F-CRC ¹ -3-R	201.51	41.05	40.91	12.52	10.56	1.15	1.12
35	8F-SRA-1-L	202.06	40.58	40.55	12.93	10.66	1.16	1.12
36	8F-SRA-1-R	201.32	41.10	40.60	10.83	12.79	1.16	1.10
37	8F-SRA-2-L	201.65	41.06	40.37	12.28	10.58	1.16	1.11
38	8F-SRA-2-R	201.49	40.86	40.32	10.14	12.22	1.14	1.11
39	8F-SRA-3-L	201.64	40.68	40.33	12.91	10.90	1.14	1.11
40	8F-SRA-3-R	201.70	40.85	40.46	12.62	10.64	1.15	1.12
41	8F-SRB-1-L	201.40	41.16	40.30	10.86	12.83	1.12	1.09
42	8F-SRB-1-R	201.00	41.06	40.28	10.81	12.80	1.14	1.10
43	8F-SRB-2-L	201.47	41.10	40.33	10.29	12.69	1.15	1.11
44	8F-SRB-2-R	201.24	40.72	40.49	10.99	12.47	1.15	1.11
45	8F-SRB-3-L	201.25	40.66	40.37	12.81	10.60	1.14	1.11
46	8F-SRB-3-R	201.85	41.05	40.37	12.19	10.85	1.15	1.11
47	8F-SRC-1-L	202.06	40.60	40.30	12.83	10.67	1.17	1.12
48	8F-SRC-1-R	201.12	40.56	40.23	12.88	10.75	1.16	1.12
49	8F-SRC-2-L	201.54	41.16	40.45	10.84	12.93	1.14	1.13
50	8F-SRC-2-R	200.94	40.57	40.64	12.84	10.90	1.14	1.12
51	8F-SRC-3-L	202.24	40.63	40.60	12.88	10.88	1.14	1.12
52	8F-SRC-3-R	201.46	41.09	40.20	10.83	12.85	1.13	1.10
Average		201.45	40.85	40.44	11.92	11.60	1.15	1.11
Standard Deviation		0.37	0.28	0.18	1.05	1.02	0.01	0.01

Note: See Figure 2.8 for the symbols.

t' - Overall thickness.

t - Base metal thickness.

All dimensions are in mm

Table 2.4: Measured geometrical dimensions of the CFS steel sections - 1200S162-97 (308.8 mm deep, $h/t = 118$)

S.N.	Specimen	D	B_c	B_t	d_c	d_t	t'	t
1	12F-N-1-L	303.90	40.61	41.26	11.85	12.15	2.47	2.44
2	12F-N-1-R	303.91	41.03	40.67	11.95	12.37	2.49	2.45
3	12F-N-2-L	304.31	40.71	41.22	11.70	12.06	2.46	2.44
4	12F-N-2-R	304.20	41.16	41.29	11.50	12.02	2.46	2.47
5	12F-N-3-L	304.26	40.76	41.29	12.12	12.09	2.48	2.44
6	12F-N-3-R	304.01	40.76	41.42	12.22	11.73	2.46	2.44
7	12F-C-1-L	303.83	41.00	40.81	11.57	12.42	2.49	2.43
8	12F-C-1-R	303.53	41.06	41.16	11.90	11.77	2.47	2.43
9	12F-C-2-L	303.60	40.89	41.14	12.48	11.89	2.49	2.46
10	12F-C-2-R	303.93	40.55	40.52	12.47	12.04	2.49	2.46
11	12F-C-3-L	303.68	40.79	40.82	12.09	12.07	2.47	2.46
12	12F-C-3-R	303.60	40.53	40.75	12.46	11.82	2.48	2.46
13	12F-S-1-L	304.31	41.40	40.57	11.85	11.83	2.49	2.44
14	12F-S-1-R	304.48	40.52	40.73	11.98	11.55	2.48	2.45
15	12F-S-2-L	303.83	41.43	40.97	12.37	12.17	2.49	2.45
16	12F-S-2-R	303.73	40.90	41.27	11.92	12.08	2.47	2.46
17	12F-S-3-L	303.69	41.43	40.69	11.77	12.41	2.48	2.47
18	12F-S-3-R	303.74	40.54	41.16	11.91	11.91	2.48	2.46
19	12F-CRA-1-L	303.67	40.99	40.97	12.30	11.55	2.50	2.45
20	12F-CRA-1-R	303.96	40.74	40.94	12.12	11.97	2.48	2.46
21	12F-CRB-1-L	304.46	40.59	40.70	11.83	12.48	2.47	2.47
22	12F-CRB-1-R	303.60	41.32	40.87	11.76	12.03	2.46	2.45
23	12F-CRC-1-L	304.04	40.63	40.93	12.38	11.67	2.48	2.47
24	12F-CRC-1-R	303.85	41.22	40.88	12.26	12.32	2.47	2.45
25	12F-CRC-2-L	303.60	40.80	40.71	12.09	12.22	2.46	2.45
26	12F-CRC-2-R	304.11	41.43	41.34	12.04	12.42	2.48	2.44
27	12F-CRC-3-L	304.16	40.54	40.71	11.92	11.69	2.48	2.47
28	12F-CRC-3-R	304.21	41.35	40.89	11.96	12.43	2.50	2.44
29	12F-CRC'-1-L	303.98	41.07	41.25	12.12	12.31	2.47	2.46
30	12F-CRC'-1-R	304.31	40.83	41.05	12.29	12.22	2.47	2.43
31	12F-CRC'-2-L	304.02	41.12	40.68	12.37	11.76	2.46	2.43

Continued on Next Page...

Table 2.4 – Continued

S.N.	Specimen	D	B_c	B_t	d_c	d_t	t'	t
32	12F-CRC'-2-R	303.93	41.16	41.36	12.12	12.36	2.48	2.44
33	12F-CRC'-3-L	303.77	41.09	41.06	11.90	11.52	2.47	2.46
34	12F-CRC'-3-R	303.92	41.04	40.76	12.45	12.44	2.49	2.47
35	12F-CRC-1-L	303.67	41.39	40.85	11.95	12.39	2.50	2.46
36	12F-CRC-1-R	303.70	41.27	41.24	12.08	12.49	2.48	2.45
37	12F-CRC-2-L	303.77	41.10	40.85	11.99	11.79	2.48	2.45
38	12F-CRC-2-R	303.92	40.84	41.10	11.99	11.95	2.46	2.46
39	12F-CRC-3-L	303.99	40.84	41.03	11.54	12.18	2.49	2.45
40	12F-CRC-3-R	303.70	41.16	41.15	11.78	12.31	2.50	2.46
41	12F-SRA-1-L	303.91	41.05	41.35	11.67	12.03	2.47	2.45
42	12F-SRA-1-R	304.14	41.08	41.16	11.86	12.18	2.48	2.46
43	12F-SRB-1-L	303.88	40.97	40.50	11.57	11.73	2.46	2.44
44	12F-SRB-1-R	304.20	40.71	41.29	11.79	12.25	2.48	2.43
45	12F-SRC-1-L	304.12	41.12	40.99	12.19	12.42	2.49	2.44
46	12F-SRC-1-R	304.27	40.96	40.88	12.16	11.78	2.50	2.44
47	12F-SRC-2-L	304.15	40.70	41.03	12.02	12.33	2.48	2.46
48	12F-SRC-2-R	303.51	41.32	41.44	12.46	11.82	2.49	2.45
49	12F-SRC-3-L	303.51	40.56	40.89	12.12	12.35	2.49	2.44
50	12F-SRC-3-R	304.29	40.76	40.75	12.15	12.49	2.49	2.45
Average		303.94	40.96	40.99	12.03	12.09	2.48	2.45
Standard Deviation		0.26	0.28	0.25	0.26	0.28	0.01	0.01

Note: See Figure 2.8 for the symbols.

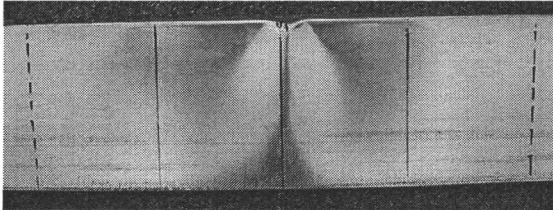
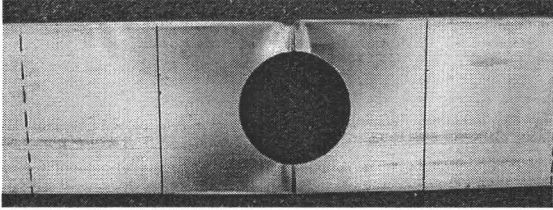
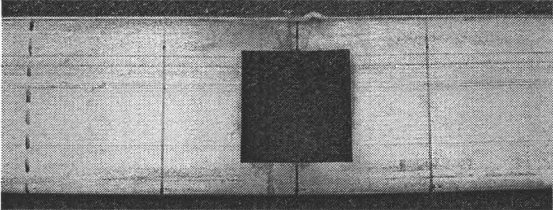
t' - Overall thickness.

t - Base metal thickness.

All dimensions are in mm

Table 2.5: Flexural resistance of CFS joists with and without web opening in high moment regions

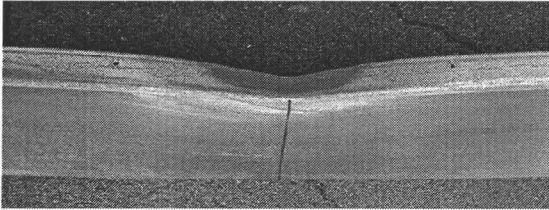
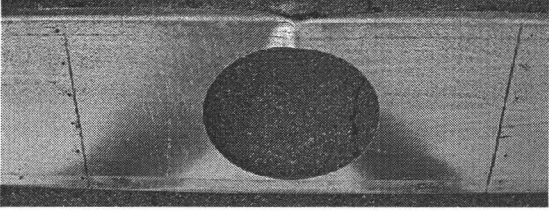
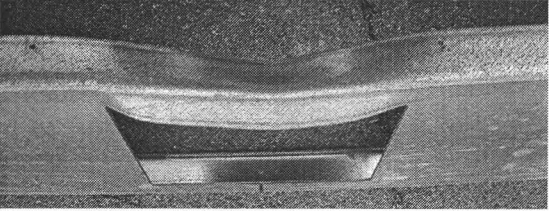
Section: 800S162-43 ; $\frac{h}{t} = 180$; Moment Capacity (AISI, 007a), Solid: $M_n = 4.35$ kN-m; Openings: $M_{no} = 4.06$ kN-m

Test Designation	Moment at the Opening Region (kN-m)	Percentage Reduction in Moment Capacity	Sample Pictures	Remarks
8F-N	Test 1: 4.47 Test 2: 4.37 Test 3: 4.37 Average: 4.40 Std Dev: 0.06	0.00%		Compression flange local buckling at mid span
8F-C	Test 1: 4.22 Test 2: 4.21 Test 3: 3.97 Average: 4.13 Std Dev: 0.14	-6.13%		Compression flange and web local buckling on the opening region at mid span
8F-S	Test 1: 3.68 Test 2: 3.92 Test 3: 3.75 Average: 3.78 Std Dev: 0.25	-14.09%		Compression flange and web local buckling on the opening region at mid span

1kN-m = 8.85 kips-inch

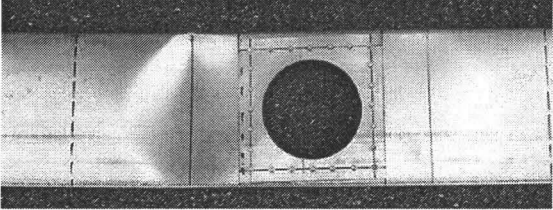
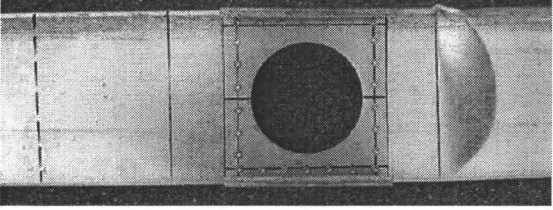
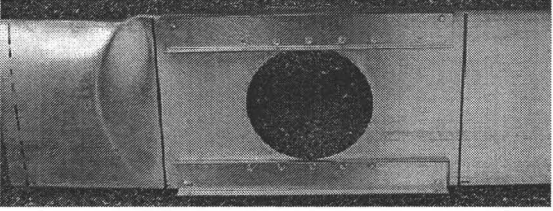
Table 2.6: Flexural resistance of CFS joists with and without web opening in high moment regions

Section: 1200S162-97 ; $\frac{h}{t} = 118$; Moment Capacity (AISI, 007a), Solid: $M_n = 21.41$ kN-m ; Openings: $M_{no} = 17.93$ kN-m

Test Designation	Moment at the Opening Region (kN-m)	Percentage Reduction in Moment Capacity	Sample Pictures	Remarks
12F-N	Test 1: 22.94 Test 2: 23.63 Test 3: 22.97 <i>Average: 23.18</i> <i>Std Dev: 0.39</i>	0.00%		Compression flange local buckling at mid span
12F-C	Test 1: 19.90 Test 2: 19.44 Test 3: 19.80 <i>Average: 19.71</i> <i>Std Dev: 0.14</i>	-14.97%		Compression flange and web local buckling on the opening region at mid span
12F-S	Test 1: 17.29 Test 2: 17.67 Test 3: 18.36 <i>Average: 17.77</i> <i>Std Dev: 0.25</i>	-23.34%		Compression element acted as column buckling

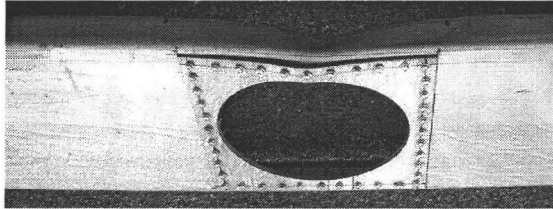
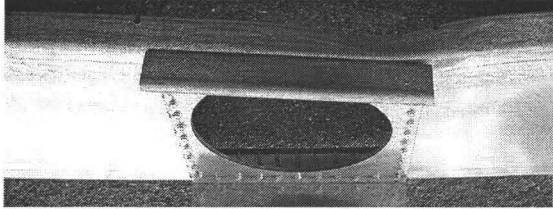
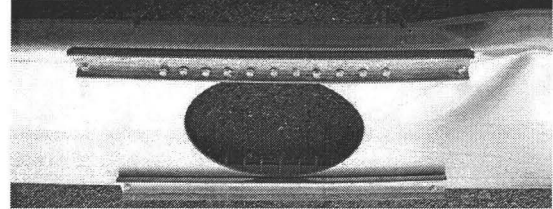
$1\text{kN-m} = 8.85 \text{ kips-inch}$

Table 2.7: Flexural resistance of CFS joists with reinforced circular web opening in high moment regions

Section: 800S162-43		$\frac{h}{t} = 180$		Moment Capacity (AISI, 007a), $M_n = 4.35$ kN-m	
Test Designation	Moment at the Opening Region (kN-m)	Percentage Reduction in Moment Capacity	Re-	Sample Pictures	Remarks
8F-CRA Plate Reinforcement (Scheme-“A”)	Test 1: 4.59 (one test only)	+4.31%			Compression flange and web local buckling out of reinforced region
8F-CRB Stud Reinforcement (Scheme-“B”)	Test 1: 4.58 (one test only)	+4.09%			Compression flange and web local buckling out of reinforced region
8F-CRC Bridging Channel Reinforcement (Scheme-“C”)	Test 1: 4.60 Test 2: 4.59 Test 3: 4.66 Average: 4.62 Std Dev: 0.04	+5.00%			Compression flange and web local buckling out of reinforced region

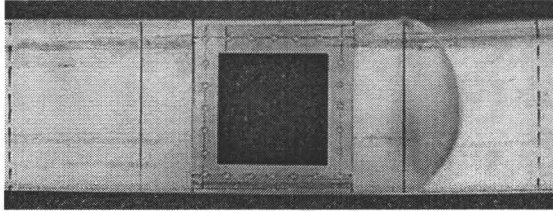
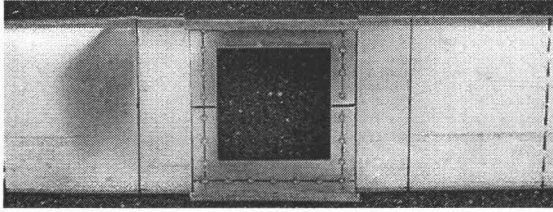
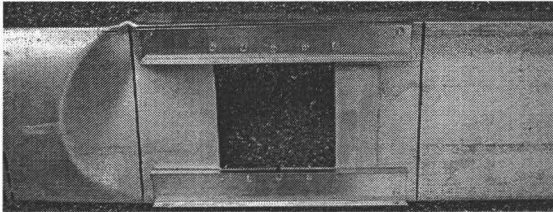
$1\text{kN-m} = 8.85$ kips-inch

Table 2.8: Flexural resistance of CFS joists with reinforced circular web opening in high moment regions

Section: 1200S162-97		$\frac{h}{t} = 118$		Moment Capacity (AISI, 007a), $M_n = 21.41$ kN-m	
Test Designation	Moment at the Opening Region (kN-m)	Percentage Reduction in Moment Capacity	Re-	Sample Pictures	Remarks
12F-CRA Plate Reinforcement (Scheme-“A”)	Test 1: 21.77 (one test only)	-6.08%			Compression flange and web local buckling on the opening region at mid span
12F-CRB Stud Reinforcement (Scheme-“B”)	Test 1: 22.42 (one test only)	-3.28%			Compression flange local and distortional buckling on the opening region at mid span
12F-CRC Bridging Channel Reinforcement (Scheme-“C”)	Test 1: 24.20 Test 2: 24.05 Test 3: 22.89 <i>Average: 23.71</i> <i>Std Dev: 0.04</i>	+2.29%			Compression flange and web local buckling out of reinforced region

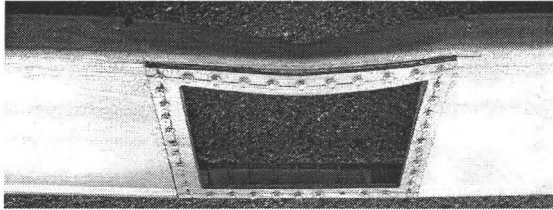
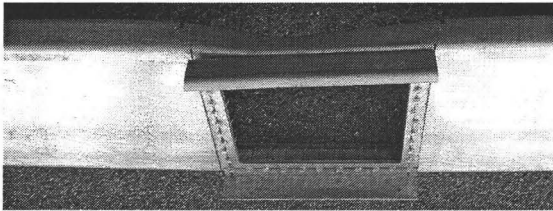
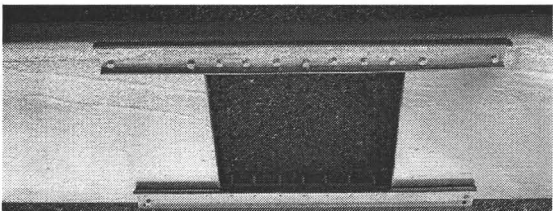
$1\text{kN-m} = 8.85 \text{ kips-inch}$

Table 2.9: Flexural resistance of CFS joists with reinforced square web opening in high moment regions

Section: 800S162-43		$\frac{h}{t} = 180$		Moment Capacity (AISI, 007a), $M_n = 4.35$ kN-m	
Test Designation	Moment at the Opening (kN-m)	at the Region	Percentage Reduction in Moment Capacity	Sample Pictures	Remarks
8F-SRA Plate Reinforcement (Scheme-“A”)	Test 1: 4.59 Test 2: 4.66 Test 3: 4.57 <i>Average: 4.61</i> <i>Std Dev: 0.05</i>	4.59	+4.77%		Compression flange and web local buckling out of reinforced region
8F-SRB Stud Reinforcement (Scheme-“B”)	Test 1: 4.31 Test 2: 4.67 Test 3: 4.63 <i>Average: 4.53</i> <i>Std Dev: 0.20</i>	4.31	+2.95%		Compression flange and web local buckling out of reinforced region
8F-SRC Bridging Channel Reinforcement (Scheme-“C”)	Test 1: 4.69 Test 2: 4.45 Test 3: 4.48 <i>Average: 4.54</i> <i>Std Dev: 0.13</i>	4.69	+3.18%		Compression flange and web local buckling out of reinforced region

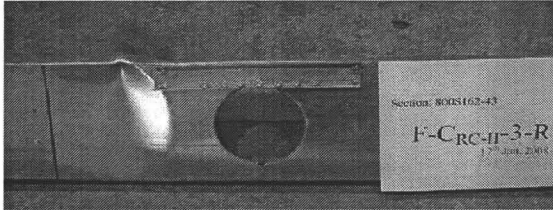
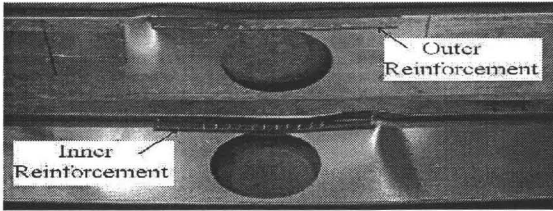
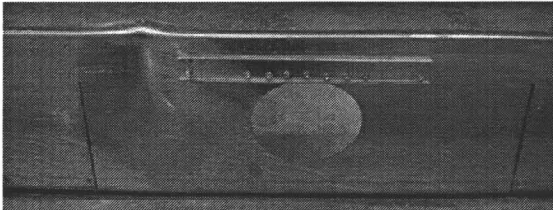
$1\text{kN-m} = 8.85$ kips-inch

Table 2.10: Flexural resistance of CFS joists with reinforced square web opening in high moment regions

Section: 1200S162-97		$\frac{h}{t} = 118$		Moment Capacity (AISI, 007a), $M_n = 21.41$ kN-m	
Test Designation	Moment at the Opening Region (kN-m)	Percentage Reduction in Moment Capacity	Re-	Sample Pictures	Remarks
12F-SRA Plate Reinforcement (Scheme-“A”)	Test 1: 18.39 (one test only)	-20.66%			Compression flange and web local buckling on the opening region at mid span
12F-SRB Stud Reinforcement (Scheme-“B”)	Test 1: 21.07 (one test only)	-9.10%			Compression flange local and distortional buckling on the opening region at mid span
12F-SRC Bridging Channel Reinforcement (Scheme-“C”)	Test 1: 23.39 Test 2: 23.55 Test 3: 24.05 <i>Average: 23.66</i> <i>Std Dev: 0.04</i>	+2.07%			Compression flange and web local buckling out of reinforced region

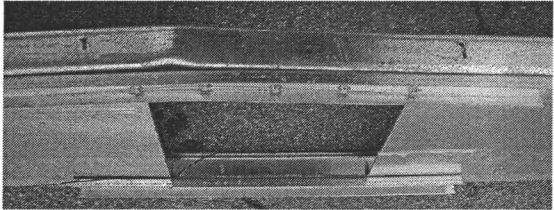
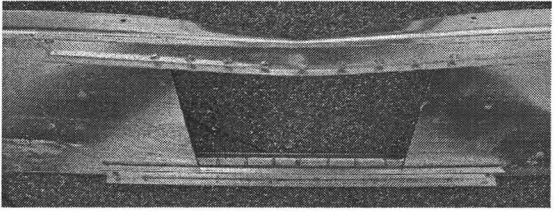
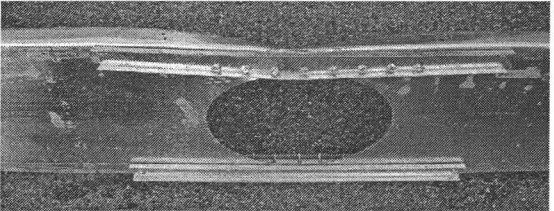
$1\text{kN-m} = 8.85 \text{ kips-inch}$

Table 2.11: Alternative flexural reinforcement schemes for scheme -c

Test Designation	Moment at the Opening Region (kN-m)	Percentage Reduction in Moment Capacity	Sample Pictures	Remarks
8F-CRC' Plate Matching (43 mils) Bridging Channel Reinforcement only on Compression side	Test 1: 4.86 Test 2: 4.51 Test 3: 4.65 <i>Average:</i> 4.67 <i>Std Dev:</i> 0.18	+6.13%		Opening Size 5" (64 % of web). Local buckling out of reinforced region
12F-CRC' Two Bridging Channels (54 mils , inside and outside) Reinforcement only on Compression side)	Test 1: 24.42 Test 2: 24.12 Test 3: 24.28 <i>Average:</i> 24.27 <i>Std Dev:</i> 0.15	+4.70%		Opening Size 9" (75 % of web). Local buckling out of reinforced region
12F-C'RC' One Bridging Channel (43 mils) Reinforcement only on Compression side	Test 1: 24.03 Test 2: 24.06 Test 3: 23.76 <i>Average:</i> 23.95 <i>Std Dev:</i> 0.17	+3.40%		Opening Size 6" (50 % of web). Local buckling out of reinforced region

1kN-m = 8.85 kips-inch

Table 2.12: Trial stages to develop the reinforcement schemes for high moment regions

Section: 1200S162-97		$\frac{h}{t} = 118$	Nominal Moment Capacity (AISI, 007a), $M_n = 21.41 \text{ kN-m}$	
Stages	Reinforcements Detailing	Sample Picture	Observations	
Stage: One	Reinforced by 1-1/2"x1/2"-54 mils bridging channel with "d/4" (2.25 inch) screw spacing above and below the square hole where, d = width of the square hole		<i>Observation:</i> Began with local buckling on compression flange and web between the screws. <i>Solution:</i> Decrease the spacing of the screws.	
Stage: Two	Reinforced by 1-1/2"x1/2"-54 mils bridging channel with "w" (1.25 inch) screw spacing above and below the square hole, where, w = flat width of the web above/below the square hole.		<i>Observation:</i> The compression element above the opening acted as a column. A column buckling action on compression element was observed. <i>Solution:</i> Increase the size of the reinforcement to increase over all flexural stiffness of the compression element.	
Stage: Three	Reinforced by 1-1/2"x1/2"-54 mils bridging channel with "w" (1.25 inch) screw spacing above and below the circular hole, where, w = flat width of the web above/below the circular hole		<i>Observation:</i> The compression element above the opening acted as a column. A column buckling action on compression element was observed. <i>Solution:</i> Increase the size of the reinforcement to increase over all flexural stiffness of the compression element.	

$1\text{kN-m} = 8.85 \text{ kips-inch}$

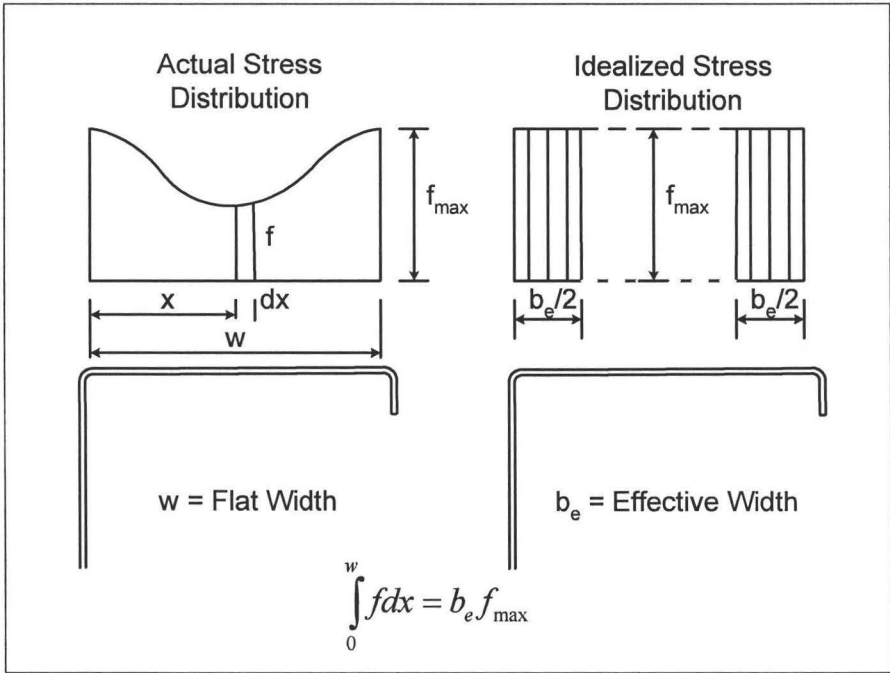


Figure 2.1: Stress distribution and effective width in a stiffened flange

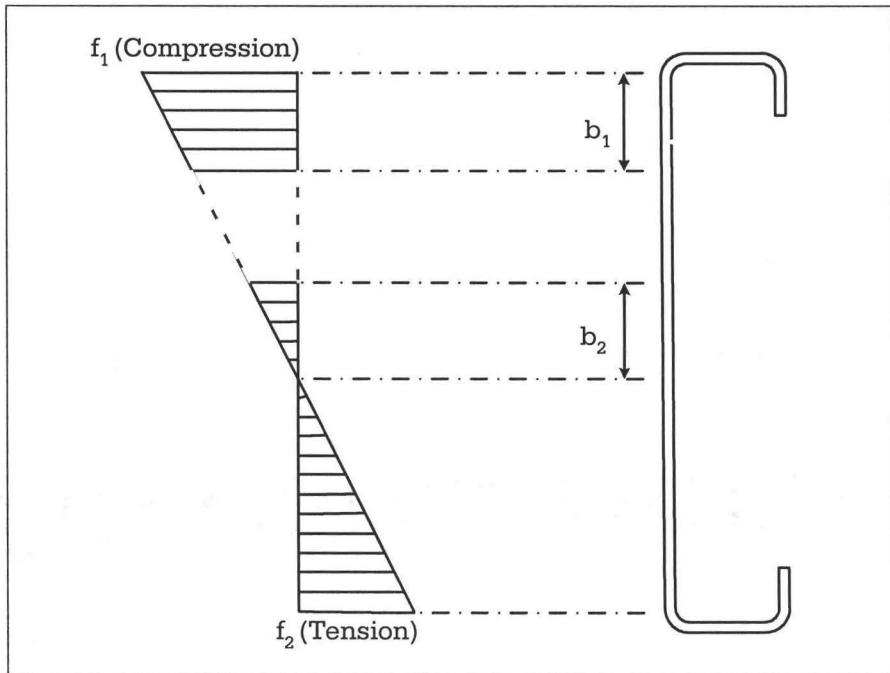


Figure 2.2: Stress distribution and effective width of a web in flexure

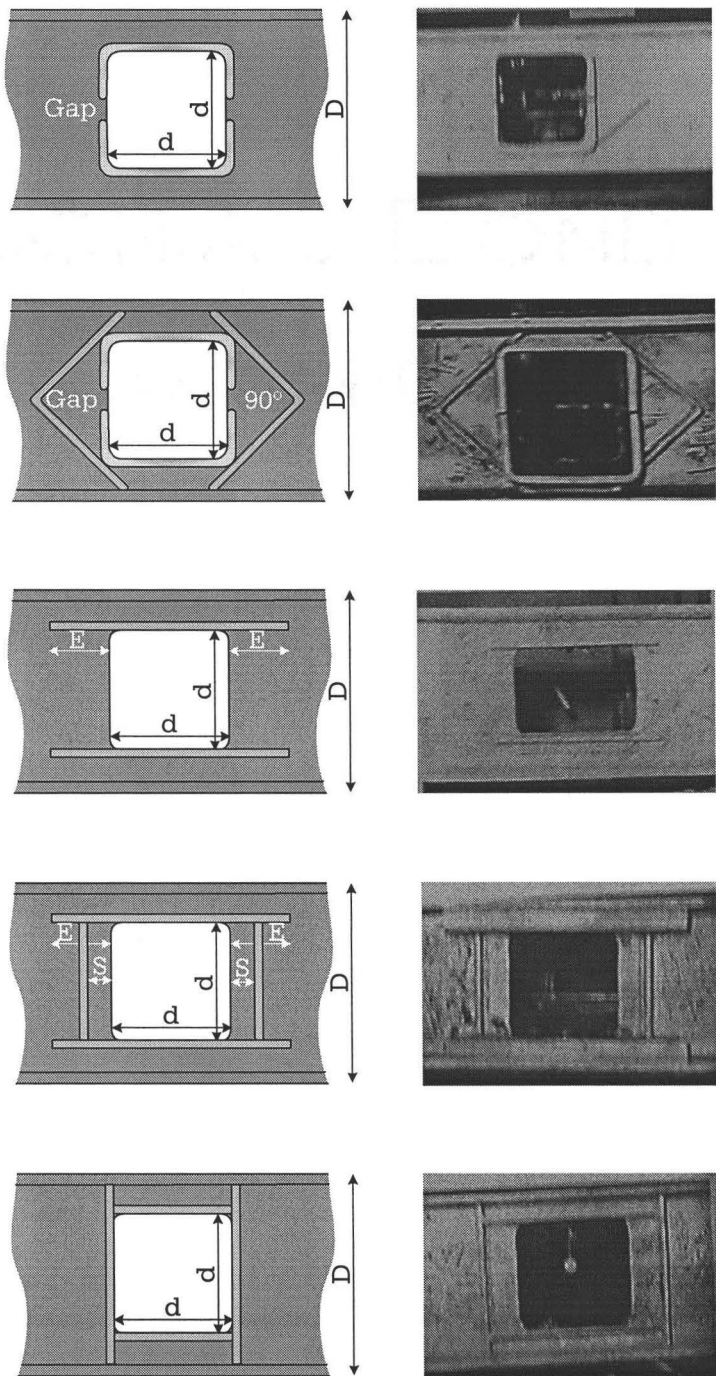


Figure 2.3: Various reinforcement schemes recommended for hot-rolled steel beams (Segner, 1964)

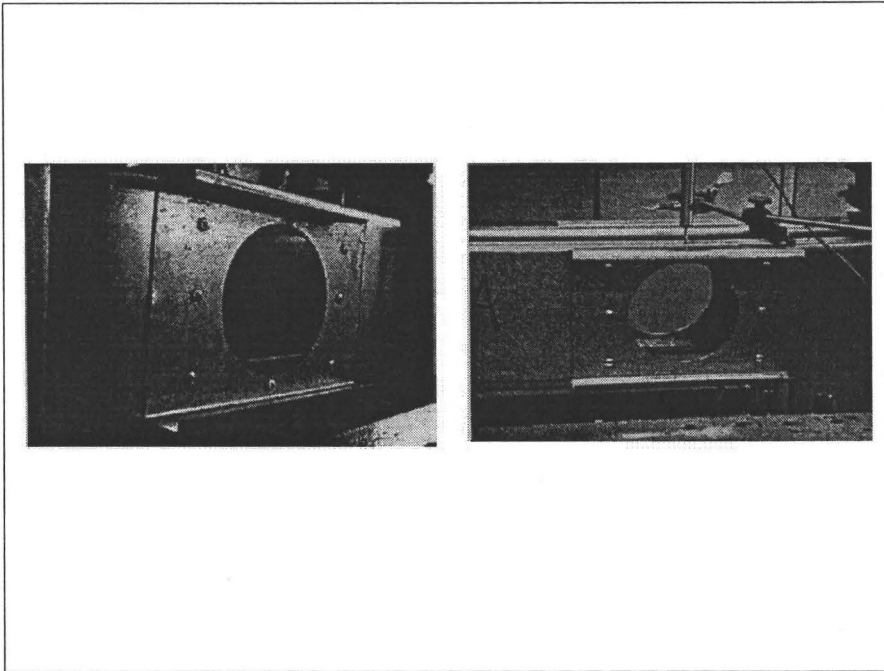


Figure 2.4: Reinforcement schemes for CFS joists considered by Pennock, (2001)

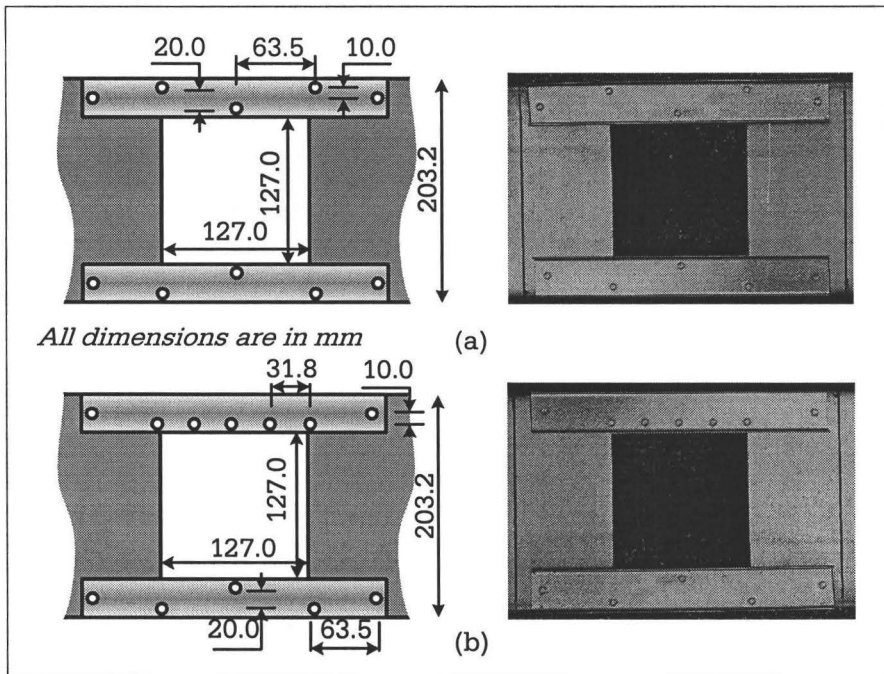


Figure 2.5: Typical reinforcement schemes for CFS joists tested by Ng, (2004) (a) scheme A (b) scheme B

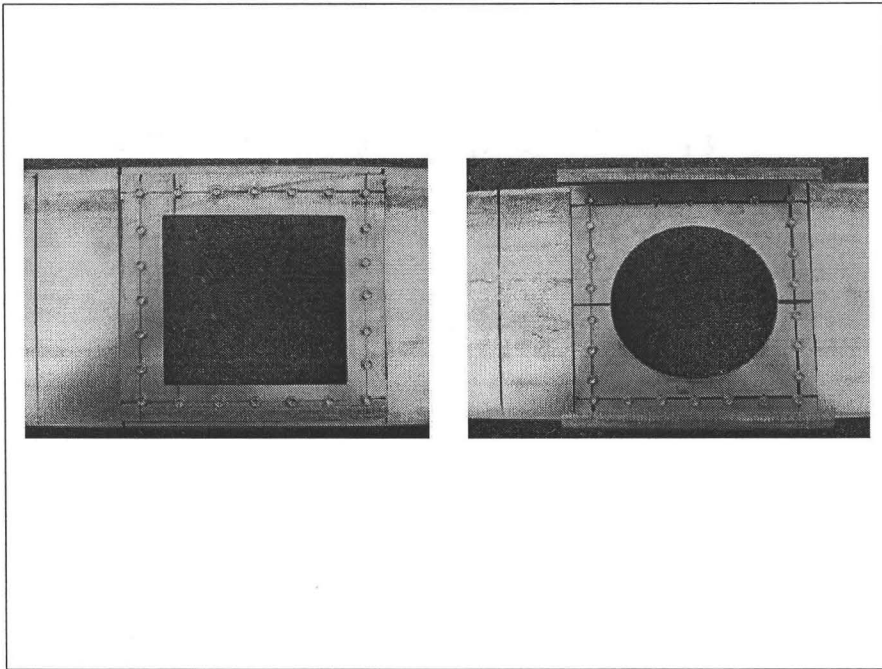


Figure 2.6: Reinforcement schemes for CFS joists suggested by AISI, (2001)

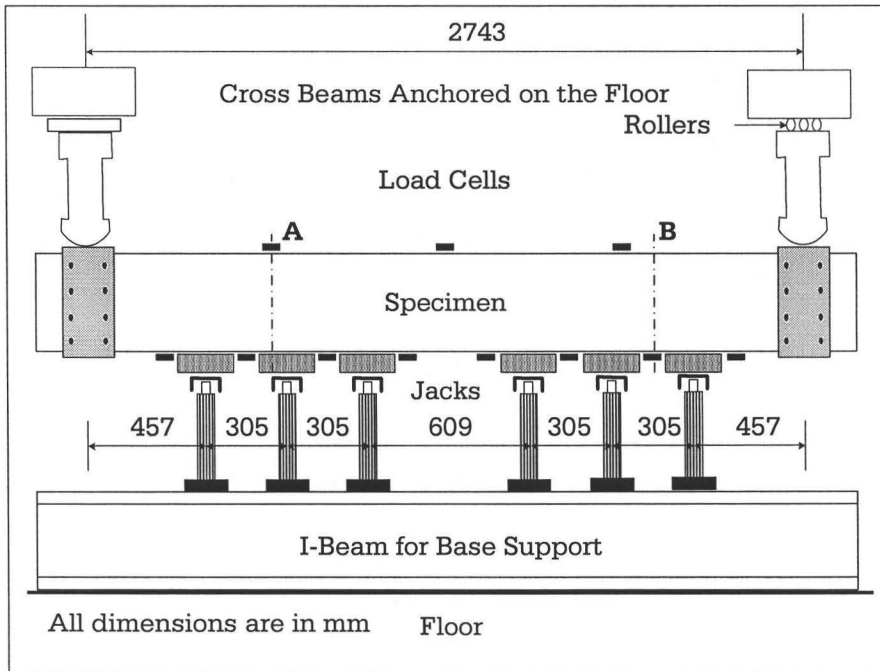


Figure 2.7: Flexural test setup-I

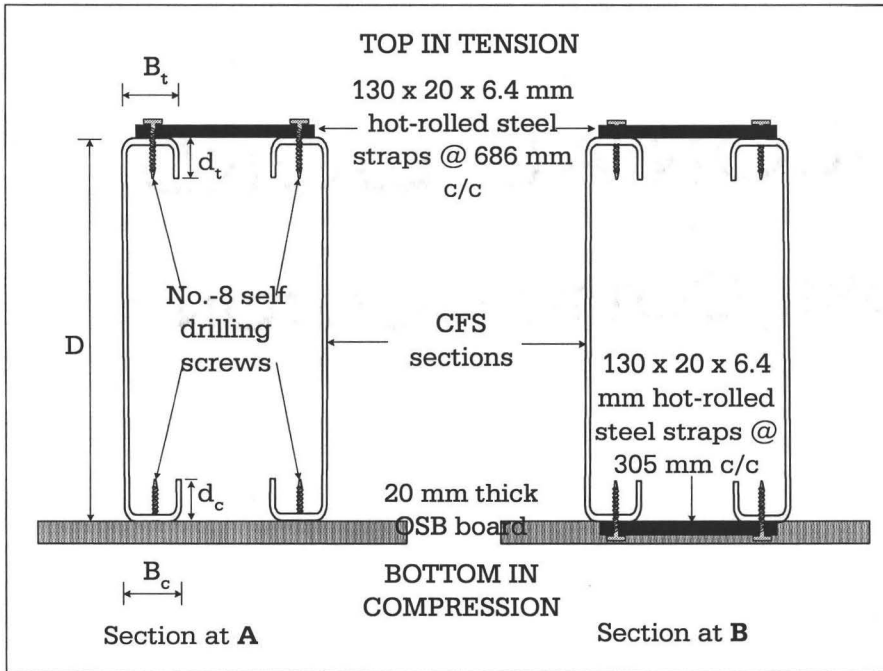


Figure 2.8: Cross sections at A and B

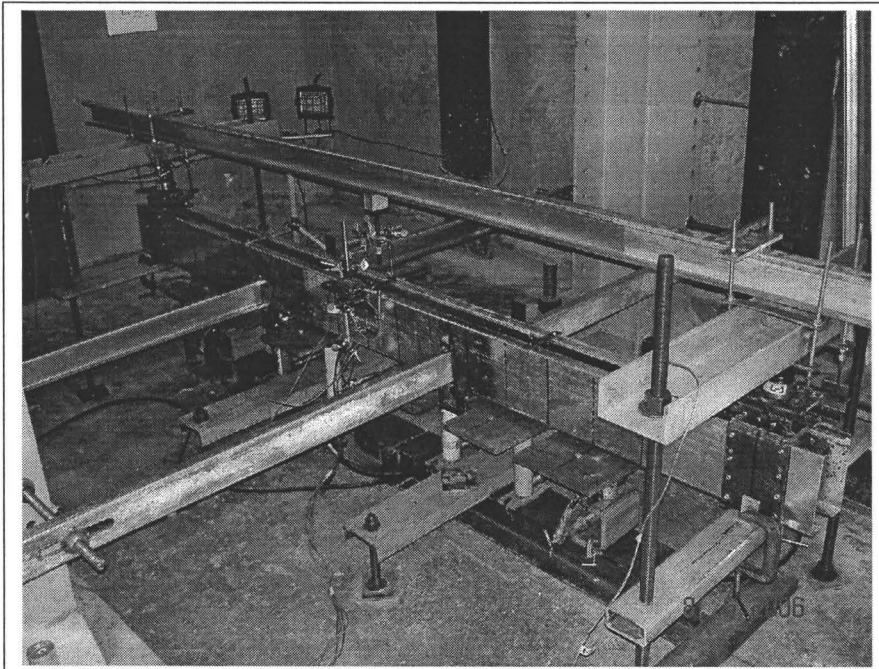


Figure 2.9: Photograph of flexural test setup-I

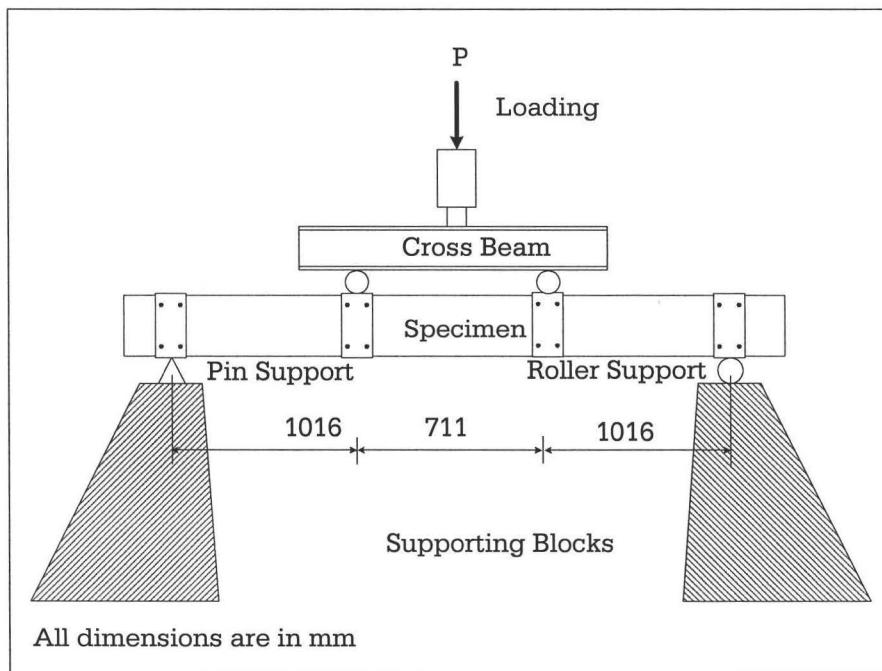


Figure 2.10: Test setup-II for flexural test



Figure 2.11: Test setup-II picture for flexure test

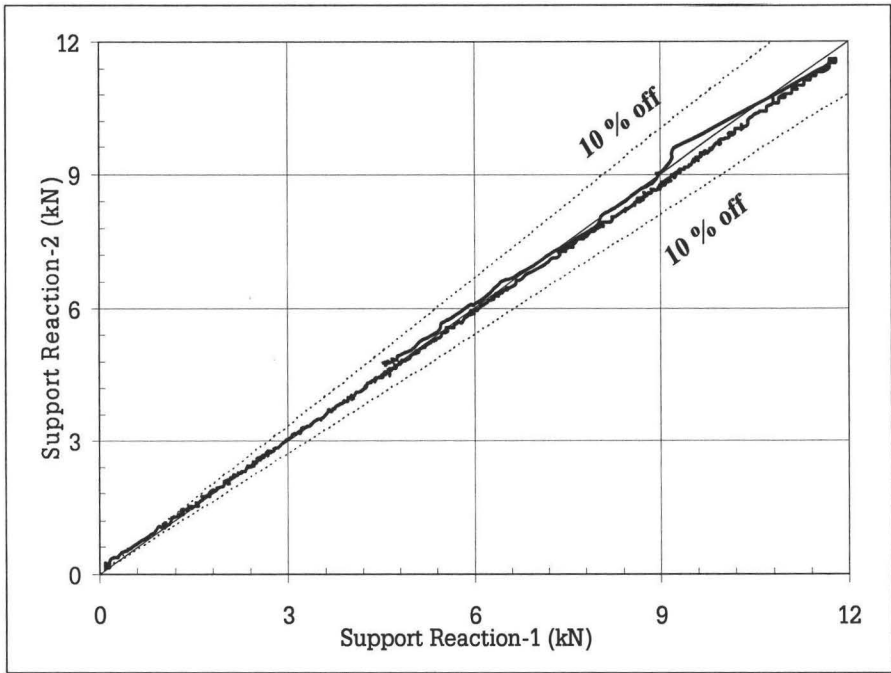


Figure 2.12: Comparative plot for two support reactions

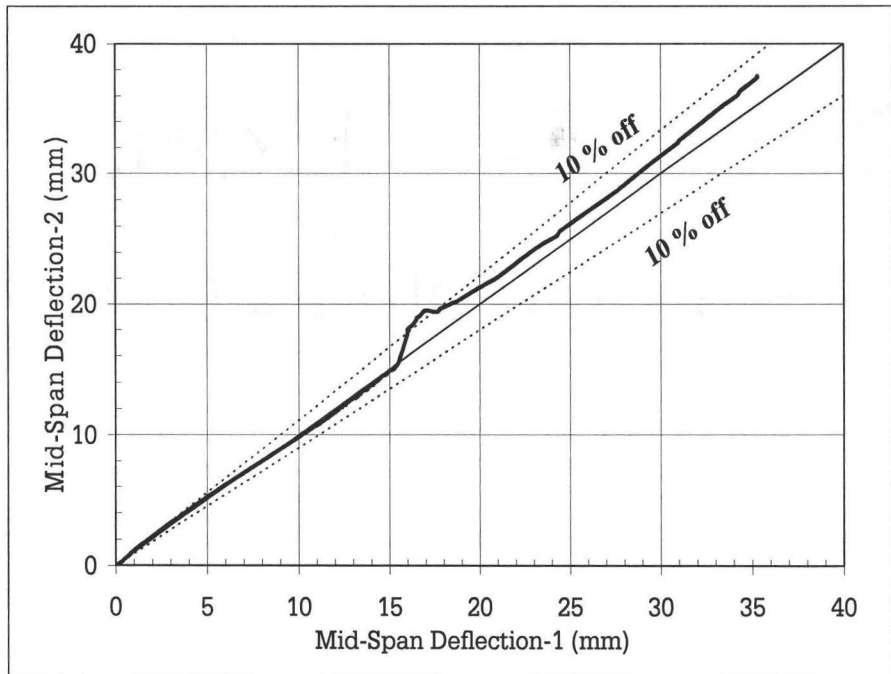


Figure 2.13: Comparative plot for two mid-span deflections

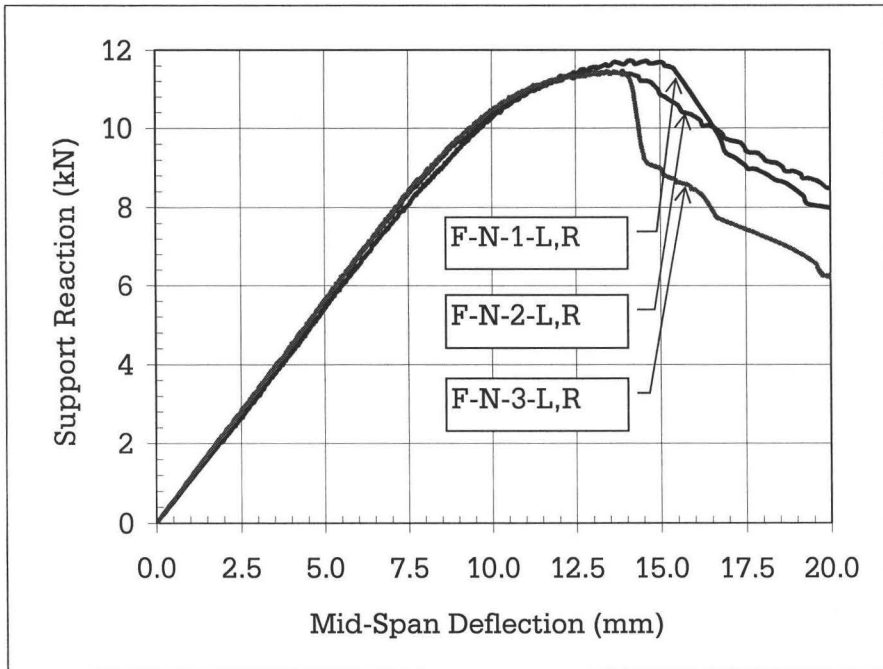


Figure 2.14: Load deflection curve for solid joist ($h/t = 180$)

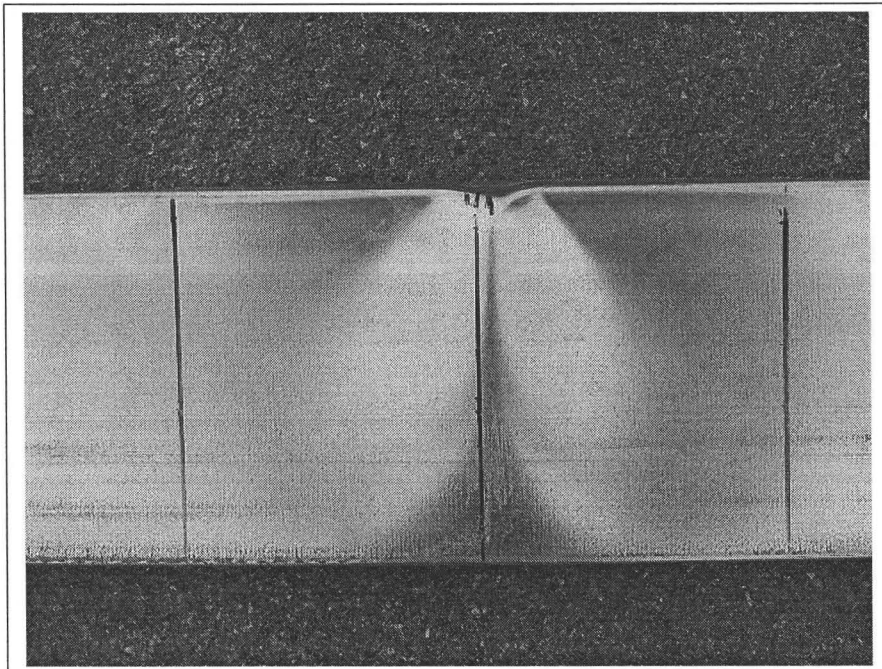


Figure 2.15: Typical flexural failure of solid joist ($h/t = 180$)

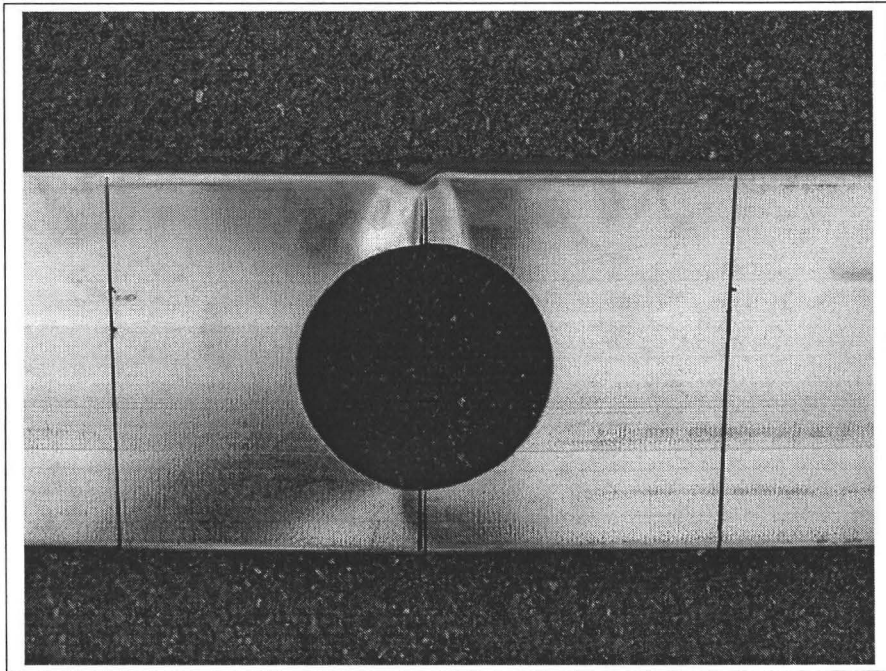


Figure 2.16: Typical flexural failure of joist having circular openings ($h/t = 180$)

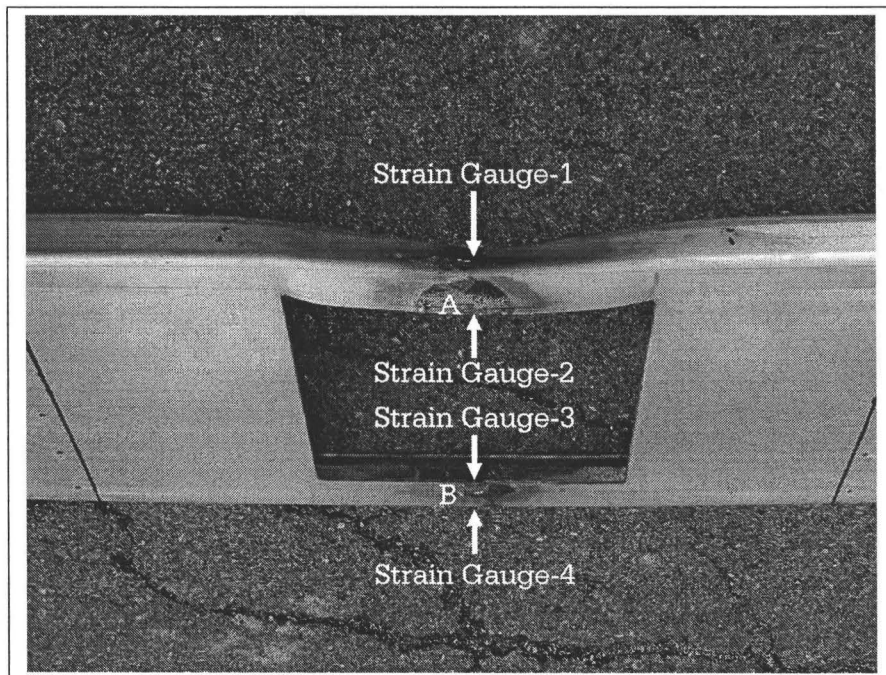


Figure 2.17: Typical flexural failure of joist having square openings ($h/t = 118$)

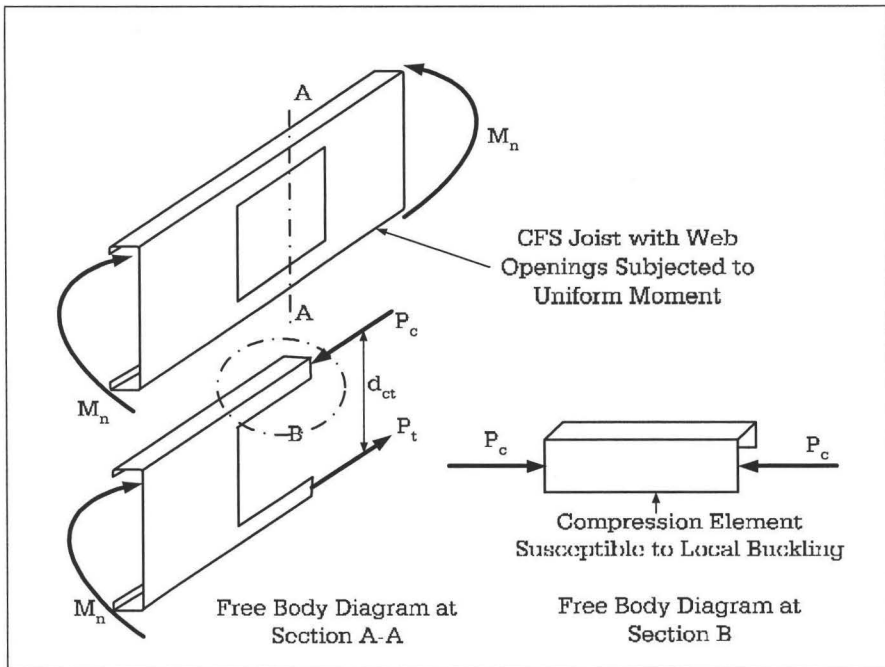


Figure 2.18: Free body diagram of CFS joist at the opening region

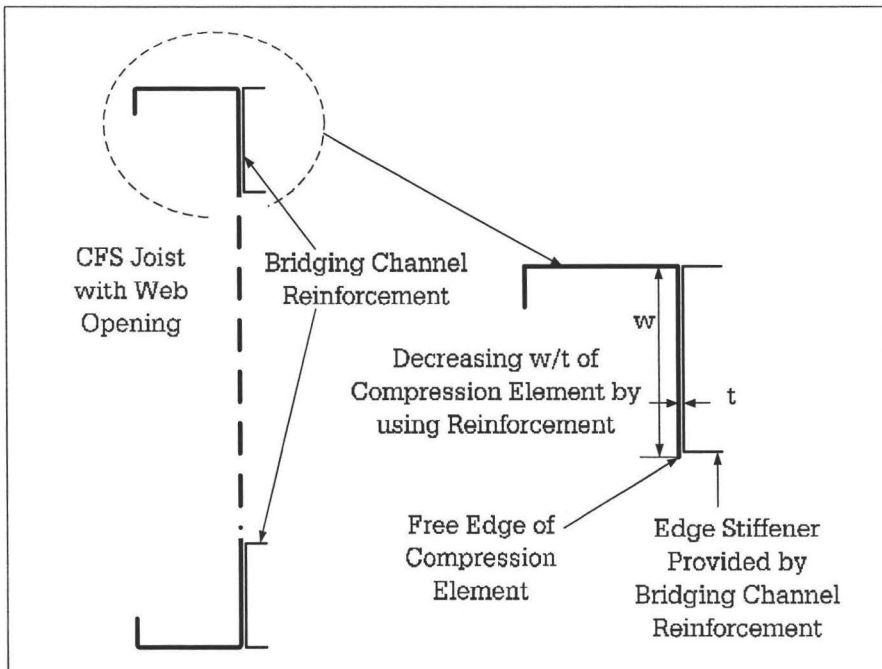


Figure 2.19: Reinforcement for compression element

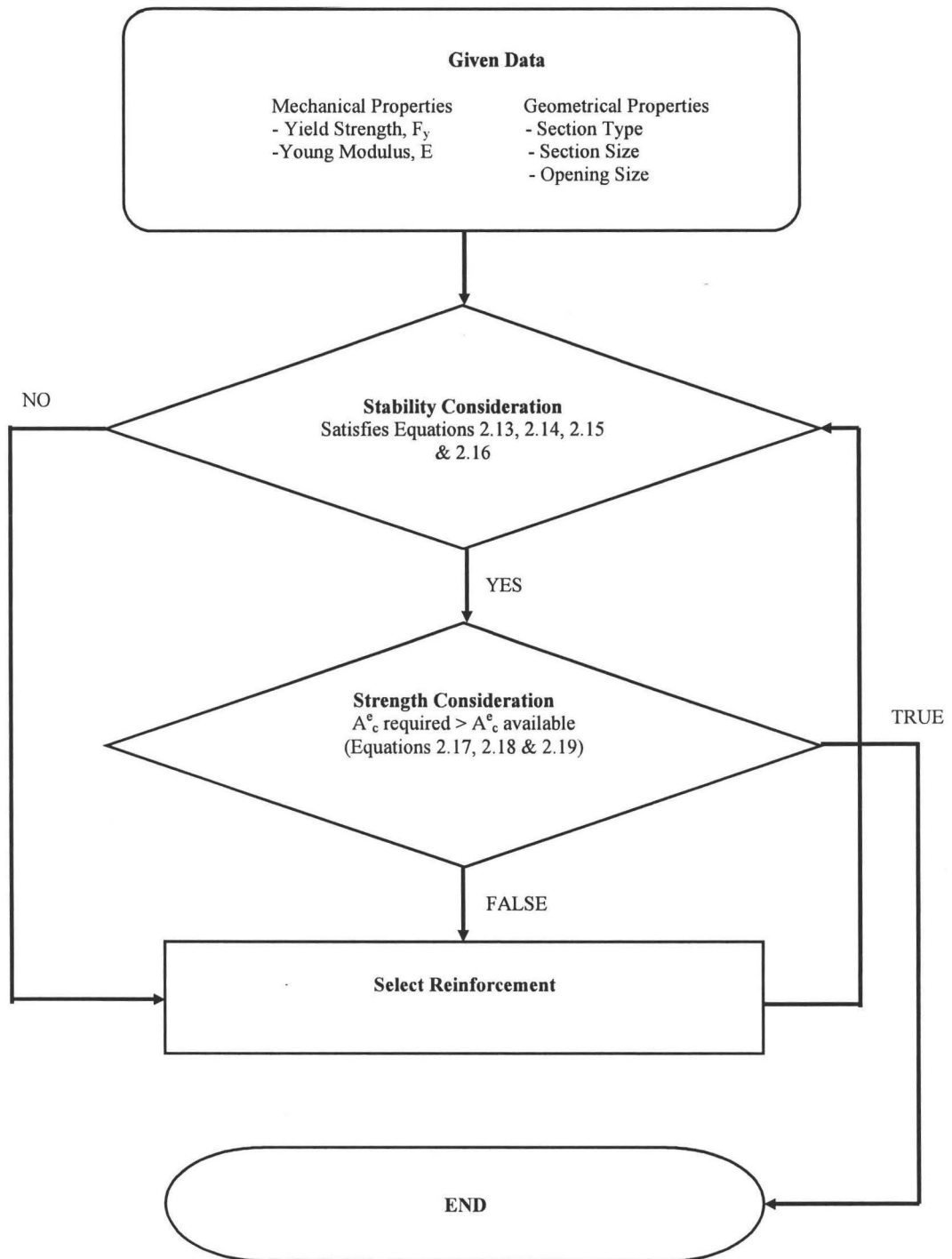


Figure 2.20: Flowchart to design flexural reinforcement

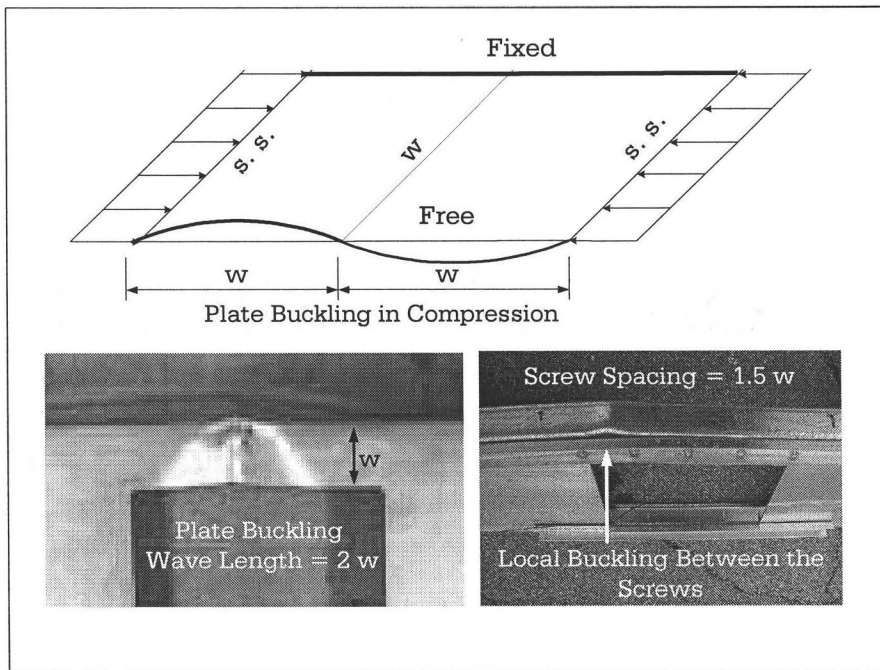


Figure 2.21: Local plate buckling because of inadequate screw spacing

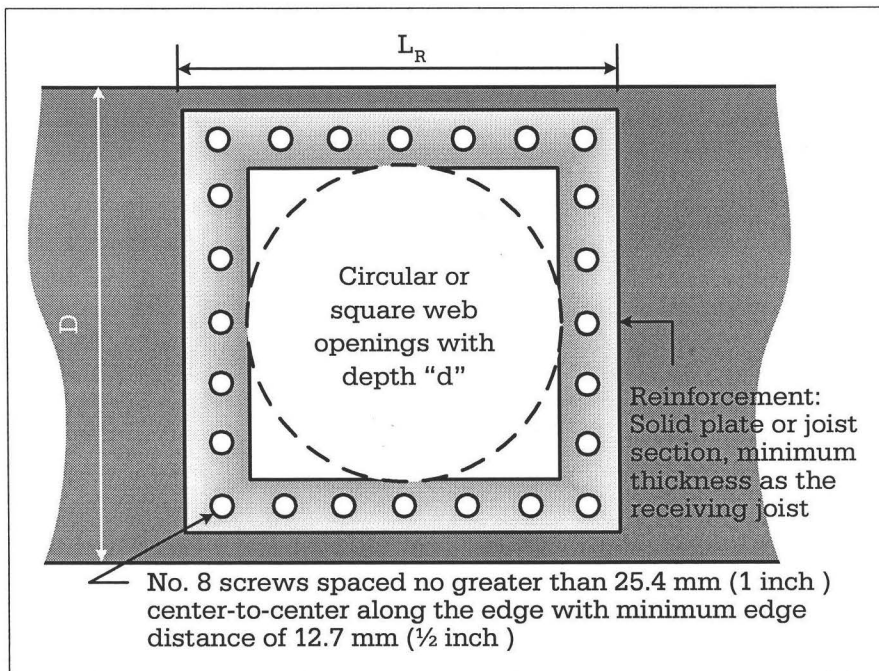


Figure 2.22: Reinforcement scheme-A and B for flexural zone, (AISI, 2007a)

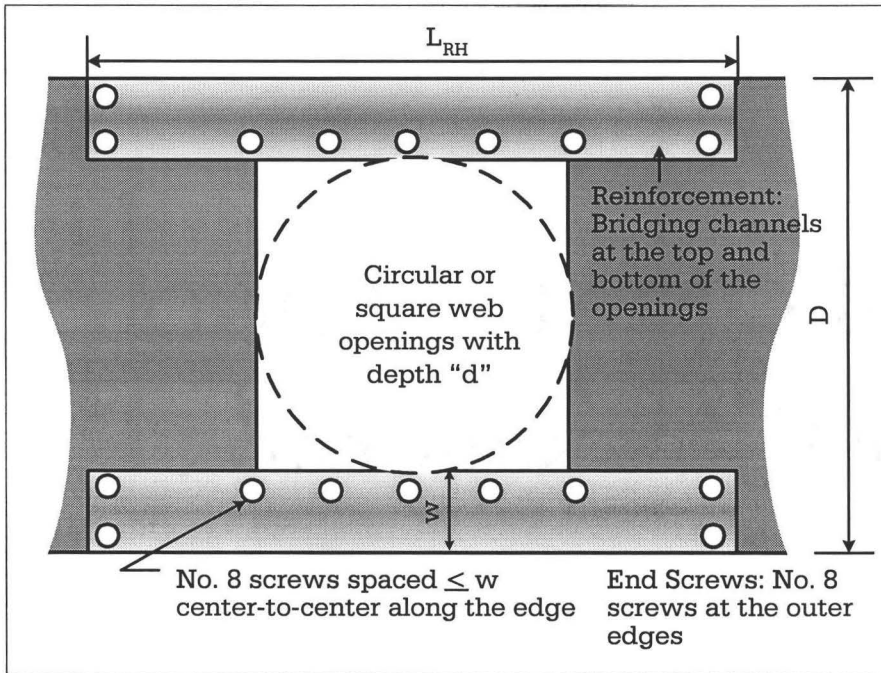


Figure 2.23: Reinforcement scheme-C, for flexural zone (Current study)

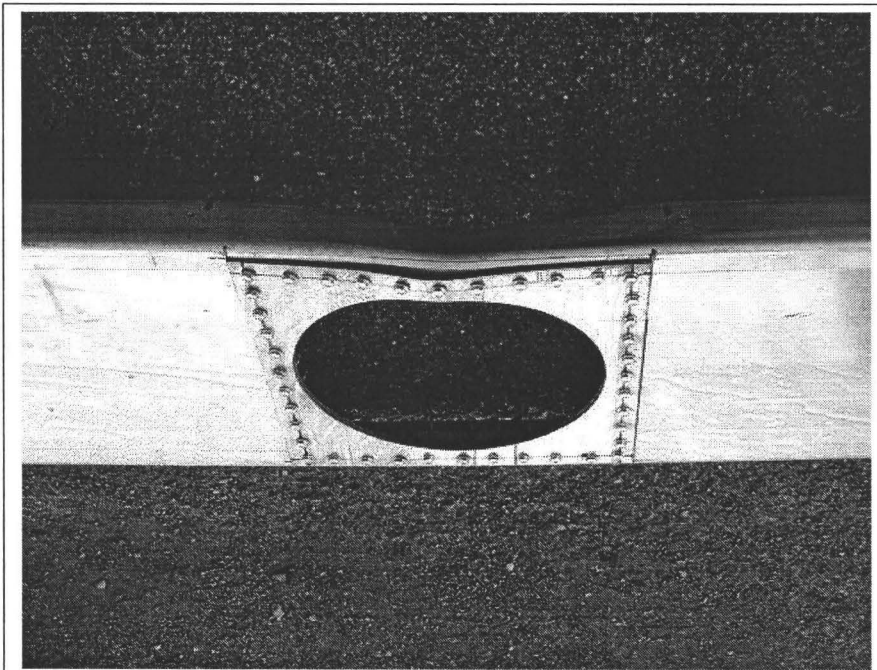


Figure 2.24: Typical failure of plate reinforcement (Scheme-A)

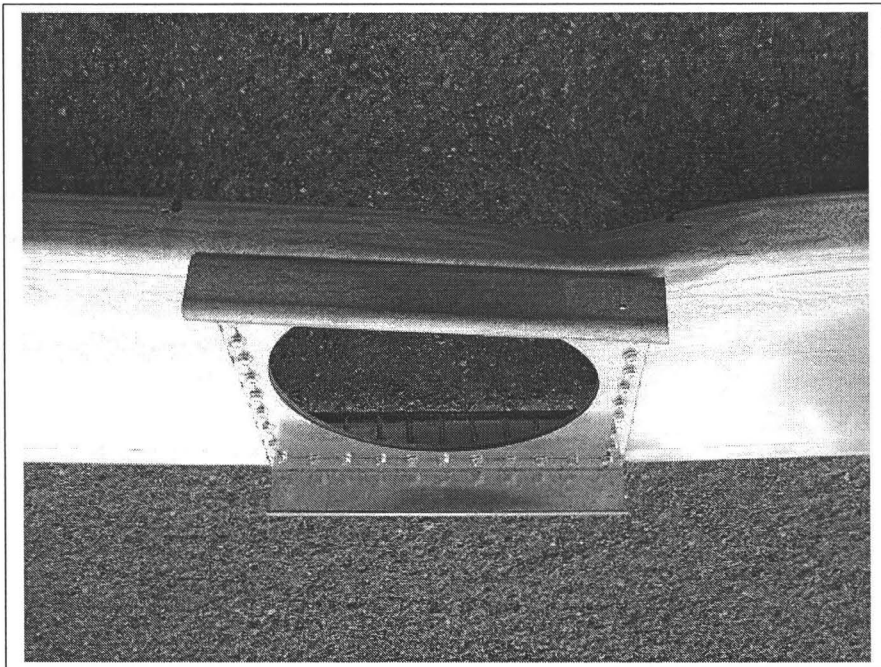


Figure 2.25: Typical failure of stud reinforcement (Scheme-B)

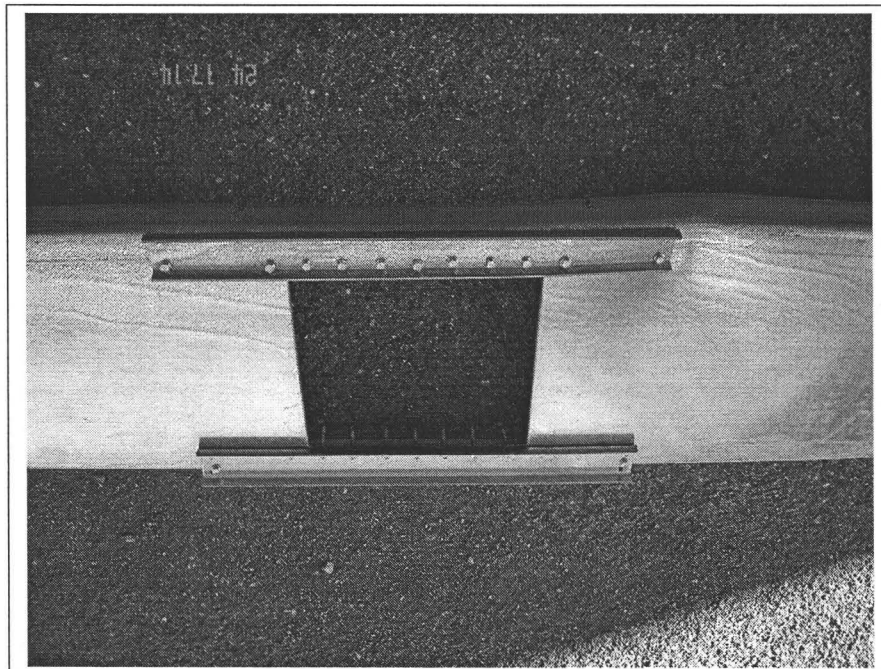


Figure 2.26: Matching bridging channel reinforcement (Scheme-C)

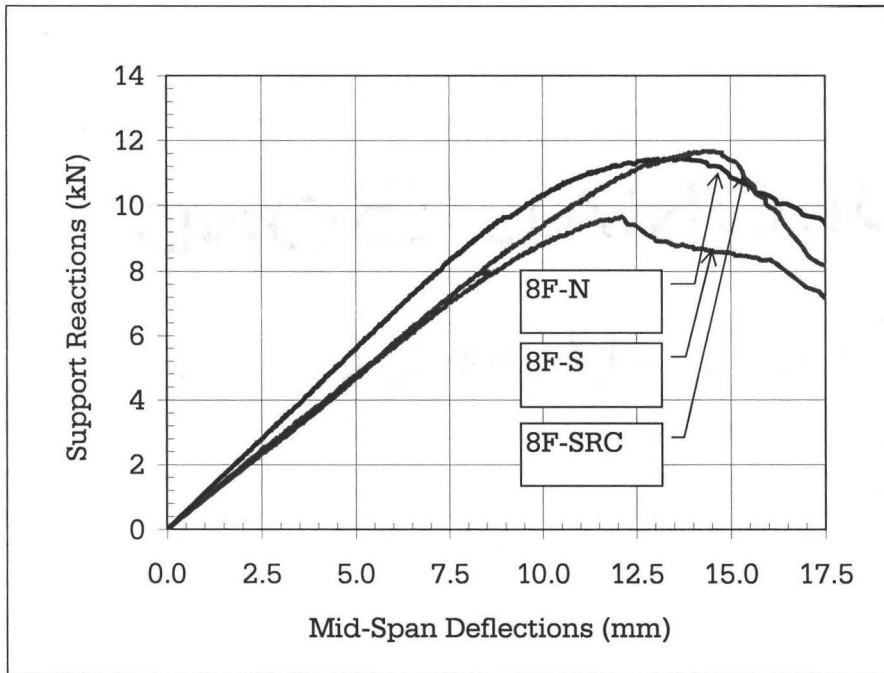


Figure 2.27: Typical comparative plot of solid, unreinforced and reinforced studs

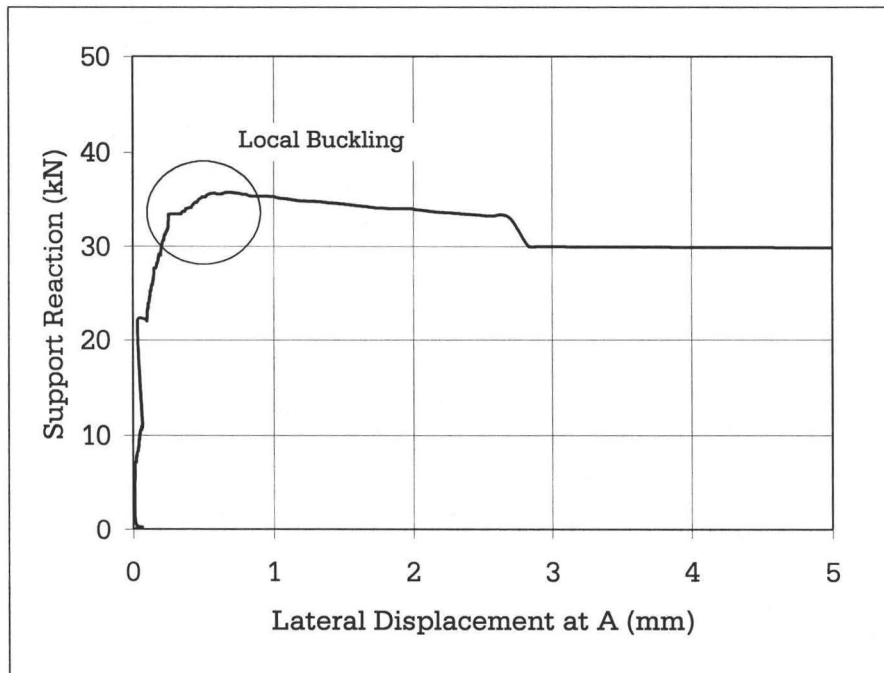


Figure 2.28: Lateral deflection showing beginning of local buckling

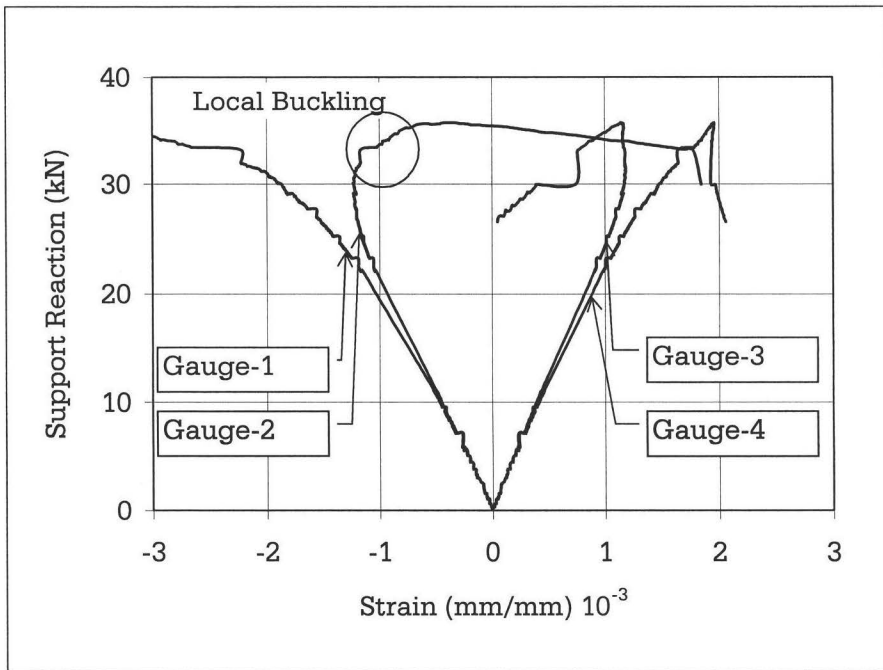


Figure 2.29: Strain measurements showing beginning of local buckling

Chapter 3

Reinforcements for CFS Joists with Web Openings in Shear Zone: Experimental Study

3.1 Introduction

Shear resistance of cold-formed steel (CFS) joists is determined by the shear stress prior to buckling and the cross-sectional area of the web. Contribution to the shear resistance by the flanges is relatively small and is often neglected. Therefore, the presence of openings in the web could drastically reduce the shear strength of the CFS joists. The primary objective of this part of the research was to develop reinforcement schemes to restore the shear capacity of CFS joists to values which would have been obtained had the openings not been made.

This chapter discusses the experimental investigation on the shear strength of CFS solid joists, joists with unreinforced web openings, and joists with reinforced web openings. The investigation is focused on circular and square web openings. The test program included three types of reinforcement schemes; two schemes prescribed by the current AISI Standard (AISI, 2007a) and the third scheme consisted of a Vierendeel truss type reinforcement arrangement. The investigation assessed the effectiveness of

these reinforcement schemes for CFS steel joists having web openings in a high shear zone. A total of 66 short span CFS joists were subjected to shear tests.

The AISI Standard (AISI, 2007a) provides a design table for CFS joists subjected to two intensities of loading for different applications. The maximum span that can be used for various joists was reproduced and is shown in Table 3.1. One of the controlling factors in selecting the maximum clear span is the shear resistance of the joists. Ratios of factored shear load to factored shear resistance are presented in Table 3.2. As shown in this table, thicker joists experience lower shear loads compared to the shear resistance of joists because the overall capacity of thicker joists is governed by flexure. The table also shows that relatively thinner solid joists are likely to experience higher shear force compared to the shear resistance of the joists. Such joists are indicated by the higher shear ratio in Table 3.2. In this investigation, 1.09 mm (43 mils) thick, 203.20 mm (8 inch) deep joist joists (800S162-43), which can experience shear loads up to 86 percent of the shear resistance in practical applications, were selected for testing.

3.2 Shear Resistance of the Cold-Formed Steel Joists

3.2.1 Shear Resistance of Solid Joists

Shear failure of cold-formed steel (CFS) joists can occur in one of three different modes, depending upon the h/t ratio of the web, where h is the flat depth of the web and t is thickness of the web. Such failure modes are: shear yielding, elastic shear buckling and inelastic shear buckling. The shear strength of cold-formed steel joists is determined as follows (Yu, 2000):

$$V_n = (ht)F_v \quad (3.1)$$

where, V_n = nominal shear resistance, F_v = nominal shear stress, h = flat web depth and t = web thickness. When a web with a relatively small h/t ratio is subjected to shear stress, the shear capacity of the joists is governed by shear yielding. The nominal shear stress for shear yielding is given as (Yu, 2000):

$$F_v = F_y/\sqrt{3} \quad (3.2)$$

where, F_y is the tensile yield stress. For the webs with large h/t ratios, the shear capacity of the web is governed by elastic critical shear buckling. The elastic critical shear buckling stress can be computed by the following equation (Yu, 2000).

$$F_v = k_v \frac{\pi^2 E}{12(1 - \mu^2)} \left(\frac{t}{h} \right)^2 \quad (3.3)$$

where, k_v is shear buckling coefficient, E is modulus of elasticity, and μ is Poisson's ratio. For webs having moderate h/t ratios, the computed theoretical buckling stress using Equation 3.3 may exceed the proportional limit in shear. The theoretical value of critical shear buckling stress should be reduced according to the change in the modulus of elasticity (Yu, 2000). Considering strain hardening, the nominal shear stress is computed as (Basler, 1961):

$$F_v = \sqrt{F_{vp}F_{vi}} \quad (3.4)$$

where, F_{vp} = proportional limit in shear = $0.8F_y/\sqrt{3}$ and F_{vi} = initial critical shear buckling stress given by Equation 3.3.

The AISI Standard (AISI, 2007) groups the shear failure of CFS joists into three different modes (shear yielding, inelastic shear buckling, elastic shear buckling) based on the h/t ratio. The shear design criteria in AISI Standard (AISI, 2007) Section C3.2 are as follows:

$$V_n = A_w F_v \quad (3.5)$$

(a) For $\frac{h}{t} \leq \sqrt{\frac{Ek_v}{F_y}}$

$$F_v = 0.60F_y \quad (3.6)$$

(b) For $\sqrt{\frac{Ek_v}{F_y}} < \frac{h}{t} \leq 1.51\sqrt{\frac{Ek_v}{F_y}}$

$$F_v = \frac{0.60\sqrt{Ek_v F_y}}{h/t} \quad (3.7)$$

(c) For $\frac{h}{t} > 1.51\sqrt{\frac{Ek_v}{F_y}}$

$$F_v = k_v \frac{\pi^2 E}{12(1 - \mu^2)} \left(\frac{t}{h}\right)^2 = 0.904 \frac{Ek_v}{(h/t)^2} \quad (3.8)$$

where,

A_w = Area of web element = ht

E = Modulus of elasticity of steel

F_v = Nominal shear stress

V_n = Nominal shear resistance

t = Web thickness

h = Depth of flat portion of web measured along plane of web

μ = Poisson's ratio = 0.3

k_v = Shear buckling coefficient determined as follows:

(i) For unreinforced webs, $k_v = 5.34$

(ii) For webs with transverse stiffeners

when $\frac{a}{h} \leq 1.0$

$$k_v = 4.00 + \frac{5.34}{(a/h)^2} \quad (3.9)$$

when $\frac{a}{h} > 1.0$

$$k_v = 5.34 + \frac{4.00}{(a/h)^2} \quad (3.10)$$

where,

a = Shear panel length of unreinforced web element

= Clear distance between transverse stiffeners of reinforced web elements.

Figure 3.1 shows the modes of shear failure determined by AISI design equations (Equations 3.6 to 3.8).

3.2.2 Shear Resistance of the Joists having Web Openings

The shear resistance of perforated plates has been of interest to engineers as early as 1944. Researchers (Biskin, 1944; Wang, 1946) have conducted analytical studies on the influence of holes on plates subjected to shear. Further analytical and experimental investigations for the behavior of perforated shear plates have been conducted by Kroll (1949), Kawai and Ohtsubo (1968), and Rockey et al. (1969). One of the prominent research series on the behavior of perforated shear plates was performed by Narayanan and Der-Avanessian (1983b), Narayanan et al. (1983), Narayanan and Der-Avanessian (1984), Chow and Narayanan (1984), Narayanan and Der-Avanessian (1985) and Narayanan and Der-Avanessian (1986). In these studies, the ultimate

shear capacity of a plate girder was studied with its web containing rectangular openings. Seventy tests were completed with web slenderness ratios ranging from 200 to 360; the ratio of the web plate width-to-depth ranged from 1.0 to 1.5 and the hole size did not exceed one-half of the depth of web plate or one-half of the width of the web plate. Based on a parametric study by Narayanan and Der-Avanessian (1984), an approximate method for computing the ultimate shear capacity of a web with a hole was developed. The elastic shear buckling stress appropriate to a perforated plate was expressed in a form similar to Equation 3.3:

$$F_{vo} = k_{vo} \frac{\pi^2 E}{12(1 - \mu^2)} \left(\frac{t}{h} \right)^2 \quad (3.11)$$

where, k_{vo} is the modified value of shear buckling coefficient. Expressions for k_{vo} were given for plates with circular and rectangular openings. The shear buckling coefficient for plates containing a central circular openings of diameter d_h and $d_h/h \leq 0.5$ was given as (Narayanan and Der-Avanessian, 1984):

$$k_{vo} = k_v \left(1 - \alpha_c \frac{d_h}{\sqrt{(h^2 + b_h^2)}} \right) \quad (3.12)$$

where, $\alpha_c = 1.5$ for clamped edges and 1.8 for simply supported edges. Where the circular openings are larger ($d_h/h > 0.5$), the coefficient of elastic critical buckling was given as (Narayanan and Der-Avanessian, 1984):

$$k_{vo} = k_v \left(1 - \frac{d_h}{h} \right) \quad (3.13)$$

Similarly, the shear buckling coefficient for a square plate having rectangular openings of depth d_h and width b_h ($d_h/h \leq 0.5$, and $b_h/h \leq 0.5$) was given as:

$$k_{vo} = k_v \left(1 - \alpha_r \frac{A_o}{A} \right) \quad (3.14)$$

where, $A_o = bd$, $A =$ area of the plate, and $\alpha_r = 1.25$ for clamped edges and 1.5 for simply supported edges. For larger rectangular openings, elastic critical buckling coefficient was the smaller of two values:

$$k_{vo} = k_v \left(1 - \frac{b_h}{h} \right), \text{ or, } k_{vo} = k_v \left(1 - \frac{d_h}{h} \right) \quad (3.15)$$

All of the analytical and experimental studies discussed above involved testing of plates rather than structural members.

Based on experimental information, guidelines for the design of hot-rolled beam sections with perforated webs was developed by Fowler et al. (1971). In that study, the allowable shear stress was taken as 40 percent of the tensile yield stress. The study also found that the shear force caused secondary bending of the plate elements above and below the openings. Two design criteria were proposed based on the elastic and plastic behavior for a perforated web subjected to shear. Because of high h/t ratios, the failure mode of CFS joists is somewhat different than that of the failure mode of hot-rolled steel members. Therefore, separate studies are needed for CFS members.

Yu and Devis (1973) studied the structural behavior of cold-formed steel members with perforated elements. Based on twelve tests of back-to-back channel sections having a web depth-to-thickness ratio ranging from 66.2 to 99.5 and a ratio of hole width-to-web depth varying from 0 to 0.505, the authors concluded that the presence of circular openings resulted in a significant reduction of shear capacity significantly. Yu and Davis (1973) developed a relation for the shear reduction factor that was

applicable only for circular openings located at mid-depth in a web element. The factor was expressed as,

$$q_s = 1.0 - 1.1 \left(\frac{d_h}{h} \right) \quad (3.16)$$

Where, d_h = the diameter of circular openings and h = the clear distance between flanges measured along the plane of the web.

Based on a finite element study, Redwood and Uenoya (1979) developed reduced shear reduction factors for both circular and rectangular openings. The shear reduction factor were expressed as follows:

For rectangular openings,

$$q_s = 1.24 - 1.16 \left(\frac{d_h}{h} \right) - 1.17 \left(\frac{b_h}{2d_h} \right) \quad (3.17)$$

For circular openings,

$$q_s = 1.15 - 1.05 \left(\frac{d_h}{h} \right) \quad (3.18)$$

Where, d_h = height/diameter of the openings, h = clear height of the web, b_h = width of a rectangular openings.

Schuster (1995) conducted a study to determine the effect of perforated CFS channel sections in shear. Each test specimen consisted of two channel sections strapped together using aluminum angles to form a box beam to prevent torsion. The web perforations were either diamond or elliptical shaped and the depths of the openings varied from 20 percent to 78 percent of the web depth. This study also indicated that the presence of web openings resulted in a significant reduction of the shear capacity of CFS sections.

Shan (1996) conducted an experimental investigation to study the behavior of CFS joists with elliptical web openings subjected to a shear load. Based on 26 beam specimen tests, modified equations using either linear or a non-linear relationship were developed to determine the capacity of the CFS joists having elliptical web openings. The d_h/h ratio was found to be the primary parameter contributing to the reduction in capacity for joists having web openings, where d_h and h represent for opening depth and height of flat portion of the web, respectively. Based on the investigations (Shan and LaBoube, 1994; Shan et al., 1996; LaBoube et al., 1997), the following design recommendations for the shear capacity of the CFS joists with elliptical web openings having a limitation of $34.43 \leq h/t \leq 210.32$ were proposed.

when $d_h/h \leq 0.383$

$$q_s = 1.711 - 3.661 \left(\frac{d_h}{h} \right) \quad (3.19)$$

when $d_h/h > 0.383$

$$q_s = 0.456 - 0.377 \left(\frac{d_h}{h} \right) \quad (3.20)$$

Equation 3.19 and 3.20 apply to the linear behavior of CFS joists. The non-linear relation for the shear reduction factor was expressed as,

$$q_s = 1.506x10^{-1.33 \frac{d_h}{h}} \quad (3.21)$$

The AISI Standard (AISI, 2007) included a procedure for calculating the shear resistance of CFS joists having web openings. The standard classifies openings as circular or non-circular. The provisions are limited for:

- $d_h/h \leq 0.7$

- $h/t \leq 200$
- Openings Centered at mid-depth of web
- Clear distance between openings $\geq 457mm$
- Non-circular openings: corner radii $\geq 2t$
- Non-circular openings: $d_h \leq 64mm$ and $b_h \leq 114mm$
- Circular openings: $14 \leq d_h \leq 152mm$

Under these limitations, the shear resistance of joists having web openings is given by $q_s V_n$ where V_n is nominal shear resistance of solid joists and q_s is given by, when $c/t \geq 54$

$$q_s = 1.0 \quad (3.22)$$

when $5 \leq c/t < 54$

$$q_s = \frac{c}{54t} \quad (3.23)$$

where, $c = h/2 - d_h/2.83$ for circular openings and $c = h/2 - d_h/2$ for non-circular openings. The AISI Standard (AISI, 2007) provisions show that non-circular openings cause large reductions in shear resistance compared to circular openings.

Plots showing the various shear reduction factors are given in Figures 3.2 and 3.3. The experimental results for the joists considered in this study having 64 percent web openings are also shown in these figures. The plots show that the shear reduction factor given by Shan (1996) is the most conservative. The AISI Standard (AISI, 2007) gives the lowest reduction in shear resistance compared to other recommendations.

3.3 Shear Reinforcements for Web Openings

3.3.1 Previous Studies

Various studies (Segner, 1964; Congdon, 1968; Copper and Snell, 1972; Wang et al., 1975; Larson and Shah, 1976) have addressed the behavior of hot-rolled steel beams with reinforced web holes. Segner (1964) studied various reinforcement schemes and presented a method for determining the amount of reinforcement around large rectangular openings in the webs of wide-flange beams (depth of the openings as compared to the depth of the beams ranged from 0.4 to 0.7). These studies primarily focused on square and rectangular openings, having a particular form of web reinforcement. The beams were subjected to varying combinations of bending moment and shear. The reinforcement schemes suggested by Segner (1964) consisted of horizontal, vertical and inclined bars welded to the web around the openings, as discussed in Chapter 2 (see Figure 2.3). Segner (1964) observed that, for a high shear zone, the reinforcement consisting of a combination of horizontal and inclined bars were more economical and more effective than the reinforcements consisting of only horizontal bars. The proposed method of reinforcement was based on the theory that a member having web openings located on the neutral axis acts as a Vierendeel truss in the vicinity of such openings. The reinforcement techniques suggested by Segner (1964) are widely used in hot-rolled steel construction because of the effectiveness, economy and ease of fabrication.

Shrivastava and Redwood (1979) presented design recommendations for W-shaped hot-rolled beams with and without reinforced openings. Both square and rectangular openings with a height of the openings ranging between 30-70 percent of the beam depth were studied. Based on an analytical study, (Narayanan and Der-Avanessian, 1984; Narayanan and Der-Avanessian, 1985) design procedure for reinforcement were

developed. In this procedure, the amount of the reinforcements and anchorage length of the reinforcements beyond the openings were determined. The reinforcement considered was in the form of flat strips welded symmetrically above and below the openings. Finite element studies (Narayanan and Der-Avanessian, 1983a; Narayanan and Der-Avanessian, 1984; Narayanan and Der-Avanessian, 1985) on the buckling of the perforated plates with flat strip reinforcement have shown that in order for the reinforced web to develop a buckling resistance equal to that of an unperforated web, the width and thickness of the reinforcements must satisfy the following condition:

$$\left(\frac{t_r}{t}\right)^2 \left(\frac{w_r}{h}\right) > 2.76 \sqrt{\frac{b_h d_h}{ah}} \quad (3.24)$$

where, t_r = thickness of the reinforcements, t = thickness of the web, w_r = width of the reinforcements, h = height of the web, b_h = width of the openings, d_h = depth of the openings and a = clear distance between transverse stiffeners of the web. The following anchorage length of the reinforcement beyond the openings was suggested:

$$l = \begin{cases} 0.5(d_h \cot \phi_m - b_h) \\ 0.25b_h \end{cases} \quad (3.25)$$

whichever is greater. Here, ϕ_m is function of area of the hole and area of the web and varies linearly with $\sqrt{b_h d_h / ah}$. This design method was limited to webs of hot-rolled steel plate girders having h/t ratios between 200 and 300 and a web panel aspect ratio, a/h , between of 1.0 and 1.5. Such design procedures were applicable only for welded reinforcements on the web of hot-rolled steel plate girders.

Pennock (2001) conducted an experimental investigation on the strength of CFS joists with web openings. Fifty six specimens were tested under a eight point-load

configuration. The purpose of this study was to assess the effects of various reinforcement schemes. The tested specimens were mainly subjected to bending and the combined effect of shear and bending under simply supported conditions. The CFS joists with web openings were tested under two point loading conditions. Circular and square web openings which reduced the web area by 75 percent were investigated. The opening locations were varied so that the effect of varying levels of moment and shear could be evaluated. In this study, the web was reinforced with a web perforated joist of the same shapes and size. It was observed that the use of web perforated joists as reinforcement was ineffective in improving shear capacity of CFS joists.

The AISI Standard (AISI, 007a) recommends a procedure for reinforcing the web openings in CFS joists when the web openings violate specified requirements. The reinforcement schemes recommended by AISI Standard (AISI, 007a) are similar as those recommended for flexure discussed in Section 2.3.2.

3.3.2 Shear Buckling and Vierendeel Action

When a cold-formed steel (CFS) joist is subjected to shear load, the web of the joist would form a tensile and a compression band along its diagonal direction as shown in Figure 3.4. Failure of CFS joist subjected to shear would be by buckling along the compression band known as shear buckling. Figure 3.5 shows a typical example of shear failure pattern of web of CFS joist having circular opening. Presence of such opening on compression band would reduce the shear strength of the CFS joist significantly. The reduction of shear strength of CFS joist with web opening can be determined as:

$$V_r = V_s - V_o \quad (3.26)$$

Where, V_r is reduction in shear strength, V_s is shear strength of solid web and V_o is shear strength of the web with opening.

Shear strength of web of CFS joist with web opening can be restored by applying a Vierendeel truss type reinforcement. As shown in Figure 3.6 the Vierendeel truss does not use diagonals, thus, provides a clear open rectangular area between members (chords and verticals). However, when the diagonals are removed, a significant portion of truss action is lost, i.e, forces are no longer transmitted exclusively by creating only axial forces in the chords and verticals. Instead, forces are transmitted by axial force, shear force and moment in the members called Vierendeel action as shown in Figure 3.6. The member joints are also fixed to transmit the moments between the members.

When a Vierendeel truss type reinforcement is applied around the openings of web of the CFS joist, the diagonal compression on the web is shared by the reinforcement. Assuming that the resultant of diagonal compression load would pass through the joint of the truss, the resultant diagonal load to be carried by the reinforcement is given by:

$$P_r = \sqrt{2}V_r \quad (3.27)$$

The resultant diagonal force on the truss would be carried by the members by Vierendeel action as shown in Figure 3.6. Axial force, shear force and moment on the reinforcement can be derived using slope deflection equations. The axial load P_m , shear load V_m and moment M_m are given by:

$$P_m = \frac{P_r}{2\sqrt{2}} \quad (3.28)$$

$$V_m = \frac{P_r}{2\sqrt{2}} \quad (3.29)$$

and

$$M_m = \frac{6EIP_rL}{12EI - P_rL^2} \quad (3.30)$$

Where, E = modulus of elasticity of reinforcement, I = moment of inertia of reinforcement about its centroidal axis and L = Length of one side of the reinforcing frame

3.4 Experimental Program

3.4.1 Test Designation

Each of the shear tests in the present experimental program was designated by a specific name that describes the size of the joist, the type of the test, the opening type, the sequence of the test and the position of the joist on the specimen assembly.

For example, test “**8S-CRA-1-R**” indicates the following:

8 : 8-inch (203.2 mm) deep joist

S : Shear test

CRA : “C” for circular hole, “R” for reinforced and “A” for reinforcement scheme “A” (see Section 3.4.3 for various reinforcement schemes)

1 : First set of tests, and

R : Right hand side section of the test specimen assembly

The measured dimensions of each of the joists used in this experimental program are presented in Table 3.3.

3.4.2 Test Setup

This section describes the experimental set-up, and the configuration of the test specimens corresponding to this part of the investigation. Figure 3.7 shows a sketch of the test setup. It is impossible to create a pure shear zone for shear testing because of the presence of a bending moment. In practice, a shear test is performed by creating a high shear and low moment region. Here, a 914 mm (36 inch) short span with a mid-span point load was considered as an appropriate test setup to achieve high uniform shear and low moment. One end of the test specimen was pin-supported, whereas the other end was roller-supported in order to allow for horizontal movements. The test arrangement, as described above, and as shown in Figure 3.7, results in a uniform shear force and an increasing moment between the support and the mid-span load point. The load was applied at mid-span through a 600 kN capacity Tinius Olsen test machine. To prevent web crippling under the concentrated loads at the load point and at the supports prior to the anticipated shear failure the webs were reinforced. In this investigation, as shown in Figures 3.7, 3.8 and 3.9, the applied load, and the support reactions were transmitted to the web of the specimen through steel brackets. Furthermore, the vertical planes of the steel brackets were fastened to the webs of the test specimens using self-drilling screws, which was to help to transfer the concentrated loads effectively into the web. Figure 3.8 shows the cross-sectional configurations of the test specimens at load location A and support condition B.

The investigation considered mono-symmetric 203.20 mm (8 inch) deep 1.09 mm (43 mils) thick galvanized lipped channel CFS joists. Mono-symmetric sections are generally susceptible to torsional loadings, due to the fact that the shear center does not coincide with the centroid of the section. However, it is not convenient to apply a load through the shear center of a single channel section, as its shear center is

outside of the section. Therefore, in this investigation two lipped channel sections with a length of about 1220 mm (48 inch) were arranged face-to-face to form the test specimen. In this arrangement the torsional effects are counterbalanced by each other, since torsional restraints were provided at several locations along the span. The steel brackets that were used to prevent web crippling at the load and the support locations provide some torsional restraints at these locations. In addition, 6 mm (1/4 inch) thick steel plate strips were attached to the non-bearing flanges at the load and at the support locations which enhanced the torsional resistance at these locations. Furthermore, additional steel plate strips were fastened to the compression flanges of the two sections of the test specimen at about 304 mm (12 inch) intervals. Two vertical linear variable displacement transducers (LVDTs) were mounted on the top of two sections to measure central vertical displacement of the specimen. Two lateral LVDTs were set to measure lateral displacements of the web at the central region. Lateral measurements were measured at the edge of the openings located on the diagonal of the shear panels. Four strain gauges were mounted on one of the three identical tests to measure longitudinal strain on the top flange, bottom flange, and at the edge of the openings near the diagonal of the shear panels. Web strains were measured at 45 degrees with respect to the horizontal (maximum strain expected in this direction).

3.4.3 Test Procedure

At first, the longitudinal and transverse centerlines of the whole test set-up were checked so that the specimen's centerlines coincided with the corresponding centerlines of the loading machine and the end supports. Then, the span length and the

position of the central load were measured and recorded. Each specimen was subjected to a low load (about 2 kN), to ensure proper functioning of the load cells and transducers. After this initial loading, the load cells, the displacement transducers and the strain gauge readings were initialized to zero. The specimens were thus subjected to a continuous loadings until failure. The loading rate was 2.0 kN per minute. This loading rate was selected such that (a) sufficient load increments could be recorded to establish adequate load-displacement relationships and (b) stress rate at any point of the section did not exceed the stress rate specified by ASTM for tensile coupon tests (690 MPa/min). Prior to testing, the shear capacity of the sections was estimated on the basis of the AISI Standard (AISI, 2007) design criteria. Accordingly, the shear resistance of the sections under consideration, with $a/h = 1.5$, was computed to be 8.81 kN. The loading was applied in three equal intervals pausing for 3 minutes. This pause in loading allowed the stress to distribute on the entire beam. The readings from the load cells, LVDTs and the strain gauges were recorded to a data file using a computer controlled data acquisition system. The loading was continued until the load dropped to 70 percent of the failure load or until a clear failure shape was evident.

The support reactions at both ends were recorded and averaged. Since a point load was applied at the center of the span, the reactions were expected to be equal. Similarly, the vertical mid-span displacement on both joists were measured and averaged. Figure 3.10 shows the typical plot of two support reactions. Similarly, Figure 3.11 shows a sample plot for the mid-span deflection of two solid joists. It can be seen from these figures that the both reactions and displacements were within the 10 percent of the average value until failure. The average support reaction and average mid-span displacement were plotted for all tests. Such plots are presented in Appendix D. Only the peak values from the test plots are presented in this chapter

(Table 3.4 to Table 3.7). The shear strength of the sections was established based on the average of three tests.

3.5 Solid Joists and Joists with Unreinforced Web Openings

In this section, the shear capacity of (a) joists with no openings ($a/h = 1.0$ and 1.5), (b) joists with circular openings ($a/h = 1.5$), and (c) joists with square openings ($a/h = 1.5$) is described. Water-jet cutting was used to cut out these web openings. Three identical tests were conducted for each case. Thus, this part of the investigation includes twelve tests. Circular and square openings with 127 mm (5 inch)-diameter and 127 mm (5 inch)-side, respectively, were considered. The opening depth was 64 percent of the flat width of the web, and the openings were located between the central load and one of the supports (at quarter span).

Solid Specimens: Detail test results and photographs of the failed specimens are given in Appendix D. The shear strength of the three tested solid sections ($a/h = 1.0$) were 16.45 kN, 16.71 kN and 15.90 kN. The average value was 16.35 kN. The calculated shear capacity (based on measured mechanical properties) of the joists according to AISI Standard (AISI, 2007) design provisions (Equation 3.5 to Equation 3.10) was 11.56 kN. Table 3.4 summarizes the shear strength of CFS joists ($a/h = 1.5$) with and without a web opening in the high shear zone. The picture of the shear failure and corresponding load displacement curve are shown in Figures 3.12 and 3.13. Though short spans were used in the test, these specimens experience high shear and high moments at the load location. The load displacement behavior was observed to be consistent for all three tests. Based on the results from the three identical tests,

the peak shear values for a solid joist with a/h ratio equal to 1.5 were established as 12.23 kN, 12.56 kN and 12.49 kN. Therefore the average shear capacity of a single joist based on these tests was 12.43 kN. The calculated shear capacity of the joist based on the AISI Standard (AISI, 2007) design provisions was 8.81 kN. Though shear buckles were evident in these test specimens well prior to failure, the eventual failure of the solid specimens was right at the edges of the loading bracket, indicating that the failure was due to a combination of shear and moment. All three specimens experienced similar failure modes.

Specimens with Circular Web Openings: The test results from specimens with circular web openings are presented in Table 3.4. It was observed that the failure was governed by diagonal shear buckling of the web as shown in Figure 3.14. All three specimens failed at the region of the openings. The peak shear forces experienced by these joists were 7.37 kN, 7.45 kN and 7.48 kN. The load displacement curves for the three tests are presented in Figure 3.15 which show that all three test results were consistent. The average shear capacity for a single joist with a circular web opening based on these tests was 7.43 kN. The value obtained from the AISI Standard (AISI, 2007) for joists having 64 percent circular web openings was equal to 8.0 kN. This value was based on Equations 3.22 and 3.23. Thus the AISI Standard (AISI, 2007) overestimated the shear resistance of CFS joists having a circular opening. The test results showed that a circular opening of 64 percent web depth reduces the shear strength by 40 percent.

Specimens with Square Web Openings: The test results for specimens with square web openings are presented in Table 3.4. These specimens also failed due to diagonal shear buckling of the web at the opening region, which is evident in the photographs given in Table 3.4. All three specimens failed at the opening region in a similar manner. The peak shear values recorded from three joist tests were 5.10 kN, 5.27

kN and 5.06 kN. The average shear capacity of a single 1.092 mm (43 mils) thick, 203.2 mm (8 inch) deep joist, based on three identical tests, was 5.14 kN. The value according to the AISI Standard (AISI, 2007) was equal to 5.21 kN. Thus the AISI Standard (AISI, 2007) overestimated the shear resistance of the joists having square web openings. A typical diagonal shear failure of a CFS joist having square openings is depicted in Figure 3.16. The shear capacity of the joist was 59 percent lower due to the presence of a square web opening. The impact of square openings seems to be more severe compared to circular openings.

3.6 Joists with Reinforced Web Openings

3.6.1 Shear Reinforcement Schemes

Three reinforcement schemes, namely, Scheme-A, Scheme-B and Scheme-C, were considered for shear tests. These reinforcement schemes were used for both circular and square openings. Reinforcement schemes A and B are based on the AISI (AISI, 2007a) reinforcement requirements.

Reinforcement Scheme - A (AISI, 2007a): In this scheme the web openings were reinforced with a steel plate having the same size and shape openings of the joist. The thickness of the steel plates was equal to the thickness of the receiving joists (1.09 mm) and extended 25.4 mm (1 inch) beyond all edges of the openings. The steel plates were fastened to the web of the section with No. 8 screws spaced 25.4 mm (1 inch) center-to-center along the edges of the patch with an edge distance of 12.7 mm (1/2 inch). Figure 3.17 shows the details of Scheme-A reinforcement.

Reinforcement Scheme - B (AISI, 2007a): In this scheme the web openings were reinforced with a CFS stud section having same size and shape openings of the

joist. The thickness of the reinforcements was equal to the thickness of the receiving joists (1.09 mm) and extended 25.4 mm (1 inch) beyond all edges of the openings. The stud reinforcement was fastened to the web of the joist with No. 8 screws spaced 25.4 mm (1 inch) center-to-center along the edges of the patch with an edge distance of 12.7 mm (1/2 inch). The detail associated with reinforcement "B" is also shown in Figure 3.17.

Reinforcement Scheme - C: The reinforcement Scheme-C was developed based on several trial reinforcement schemes involving different channel types and screw patterns. The development of this reinforcement scheme began with two horizontal bridging channels on the top and bottom of the opening, as suggested for hot-rolled steel by Narayanan (Narayanan and Der-Avanessian, 1984; Narayanan and Der-Avanessian, 1985). However, it was observed during testing that such a reinforcement was totally ineffective in restoring the shear capacity of the joists. The results from the tests are shown in Table 3.5.

The shear reinforcement in Scheme-C involved the use of screw fastened (No. 8 self-drilling screws) bridging channels of depth 38.1 mm (1-1/2 inch) and thickness of 1.37 mm (54 mils) along all four edges of the openings. The bridging channels were 1.37 mm (54 mils) thick whereas the main joists were 1.092 mm (43 mils) thick. The shear reinforcement consisted of horizontal and vertical reinforcement comprising a Vierendeel truss type arrangement. The horizontal reinforcement consisted of two bridging channels where length was determined by the width of the openings, 127 mm (5 inch) plus one half of the depth of the openings on both sides of the opening and a minimum edge distance for screws of 10 mm. Therefore, the total length of the horizontal reinforcement was 274 mm (10.7 inches). The vertical reinforcement included two bridging channels of length equal to the depth of the web of receiving joists. Horizontal reinforcements were fastened along the top and bottom edge of the

openings. The channels were screw fastened at a spacing of 31.75 mm (1.25 inch) close to the opening edges within the opening region starting from the central screw. The requirement of screw spacing was discussed in Section 2.7.1. Furthermore, vertical reinforcement was placed closer to the vertical edges of the openings. Four screws were used at the corners of the horizontal and vertical reinforcement to create rigid joints. This system produced a Vierendeel truss type reinforcement system, as shown in Figure 3.18.

3.6.2 Test Results

The shear resistance of joists having reinforced circular web openings and joists having reinforced square web openings is discussed in this section. Both circular and square openings were reinforced by plates, studs and bridging channels, Schemes-A, B and C, respectively. Three tests for each of plate, stud and bridging channel reinforcement on circular and square openings were carried out. Thus a total of 18 tests were conducted. The test results are presented in Tables 3.6 and 3.7. It was observed that joists with reinforcement Scheme-A and B failed in diagonal shear failure mode at the opening region and this reinforcement was not adequate to restore the shear strength of the joists. Typical failure modes for reinforcement Scheme-A and B are shown in Figures 3.19 and 3.20. Specimens with reinforcement Scheme-C failed outside the reinforced area and the failure was initiated by shear buckling on the web followed by local buckling of the compression flange (see Figure 3.21). It was observed that reinforcement Scheme-C was fully capable of restoring the original shear strength of the joists. Typical results from joists with and without circular web opening and with Scheme-C reinforced web opening are shown in Figure 3.22.

3.6.3 Strains on the Main Joists and Reinforcement Channels

Strains were measured at four different locations of the specimen using electrical resistance strain gauge. Two strain gauges were mounted on the top and bottom flanges. Another two strain gauges were placed at the edge of the openings located on the diagonal line on the web. Strain gauges on the web were placed at 45 degrees with respect to the horizontal plane in which the direction the maximum strains were expected because of diagonal failure. One strain gauge was placed to measure the diagonal tension strain and another was placed to measure diagonal compression strain. The location and orientation of the strain gauges are shown in Figure 3.16.

The recorded strains are presented in Figure 3.23. The figure shows that the strains on the flanges are smaller than the strains on the web. Since the joist was subjected to high shear, the longitudinal strains on the flange would be lower than the diagonal strains on the web. The results also shows that the strain gauge at the compression band started to experience tension after a certain load level. This is because of the local buckling at the strain gauge region where the strain gauge was on tensile face of the buckled surface. The plot clearly shows the beginning of shear buckling. Figures 3.21 and 3.24 show the locations of strain gauges on the reinforcements and the strain readings, respectively. The plot in Figure 3.24 shows that the top reinforcement and two vertical reinforcements experienced compression load and the bottom reinforcement experienced tensile load.

3.6.4 Lateral Displacements and Initiation of Shear Buckling

Figure 3.25 shows the lateral displacements of the web at diagonal points A and B. The locations of lateral displacement measurements (A and B) are identified in Figure 3.16.

Figure 3.225 shows that the web experienced significantly high lateral displacement beginning at some load level because of buckling. This load level corresponds to the shear buckling load level observed in the strain measurements.

3.7 Conclusions

The shear strength of CFS solid joists according to AISI Standard (AISI, 2007) procedures was very conservative. The experimental values were 41 percent higher than the calculated values. The reduction in the shear strength of CFS joists due to web openings (up to 64 percent of web height) was as high as 60 percent. The AISI Standard (AISI, 2007) overestimated the shear strength of joists with web openings. Reinforcement Schemes-A, and B, recommended by AISI Standard (AISI, 2007a) were not adequate to restore the shear strengths of CFS joists having web openings. Reinforcement Scheme-C, which is a Vierendeel type reinforcement system, for web openings is capable of restoring the original shear resistance of cold-formed steel joists.

3.8 Recommendation for Flexural and Shear Reinforcement

3.8.1 Flexural and Shear Zones

Chapter 2 and 3 presented the experimental flexural strength and the shear strength of cold formed steel (CFS) joist having web opening. These chapters established the impact of such web opening, and they also determined the reinforcement schemes which restored the original strength of CFS joist. In these chapters, the flexural effect and the shear effect were studied separately, and the flexural zone and the shear zone

were not defined. The flexural zone and shear zone for a joist member depend on the structural arrangement and the loading. This section establishes definition for the flexural zone and shear zone for CFS joists.

Cold-formed steel (CFS) floor joists are expected to carry uniformly distributed load imposed by the floor deck. Therefore, in the analysis and design of CFS floor joists for house construction, it is reasonable to assume that the floor joist is subjected to uniformly distributed load.

Figure 3.26 shows the non-dimensional shear variation in a floor joist having three different structural arrangements (simple support, continuous support and moment optimized two-span joist). The figure shows that if the joist is simply supported, then the maximum shear (V_{max}) occurs at the supports. The test results described in Chapter 3 show that web opening depth up to 65 percent of web depth would reduce the shear strength of cold-formed joist by 60 percent. In other word, CFS joist having such web openings (opening depth up to 65) possesses 40 percent shear capacity of the joist. Therefore, shear reinforcement is required when shear load is greater than 40 percent of design shear (maximum shear, V_{max}). Figure 3.26 shows that shear grater than $0.40V_{max}$ exists outside $0.30L$ and $0.70L$, where L is the span length. The shear within the region $0.30L$ and $0.70L$ (mid-span region) for this structural arrangement will be less than $0.40V_{max}$.

If the joist is continuous over two or more spans, then the maximum shear, V_{max} , occurs over the support. Shear greater than $0.40V_{max}$. exists outside $0.125L$ and $0.625L$, where L is the span length.

If the joist has an over-hang and the joist had been designed such that the moment over the support is equal to moment at the mid-span (moment optimized two-span joist), then the maximum shear, V_{max} , occurs over the support. Shear grater than $0.40V_{max}$. exists outside $0.18L$ and $0.65L$, where L is the span length.

Considering these three possible structural arrangements, and choosing $0.30L$ from end-support and $0.375L$ from intermediate-support the shear within this region will be less than $0.40V_{max}$. The region within $0.30L$ from end-support and $0.357L$ from intermediate-support will be greater than $0.40V_{max}$. Thus, the openings within $0.30L$ from end-support and $0.375L$ from intermediate-support of a joist will need shear reinforcement.

Figure 3.27 shows non-dimensional moment variations in a floor joist subjected to a uniformly distributed load. If the joist is simply supported, then the maximum moment M_{max} occurs in the mid-span. Focusing on the mid-span region, moment greater than $0.75M_{max}$ exists between $0.255L$ and $0.75L$, where L is the span length and $0.75M_{max}$ is moment resistance of CFS joist having web opening established by experiment (Chapter 2).

If the joist is continuous over two or more spans, then the maximum moment M_{max} occurs over the support. Focusing on the mid-span region, no location experiences moment greater than $0.75M_{max}$. If the joist has an over-hang and the joist had been designed such that the moment over the support is equal to moment at the mid-span (moment optimized two-span joist), then the maximum moment M_{max} occurs over the support and in the mid-span region at $0.41L$. Focusing on the mid-span region, moment greater than $0.75M_{max}$ exists between $0.21L$ and $0.625L$, where L is the span length.

For all other structural span arrangement for the joist, the maximum moment occurs either in the mid-span or at the support. Further more, it can be stated that regardless of the joist structural arrangement, moment more than $0.75M_{max}$ may exist between $0.21L$ and $0.625L$, where L is the span length.

3.8.2 Conclusion

In summary, the shear and moment diagrams (Figures 3.26 and 3.27), show that when there is a opening at the region $0.30L$ from the end-support and $0.375L$ from the intermediate-support, CFS floor joist always need shear reinforcement as shown in Figures 3.18 and 3.21. Thus, these zones can be defined as “Shear Zone”. Presence of opening in the remaining region needs only flexural reinforcement (see Figure 2.23) hence can be defined as “Flexural Zone”. Figure 3.28 shows a clear picture of “Shear Zone” and “Flexural Zone” for a simply supported and a multiple supported floor joist.

Table 3.1: Maximum spans for CFS joists in meter (AISI, 007a)

Floor Joists - Multiple Spans, $F_y = 345$ MPa (50 ksi)

Joist	1.44 kN/m^2 (30 psf) Live Load				1.92 kN/m^2 (40 psf) Live Load			
	Joist Spacing				Joist Spacing			
	0.31 m 12 in	0.41 m 16 in	0.49 m 19.2 in	0.61 m 24 in	0.31 m 12 in	0.41 m 16 in	0.49 m 19.2 in	0.61 m 24 in
550S162-33	4.2	3.7	3.3	2.8	3.7	3.2	2.9	2.5
550S162-43	4.9	4.3	3.9	3.5	4.4	3.8	3.4	3.1
550S162-54	5.5	5.0	4.7	4.2	5.0	4.5	4.1	3.7
550S162-68	5.9	5.4	5.1	4.7	5.4	4.9	4.6	4.2
550S162-97	6.6	6.0	5.6	5.2	6.0	5.4	5.0	4.7
800S162-33	4.7	3.8	3.3	2.8	4.0	3.2	2.7	2.0
800S162-43	6.7	5.8	5.3	4.6	6.0	5.2	4.5	3.8
800S162-54	7.4	6.8	6.3	5.5	6.8	6.0	5.4	4.8
800S162-68	8.0	7.3	6.9	6.4	7.3	6.7	6.2	5.8
800S162-97	8.9	8.1	7.7	7.1	8.1	7.3	6.9	6.5
1000S162-43	7.1	5.8	5.1	4.3	6.1	4.9	4.2	3.5
1000S162-54	8.6	7.3	6.6	5.8	7.5	6.3	5.7	5.5
1000S162-68	9.7	8.8	8.3	7.7	8.8	8.0	7.5	6.9
1000S162-97	10.8	9.8	9.2	8.6	9.8	8.8	8.3	7.7
1200S162-43	6.9	5.6	4.8	4.0	5.8	4.6	4.0	3.2
1200S162-54	9.9	8.5	7.5	6.4	8.8	7.2	6.3	5.4
1200S162-68	11.3	9.8	8.9	7.8	10.1	8.6	7.8	6.8
1200S162-97	12.5	11.4	10.7	9.9	11.4	10.3	9.7	9.0

Notes:

- Table provides the maximum clear span in meter to either side of the interior support.
- Interior bearing supports for multiple span joists shall consist of structural (bearing) walls or beams.
- Bearing stiffeners shall be installed at all support points and concentrated loads.
- Deflection criteria : $L/480$ for live loads, $L/240$ for total loads.
- Floor dead load = 0.479 kN/m^2 (10 psf).
- Interior supports shall be located within 0.61 m (2 feet) of mid-span provided that each of the resulting spans does not exceed the appropriate maximum span shown in the above.

Table 3.2: Shear ratios (Shear Force / Shear Resistance)

Floor Joists - Multiple Spans, $F_y = 345 \text{ MPa}$ (50 ksi)

Joist	1.44 kN/m^2 (30 psf) Live Load				1.92 kN/m^2 (40 psf) Live Load			
	Joist Spacing				Joist Spacing			
	0.31 m 12 in	0.41 m 16 in	0.49 m 19.2 in	0.61 m 24 in	0.31 m 12 in	0.41 m 16 in	0.49 m 19.2 in	0.61 m 24 in
550S162-33	0.56	0.64	0.71	0.74	0.62	0.72	0.78	0.85
550S162-43	0.29	0.34	0.37	0.42	0.33	0.38	0.42	0.47
550S162-54	0.17	0.20	0.22	0.25	0.19	0.23	0.25	0.28
550S162-68	0.10	0.12	0.14	0.16	0.11	0.14	0.16	0.18
550S162-97	0.06	0.07	0.08	0.09	0.07	0.08	0.09	0.11
800S162-33	0.92	0.99	1.03	1.08	0.98	1.05	1.07	1.02
800S162-43	0.59	0.68	0.75	0.80	0.67	0.77	0.81	0.86
800S162-54	0.33	0.40	0.44	0.48	0.38	0.45	0.49	0.54
800S162-68	0.18	0.22	0.24	0.28	0.21	0.25	0.28	0.33
800S162-97	0.07	0.09	0.10	0.12	0.08	0.10	0.12	0.14
1000S162-43	0.79	0.86	0.91	0.96	0.85	0.92	0.96	1.01
1000S162-54	0.48	0.54	0.59	0.64	0.53	0.60	0.65	0.79
1000S162-68	0.27	0.33	0.37	0.43	0.31	0.38	0.43	0.49
1000S162-97	0.10	0.12	0.14	0.16	0.12	0.14	0.16	0.19
1200S162-43	0.94	1.00	1.04	1.09	0.99	1.06	1.09	1.09
1200S162-54	0.67	0.77	0.81	0.87	0.76	0.83	0.87	0.92
1200S162-68	0.38	0.44	0.48	0.53	0.43	0.49	0.54	0.59
1200S162-97	0.15	0.18	0.20	0.23	0.17	0.20	0.23	0.27

Note:

- Total factored load (w_f) = $1.2 * D + 1.6 * L$
- Maximum factored shear force (V_f) = $5/8 * w_f * \text{clearspan} * \text{spacing}$
- Shear resistance factor = 0.95

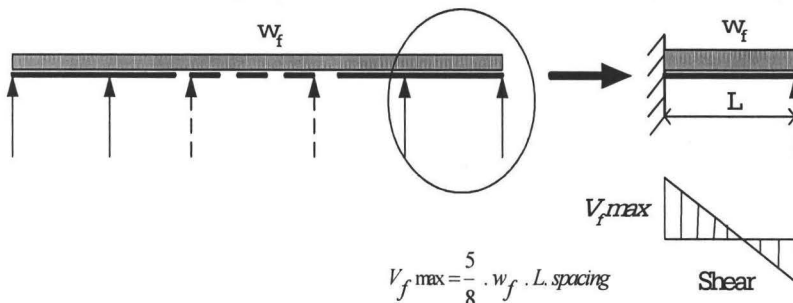


Table 3.3: Measured geometrical dimensions of the CFS joists tested in shear

S.N.	Specimen	D	B_c	B_t	d_c	d_t	t'	t
1	8S-N-1-L	200.98	41.16	40.47	10.92	12.84	1.14	1.12
2	8S-N-1-R	202.06	41.24	40.35	10.88	12.93	1.17	1.12
3	8S-N-2-L	201.70	40.63	40.43	12.96	10.67	1.14	1.10
4	8S-N-2-R	201.16	41.24	40.42	10.84	12.80	1.16	1.12
5	8S-N-3-L	201.70	40.73	40.36	12.88	10.72	1.14	1.12
6	8S-N-3-R	201.88	40.68	40.51	12.84	10.80	1.13	1.09
7	8S-C-1-L	201.08	41.27	40.26	10.95	12.94	1.17	1.12
8	8S-C-1-R	201.38	40.60	40.58	12.83	10.68	1.16	1.12
9	8S-C-2-L	202.32	40.65	40.29	12.95	10.85	1.16	1.12
10	8S-C-2-R	201.16	41.06	40.29	10.74	12.80	1.17	1.12
11	8S-C-3-L	201.26	40.66	40.20	13.04	10.73	1.16	1.10
12	8S-C-3-R	201.46	41.16	40.40	10.79	12.81	1.14	1.10
13	8S-S-1-L	201.12	40.65	40.59	12.97	10.72	1.17	1.12
14	8S-S-1-R	201.36	41.06	40.64	10.65	12.88	1.17	1.13
15	8S-S-2-L	201.08	40.61	40.34	12.73	10.89	1.17	1.13
16	8S-S-2-R	201.48	41.17	40.37	10.47	12.85	1.17	1.12
17	8S-S-3-L	202.04	40.66	40.27	12.76	10.79	1.13	1.10
18	8S-S-3-R	201.48	41.14	40.61	10.43	12.89	1.14	1.12
19	8S-CRA -1-L	201.18	40.67	40.60	12.63	10.91	1.16	1.12
20	8S-CRA-1-R	201.72	40.64	40.58	12.86	10.91	1.14	1.13
21	8S-CRA -2-L	201.13	40.71	40.33	10.76	12.46	1.14	1.12
22	8S-CRA-2-R	201.20	40.77	40.55	12.09	10.62	1.14	1.10
23	8S-CRA -3-L	201.87	40.92	40.58	12.50	10.20	1.16	1.11
24	8S-CRA-3-R	201.24	40.84	40.39	12.46	10.82	1.16	1.11
25	8S-CRB -1-L	201.42	41.13	40.54	10.86	12.88	1.14	1.12
26	8S-CRB-1-R	202.28	40.72	40.48	12.88	10.64	1.14	1.12
27	8S-CRB -2-L	201.51	40.61	40.36	10.07	12.17	1.14	1.12
28	8S-CRB-2-R	201.39	40.70	40.63	10.67	12.60	1.16	1.12
29	8S-CRB -3-L	201.86	41.03	40.37	12.33	10.41	1.15	1.10

Continued on Next Page...

Table 3.3 – Continued

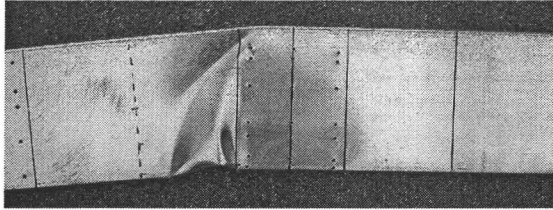
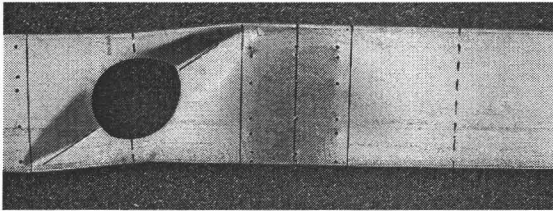
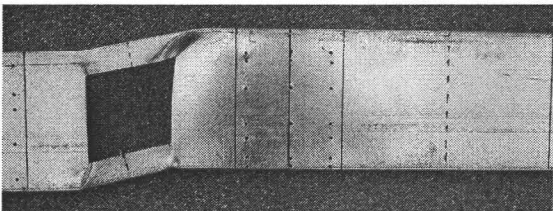
S.N.	Specimen	D	B_c	B_t	d_c	d_t	t'	t
30	8S-CRB-3-R	201.41	40.73	40.49	12.61	10.61	1.15	1.12
31	8S-CRC-1-L	200.76	41.14	40.62	10.46	12.95	1.14	1.10
32	8S-CRC-1-R	201.20	40.63	40.57	12.81	10.66	1.17	1.13
33	8S-CRC-2-L	201.34	41.26	40.58	10.90	12.90	1.16	1.12
34	8S-CRC-2-R	201.80	40.57	40.35	12.88	10.75	1.14	1.10
35	8S-CRC-3-L	202.16	41.33	40.58	10.75	12.84	1.14	1.12
36	8S-CRC-3-R	201.66	40.64	40.70	12.62	10.72	1.14	1.12
37	8S-SRA -1-L	201.56	41.06	40.62	12.82	10.69	1.14	1.13
38	8S-SRA-1-R	201.22	40.51	40.21	12.78	10.86	1.19	1.08
39	8S-SRA -2-L	201.81	40.62	40.42	12.80	10.50	1.15	1.11
40	8S-SRA-2-R	201.96	40.95	40.48	12.07	10.01	1.16	1.12
41	8S-SRA -3-L	201.62	40.92	40.54	12.93	10.99	1.14	1.12
42	8S-SRA-3-R	201.48	40.68	40.33	10.39	12.16	1.14	1.12
43	8S-SRB -1-L	202.32	40.76	40.32	12.88	10.62	1.13	1.10
44	8S-SRB-1-R	202.88	41.23	40.58	10.81	12.83	1.12	1.10
45	8S-SRB -2-L	201.21	40.89	40.55	12.85	10.37	1.16	1.11
46	8S-SRB-2-R	201.73	40.93	40.33	12.65	10.69	1.14	1.12
47	8S-SRB -3-L	201.89	41.00	40.56	12.28	10.23	1.16	1.12
48	8S-SRB-3-R	201.13	40.88	40.61	10.24	12.06	1.16	1.12
49	8S-SRC-1-L	201.56	40.66	40.64	13.10	10.71	1.14	1.12
50	8S-SRC-1-R	201.32	41.34	40.23	10.93	12.76	1.16	1.12
51	8S-SRC-2-L	201.36	40.65	40.71	12.86	10.86	1.14	1.12
52	8S-SRC-2-R	200.98	41.23	40.55	10.82	12.93	1.14	1.10
53	8S-SRC-3-L	201.58	41.25	40.51	10.72	12.85	1.14	1.12
54	8S-SRC-3-R	200.94	40.51	40.32	12.89	10.89	1.16	1.13
Average		201.53	40.88	40.47	11.90	11.51	1.15	1.11
Standard Deviation		0.42	0.25	0.14	1.05	1.05	0.01	0.01

Note: See Figure 3.8 for the symbols.

t' - Overall thickness.

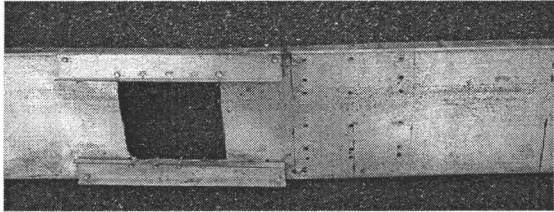
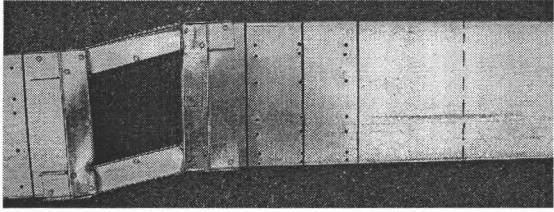
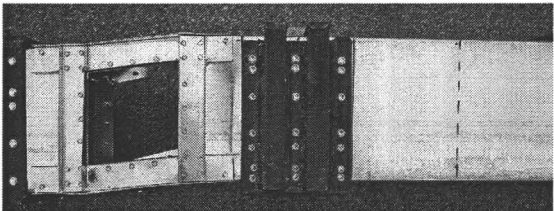
t - Base metal thickness.

Table 3.4: Shear resistance of CFS joists with and without web openings in high shear zones

Section: 800S162-43		$\frac{h}{t} = 180$	$\frac{a}{h} = 1.5$	Nominal Shear Capacity (AISI, 007a), $V_n = 8.81kN$	
Test Designation	Shear at the Opening (kN)	at the Region	Percentage Reduction in Shear Capacity	Sample Pictures	Remarks
8S-N	Test 1:	12.23	0.00%		Primarily shear failure mixed in with flexural failure
	Test 2:	12.56			
	Test 3:	12.49			
	Average:	12.43			
	Std Dev:	0.17			
8S-C	Test 1:	7.37	-40.22%		Shear diagonal failure
	Test 2:	7.45			
	Test 3:	7.48			
	Average:	7.43			
	Std Dev:	0.06			
8S-S	Test 1:	5.10	-58.65%		Shear diagonal failure
	Test 2:	5.27			
	Test 3:	5.06			
	Average:	5.14			
	Std Dev:	0.11			

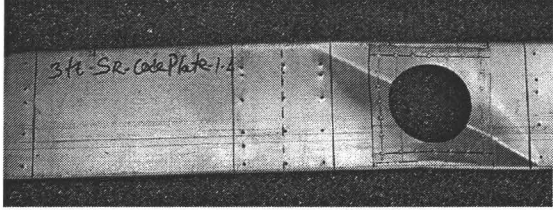
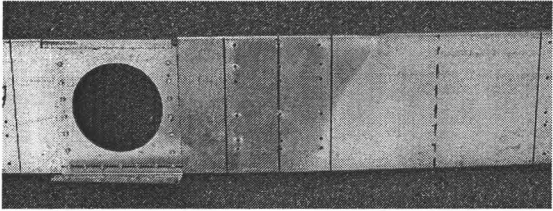
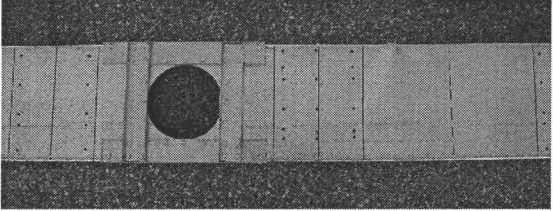
1kN = 0.225 kips

Table 3.5: Trial stages to develop the reinforcement schemes for high shear zones

Section: 800S162-43		$\frac{h}{t} = 180$	$\frac{a}{h} = 1.5$	Nominal Shear Capacity (AISI, 007a), $V_n = 8.81kN - m$
Stages	Reinforcements Detailing	Sample Picture		Observations
Stage: One	Reinforced by 1-1/2"x1/2"-43 mils bridging channels with d/4 (1.25 inch) screw spacing above and below the square openings where, d = width of the square openings, failure load = 5.12 kN.			<i>Observation:</i> Began with diagonal shear buckling at the opening region. No significant recovery in the shear strength. <i>Solution:</i> Change the reinforcement pattern. Vertical reinforcements are expected to prevent from diagonal shear buckling.
Stage: Two	Reinforced by 1-1/2"x1/2"-43 mils bridging channels with d/2 (2.5 inch) spacing around square openings where, d = width of the square openings, failure load = 7.34 kN			<i>Observation:</i> Began with local buckling between the screws, failure was around the opening region. <i>Solution:</i> Decrease the spacing of the screws.
Stage: Three	Reinforced by 1-1/2"x1/2"-43 mils bridging channels with d/4 (1.25 inch) spacing around square openings where, d = width of the square openings, failure load = 8.44 kN			<i>Observation:</i> Failure was around the opening region. <i>Solution:</i> Increase the size of the reinforcement to increase over all stiffness of the reinforcements.

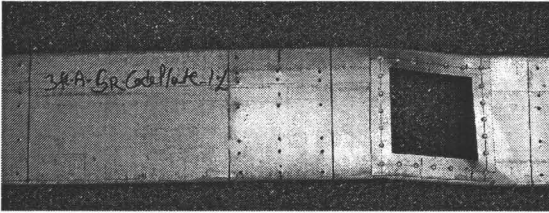
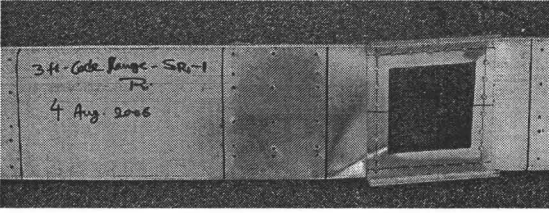
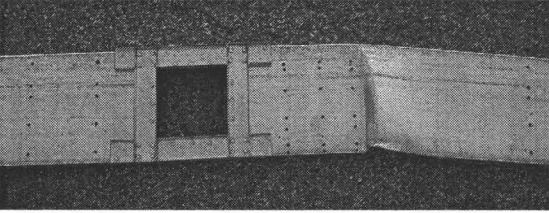
$1kN = 0.225 kips$

Table 3.6: Shear resistance of CFS joists with reinforced circular web opening in high shear zones

Section: 800S162-43		$\frac{h}{t} = 180$	$\frac{a}{h} = 1.5$	Nominal Shear Capacity (AISI, 007a), $V_n = 8.81kN$	
Test Designation	Shear at the Opening (kN)	at the Region	Percentage Reduction in Shear Capacity	Sample Pictures	Remarks
8S-CRA	Test 1:	11.52	-7.32%		Shear diagonal failure at the opening region
	Test 2:	11.12			
	Test 3:	11.06			
	Average:	11.52			
	Std Dev:	0.25			
8S-CRB	Test 1:	12.46	+0.24%		Shear diagonal failure at opening + shear-flexural failure out of the opening region
	Test 2:	12.05			
	Test 3:	11.98			
	Average:	12.46			
	Std Dev:	0.11			
8S-CRC	Test 1:	12.77	+4.18%		Shear + flexural failure out of the opening region
	Test 2:	12.86			
	Test 3:	13.22			
	Average:	12.95			
	Std Dev:	0.24			

$1kN = 0.225 kips$

Table 3.7: Shear resistance of CFS joists with reinforced square web opening in high shear zones

Section: 800S162-43		$\frac{h}{t} = 180$	$\frac{a}{h} = 1.5$	Nominal Shear Capacity (AISI, 007a), $V_n = 8.81kN$	
Test Designation	Shear at the Opening Region (kN)	at the Region	Percentage Reduction in Shear Capacity	Sample Pictures	Remarks
8S-SRA	Test 1:	8.40	-35.00%		Shear diagonal failure at opening region
	Test 2:	8.22			
	Test 3:	7.63			
	Average:	8.08			
	Std Dev:	0.40			
8S-SRB	Test 1:	9.25	-31.57%		Shear diagonal failure at opening region
	Test 2:	8.11			
	Test 3:	8.18			
	Average:	8.52			
	Std Dev:	0.64			
8S-SRC	Test 1:	12.44	+0.56%		Shear + flexural failure out of opening region
	Test 2:	12.61			
	Test 3:	12.47			
	Average:	12.50			
	Std Dev:	0.09			

$1kN = 0.225 kips$

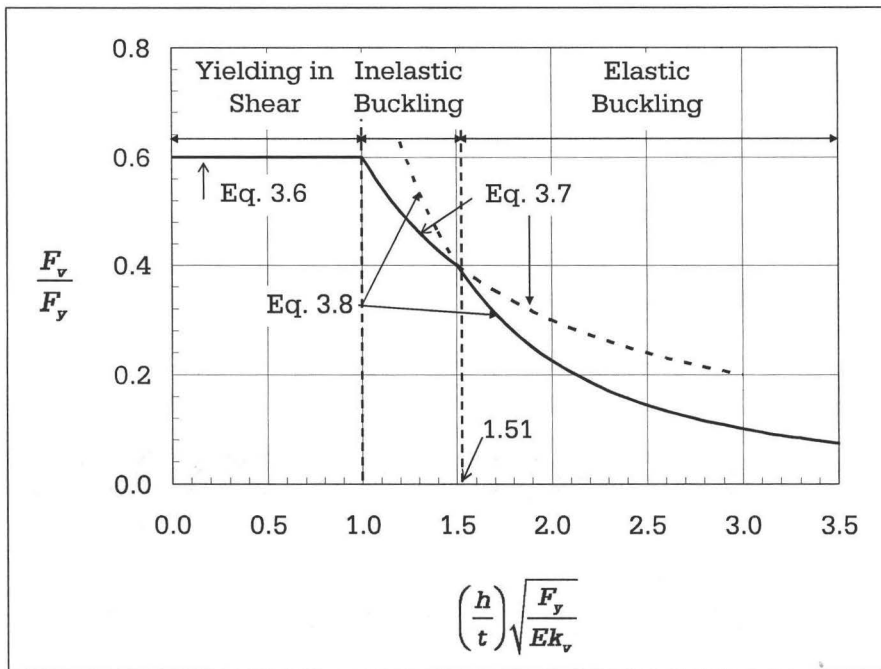


Figure 3.1: Nominal shear stress variation with slenderness (AISI, 2007)

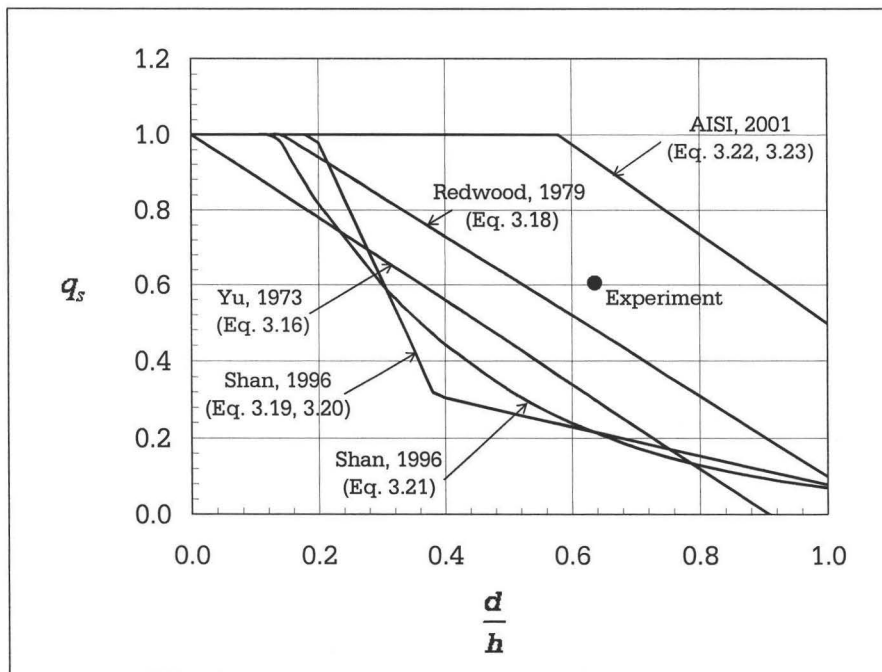


Figure 3.2: Shear resistance reduction factor for the joists having circular web openings

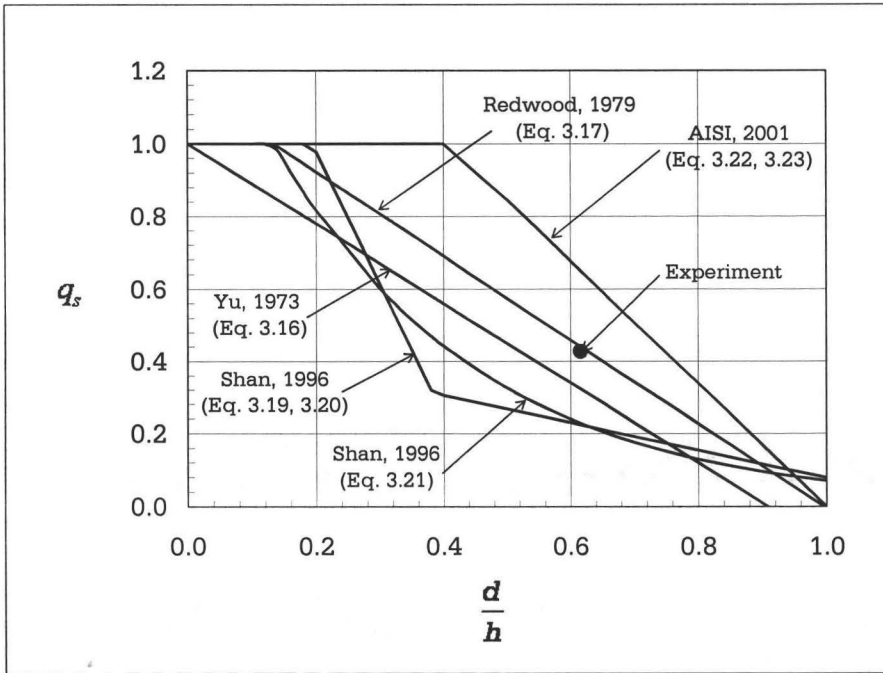


Figure 3.3: Shear resistance reduction factor for the joists having square web openings

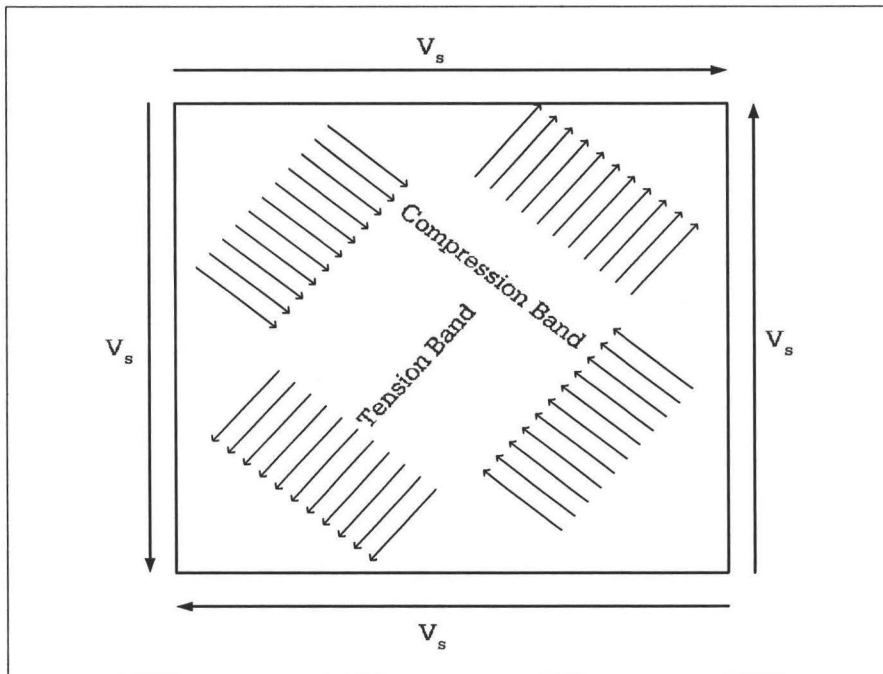


Figure 3.4: Web of CFS joists subjected in shear forming compression and tension band along the diagonals

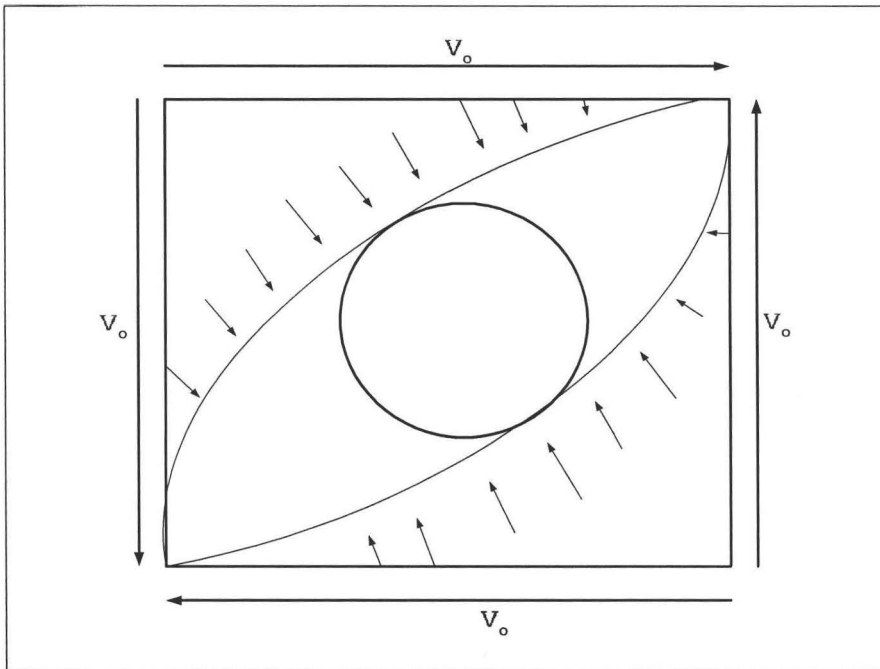


Figure 3.5: Shear buckling of the web of CFS joists having opening

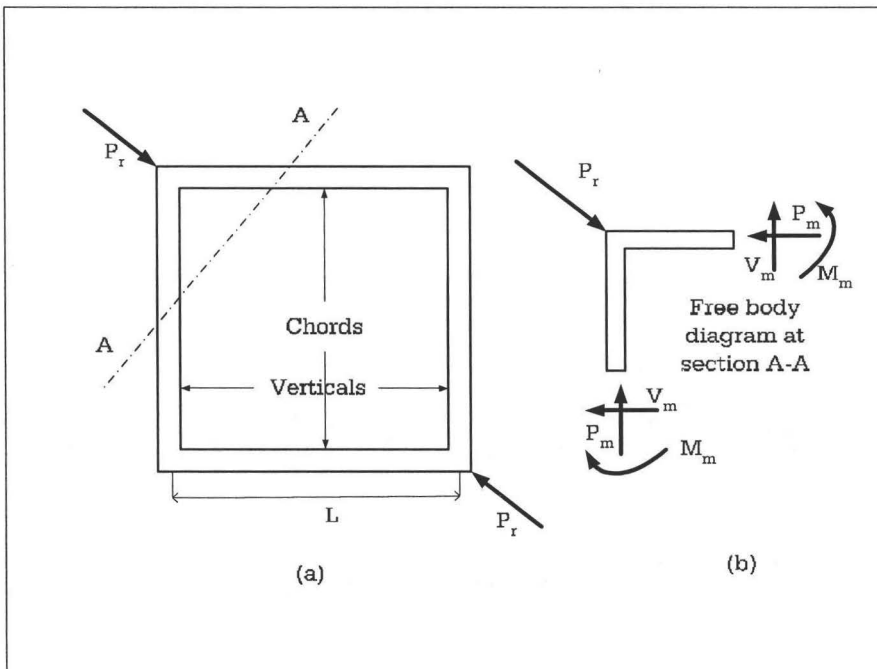


Figure 3.6: Shear reinforcement (a) Vierendeel truss (b) Vierendeel action

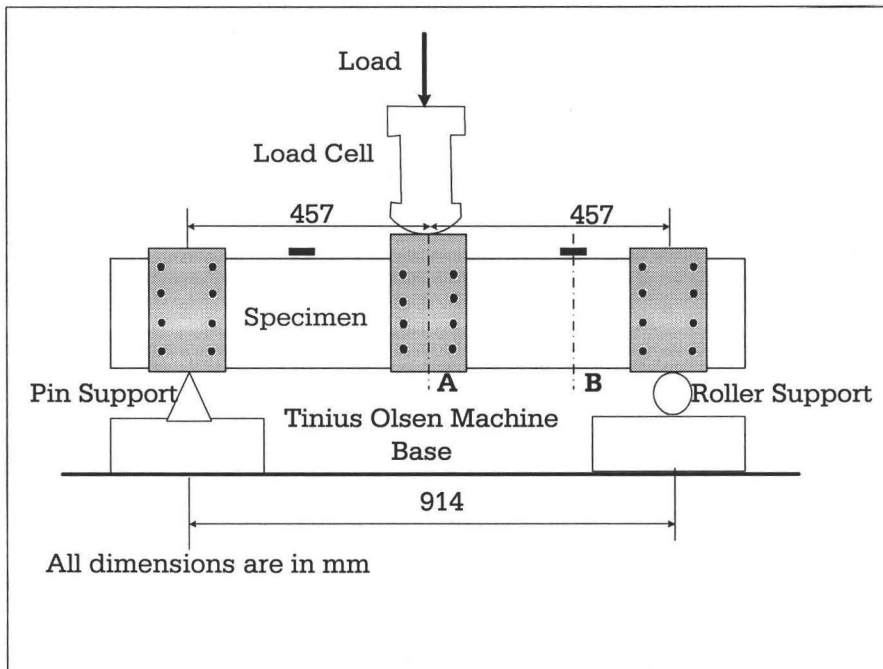


Figure 3.7: Test setup for shear test

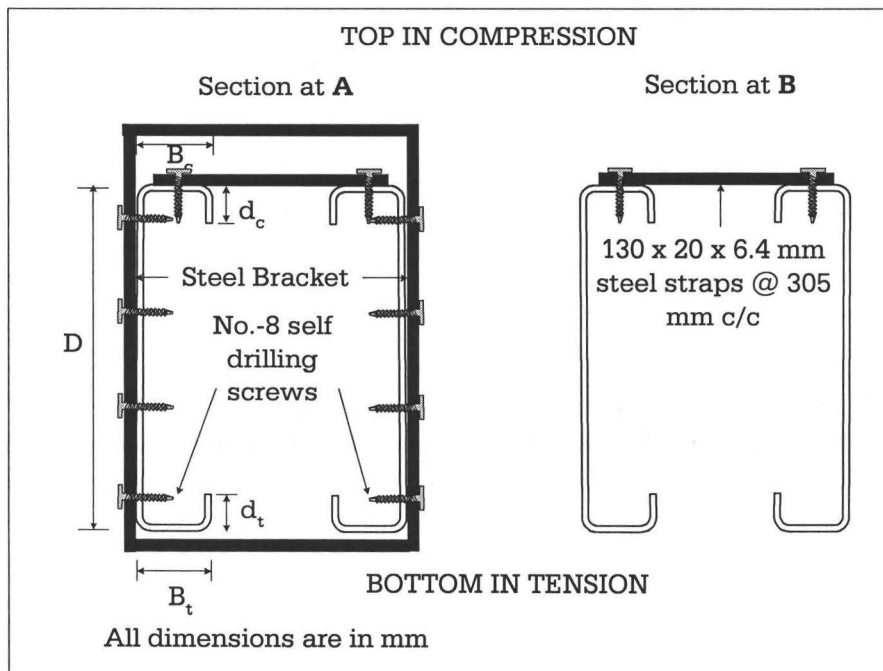


Figure 3.8: Section at A and B

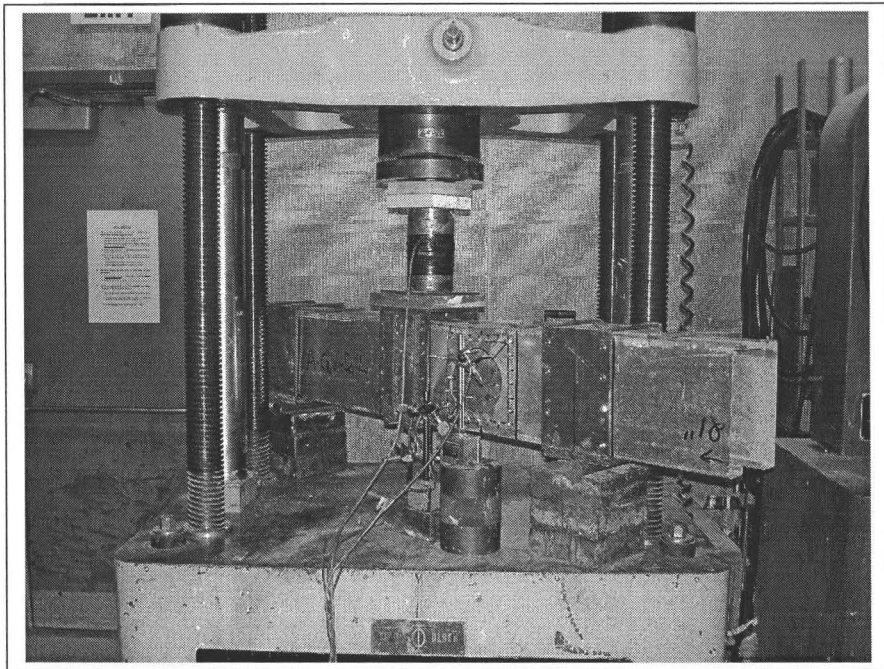


Figure 3.9: Test setup picture for shear test

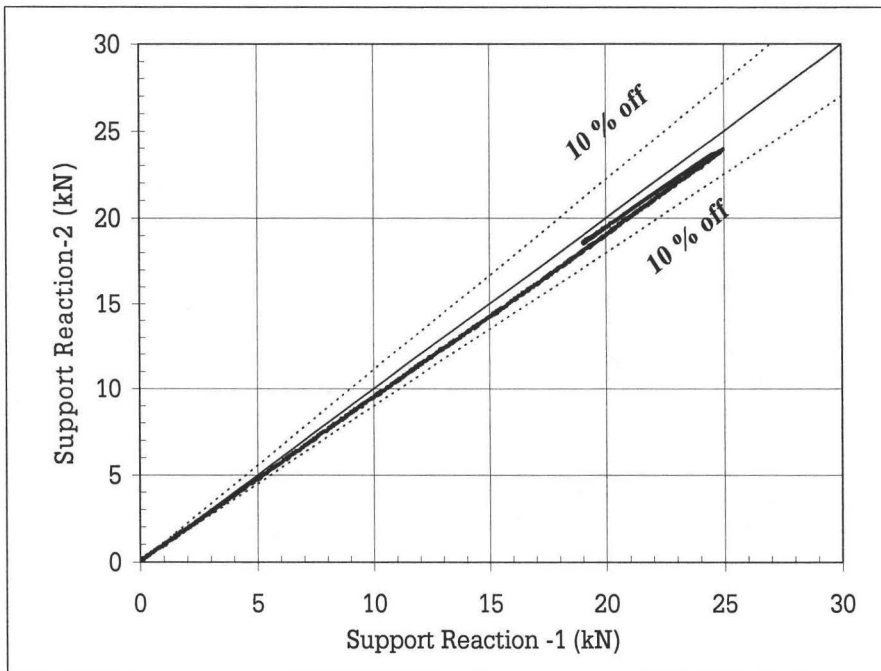


Figure 3.10: Comparative plot for two support reactions

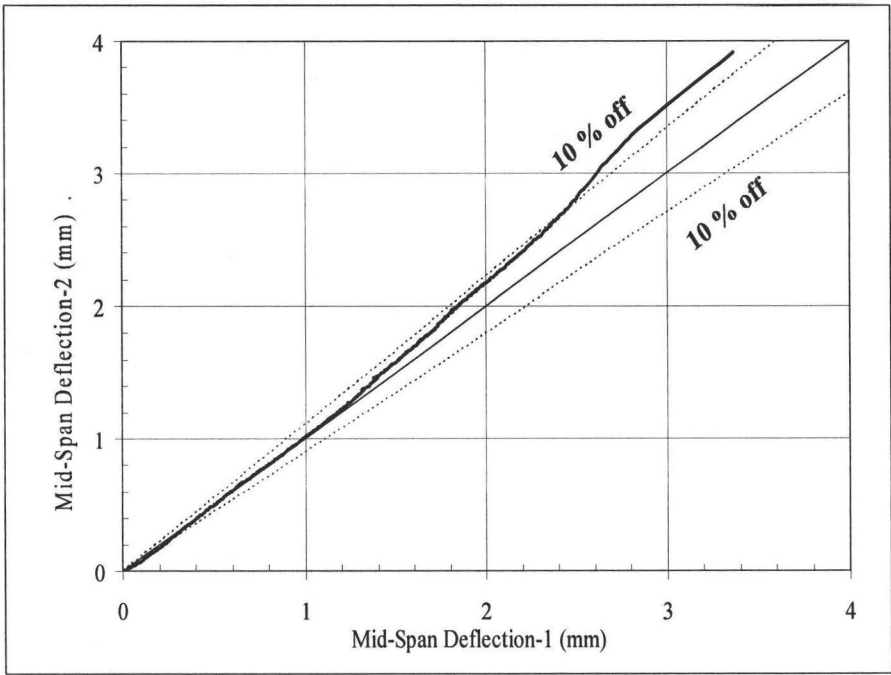


Figure 3.11: Comparative plot for two mid-span deflections

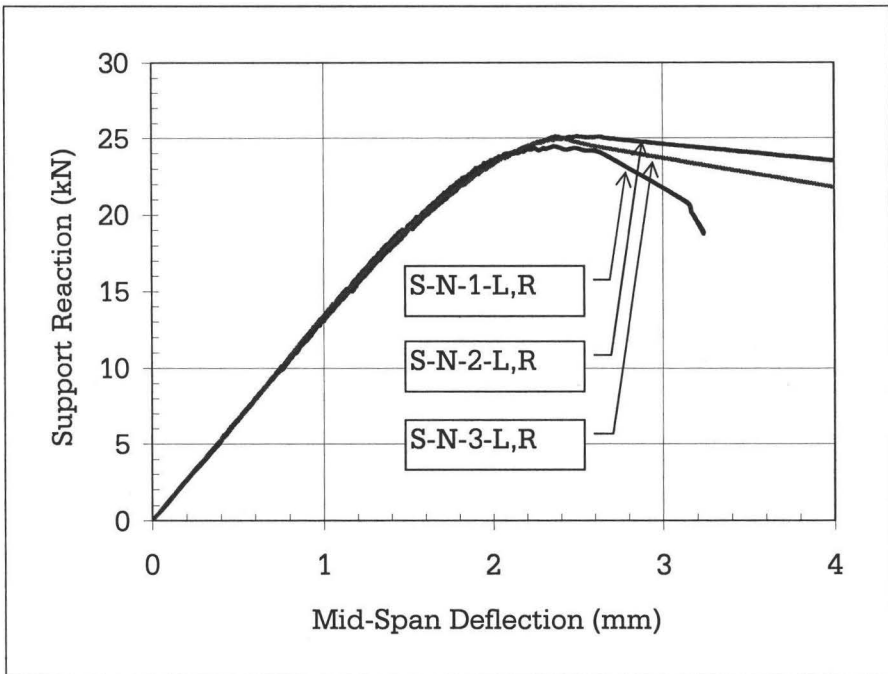


Figure 3.12: Load displacement curve for solid joists in shear

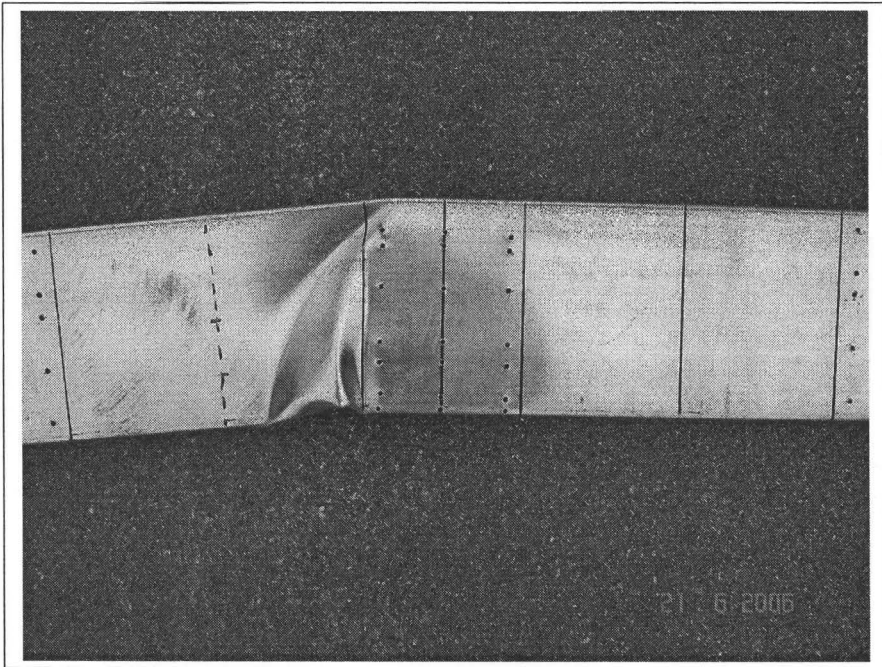


Figure 3.13: Typical failure of solid joists ($a/h = 1.5$)

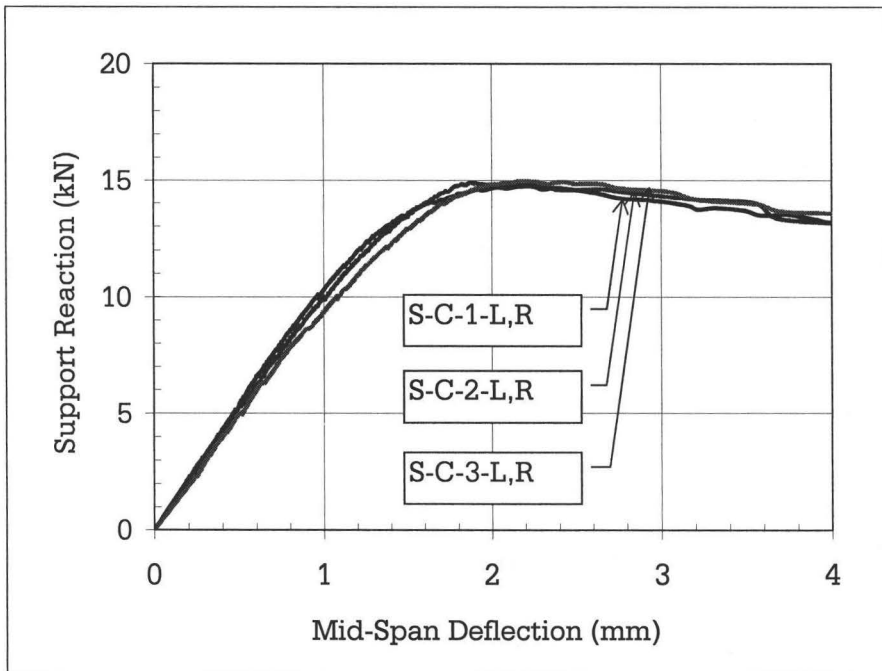


Figure 3.14: Sample test result for the shear test of joists having circular web openings

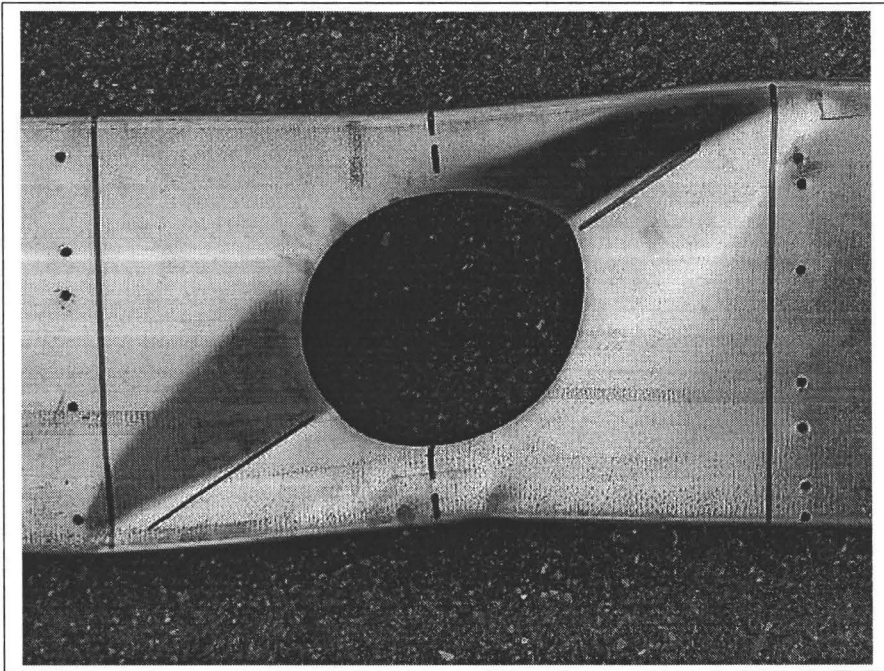


Figure 3.15: Diagonal shear buckling failure for the joists having circular web opening

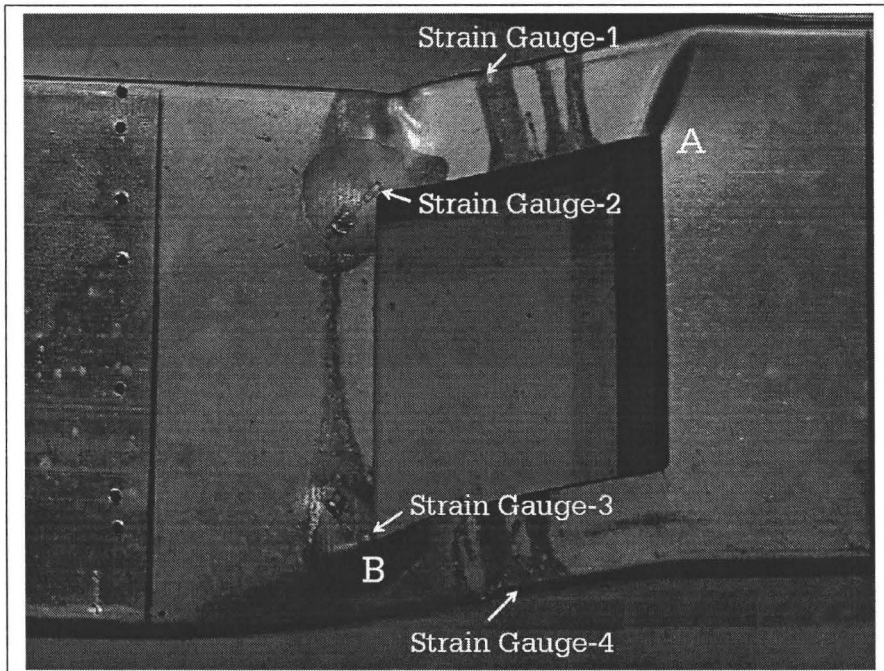


Figure 3.16: Typical diagonal shear failure of joists having square web openings

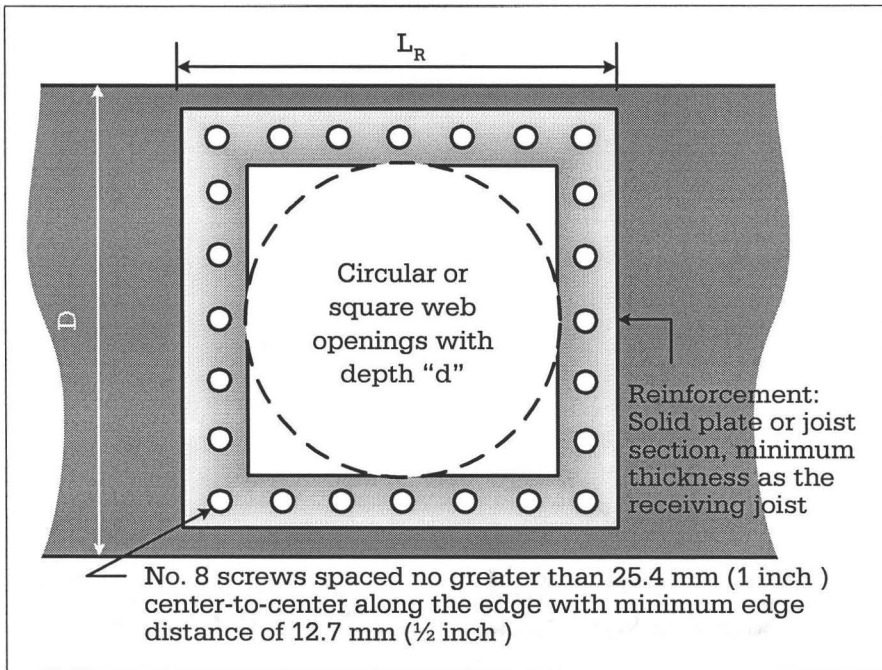


Figure 3.17: Shear reinforcement schemes "A" and "B" (AISI, 007a)

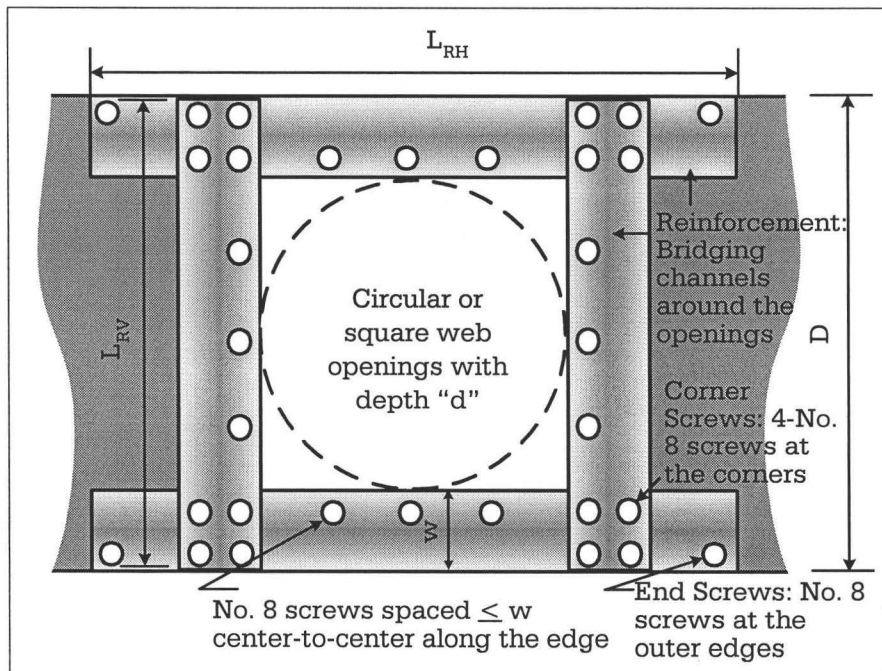


Figure 3.18: Shear reinforcement scheme "C" (Current study)

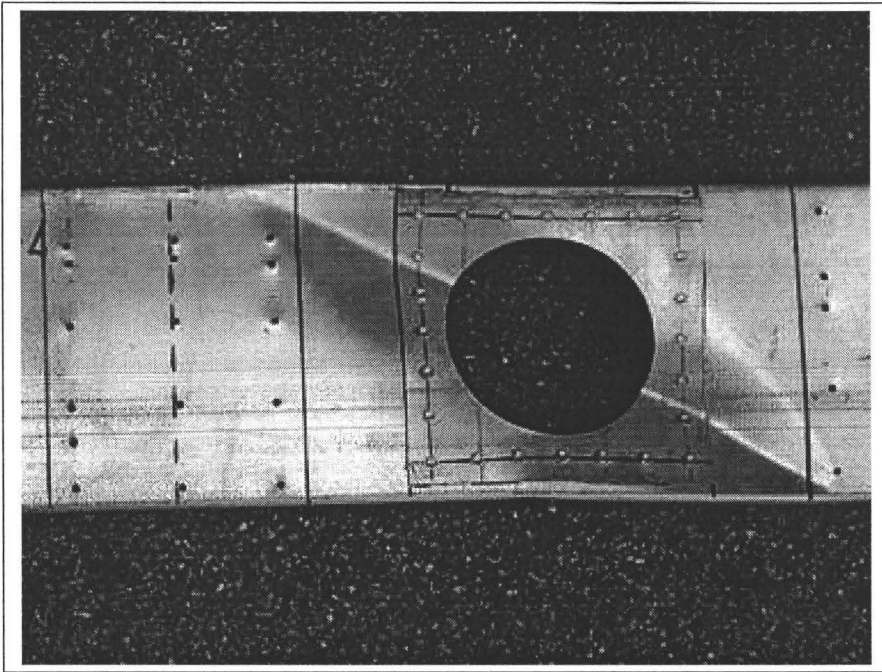


Figure 3.19: Typical shear failure of joists having reinforced (Scheme-A) web openings

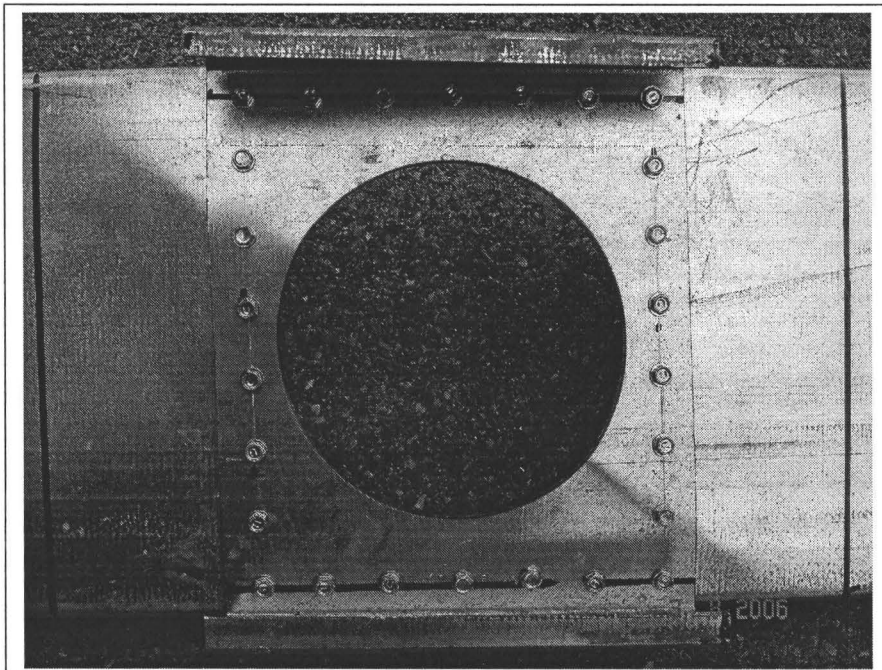


Figure 3.20: Typical shear failure of joists having reinforced (Scheme-B) web openings

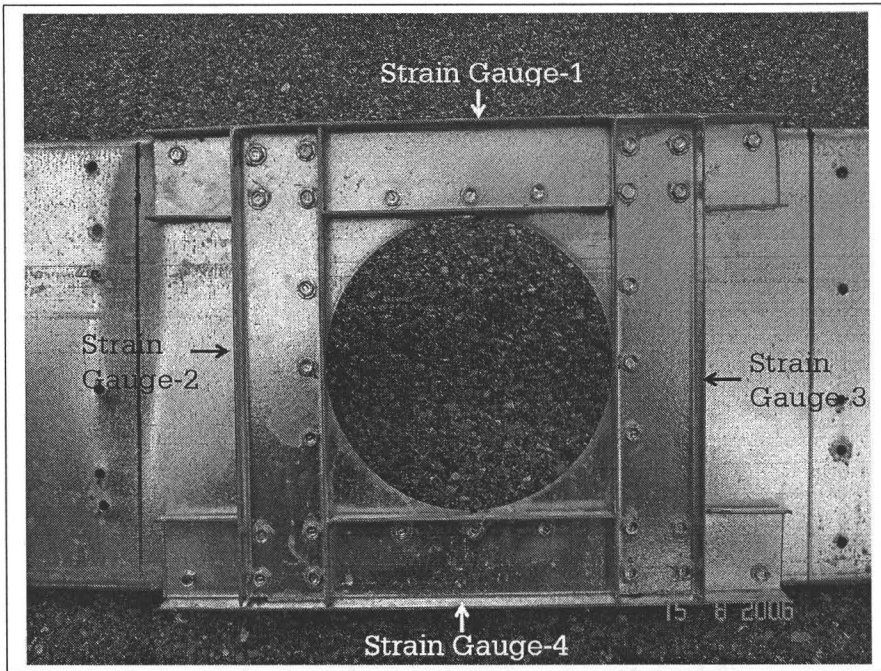


Figure 3.21: Typical failure of joists having reinforced (Scheme-C) web openings

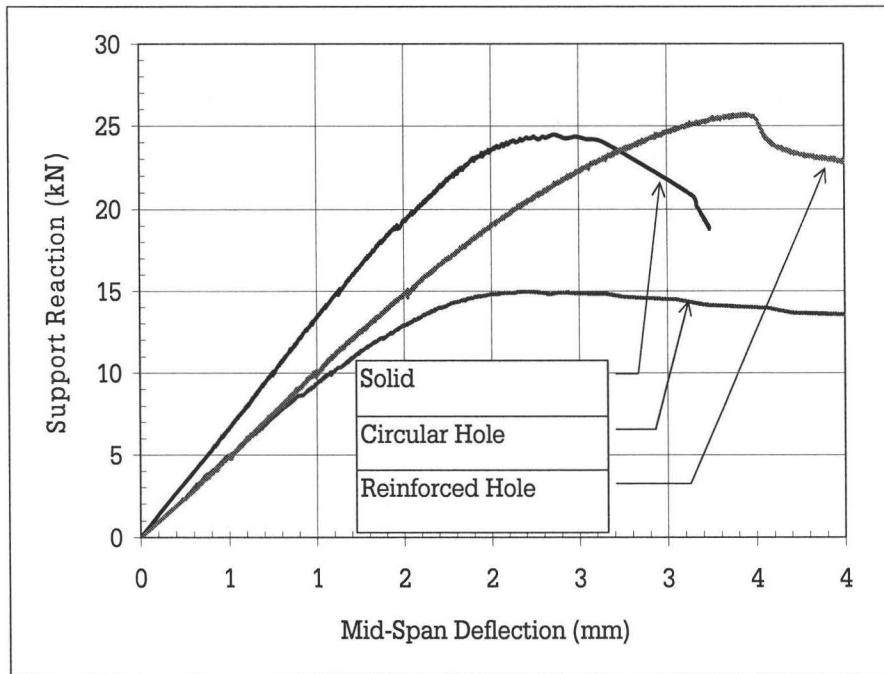


Figure 3.22: Comparison of reinforced and unreinforced (circular openings) specimens with solid specimen in shear

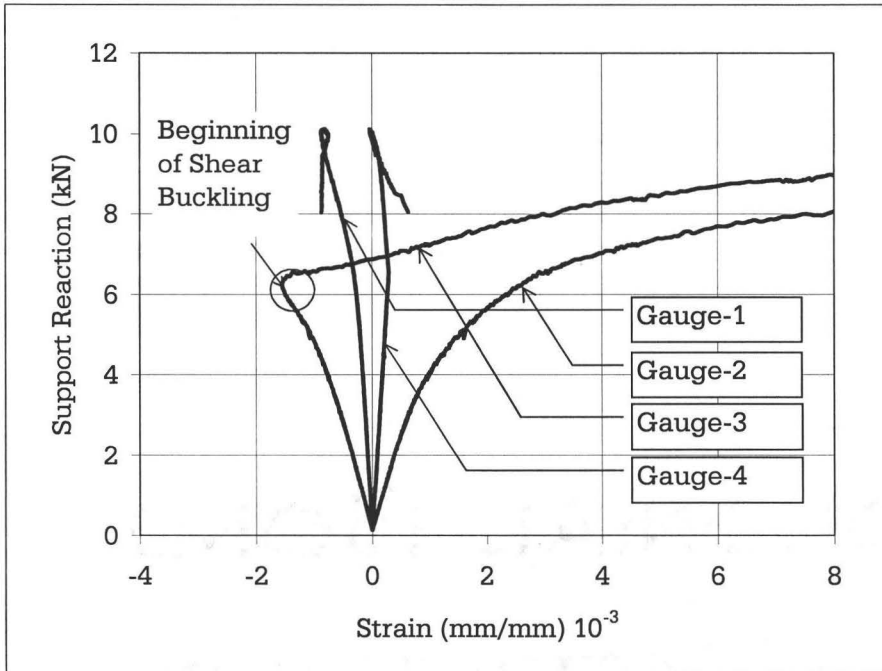


Figure 3.23: Strain measurements on the joist having square web openings in shear test

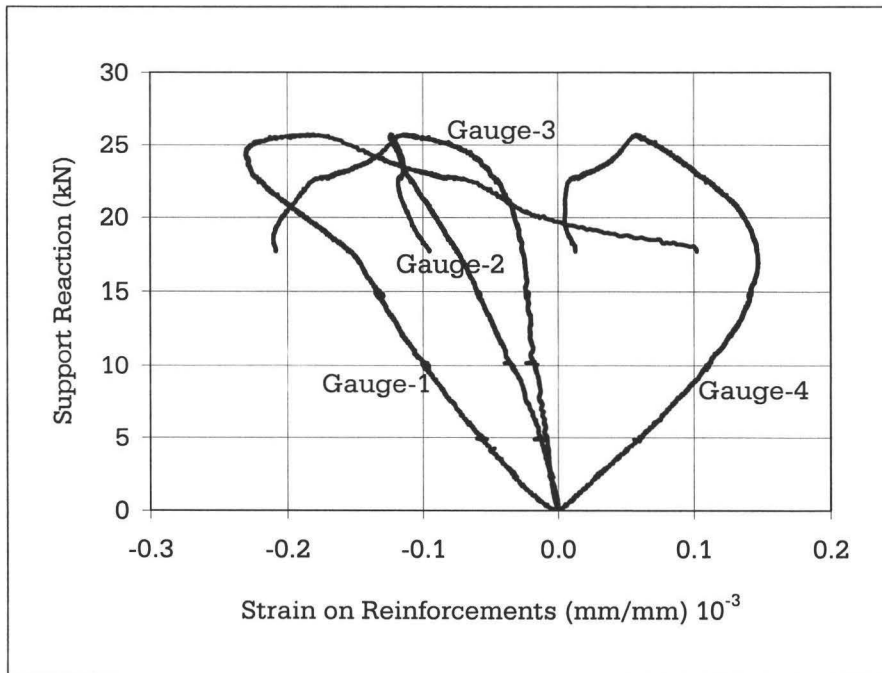


Figure 3.24: Strain measurements on the reinforcements of joists having circular web openings in shear test

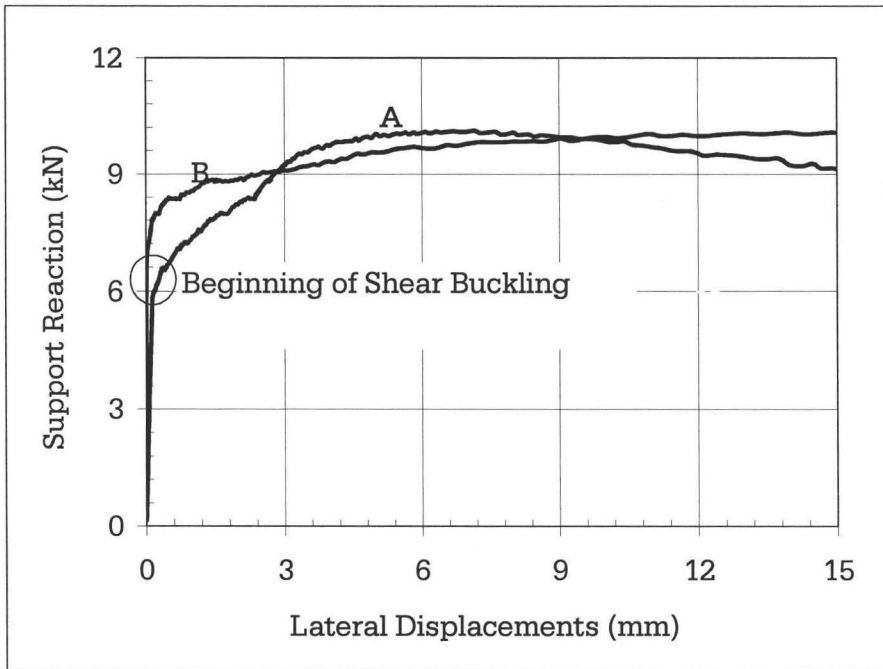


Figure 3.25: Typical lateral displacement measurements of joists having square web openings in shear test

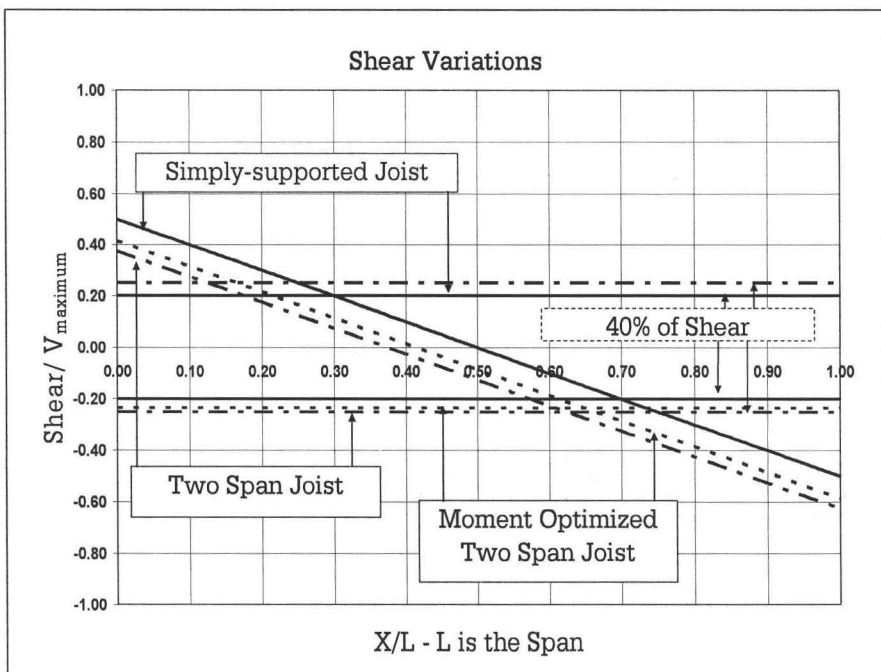


Figure 3.26: Shear variations on floor joist

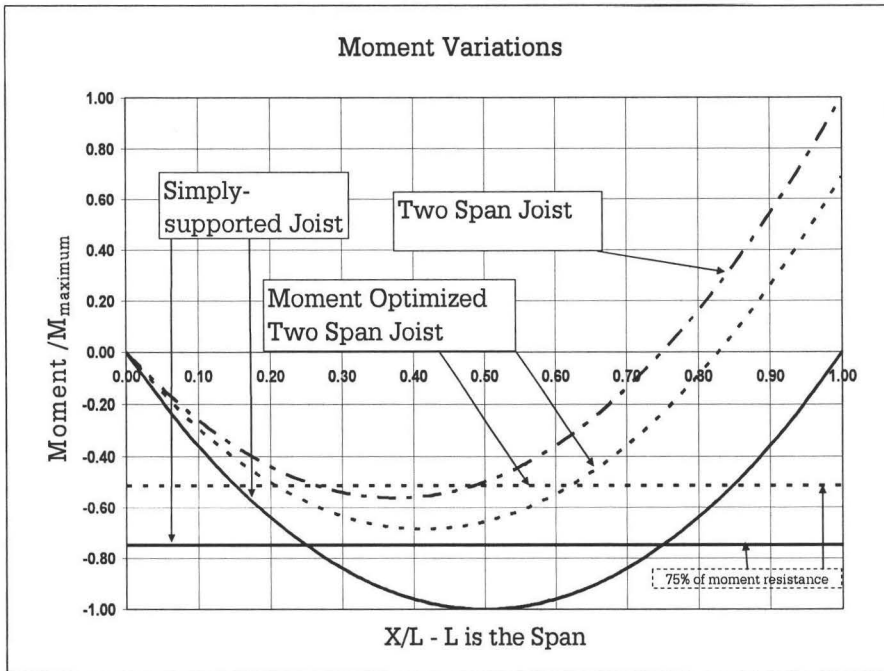


Figure 3.27: Moment variations on floor joist

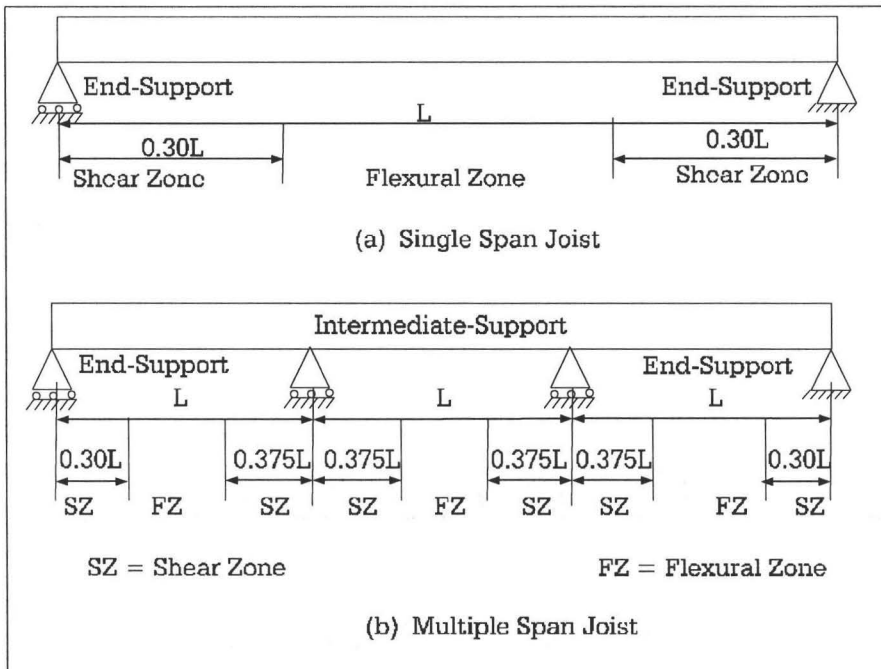


Figure 3.28: Shear zone and flexural zone for a floor joist

Chapter 4

Finite Element Models for Lap Connections in Thin Walled Members

4.1 Introduction

Welding and mechanical fastening are the common types of connections in steel construction. The behavior of connections in thin walled steel members, such as cold-formed steel members, is however, different from that of the connections in hot-rolled steel constructions, primarily because of the thinness of the connected parts. Though thin-walled members may be welded together, mechanical connections for such members are convenient and are thus widely used. Mechanical fasteners include screws, bolts and nuts, blind rivets and short pins. The behaviors of screw connections and bolt connections associated with the cold-formed steel members are influenced by the low plate stiffness. The mechanisms that play important role in the behavior of cold-formed steel connections are tilting of fasteners in the hole, pull-over of the screws, distortion of the sheet metal around the hole in tension, etc.

Most of the previous studies on screw connections and bolted connections were carried out focusing on the ultimate strength of connections experiencing various

failure modes (Winter, 1956; Fan et al., 1997; Kim and Yura, 1999; Aceti et al., 2004; Kim and Kuwamura, 2007). These studies concentrated on the stress and strain state in the vicinity of the screws or bolts, screw/bolt-plate interaction, friction between plates, effect of grips of bolts, effect of bolt tightening on the connection, etc. Therefore, previously proposed finite element models focused on detailed modeling of the connection region. Such a model may be effective for a comprehensive study of a connection associated with various mechanical parts or for a comprehensive study of a structural connection in which the strength of the overall structure is governed by the strength of a particular connection. However, structural engineers frequently encounter structures with large number of connections, where the connections may not be the weakest link, and that the member failure may determine the strength of the structure. Screw fastened reinforcements, screw fastened web stiffeners, and screw fastened sheet metal flooring are some of the examples of such type of connections. In such connections the stiffness of the connection plays a larger role on the strength behavior of the structure rather than the strength of the connections itself. Detail modeling of large number of such connections is not only very tedious and time consuming but also may cause difficulties in the numerical convergence because of the large number of nonlinearities involved. Therefore, it is advantageous to develop a simplified finite element model of a connection which accurately captures the joint stiffness, without much regard to the joint failure modes, stress state, and strain state in the vicinity of the screws or bolts.

This chapter discusses the simplified finite element models for cold-formed steel member connections using self-drilling screws and bolts. ADINA, a finite element analysis program (ADINA, 2001) was used for the analysis. The connections considered herein were lap connections of two plates using self-drilling screws and bolts. Two types of modeling techniques for screw/bolt connections were investigated. The

finite element models built herein were validated against corresponding experimental results.

4.2 Self-Drilling Screw Connection

4.2.1 General

Self-drilling screws are externally threaded fasteners with the ability to self drill and form their own internal threads. A picture of self-drilling screws is shown in Figure 4.1. Self-drilling screws are normally made with carbon steel plated with zinc for corrosion protection or stainless steel with carbon steel drill point and plated with zinc for lubrication. Use of self drilling screws has become popular because of their various advantages. Self drilling screws drill holes themselves, form mating thread and clamp two or more elements in one easy operation. The fastening process does not need power drills and drill bits. Furthermore it does not require elaborate and costly press tools, machine taps and associated maintenance. The tool required is a screw driver. Self drilling ensures correct hole size every time, resulting in better thread engagement and tighter clamp. In summary, self-drilling screws can provide a rapid, effective and economical mean to fasten cold-formed steel members and structures. It is no wonder that the self drilling screw connections are very popular in connecting thin structural and non-structural elements such as cold-formed steel construction.

4.2.2 Modes of Failure

The failure modes associated with the screw connections in cold-formed steel members can be categorized into two types: plate (main member) failure and screw failure. Plate failure includes: net section failure, bearing failure of the plate and pull-over

of the plate. Screw failure consists of shear failure of screws, pull-out failure and excessive screw tilting. A brief introduction to these failure modes is given below.

Net Section Failure: The net section failure is characterized by the fracture of the connected plate across the screw holes perpendicular to the loading direction. The AISI Standard (AISI, 2007) has the following provision to calculate the net section failure.

$$P_n = A_{net}F_u \quad (4.1)$$

where, P_n is nominal load capacity, A_{net} is net cross sectional area and F_u is ultimate strength of the material.

Bearing Failure of Plate: The connection may experience bearing failure, which is essentially piling up of steel sheet in front of the screws. Studies indicate that the bearing strength of the connected plate depends on: the thickness of plates, the tensile strength of the connected plates, and the F_u/F_y ratio of the connected part. The AISI Standard (AISI, 2007) provision to calculate the bearing failure is given as:

$$P_n = m_f C d t F_u \quad (4.2)$$

where, P_n is nominal load capacity, m_f modification factor for the type of bearing connection, C is bearing factor, t is the thickness of the connected plate, d is diameter of the screw and F_u is ultimate strength of the material.

Pull-Over: The pull-over mode of failure occurs only in thin metal connections. The thin plate wraps itself around the head of the screw and tears and pulls over the screw head. AISI Standard (AISI, 2007) gives the following provision to calculate pull-over strength.

$$P_{nov} = 1.5tdF_u \quad (4.3)$$

Where, t is the thickness of the connected plate in contact with the screw head, d is the larger of screw head diameter and washer diameter, and F_u is the tensile strength of the plate in contact with screw head. To increase the pull-over strength, flat washers under the screw head are often used thus increasing the thin plate effective area participating in the pull-over mechanism.

Shear Strength of Screws: A screw lap connection transfers the load from one plate to another plate by means of shear in screws. As per AISI Standard (AISI, 2007), the nominal shear strength of the screw shall be calculated as follows:

$$P_{ns} = 0.8P_{ss} \quad (4.4)$$

Where P_{ns} is the nominal shear capacity per screw and P_{ss} is the nominal shear strength of screws, as reported by the manufacturer, which is determined by independent laboratory testing.

Pull-Out Strength of Screws: : Screw pull out from the thin plate base is termed as Pull-Out mode of failure. The often stated reasons of pull-out failure are: inadequate stiffness of connected thin plate to grab the screw thread around the opening, shearing of screw threads and pulled out, and elongation of screw and eventual breaking in tension. The nominal pull-out strength of a screw is given by AISI Standard (AISI, 2007) as:

$$P_{not} = 0.85tdF_u \quad (4.5)$$

Where, t is the least thickness of the connected plate, d is the nominal screw diameter, F_u is the tensile strength of the plate which is not in contact with screw head.

Screw Tilting: Because of inherent eccentricity associated with the lap connection, the screw is always subjected to tilting action. For thick plate connections, the screw tilting is controlled by yield strength of the connected plate. However, for thin plate connections, screw tilting is controlled by the plate thickness (bending stiffness around the openings). Tilting of the plate often triggers the screw pull-out and pull-over failures.

4.3 Finite Element Modeling

4.3.1 Physical Actions in Lap Connections

In order to develop an accurate finite element model, first of all, it is necessary to identify all possible physical actions involved within the structure under consideration. Some of the other important factors to be considered in finite element modeling are: boundary conditions, load paths, large displacement of any structural part because of buckling/bending/rotation, and contact actions. The following actions are dominant in a lap screwed or a lap bolted connection.

Shear Transformation: The main function of a structural connection is to transfer a load from one structural part to another structural part. Depending on the type of connection and types of applied load, the connecting elements such as screws, bolts, rivets, welds, etc. may be subjected to compression, tension, shear, torsion and bending. In lap connections the load is transferred into another plate primarily by means of shear transfer through the screws.

Screw-to-Plate Contact: Load from the plate to the screws is primarily transferred through a direct contact action. A 3-D no penetration contact surface element available in ADINA (2001) was used to incorporate such contact actions between the plate and the screw.

Plate-to-Plate Contact: In a lap joint, two plates are fastened together. Such plates make two parallel planes. When the lap joint is subjected to tensile loading, these two parallel planes would attempt to align themselves into a single plane. In such a process, the two plates would begin to come into contact with each other. A 3-D no penetration contact surface element was also used to handle such contact action between the main connecting plates.

Screw Tilting: Eccentricity of the lap connection would cause tilting of screws. Screw tilting decreases the overall stiffness of the connection.

Curling: The out of plane deformation of the free end of the connection is known as curling. Effects of curling on the ultimate strength of a connection has been discussed in various studies (Chong and Matlock, 1975; Winter, 1956; Kim and Kuwamura, 2007). In the first two studies the experiments demonstrated considerable curling or bending of ends out of original plane. However it was also suggested that the load carrying capacity of a light-gauge steel connection may not be significantly affected by curling. However, another study (Kim and Kuwamura, 2007) showed that the reduction of ultimate strength of curled specimen may be about 4-25 percent compared with the specimen restrained against curling. It was also reported that curling has a considerable effect on the ultimate strength of connections and should be considered in estimating the ultimate strength. The effect of curling on the connection stiffness was also incorporated in this study.

4.3.2 Finite Element Formulations

The connection problem in thin-walled structures such as cold-formed steel is small strain and large deformation problem. The Total Lagrangian formulation can be used for such small strain and large deformation problem (Bathe, 1996). The Total Lagrangian formulation includes all kinematic non-linear effects due to large displacements and rotations, but small strains. In this formulation, all the current static and kinematic variables at time t are referred to the initial configuration before deformation (at time $t = 0$). The equilibrium condition in incremental term is now introduced by means of the virtual work equation.

$$\int \mathcal{C}_{ijkl} \, {}_0\Delta\varepsilon_{kl} \, \delta_0\Delta\varepsilon_{ij} \, dv + \int {}^tS_{ij} \, \delta_0\Delta\eta_{ij} \, dv = \delta W - \int {}^tS_{ij} \, \delta_0\Delta\varepsilon_{ij} \, dv \quad (4.6)$$

Where δW is the external incremental virtual work at the current time t . The ${}_0\Delta\varepsilon_{ij}$ can be divided into a linear part ${}_0\Delta\varepsilon_{0ij}$ and an initial displacement part ${}_0\Delta e_{ij}$ as follows.

$${}_0\Delta\varepsilon_{ij} = {}_0\Delta\varepsilon_{0ij} + {}_0\Delta e_{ij} = \frac{1}{2}({}_0\Delta u_{i,j} + {}_0\Delta u_{j,i}) + \frac{1}{2}(\mathcal{U}_{k,i} \, \mathcal{U}_{k,j} + \mathcal{U}_{k,i} \, \mathcal{U}_{k,j}) \quad (4.7)$$

${}^tS_{ij}$ is the stress at time t referred to the initial configuration. The incremental stress is defined as:

$${}_0\Delta S_{ij} = \mathcal{C}_{ijkl} \, {}_0\Delta\varepsilon_{kl} \quad (4.8)$$

The non-linear incremental strain ${}_0\Delta\eta_{ij}$ can be expressed as:

$${}_{0}\Delta\eta_{ij} = \frac{1}{2}({}_{0}u_{k,i} \quad {}_{0}\Delta u_{k,j}) \quad (4.9)$$

By substituting Equations 4.7, 4.8 and 4.9 in Equation 4.6 and by realizing the virtual displacements $\delta\Delta u$ are arbitrary displacements, the incremental virtual work equation can be written in a matrix form as follows:

$$\int {}_{0}B^T D_{ep} \quad {}_{0}B \quad dv + \int {}_{0}B_{NL}^T S \quad {}_{0}B_{NL} \quad dv = {}_tR - \int {}_{0}B^T S dv \quad (4.10)$$

D_{ep} represents the idealized elasto-plastic stress-strain relationship of cold-formed steel. The incremental strain-displacement matrix ${}_{0}B$ consists of the small deformation matrix ${}_{0}B_0$ and the initial displacement matrix ${}_{0}B_L$ associated with ${}_{0}\Delta\varepsilon_0$ and \mathcal{E}_0 , respectively. Therefore the matrix ${}_{0}B$ is defined as,

$${}_{0}B = {}_{0}B_0 + {}_{0}B_L \quad (4.11)$$

By substituting Equation 4.11 into 4.10 and collecting the corresponding terms, the finite element incremental equation can be obtained as:

$$[K_0 + K_L + K_{NL}] \Delta d = {}_tR - f \quad (4.12)$$

Where, R and f are current external force and internal force, respectively. Internal force is taken from previous iteration. The three stiffness matrixes are defined as:

Small displacement stiffness matrix:

$$K_0 = \int {}_{0}B^T D_{ep} \quad {}_{0}B \quad dv \quad (4.13)$$

Initial displacement stiffness matrix:

$$K_L = \int \mathbf{0}B^T D_{ep} \mathbf{0}B_L \mathbf{0}dv + \int \mathbf{0}B_L^T D_{ep} \mathbf{0}B_L \mathbf{0}dv + \int \mathbf{0}B_L^T D_{ep} \mathbf{0}B_0 \mathbf{0}dv \quad (4.14)$$

and

Large displacement stiffness matrix:

$$K_{NL} = \int \mathbf{0}B_{NL}^T S \mathbf{0}B_{NL} \mathbf{0}dv \quad (4.15)$$

4.3.3 Shell Elements

A shell element can be obtained by superimposing the plate bending behavior and the plane stress (membrane) behavior. Since the plate element has three degrees of freedom and plane stress (membrane) element has two degrees of freedom, the resulting shell element would have five degrees of freedom. Figure 4.2 shows the degrees of freedom for a node of plate, plane stress and shell elements. Let K_B and K_M be the stiffness matrices corresponding to bending and membrane behavior of the element, respectively then the shell element stiffness matrix K_S is given as (Bathe, 1996):

$$K_s = \begin{bmatrix} K_B & 0 \\ 0 & K_M \end{bmatrix} \quad (4.16)$$

The detail procedure of shell element formulation for the elements used in this study can be found in the literature (Bathe, 1996).

4.3.4 Contact Elements

Contact surfaces are defined as surfaces that are initially in contact, or are anticipated to come into contact during the response solution. Plate to plate or plate to screw contacts can be expected in screw connections. Three dimensional contact elements are available in ADINA element library to define contacts between two surfaces. The contact surfaces that are initially in contact or that are expected to come into contact during the response solution are defined as contact pairs. One of the contact surfaces in the pair is designated as the contactor surface and the other contact surface is designated as the target surface. Action of contact occurs when the plane or line defined by the contact segment nodes of target surface is penetrated by the nodes of contractor surfaces. The contact elements available in ADINA are capable of taking into account of repeated contact and separation actions.

4.3.5 Failure Criteria

The purpose of failure criteria is to predict failure of the material during the analysis. A considerable number of theories have been proposed to define the failure of the materials. Such failure theories are divided into two major groups: failure criteria for brittle materials and failure criteria for ductile materials. Cold-formed steel is a ductile material. The maximum distortion energy criterion also known as the von Mises Criterion, is often used to estimate the yield of ductile materials. This study uses von Mises criterion as the failure criterion. The von Mises criterion states that failure occurs when the energy of distortion reaches the same energy for yield/failure in uniaxial tension. Mathematically, this is expressed as,

$$\sigma_{von} \leq \sigma_y \tag{4.17}$$

where

$$\sigma_{von} = \sqrt{\frac{1}{2} [(\sigma_1 - \sigma_2)^2 + (\sigma_2 - \sigma_3)^2 + (\sigma_3 - \sigma_1)^2]} \quad (4.18)$$

where σ_1 , σ_2 and σ_3 are principle stresses. In the case of plane stress, $\sigma_3 = 0$. The von Mises criterion reduces to,

$$\sigma_{von} = \sqrt{\sigma_1^2 - \sigma_1\sigma_2 + \sigma_2^2} \quad (4.19)$$

The Equation 4.19 represents a principal stress ellipse as illustrated in the Figure 4.3.

4.3.6 Material Modeling

The material properties of cold-formed steel (CFS) sections are significantly different from that of the virgin sheet steel due to the manufacturing process, such as cold-roll forming, cold bending etc. The cold work of forming causes changes in the mechanical properties; particularly at the corners of cold-formed structural shapes. However, previous studies showed that the material properties on the flat region can be approximated by the properties of virgin steel (Karren, 1967a; Karren, 1967b; Coetsee et al., 1990; Abdel-Rahman and Sivakumaran, 1997). The material properties considered herein was based on three tensile coupon tests of flat portion of the CFS joist. The experimental stress-strain relation was idealized into a multi-linear shape as shown in Figure 4.4. In this study it is assumed that the plate fails and that the screws do not fail. Since the screws are usually made from higher strength steel, screws were assumed to be made of perfectly elastic material with modulus of elasticity of 203 GPa and a Poissons' ratio of 0.3.

4.3.7 Structural Modeling

Numerous studies on the bolted and screw connection behavior of thin plates can be found in the literature (Winter, 1956; Fan et al., 1997; Kim and Yura, 1999; Aceti et al., 2004; Kim and Kuwamura, 2007). As discussed earlier, most of these studies focused on the failure modes of the connection. Therefore, these studies concentrated on the stress and strain state in the vicinity of the bolts and screws. Most of these previous finite element models were constructed using three dimensional solid elements. The primary objective of this study is to build a simple model resulting in a sufficiently accurate description of connection stiffness. Such a simple finite element model may not be able to fully capture the state of stresses and strains in the vicinity of the connection.

Two of the connection models proposed herein are identified as Model-I and Model-II. Figure 4.5 shows the detail of modeled surfaces for finite element model-I. The surfaces identified as 1 and 2 in the figure show the finite elements for plate 1 and 2. Surface 3 represents the edge of the plates around the screws. Similarly, surface 4 represents for the finite elements for screws. In Model-I, the plate-to-screw contacts and plate-to-plate contacts have been modeled using 3-D no penetration contact surface elements. Contact elements were generated between the surfaces 1 and 2 to represent plate-to-plate contact. Plate to plate interaction is captured by the contact elements between the surfaces 1 and 2. Moreover, contact elements were also generated between the surfaces 3 and 4 to represent plate-to-screw contact. The force from plate to the screw is transferred through the contact elements between surfaces 3 and 4. The details at A of such contact elements are also shown in Figure 4.5. Model-I represents a realistic connection model. However, this model involves

cumbersome modeling technique. It would be tedious and time consuming to use such a model if the structural model involves a large number of such connections.

Figure 4.6 shows the details of modeled surfaces for finite element model-II. Once again, the surfaces identified as 1 and 2 in the figure represents the finite elements for two plates. However, the surfaces 3 and 4 shown in model-I (Figure 4.5) were merged and produced as single surface (surface 3) in model-II. Therefore there is no contact action between screws and plates. Screws were assumed to be continuously connected to the plates. In other word, only the outer surfaces of screws were modeled, using shell elements, as a hollow shaft between two plates. Same nodes were assigned to the screws and plates around the edge of plate holes. Therefore, Model-II incorporates only the plate-to-plate contact phenomenon. Such contact phenomenon were captured by the contact surfaces generated between surfaces 1 and 2. Figure 4.6 also shows the details at A. Friction between two plates was assumed to be zero. This model is far simpler than the Model-I. Such a connection model can be built very fast. Both connection models were used to investigate a 70 mm lap joint. A gap between two plates within the overlap region was set as equal to the thickness of plate. Such a gap is essential to represent the eccentricity of loading in the lap connections.

4.3.8 Mesh Quality

The quality of mesh was checked in terms of aspect ratio, warpage and skew of the elements. Ratio of the longest edge to shortest edge was maintained less than 5 and ratio of shortest edge to thickness also maintained to be 5. Warpage (the amount by which an element deviates from being planer) was kept less than 15 degree. Similarly, the skew of the element was less than 60 degree (Bakker and Pekoz, 2003).

4.3.9 Boundary Conditions

Displacement control analysis was used that enforces prescribed displacement at selected points. One end of the connection-assembly was fixed in all translations and rotations. Such boundary would represent the clamping of test specimen. Other end was subjected to uniform translation in X-direction. Figure 4.5 and 4.6 show the boundary conditions of the connection assembly.

4.4 Experimental Work

4.4.1 Specimen Preparation

The experimental part of this research presented was carried out primarily to establish results that could be used to validate the finite element model of screw and bolt connections. Once the finite element model was experimentally verified, the model could then be used for other connection applications.

The connection type under consideration was a lap connection with four screws or bolts arranged in a square pattern as shown in Figure 4.7. The connection was designed in such a way that it would fail at the net section. In other word, the tensile strength of the net section across the width along the screw line was less than the strength given by Equations 4.3, 4.4 and 4.5. The width of the connection and the length of the overlapped portion of the connection were selected in such a way that it satisfies the connection requirements of AISI Standard (AISI, 2007). Accordingly, the minimum overlap and width of the connection is governed by the size of the screws or bolts, minimum spacing of the screws, minimum edge distance and minimum end distance. According to AISI Standard (AISI, 2007) the distance between the centers of fasteners should not be less than 3 times the diameter of the

screw or bolts. The distance from the centre of a fastener to the edge of any part shall not be less than 1.5 times the diameter of the screws or bolts. The end width of the specimen was made greater than the width of the connection to ensure connection failure. A transition zone with a smooth curve was provided between the end part and the actual connection part. Higher width at the end and a smooth transition were provided in order to prevent the failure of the specimen at the tension grip and failure at the transition zone due to stress concentration. Even though the test specimen under consideration looks like a tensile coupon, the dimensions of the test specimen were different than the standard tension coupon dimensions specified by the ASTM Standard (ASTM, 2003).

The specimens were cut from the web of a randomly selected cold-formed steel section along the longitudinal direction. This direction was parallel to the direction of rolling for such steel sections. The coupons were then machined to the shape and dimensions shown in Figure 4.7. Three set of the specimen were connected using number 8 self drilling screws and another three set of the specimen were connected using 5 mm diameter high strength steel bolts. Figure 4.8 and 4.9 show the connection specimen before testing.

The dimensions of the specimen were measured and presented in Table 4.1 and 4.2. The base metal thickness was measured after removing the galvanized layer on the metal surface. The galvanized surface was removed by dipping one end of tensile coupons into the hydrochloric acid for a while.

4.4.2 Test Setup

The picture of the overall test setup used in this investigation is shown in Figure 4.10. A 600 kN capacity Tinius Olsen loading machine (set at 30 kN loading range)

was used to apply the test load. A 5 mm electric resistance strain gauge was glued at the centre of connection of in all of the specimens. These strain gauges were to measure the strain at the connection zone. Strain gauges had a capacity to measure 3 percent strain with 0.5 percent accuracy. The coupons were mounted in the testing machine using gripping devices and aligned with respect to the vertical axis of the machine. An extensometer (LVDT-1) was mounted on the specimen to measure the gauge extension. A string pot (LVDT-2) was placed to measure relative displacement of the tip of the screws. The relative displacement of the tip of the screw allows us to determine the tilting of the screw relative to its initial orientation. The grip extension of the machine was also monitored using extensometer (LVDT-3).

4.4.3 Test Procedure

Once the preassembled test specimen was placed in position vertically, the specimen was checked using a machinist's level. The initial readings for load cells, LVDTs and strain gauges were set to zero. Then, the load was gradually applied. Although there exists no standard for the loading rate for such type of testing, the loading rate was controlled such that sufficient load increments can be recorded for the plotting (60 readings per kN tensile load) and the average stress rate of the section did not exceed the stress rate specified by ASTM Standard (ASTM, 2003) for tensile coupon tests (690 MPa/min). The readings from the machine (load readings), string pots and the strain gauges were recorded to a data file using a data acquisition system and a personal computer. The loading was continued until connection failure took place.

4.5 Results and Discussions

In the experiments, failure of the specimen was triggered by net section yielding. Figure 4.11 shows the connections after testing. Similarly, Figure 4.12 shows the deformed shape obtained through the finite element model. Finite element results were compared with experimental results. Both finite element and experimental result show evidence of end curling. In terms of deformed shapes, both the experimental results and finite element model results show similar deformed pattern.

Figure 4.13, 4.14 and 4.15 show the experimental results for the screw connections. Measurements were taken to observe gauge extension, screw tilting, average strains and end curling for both screw and bolt connections. Figure 4.13 shows the gauge extension of screw connection. The figure shows that both finite element models have good agreement in connection stiffness with experimental results. But, Model-I seems more accurate in determining the ultimate strength of the connection.

Figure 4.14 shows the screw tilting measurements in screw connections. Two out of three experimental results showed that no significant screw tilting at the beginning. But the finite element results show the linear screw tilting behavior from the very beginning. However, both models were capable of capturing the screw tilting at higher load levels. Figure 4.15 shows the strain at the center of the screw connection.

Similar results for the bolted connections are presented in Figures 4.16, 4.17 and 4.18. Figure 4.16 shows the gauge extension for bolted connection. The figure also compares the results from finite element models. Model-I seems promising in connection stiffness of bolted connection, but Model-II showed stiffer connection behavior than the experimental results. Both finite element connection models seem capable of capturing bolt tilting, as seen in Figure 4.17. Figure 4.18 shows the strain at the

middle of the bolted connection. Once again, Model-I was more accurate in predicting the strain at the center of the connection.

The effect of curling in the connection was also investigated in this study. Model-II was used to investigate the effect of curling on the connection stiffness of a screw connection. Curling was prevented by restricting the out of plane displacements along the connected edge of the plate. Figure 4.19 shows the effect of curling in gauge extension. The end of the connected plate was restricted from moving out of plane to prevent curling. The result shows that preventing curling makes the connection stiffer by as much as 4.6 percent. Moreover, Figure 4.20 shows that screw tilting might be decreased by up to 32.6 percent by preventing curling.

4.6 Conclusion

The behavior of screw connections associated with thin members such as cold-formed steel members is governed by the small plate stiffness. Most of the previous studies on screw connections and bolted connections have focused on the behavior and the ultimate strength of the connections in thick plates. Some of these studies have concentrated on the stress and strain state in the vicinity of screws or bolts. Thus, these previous studies were detail but involved somewhat cumbersome modeling techniques at the connection regions. Such models are very effective in examining the behavior of connection in various mechanical parts and structural connections where strength of the overall structure is governed by the strength of the connection. However, structural engineers frequently encounter large number of connection, where the load level rarely reaches to the ultimate strength of the connection. Screw fastened reinforcement, screw fastened web stiffeners, and screw fastened sheet metal flooring are some examples of such type of connections.

Detailed analysis of a large number of such connections using sophisticated finite element models is not only very tedious and time consuming but also may present numerical and computational difficulties. To overcome these difficulties, two simplified finite element models were developed in this study. The main members (connected plates) were modeled using quadrilateral shell elements, and nonlinear stress-strain relationship based on experiments. Two types of finite element models were considered. The developed finite element models were calibrated against experimental results from six specimens with the two types of fasteners (screws and bolts). A simple finite element connection model is sufficiently capable of reproducing the behavior of connections in thin-walled members. It was observed that finite element analysis results were in a good agreement with test results in terms of connection stiffness, screw tilting, end curling and average longitudinal strain. The result also shows that the prevention in curling would make the connection stiffer.

Table 4.1: Measured Dimensions of Screw Connection Specimen

Specimen	Width (mm)	Base Thickness (mm)	Gauge Distance (mm)
S-43-1-T	49.60	1.12	170.83
S-43-1-B	50.42	1.11	
S-43-2-T	49.70	1.10	172.43
S-43-2-B	49.94	1.11	
S-43-3-T	50.22	1.10	171.57
S-43-3-B	49.68	1.10	
Average	49.93	1.11	171.61
Standard Deviation	0.33	0.01	0.80

Note: S- Screw, 43- 43 mils (1.09 mm) thick plate, T- Top plate, B-Bottom plate

Table 4.2: Measured Dimensions of Bolted Connection Specimen

Specimen	Width (mm)	Base Thickness (mm)	Gauge Distance (mm)
B-43-1-T	49.59	1.10	172.74
B-43-1-B	50.13	1.11	
B-43-2-T	49.67	1.11	171.70
B-43-2-B	49.76	1.12	
B-43-3-T	49.89	1.12	170.93
B-43-3-B	49.88	1.12	
Average	49.82	1.11	171.79
Standard Deviation	0.19	0.01	0.91

Note: B-Bolt, 43- 43 mils (1.09 mm) thick plate, T- Top plate, B-Bottom plate

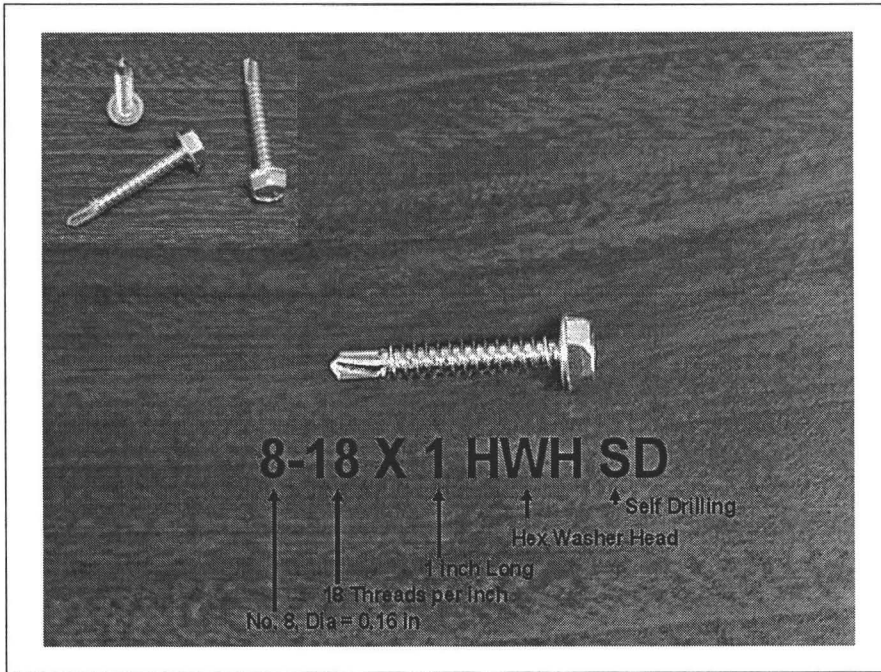


Figure 4.1: Self-drilling screws and their designations

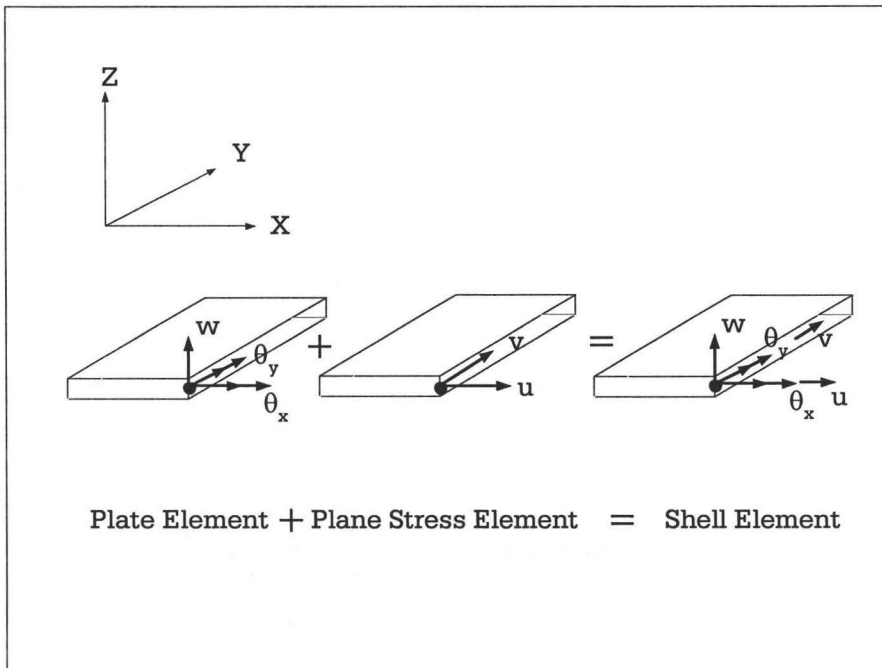


Figure 4.2: Nodal degrees of freedom for the shell elements

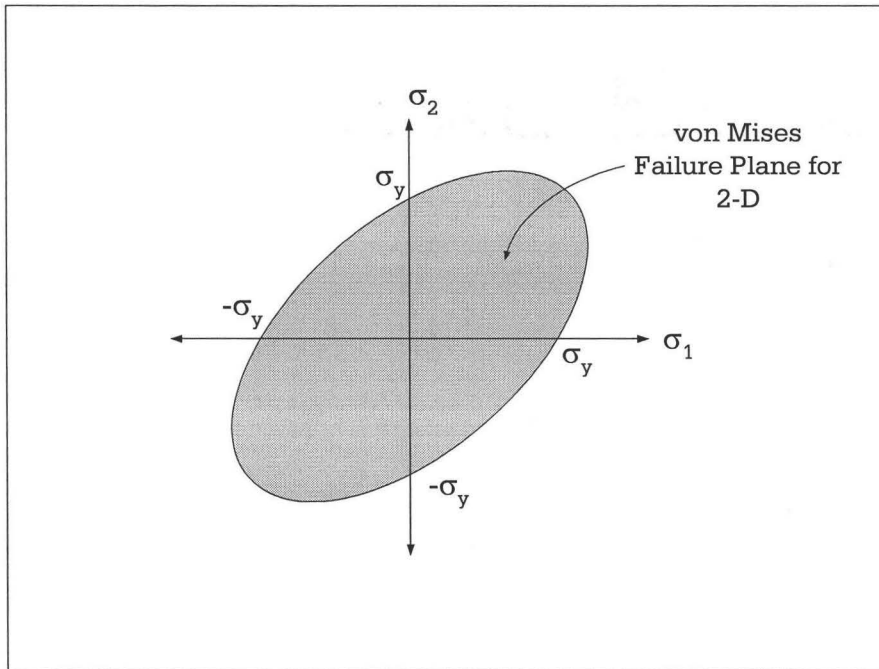


Figure 4.3: von Mises failure for two dimensional problem

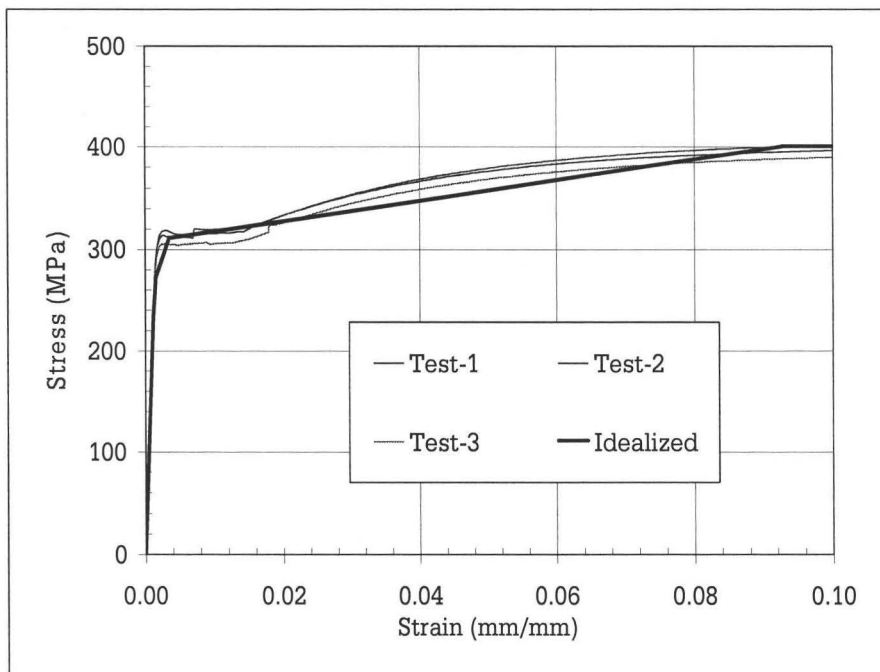


Figure 4.4: Experimental stress-strain relations and idealized stress-strain relations used in FEM

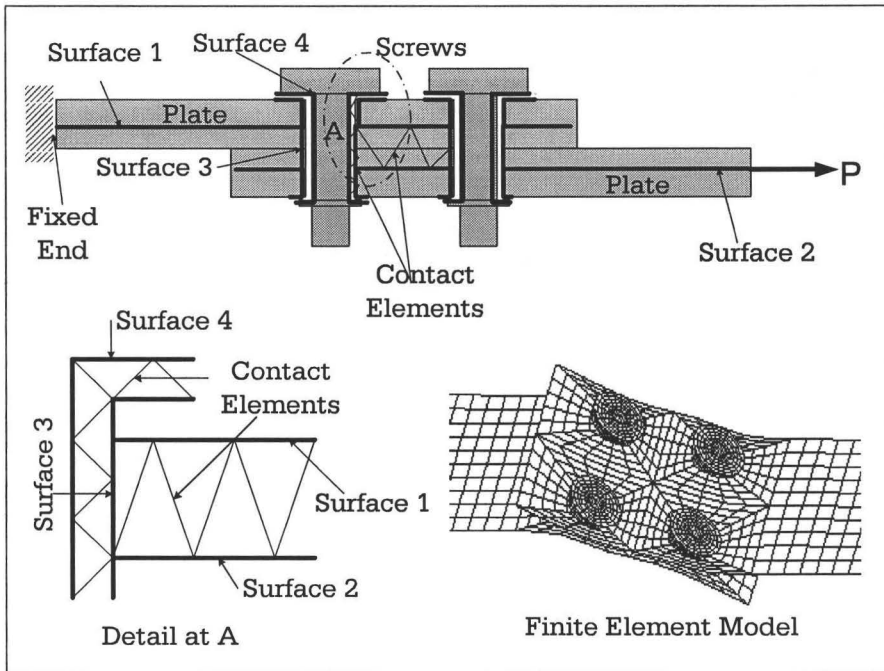


Figure 4.5: Finite element model-I

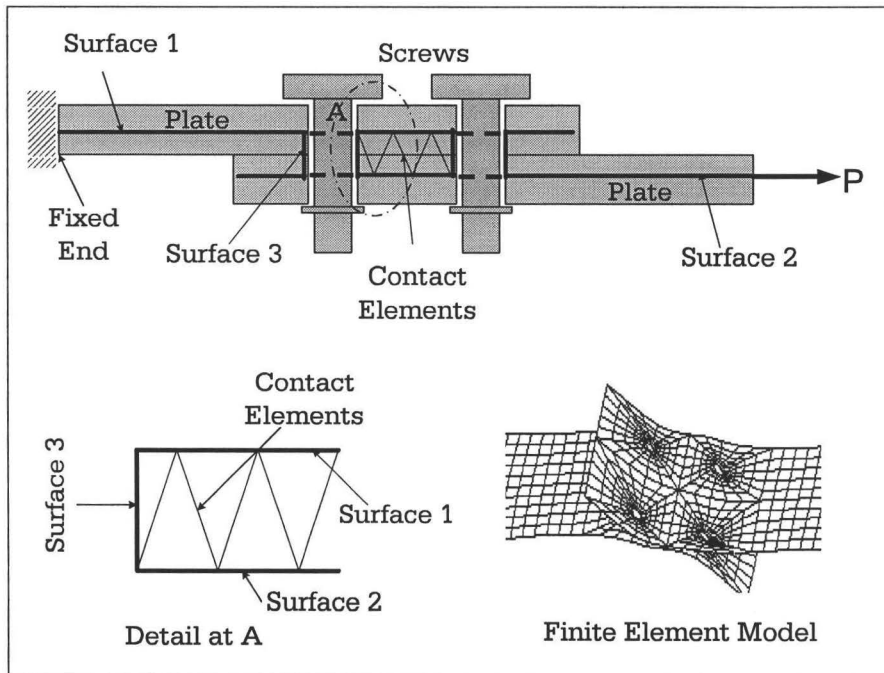


Figure 4.6: Finite element model-II

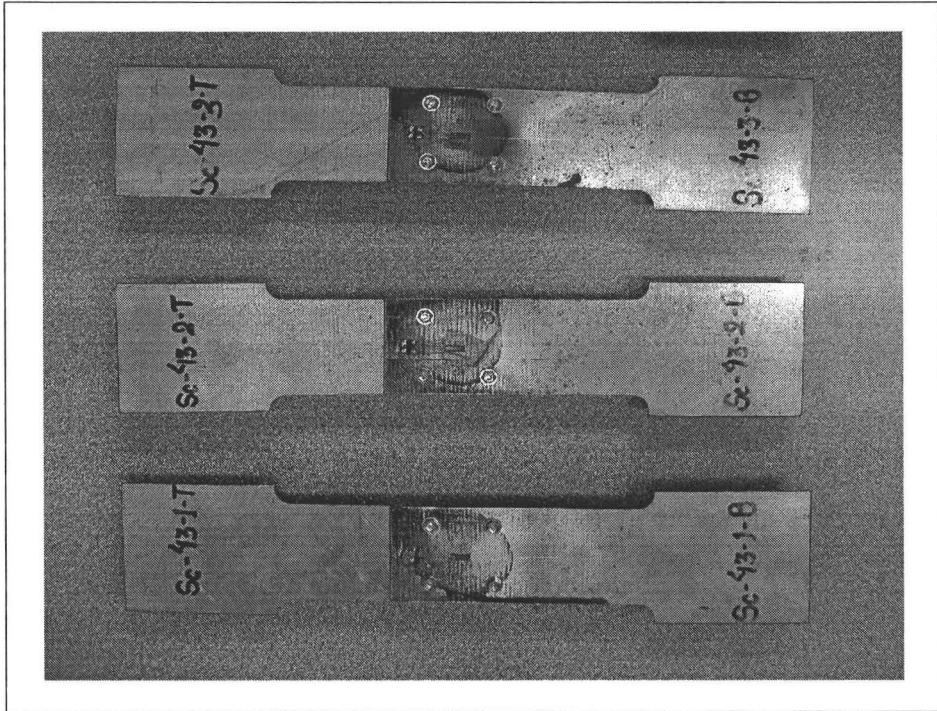


Figure 4.9: Self drilling screw connection assembly before testing

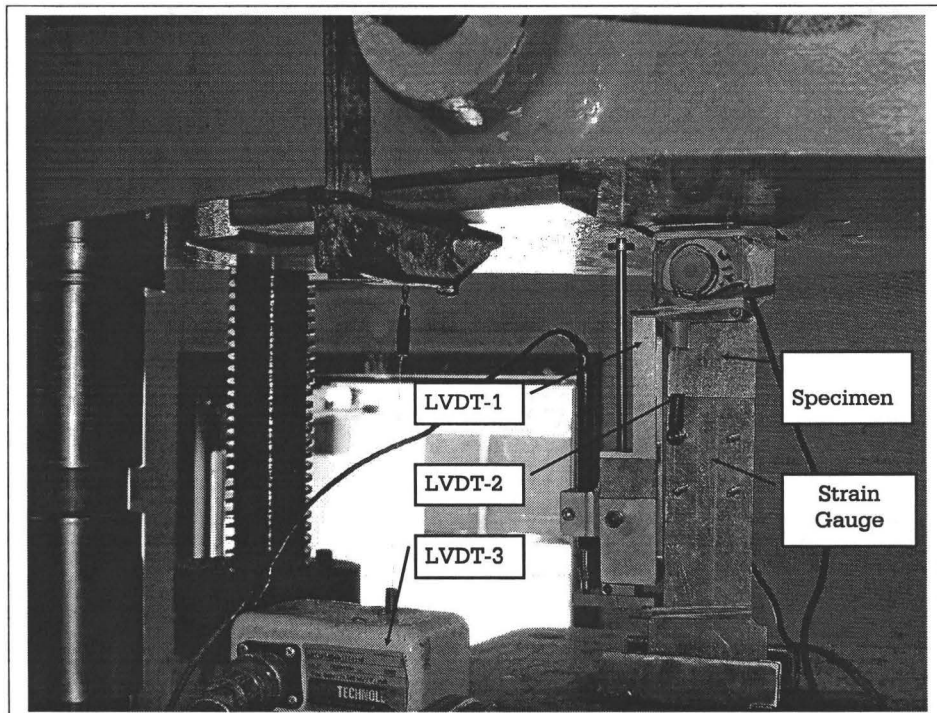


Figure 4.10: Test setup for connection test

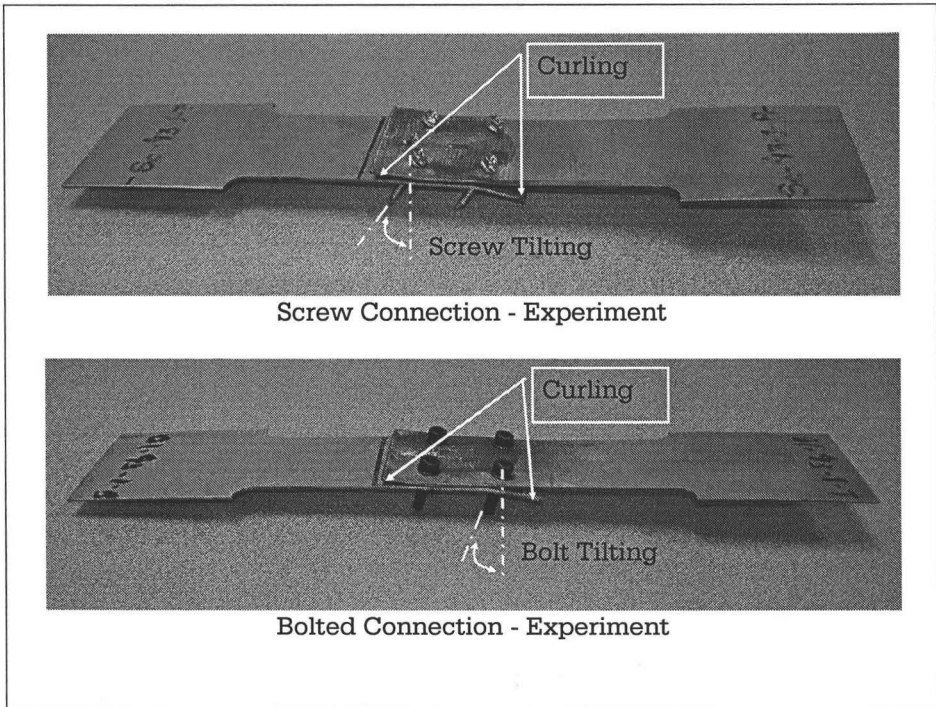


Figure 4.11: Screw/bolted connection picture after the test - experiment

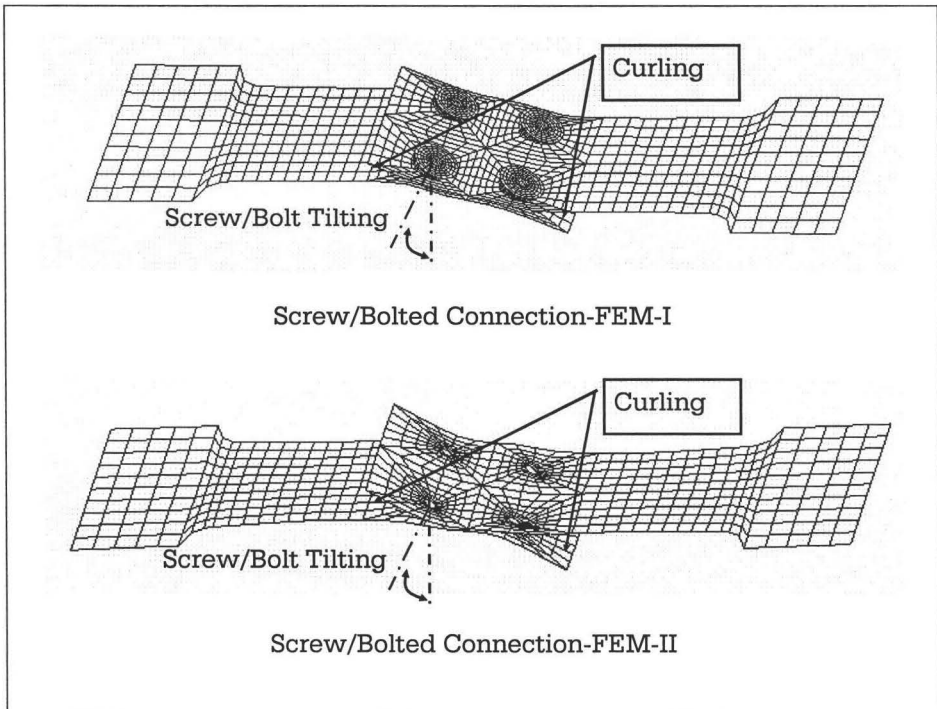


Figure 4.12: Screw/bolted connection picture after the test - FEM

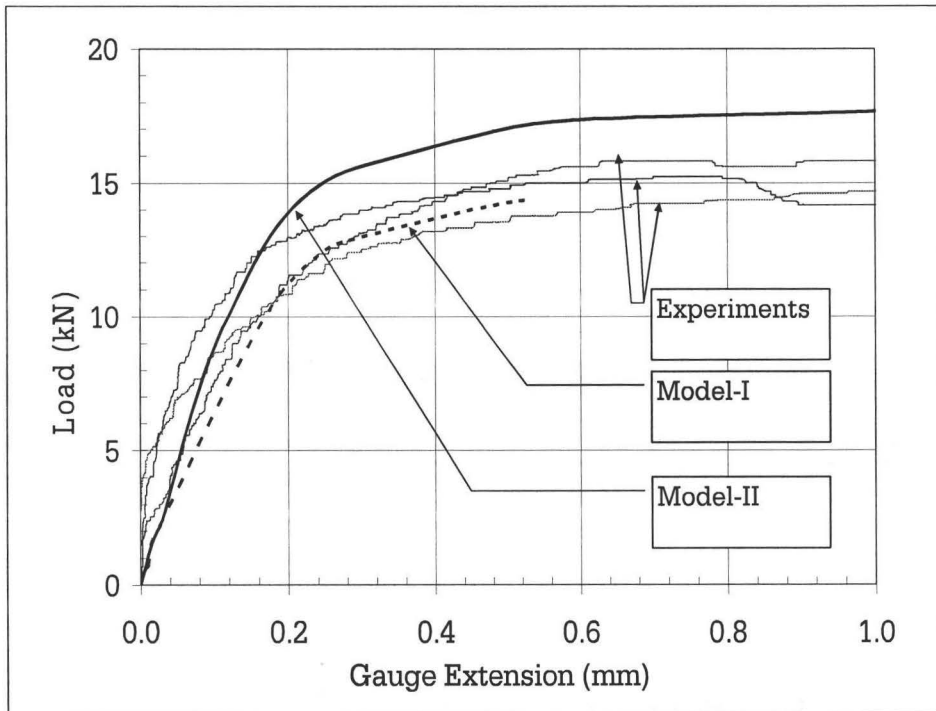


Figure 4.13: Gauge extension of the screw connection

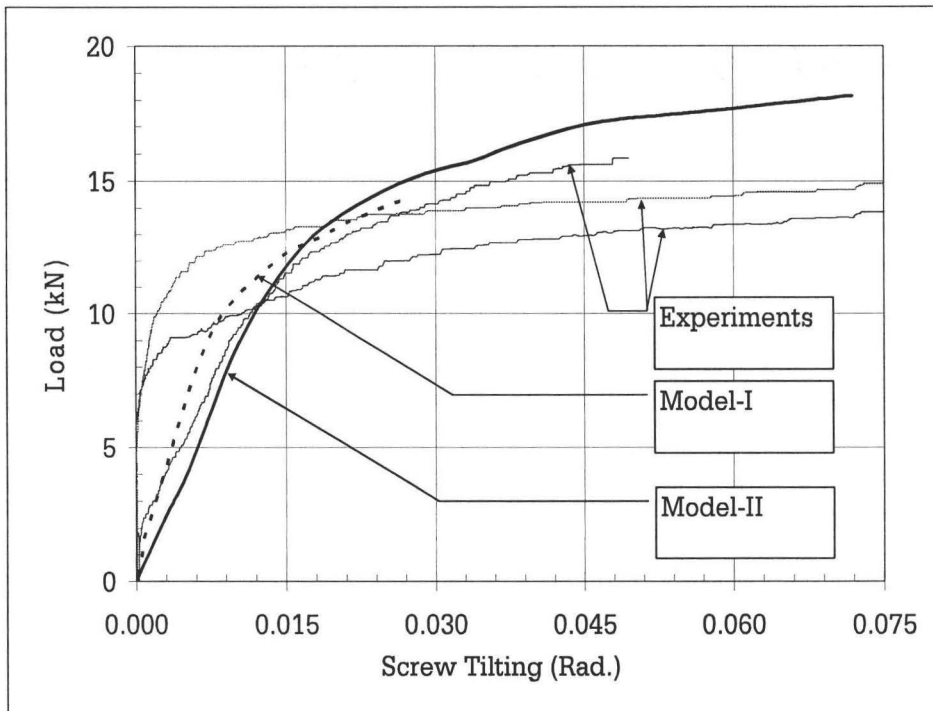


Figure 4.14: Screw tilting of the screw connection

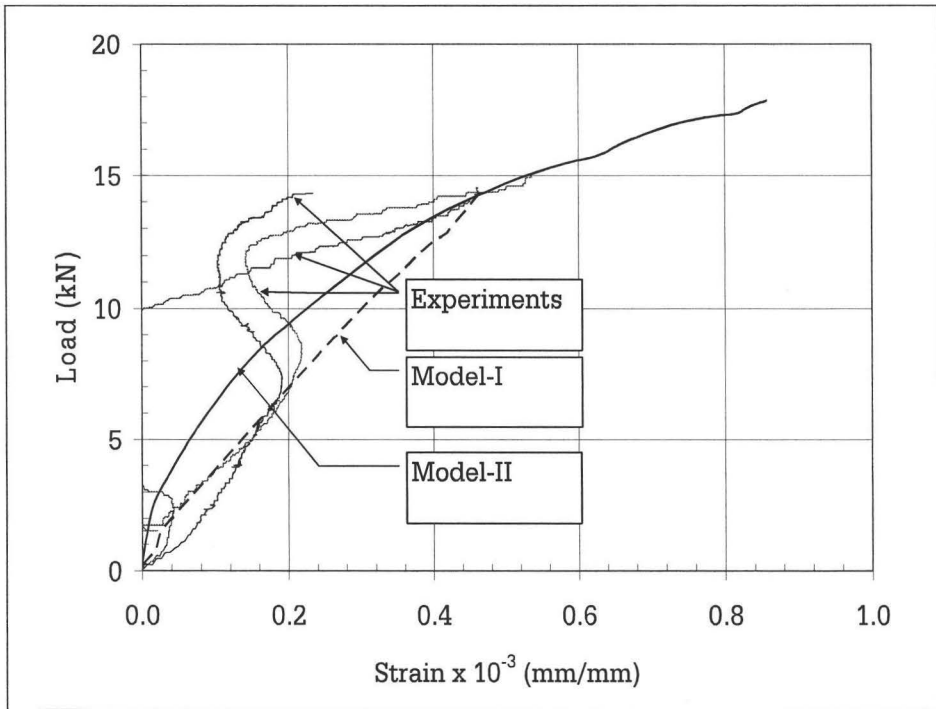


Figure 4.15: Strain at the center of the screw connection

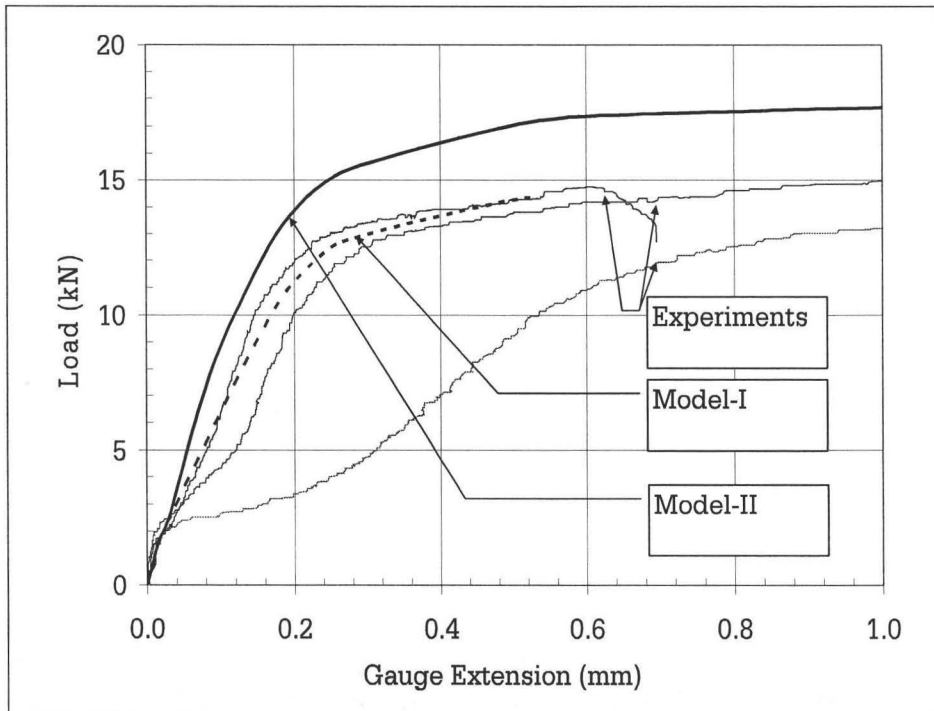


Figure 4.16: Gauge extension of the bolted connection

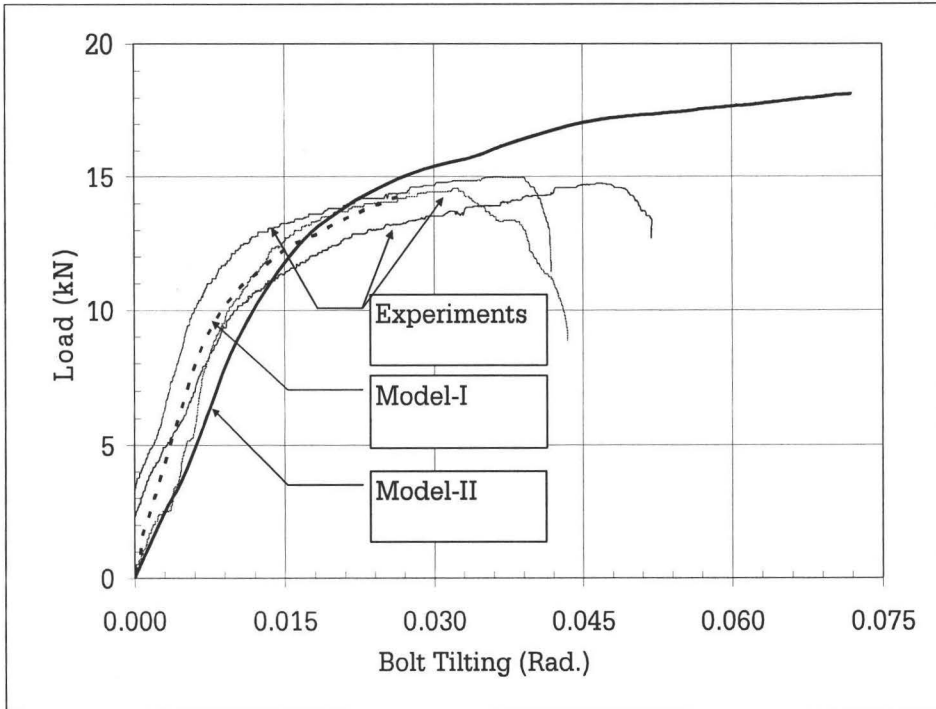


Figure 4.17: Bolt tilting of the bolted connection

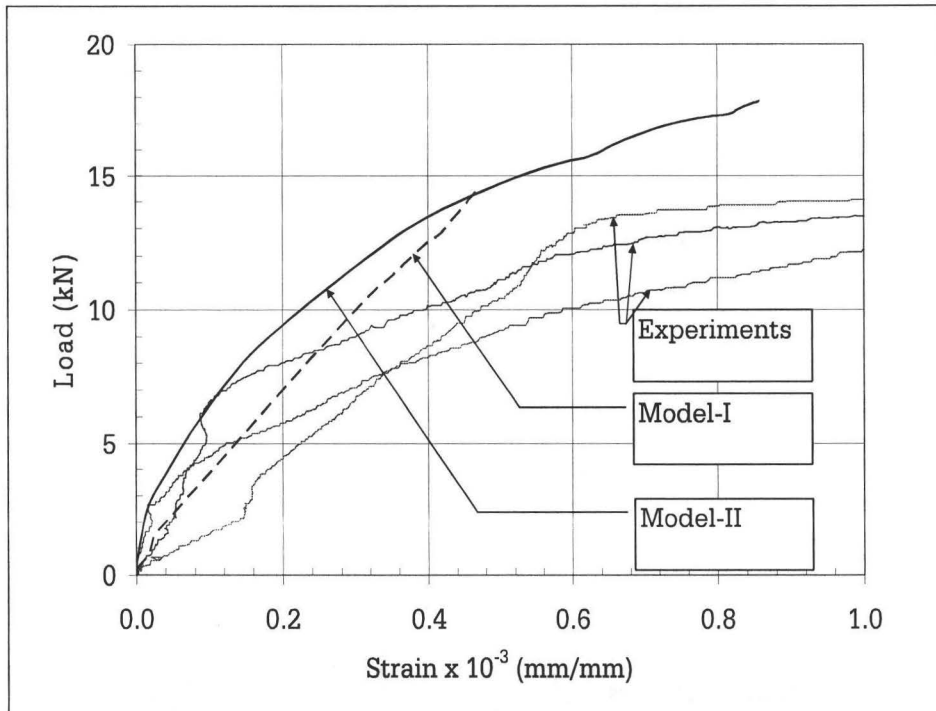


Figure 4.18: Strain at the center of the screw connection

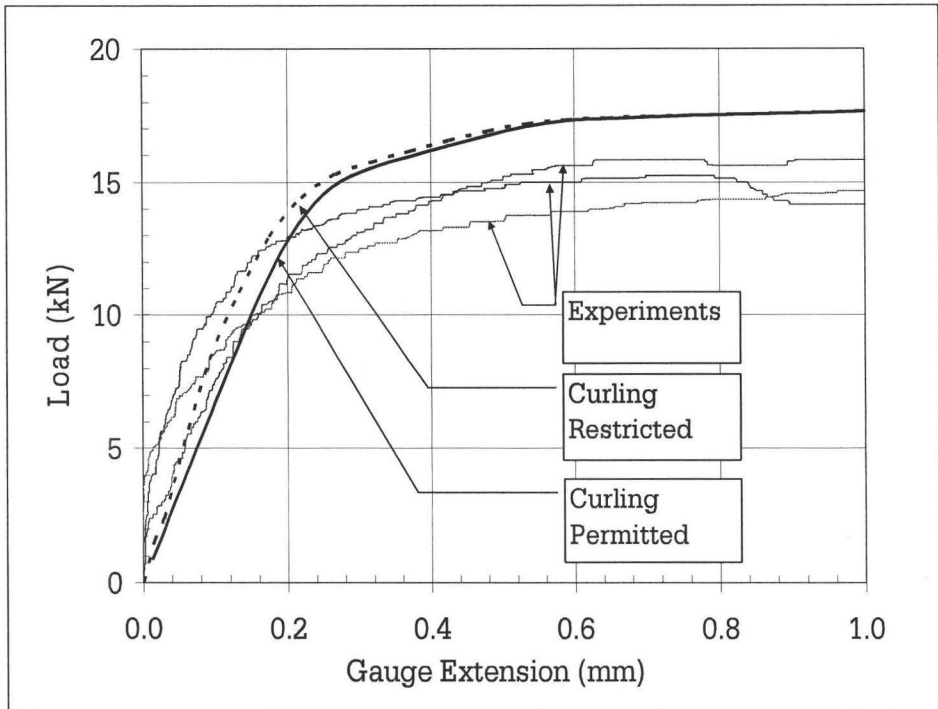


Figure 4.19: Effect of curling on gauge extension

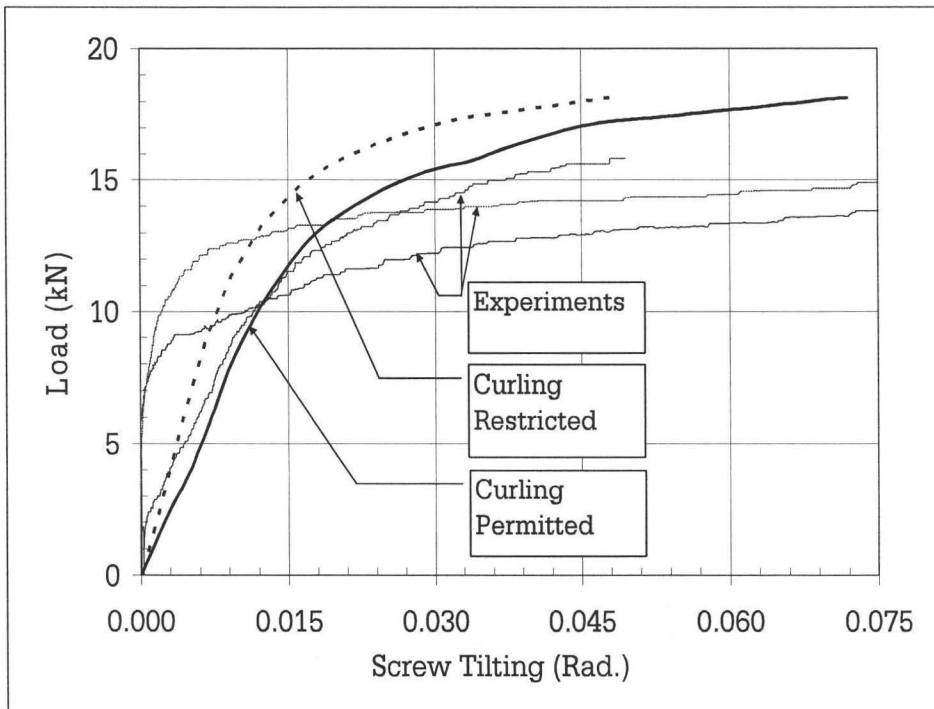


Figure 4.20: Effect of curling on screw tilting

Chapter 5

Flexural Resistance of Steel Webs with Reinforced Opening

5.1 Introduction

It is often necessary to provide openings in thin plates, such as web of cold-formed steel (CFS) members, plate and box girders and ship structures, for access and services. The behavior and the strength characteristics of such members significantly change as a consequence of redistribution of stresses around the openings and change in boundary conditions at the opening regions. Studies on thick plates and thin-walled members with openings can be found in literature (Narayanan and Der-Avanessian, 1984; Abdel-Rahman and Sivakumaran, 1998; Shanmugam et al., 2002). Abdel-Rahman and Sivakumaran (1998) studied the effects of openings on the compression capacity of cold-formed steel studs. Other studies (Narayanan and Der-Avanessian, 1984; Shanmugam et al., 2002) focused on the shear strength of the perforated web panels of the plate girders. However, structural engineers frequently encounter thin plates having openings subjected to in-plane flexural loads. Web of the CFS floor joists having openings is one such example of thin plates subjected to in-plane flexural loads.

A cost effective way to alleviate the detrimental effect of web opening is to fasten appropriate reinforcements around the opening regions. Reinforcements of openings in thick plates (for example, web of hot-rolled plate girders) had been studied in the past (Segner, 1964; Cogdon and Redwood, 1968; Copper and Snell, 1972; Wang et al., 1975; Larson and Shah, 1976). However, the reinforcement of thin plates (for example, web of cold-formed steel joists) has not been considered earnestly (Shanmugam, 1997). Recently, limited experimental studies were conducted which established reinforcement schemes for large web openings in the flexural zone of cold-formed steel joists (Pennock, 2001; Ng et al., 2004). Finite element analysis may be effectively used to establish appropriate reinforcement schemes for such problem, which may then be used in an experimental investigation.

This chapter presents a finite element analysis of thin simply-supported rectangular plates (representing the web of CFS joists) having unreinforced and reinforced openings subjected to direct compression and in-plane flexural loadings. The study, first, presents the buckling behavior of thin plates subjected to direct compression. A detail parametric study was made on various parameters such as: thickness of the plates, size of the openings, and shapes of the openings. Then the study was extended for the plates subjected to in-plane flexural loads. The opening of the plates subjected to in-plane flexural load was reinforced using the plate strips having various thicknesses. The reinforcements were taken to be screw-fastened to the main plates. The finite element model for screw fastened connections developed in Chapter 4 was used to fasten the reinforcement to the main plate.

5.2 Plates in Uniform Stress

5.2.1 Postbuckling Strength of Long Plate

Unlike one-dimensional structural members such as columns, two-dimensional elements such as simply supported plates will not collapse when the buckling stress is reached. An additional load can be carried by the plate after buckling by means of redistribution of stress. This phenomenon is known as post buckling strength.

The post buckling strength can be obtained using various relations. One of these relations given by von Karman is expressed in terms of effective width. Von Karman, in 1932, expressed the following relation for effective width,

$$b_e = 1.9t\sqrt{\frac{E}{F_y}} \quad (5.1)$$

In this approach, it is assumed that the total load is carried by an effective width subjected to a non-uniformly distributed stress. Equation 5.1 can be used to find the post buckling strength.

Winter in 1946, modified the von Karman's expression that is applicable for stress below the yield point and it also includes w/t ratio as follows.

$$b_e = 0.95t\sqrt{\frac{kE}{f_{max}}} \left(1 - 0.208 \left(\frac{t}{w} \right) \sqrt{\frac{kE}{f_{max}}} \right) \quad (5.2)$$

Post buckling capacity is reached when the maximum stress has reached the yield stress. Hence, post buckling strength can be obtained using Equation 5.2 and taking $f_{max} = F_y$.

5.2.2 Perforated Plates in Compression

Yu and Davis (1973) proposed a design approach to predict the effective design width of perforated plates with either central circular or square perforation. It was assumed that the buckling behavior of a perforated plate is similar to that of a non-perforated plate for $d_h/w < 0.7$ for circular perforation and $d_h/w < 0.7$ for square perforation. Beyond these limits, the perforated plates can be treated as two separate, but identical, unstiffened compression plates. The design equation for effective width was given as:

$$b_{eo} = 0.95t \sqrt{\frac{kE}{f_{max}}} \left(1 - X \frac{d}{w}\right) \left[\left(1 - 0.208 \left(\frac{t}{w-d}\right) \sqrt{\frac{kE}{f_{max}}}\right) \left(1 - Y \frac{d}{w}\right) \right] \quad (5.3)$$

where, d_h is diameter or width of the perforation. For a circular perforation, the constants, X and Y , are 0.226 and 0.0379, respectively. However, for a square perforation, the constant X and Y are 0.136 and 0.053, respectively.

In another study, Banwait (1987) gave a following equation to calculate effective width. The equation was based on the experimental study of cold-formed steel sections with w/t ratio of 51.5 and 112.4.

$$b_{eo} = \sqrt{\frac{w-d}{w}} b_e \quad (5.4)$$

Where, b_e is the effective design width of the corresponding non-perforated plate obtained as follows.

$$\text{for } \frac{w}{t} \leq 0.644 \sqrt{\frac{kE}{f_{max}}}$$

$$b_e = w \quad (5.5)$$

for $\frac{w}{t} > 0.644\sqrt{\frac{kE}{f_{max}}}$

$$b_e = 0.95t\sqrt{\frac{kE}{f_{max}}}\left(1 - 0.208\left(\frac{t}{w}\right)\sqrt{\frac{kE}{f_{max}}}\right) \quad (5.6)$$

Miller and Pekoz (1994) presented a simplified approach for the treatment of perforated plates with any shape of perforation. The approach consists of:

for $(w - b_e) > d_h$

$$b_{eo} = b_e \quad (5.7)$$

for $(w - b_e) < d_h$

$$b_{eo} = w - d_h \quad (5.8)$$

In other words, if the perforation does not extend into the effective portion of the plate, then it does not affect the effective design width.

AISI Standard (AISI, 2007) has following provision to find the effective width of uniformly compressed stiffened elements with openings. For circular holes, the effective width, b_{eo} , shall be calculated by:

for $\lambda \leq 0.673$

$$b_{eo} = w - d_h \quad (5.9)$$

for $\lambda > 0.673$

$$b_{eo} = \frac{w}{\lambda} \left[1 - \frac{0.22}{\lambda} - \frac{0.8d_h}{w} + \frac{0.085d_h}{w\lambda} \right] \quad (5.10)$$

In all cases $b_{eo} \leq (w - d_h)$

approximate method to find the buckling stress of unstiffened plate with stress gradient. According to the AISI Standard (AISI, 2007), the effective width of unstiffened compressive elements with stress gradient can be treated as uniformly compressed elements with k value of 0.43. The AISI Standard (AISI, 2007), procedure to calculate the effective width of unstiffened compressive elements with stress gradient is presented in Section 2.2.1 of Chapter 2 (Equation 2.3-2.6).

5.3.3 Plates with Openings in Stress Gradient

When a simply supported plate having opening is subjected to in-plane stress gradient, the problem can be simplified as combination of unstiffened plates with stress gradient (see section 5.3.2). The remaining portion of either side of the opening can be considered as one edge free (the opening edge free) and other edge simply supported element.

5.4 Geometrical Imperfection in Plates

Geometric imperfections account for the deviation of member or an element from the theoretically perfect geometry. It is practically impossible to get perfect geometry on structural steel members. Imperfection on the structural steel members can be the one or combination of bowing, warping, twisting and local deviations. In the literature, it has been proposed to use local plate imperfections similar to the expected local buckling shape of the plate (Hancock, 1981). For a long plate under uniaxial compression, the buckled shape is a half wave in the transverse direction, and a series

1998), a double sine-wave distribution represented by following equation was used to define the imperfections for CFS channel sections.

$$\delta = \delta_0 \sin \frac{\pi x}{w} \sin \frac{\pi y}{\bar{w}} \quad (5.17)$$

Where δ , δ_0 , w and \bar{w} represent for out of plane imperfection distribution, maximum imperfection amplitude, width of web plate and average of the width of the web and flange plates respectively. Equation 5.17 represents only for first fundamental buckling mode shape.

Some researchers (Schafer and Pekoz, 1998) suggested employing at least two fundamentally different deformed (eigen-mode) shapes summed together for the imperfection distribution. Deformed shape for web and flange considering m buckling modes are represented by a double series (Yu, Wei-Wen, 2000)

$$\delta = \sum_{i=1}^m A_m \sin \frac{i\pi x}{w} \sin \frac{\pi y}{\bar{w}} \quad (5.18)$$

Where, m is the number of half sine waves which is theoretically equal to the maximum possible buckling mode shape, along the length, A_m is coefficient and set such that maximum imperfection, δ_0 , after summation remains within the limit defined above. The maximum imperfection can be expressed as following (Sivakumaran and Abdel-Raheman, 1998):

$$\frac{\delta_0}{t} = 0.145 \left(\frac{w}{t} \right) \sqrt{\frac{F_y}{E}} \quad (5.19)$$

Where t is the thickness of the plate element, w/t is slenderness ratio, and E and F_y are the material properties of the plate. Another experimental study (Schafer and Pekoz, 1998) showed that maximum imperfection can also be expressed by:

$$\delta_0 \simeq 0.006w \quad (5.20)$$

or alternative rule based on an exponential curve to fit the thickness as follow.

$$\delta_0 \simeq 6te^{-2t} \quad (5.21)$$

where δ_0 and t are in mm. This study considers the maximum imperfection equal to the highest value established by Equations 5.19, 5.20 and 5.21. Equation 5.20 governed in this study, .

5.5 Finite Element Analysis of Plates Subjected to In-plane Compression

5.5.1 Square Plate in Compression

The finite element study on plate began with the analysis of a simply supported square plate. Finite element results were compared with closed-form solution discussed in Section 1.5.2 and 5.2.1. A simply supported square plate was analyzed for uniaxial compression loading. A 500 mm long and 500 mm wide plate was selected for the study. Thickness of the plate was taken as 5 mm ($w/t = 100$). This plate was expected to buckle before yielding. The plate was assumed to have geometric imperfection represented as single curvature in both X- and Y-direction. The curvature was considered as half-sinusoidal-wave with maximum out of plane imperfection equal to 3 mm (maximum of Equation 5.19, 5.20 and 5.21) at the centre.

Only a quarter part of the plate was discretized because of the symmetry in both X- and Y-direction. Symmetric lines were expected to remain in the initial

position through out the analysis. Hence zero displacement can be expected in X-direction along the symmetric line parallel to Y-axis, and also in Y-direction along the symmetrical axis parallel to X-axis. Rotation about the axis parallel to the symmetrical line is also expected to be zero. Boundary conditions for a quarter part of the plate considered here are shown in Figure 5.1.

Four-node shell element was used for the analysis. Since a large out-of-plane deformation was expected, small strain-large displacement formulation was used for the analysis. The quarter plate was discretized into total 100 (10x10) elements. This gives the element side to thickness ratio equal to 5. A plastic-bilinear with no strain hardening material model was considered. Modulus of elasticity and initial yield stress were taken as 203 GPa and 350 MPa. The von Mises failure criteria discussed in Section 4.3.4 of Chapter 4 was utilized for material yielding. The critical elastic buckling stress of such plate given by Equation 1.4 was 73 MPa.

Figure 5.2 shows the load displacements curve for the plate. The displacements shown in the figure are axial displacement at one edge and out of plane displacements at the center of the plate. Figure 5.3 shows the average stress strain curve. The elastic buckling stress was determined from the intersection of the slopes before buckling and after buckling. The elastic buckling stress given by the finite element analysis was 74 MPa. Similarly, the ultimate strength including postbuckling strength given by Equation 5.1, Equation 5.2 and finite element solution were 160 MPa, 144 MPa and 155 MPa, respectively. The results showed that the finite element results and closed-form results resemble each other.

Figure 5.4 to Figure 5.6 show the stress variation along section A-A at peak load. The stresses shown in the figures are: stress in X-direction, stress in Y-direction and von Mises stress. Since the plate failed in buckling, one side of the plate was observed convex shape and the other face of the plate was observed concave shape. Figure 5.4

shows the stress variation on the outer surface (convex face). Even though the plate was subjected to direct compression in X-direction, the middle part of the convex face of the plate experienced tensile stress in X-direction because of buckling. Similarly, Figure 5.5 shows the stress variation on the inner face (concave face) of the plate. The stresses in X-direction on the concave face were observed compressive as expected. Figure 5.6 shows the stresses on the mid-surface. Most of the mid surface experienced compressive stress in X-direction. Figure 5.7 shows the through-thickness variation of stresses at the center of the plate. It can be seen from the figure that none of the points through the thickness at the centre of the plate reached yield stress. However, Figure 5.8 shows that the von Mises stress at the edge region of the plate reached yield stress through out the thickness. In summary, it can be observed from Figure 5.4 to 5.8 that the von Mises stress only at the edge region of the plate reached yield stress at peak load . Rest of the area remained elastic. In other words, when a thin plate is subjected to compression load, the yielding would propagate from the edge to the center of the plate.

5.5.2 Rectangular Plate in Compression

A rectangular plate with length 600 mm and width 200 mm ($m = 3$) was considered for parametric studies. The parameters that were of interest are plate slenderness (w/t) ratio, size of the openings, and shape of the openings. Four different thicknesses ($t = 1$ mm, 2 mm, 4 mm and 8 mm), that would give four different w/t ratios ($w/t = 200, 100, 50$ and 25 , respectively), were selected for the study. The opening sizes were 20, 40, 60 and 80 percents of the width of the plate. Such openings were made at the center of the plate. Furthermore, the effects of square and circular openings were investigated.

The plate was simply supported on the four edges. Figure 5.9 shows the details of the support conditions and geometrical imperfection of the rectangular plate. The figure shows that the plate was analyzed on X-Y plane. To create a simply supported edge condition, four edges were restricted in Z- translation ($u_z = 0$). The edges parallel to X-axis were restricted in Y-rotations ($\theta_y = 0$) and the edges parallel to the Y-axis were restricted in X-rotations ($\theta_x = 0$). Furthermore, as none of the edges were expected to rotate about Z-axis, all four edges were restricted in Z-rotation ($\theta_z = 0$). Even though, the analysis could have been made using only quarter part of the plate model, full model was considered in order to establish a clear picture of the failure mode of the plate. Therefore, further boundary conditions were applied along the line of symmetry (centerlines of the plate). The centerline along the X-axis was restricted in Y-translation ($u_y = 0$) and X-rotation ($\theta_x = 0$). Similarly, the centerline along the Y-axis was restricted in X-translation ($u_x = 0$) and Y-rotation ($\theta_y = 0$). Such boundary conditions along the centerlines of the plate would maintain the symmetry of the plate in geometry, stresses, strains and displacements throughout the time steps of the analysis. The geometrical imperfection of the plate was also considered. The geometrical imperfection was defined by the Equation 5.18 with m equal to 3 (number of half sine wave = 3). The maximum imperfection obtained from the highest value given by the Equation 5.19 to 5.21 was utilized.

The plate model was generated using four-nodded shell elements. The quality of mesh was controlled according to the mesh requirements described in Section 4.3.7 of Chapter 4. Since the analysis was displacement controlled, uniform displacements were applied along the two opposite edges of the plate. The analysis was continued until a clear deformed shape was obtained. An axial displacement level of 2 mm on each edge was sufficient enough to get a distinct deformed shape. Total axial displacement was divided into 200 time steps during the analysis and results for each

time steps were recorded. Such time steps were necessary to: (a) get sufficient data for plotting the results, and (b) convergence of analysis in every time step. Elasto-plastic material properties ($E = 203000$ MPa, $F_y = 350$ MPa and $\mu = 0.3$) was used for the plate where E , F_y and μ are elastic modulus, yield strength and Poissons ratio of the plate. The results are discussed in the sections below.

This section discusses the stress distributions and the deformed shapes of typical thick and thin plates. The results for thickest ($t = 8$ mm, $w/t = 25$) and thinnest ($t = 1$ mm, $w/t = 200$) plates that were considered for the analysis were selected for this discussion. Figure 5.10 shows the band plot of axial stress (σ_{xx}) for thick plate and thin plate. The stress plotted here is the average stress. Even though every point of the thick plate experienced compressive stress in X direction, the stress was not uniform along and across the length of the plate. Such non-uniform stress pattern was due to the presence of geometrical imperfection on the plate. Had the plate been geometrically perfect, the axial stress would have been uniform over the plate. Figure 5.10 also shows that the thin plate would experience compressive and tensile axial stress (σ_{xx}) when subjected to compression. Such bands of compressive and tensile stresses are due to the buckling waves of the plate and redistribution of the stresses.

Figure 5.11 shows the deformed shape of thick plate ($w/t = 25$) at the axial deformation level of 2 mm. No significant out of plane deformation were observed through out the plate. Therefore it can be concluded that the failure of thick plate was due to the cross sectional yielding. This conclusion was also supported by the stress plot at section A-A as shown in Figure 5.12. The Figure 5.12 shows the plots for stress in X-direction, stress in Y-direction and von Mises stress across Section A-A. These stresses are average stress corresponding to the ultimate load level. The plot shows that a significant amount of stress in Y-direction can also be expected when a plate having out of plane imperfection is subjected to uniaxial compressive

stress of X-direction. Since the von Mises failure criterion was applied, von Mises stress reached to yield stress (350 MPa) all across the section at the ultimate load level. Stress in X-direction was higher than the uniaxial yield stress.

The deformed shape of thin plate ($w/t = 200$) subjected in uniaxial compression is presented in Figure 5.13. The figure shows that the failure of thin plate is governed by plate buckling. Figure 5.14 shows the stress distributions across the plate at the ultimate load level. It can be seen that the von Mises stress reached the yield stress at the edges of the plate, but the stress is closer to zero at the middle of the plate. Therefore, it can be concluded that when a simply supported thin plate is subjected to uniaxial compression load, most of the load will be carried by the edge portions of the plate.

5.5.3 Rectangular Plate having a Square Hole in Compression

Figure 5.15 to Figure 5.18 shows the deformed shapes and the stress distribution on the plate having a square opening. Once again, the results for thick plate ($t = 8$ mm, $w/t = 25$) and thin plate ($t = 8$ mm, $w/t = 200$) are presented here. Typical results for the plates having 40 percent openings are discussed. Figure 5.15 shows the deformed shape for the thick plate having square opening. The figure shows that the failure was in cross sectional yielding as expected. The stress distribution presented in Figure 5.16 shows that the von Mises stress across the section at the opening region reached yield stress. The deformed shape for thin plate having square opening presented in Figure 5.17, shows that the plate failed in localized buckling at the opening region. The stress distribution across the thin plate is shown in Figure 5.18. The figure shows that, only the edge of the plate was yielding at the ultimate

load level. The stresses (σ_{xx} and σ_{von}) at the opening edges are about 20 percent of the yield stress. The band plots of stress, (σ_{xx} , for both thick and thin plates having 40 percent square openings are presented in Figure 5.19. The plots show that the thick plate experienced compressive stress in X-direction all over the plate. However, higher stresses can be seen around the opening region because of stress concentration. Contrary to the thick plate, thin plate experienced bands of compressive and tensile stresses because the failure of the thin plate was governed by buckling.

5.5.4 Effects of Opening Size

Effects of four different sizes (20, 40, 60 and 80 percent of plate width) of square openings at the center of a thick plate ($t = 8$ mm, $w/t = 25$) and a thin plate ($t = 1$ mm, $w/t = 200$) are discussed here. Figure 5.20 shows the load displacement relations for thick solid plate and plates with square openings of various sizes. Ultimate load capacities of the plates having openings (P_o) were normalized by the ultimate load capacity of the solid plate (P_s). The figure shows that lower opening size would experience higher slope of descending curve after ultimate load level. This can be explained by the fact that once the cross section reached the yield stress, the plate would have zero elastic rigidity ($E = 0$). After the cross sectional yielding, the plate would be susceptible for buckling because of zero elastic rigidity. Since the plates with small opening have wider unsupported compressive element (element between simply supported edge and free opening edge), such plates would buckle rapidly.

Figure 5.21 shows the normalized load displacement curves for thin plates having square openings. The curves show that presence of small central openings (up to 40 percent) has no effect in the ultimate compressive strength of the plate. As discussed earlier, the contribution of middle strip of the plate on the compressive strength of

thin plate is negligible. This fact can be observed in the stresses plots shown in Figure 5.14 and Figure 5.18. Therefore, small openings on the middle strip of the plate would have no significant effects on the ultimate strength of the plate.

5.5.5 Effects of w/t Ratio

The strength reduction curves of plates having four slenderness ratios ($w/t = 25, 50, 100$ and 200) and having various sizes of square openings are presented in Figure 5.22. The figure shows that the reduction in ultimate strength of thick plate ($w/t = 25$) is linearly proportional to the size of the openings. However, for the plates having higher slenderness ratios ($w/t = 50, 100$ and 200) the reduction in ultimate strength varies non-linearly with the size of the openings. The figure shows that higher slenderness ratio of the plate would experience lower effects of central openings on the ultimate compressive strength of the plate. This can be explained by the following facts. Higher slenderness ratio plate would experience highly nonlinear stress distribution across the section. In other words, thinner plates would experience very low stress at the middle strip of the plates. Therefore, presence of openings at such low stress region would have less effect on the ultimate strength of the plate. The Figure 5.22 also shows that, for the plates having slenderness ratio (w/t) equal to 100 and 200 , there is no significant reduction in ultimate compressive strength, when the size of the central openings is less than 40 percent of the plate width.

5.5.6 Rectangular Plate having Circular Hole in Compression

The opening shapes that are of interest were square openings and circular openings. The results for the square openings were discussed earlier. The results for the plates

having circular openings are presented in Figure 5.23 to Figure 5.30. The results include deformed shapes, stress distributions, load displacement curves and load reduction curves. Figure 5.23 shows the deformed shape of thick plate with circular openings and Figure 5.24 shows the stress distribution across the plate at the opening region. The stress plot shows that at ultimate load level the whole cross-section of the plate had yielded. Figure 5.25 and Figure 5.26 shows the deformed shape and stress plots for thin plate having circular openings. As expected, the thin plate failed in buckling. Moreover, at ultimate load level only the edge of the plate reached yield stress. Figure 5.27 shows the band plot of stress in X-direction (σ_{xx}). The effects of various sizes of circular openings on the ultimate compressive strength of a thick plate are presented in Figure 5.28. Similarly, the effects of various sizes of circular openings on the ultimate compressive strength of thin plate are presented in Figure 5.29. The ultimate strength reduction factor for various sizes of circular openings and various slenderness ratios are summarized in Figure 5.30. The Figure 5.31 shows that presence of small circular openings at the center of the thin plate has no effect on the ultimate compressive strength of the thin plate. On the other hand, reduction of ultimate strength of thick plate is linearly proportional to the size of openings. In summary, the observations and conclusions made for square openings are again equally valid for the circular openings. No significant differences on the ultimate compressive strength were observed for the case of circular openings and for the case of square openings.

5.6 Finite Element Analysis for Plates in In-Plane Bending

5.6.1 Finite Element Model

The plate model considered here in is a rectangular plate subjected to in-plane bending. The plate was simply supported. The support conditions that were applied on the plate edges are shown in Figure 5.31. A line of symmetry for geometry, stresses, strains and displacements throughout the analysis was expected to be passing across the mid-length of the plate. Therefore, the boundary conditions were applied along the line of symmetry. A line passing through the mid-width of the plate also represents the line of geometrical symmetry of the plate. Since the neutral axis of thin plate might shift because of local buckling stresses, strains and displacements would not remain symmetrical about the geometrical symmetry line. Therefore, no boundary conditions were applied along the geometrical symmetry line that passes through the mid-width of the plate. However, to prevent the plate from rigid body motion, the mid points of the two short edges were restricted from Y-displacements. The in-plane bending region within the plate domain was created using a linear displacement gradient as shown in Figure 5.31. The geometrical imperfections were also considered, as defined by Equation 5.18 to Equation 5.21.

The parametric variables included the slenderness (w/t) ratio, the size of the openings and the shape of the openings. The plate slenderness (w/t) considered here are 25, 50, 100 and 200 ($t = 8$ mm, 4 mm, 2 mm and 1 mm) having four different sizes (20, 40, 60 and 80 percent of width) circular and square openings. Moreover, the finite elements, meshing techniques and analysis techniques described in Section 4.3.7 were utilized.

Figure 5.32 shows the stress (σ_{xx}) band plots for thick ($t = 8$ mm, $w/t = 25$) and thin ($t = 1$ mm, $w/t = 200$) plates. The thick plate experienced a constant stress along the length and linearly varying stress across the length. On the other hand, the stress pattern for the thin plate is different than that observed in the thick plate. The bottom portion of the thin plate (subjected to tension) shows the uniform tensile stress along the length. But the top portion of the thin plate (subjected to compression) shows a band of compression and tension stresses. Such band of compression and tension stress on the top portion of the thin plate is due to the buckling of the plate in the compression.

The deformed shape and the stresses throughout the width of thick plate are shown in Figure 5.33 and Figure 5.34, respectively. No out-of-plane deformations were observed on the plate. Furthermore, a progressive yielding from the edge of the plate to the center of the plate can be seen in the stress plot shown in Figure 5.34. Such yielding would keep moving towards the middle of the plate. Theoretically, the whole cross section would yield at a rotation of infinity. Figure 5.35 shows the deformed shape of the thin plate subjected on in-plane bending. The deformed shape shows that the plate failed due to buckling in the compression region. The compression portion of the plate buckled in the shape of sinusoidal wave. The wave length of the buckled plate was equal to the width of the plate which can be observed in Figure 5.35. An important point to be noticed here is that the plate had geometrical imperfections in the form of a sinusoidal wave having a wavelength of twice the plate width. However, the deformed shape (buckling shape) was different than the shape of the plate imperfection. It shows that the buckling wavelength of thin plate would be controlled by the width of the compressive element but not by the wave length of geometrical imperfection. Figure 5.36 shows the stresses at a section taken at mid-length. The figure shows that the stress variation is non-linear across the width. Such

a non-linear stress distribution was caused by the buckling of compressive element of the plate.

Figures 5.37 to 5.40 show the deformed shapes and corresponding stress distribution plots for thick and thin plates having square openings. Figure 5.41 shows the band plot of stress all over the plate domain. As it is evident from these figures (Figure 5.37 to Figure 5.41) failure of thick plates was governed by the cross sectional yielding and failure of thin plates was governed by buckling.

5.6.2 Effects of Opening Size

This section discusses the effect of openings on the in-plane flexural resistance of thick and thin plates. Figure 5.42 shows the moment rotation curves for a thick solid plate and for plates having four different sizes (20, 40, 60 and 80 percent of plate width) of openings. The moment of plates having openings (M_o) was normalized by the ultimate moment capacity of solid plate (M_s). Figure 5.42 shows that presence of small (less than 20 percent of plate width) openings located at the center of a thick plate has no significant effect on the ultimate moment capacity of the thick plate. However, larger opening sizes cause greater reduction on the ultimate moment capacity. Similarly, Figure 5.43 shows the moment rotation curves for a thin plate having centrally located square openings. The plots show that the presence of small openings at the centre of a plate is more severe for thin plates than for the thick plates. This can be explained by the fact that the presence of openings in thin plates would not only reduce the net cross section area of the plate, but it would also change the buckling characteristics of the plate. The opening would provide a free edge on the compression element and initiate localized buckling.

5.6.3 Effect of w/t Ratio

Figure 5.44 shows the moment reduction curves for plates with four different slenderness ratios ($w/t = 25, 50, 100$ and 200) and having various sizes of openings. The figure shows that the moment reduction varies non-linearly with the sizes of the openings for thick and thin plates. It can be observed from the figure that small central openings cause higher reduction in moment capacity in a thin plate (plates having high slenderness ratios) compared to the reduction in thick plates (plates having low slenderness ratios). On the other hand, large central openings would cause less reduction in the moment capacity of thin plates compared to thick plates.

5.6.4 Rectangular Plates having Circular Hole Subjected to In-plane Bending

Results from plates having circular openings are presented in Figures 5.45 to 5.52. The results presented included stress distributions, deformed shapes, moment rotation curves and moment reduction curves. The results show that there is no significant difference in the deformed shapes, ultimate moment capacity and moment reduction factors for plates having square and circular openings. However, the stress distributions around the openings were observed somewhat different for square and circular openings. Since the discussion made for plates with square openings is equally valid for plates having circular openings, no further discussion is made for the plates having circular openings.

5.7 Behavior of Plates with Reinforced Openings in Bending

5.7.1 Plate Geometry and Boundary Conditions

As discussed earlier, the main objective of Chapter 5 was to develop reinforcement schemes for thin simply-supported rectangular plates representing the web of cold-formed steel (CFS) joists having web openings. The CFS joists are popularly used as floor joists in housing construction. In cold-formed steel (CFS) housing construction practice, lipped channel sections having web depth 203.2 mm (8 inches) is one of the most commonly used floor joists size. Therefore, the rectangular plates (600 mm long, 203.2 mm wide, and various thicknesses) representing the web of a 203.2 mm x 42.3 mm x 12.7 mm lip channel CFS section is considered herein. The thicknesses of 1 mm, 2 mm, 4 mm, and 8 mm were considered to represent wide range of width-to-thickness ratios ($w/t = 25$ to 203). These plates were subjected to in-plane flexural loadings. This study considered three cases, namely: a solid plate, a plate with openings, and a plate with reinforced openings. The openings of interest included a circular (diameter 127 mm) and a square in shape (size 127 mm) located at the center of the plates. These openings would reduce the width of the plate by 62.5 percent of the width of solid plate.

The magnitude and the distribution of geometric imperfections play a significant role on pre-buckling and post-buckling behavior of plates. A double sine series given by Equation 5.18 to 5.21 was used to represent these imperfections. The plate was transversely simply supported along all edges and was subjected to flexural loading represented by equal rotations applied to the two opposite edges. The displacement control method was used. The loadings were applied until the rotation level reached

0.02 radians, which would give a clear picture of deformed shape of the plate. The details of the boundary conditions applied to the plate models are shown in Figure 5.31. Elasto-plastic material properties ($E = 203000$ MPa, $F_y = 350$ MPa and $\mu = 0.3$) were used in this investigation.

5.7.2 Reinforcements

The reinforcements were applied on the top and bottom of the openings. Strip reinforcements having a width of 38.1 mm (distance between the plate edge and the opening edge) and with various thickness (1 mm, 2 mm, 4 mm, and 8 mm) were assumed to be screw fastened to the main plate along the top and bottom edges of the openings. The length of such reinforcements was 274 mm which is the opening width plus opening depth plus two times minimum end distance for screws (10 mm). These reinforcements were modeled using four-nodded shell elements and elasto-plastic material.

5.7.3 Connections

The main plate and the reinforcements were connected by screw connections. The simplified finite element model for screw connections for thin plates developed in Chapter 4 was used to represent the screw connection between the plates and reinforcements. The connection model-II was utilized here. The effectiveness of reinforcements depends on the screw spacing and screw patterns. Here, starting from the central screw, the screws were fastened along the edge of the openings at a spacing of $d/4$ where d is depth of the openings. Such spacing was within the minimum spacing requirements established in Section 2.7.1 of Chapter 2. Two stabilizing screws were also fastened at the each edge of the reinforcements. This arrangement resulted in nine screws per

reinforcement for both circular and square openings. Since only the middle surfaces of the plates were modeled using shell elements, a reasonable gap was provided between the main plate and the reinforcements. The amount of such gaps was determined by the half of the thickness of the main plate plus the half of the thickness of the reinforcements. These gaps are essential to represent the eccentricity of loading in the main plate-to-reinforcement connections. A contact element described in Chapter 4 was defined between the plate and the reinforcements. A contact offset (equal to half of the gap) was set for this surface, so that the plate and reinforcement experience contact forces normal to the plate when the two surfaces touch each other. Friction between the plate and reinforcements was assumed to be zero.

5.7.4 Results and Discussions

The results from the finite element analysis on reinforced plates with central openings subjected to in-plane bending are presented in Figures 5.53 to 5.60. The results include the deformed shapes and the moment-rotation curves. The deformed shape of the finite element model would give a clear vision on the failure modes of the plate. The deformed shapes shown in this chapter are corresponding to the rotation level of 0.02 radians. The rotation level was selected in such a way that the deformed shape would be distinct and visible. The moment rotation curves for the corresponding plate models are presented along with the deformed shapes. The moments are normalized by the ultimate moment capacity of a solid plate (M_s). Such normalization would give the moment capacity of the plates with unreinforced openings and with reinforced openings as a fraction of the moment capacity of the solid plate.

The analysis began with a 1 mm thick plate and a w/t ratio of 203. Failure of this plate was governed by buckling of the plate in the compression region. The central

part of the plate was cut out to a square opening and then reinforced with 1 mm thick strips on the top and bottom of the opening. The deformed shape of the reinforced plate is shown in Figure 5.53. The figure shows that failure of reinforced plate was governed by buckling of the main plate. Moreover, an evidence of local buckling of the reinforcement is evident in the figure. Figure 5.54 shows the normalized moment rotation curves for the solid plate, the plate with unreinforced openings, and the plate with reinforced openings. The curves show that the reduction in the in-plane moment capacity of the plate ($w/t = 203$) having square opening ($d/h = 0.62$) is 68 percent. Failure of the plate with opening was due to local buckling at the opening region. Figure 5.54 also gives the moment rotation curve for the plate with reinforced openings. The figure shows that the reinforced plate was capable of reaching the moment capacity of the solid plate.

Figure 5.55 shows the deformed shape of a 2 mm thick ($w/t = 102$) solid plate and plates with reinforced openings. The solid plate failed in buckling mode. Two different sizes (1 mm and 2 mm) of reinforcement were considered for the square openings. The deformed shape of the plate with 1 mm thick reinforcement shows that the failure was due to local buckling of the reinforcement and overall buckling (column buckling) of the compression element of the plate. This implies that the thickness of the reinforcement was not sufficient to prevent the local buckling of the reinforcement itself and overall buckling of the compression element of the plate above the openings. However, the reinforcement was adequate to prevent the local buckling of the main plate at the opening region. The plate with a 2 mm thick reinforcement failed at a location outside the opening region. Figure 5.56 shows the normalized moment rotation curves for the solid plate, the plate with unreinforced square openings and the plate with two different reinforcements at the opening region. The curves clearly show that the 1 mm thick reinforcement was not capable of restoring the in-plane

moment capacity of the plate. However, the in-plane moment capacity of the plate with a 2 mm thick reinforcement was 5 percent higher than the in-plane moment capacity of the solid plate. Such higher moment was due to the change in the buckling shape of the plate in the presence of a reinforcement.

The deformed shapes of 4 mm thick ($w/t = 51$) plate with reinforced openings are shown in Figure 5.57. As discussed in Section 5.6, failure of such plates ($w/t = 51$) would be governed by the yielding of the cross section. Three different thicknesses (1 mm, 2 mm and 4 mm) of reinforcement were considered for the square openings. The figure shows that the plate with 1 mm and 2 mm thick reinforcement failed by local buckling of the reinforcement. However, the plate with 4 mm thick reinforcement failed in cross sectional yielding of the reinforcement and the main plate. The corresponding normalized moment rotation curves are shown in Figure 5.58. The figure shows that none of the reinforcements were capable of restoring the in-plane flexural strength of the plate with opening to the in-plane flexural strength of the solid plate. Similar results can be seen in Figures 5.59 and 5.60 for the 8 mm thick ($w/t = 25$) plates. It can be concluded from these results that as thicker plates are capable of reaching the plastic moment capacity, attention must be given to plastic analysis for the design of the reinforcement for such plates. No further attempts were made to establish the adequate reinforcements for thick plates ($w/t = 51$ and 25), because it was out of the scope of this research.

In summary, it was observed that attention must be paid to the failure modes of plates and reinforcements while designing the reinforcements for plates with openings. The failure modes include: (a) local buckling of the plate around the openings, (b) localized buckling of the reinforcements, and (c) yielding of the main plate and reinforcements.

5.8 Conclusion

An analytical study was carried out on the flexural strength of long solid plates, plates with openings and plates with reinforced openings. The parameters of interest included the type of the loading, slenderness (w/t ratio) of the plates, size of the openings, shape of the openings and sizes of reinforcements. Plate subjected to uniform compressive load and in plane flexural load were considered. The failure of plates having low slenderness ratio would be governed by cross sectional yielding and the failure of plates having high slenderness ratio would be governed by plate buckling. The analytical results show that for the plates having slenderness ratio, w/t , equal to 100, and 200, there was no significant reduction in the ultimate compressive strength when the size of the central openings was less than 40 percent of the plate width. However, for the plates subjected to in-plane bending, small central openings caused higher reduction in moment capacity of plates having higher slenderness ratios compared to plates having lower slenderness ratios. Furthermore, large central openings would cause less reduction in moment capacity of thin plate with compared to thick plates. No significant difference in behavior was observed between square and circular openings.

Plates with various slenderness ratios and an opening of 62.5 percent of the plate width were reinforced using strip reinforcements. The analytical results show that it is possible to reinforce plates having openings with flat strips. Such reinforcements are capable of restoring the in-plane flexural strength of plates with openings. The strength of a reinforced plate was as high as the strength of a corresponding solid plate. Attention must be paid on the failure modes of both plates and reinforcement while designing the reinforcements for plates with openings. The failure modes include:

(a) localized buckling of the plate around the openings, (b) localized buckling of the reinforcements, and (c) yielding of main plate and reinforcements.

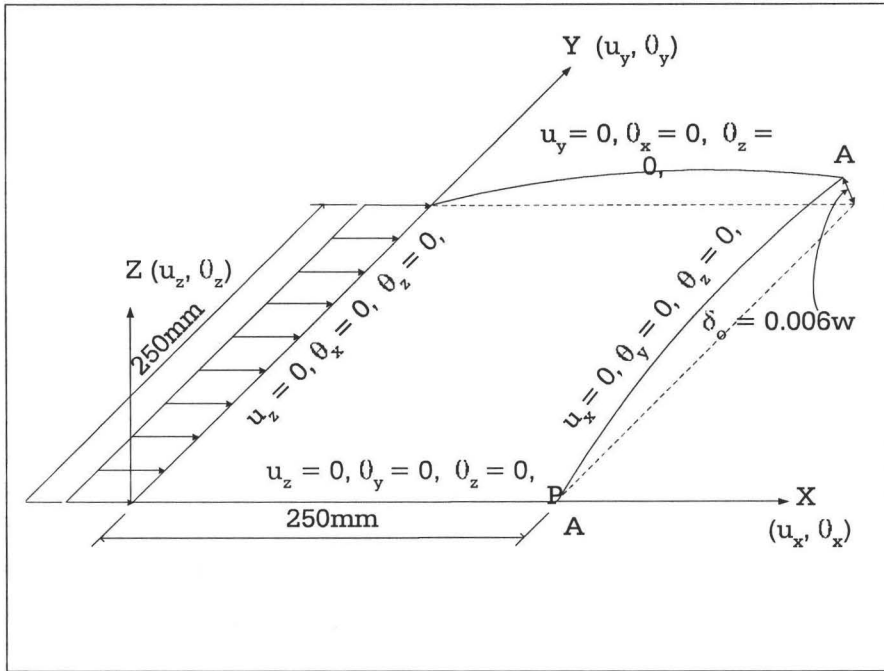


Figure 5.1: Finite element boundary conditions for a quarter plate model

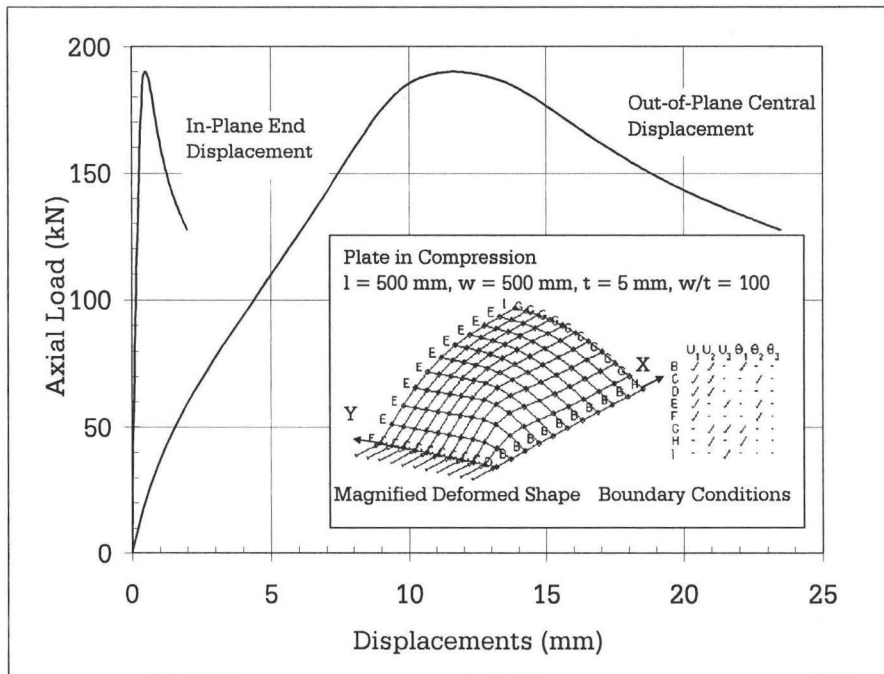


Figure 5.2: Load displacements curves for simply supported square plate subjected in compression corresponding to quarter model)

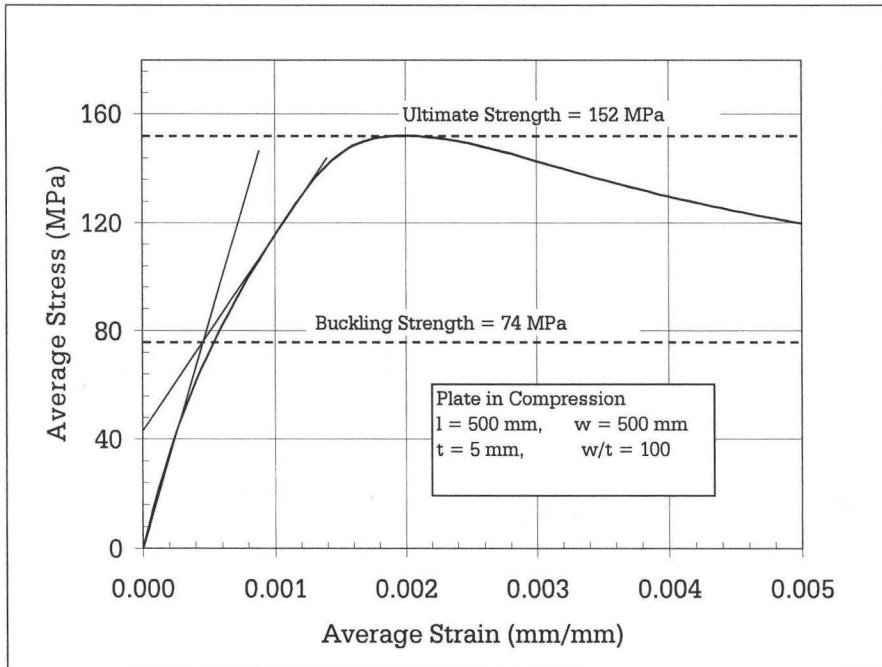


Figure 5.3: Behavior of simply supported square plate subjected in compression

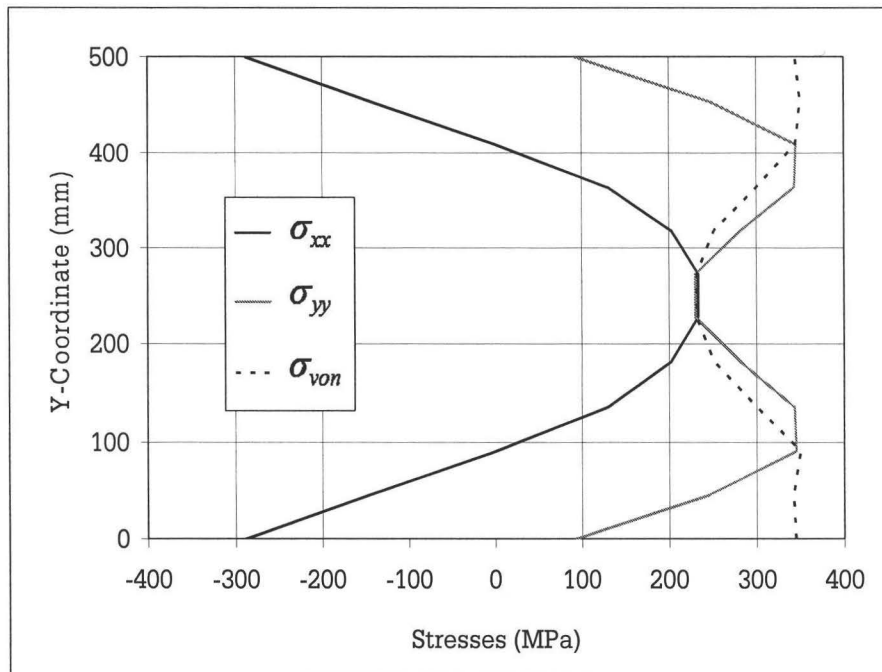


Figure 5.4: Stresses variation along A-A on the outer surface (convex face) of the plate at peak load

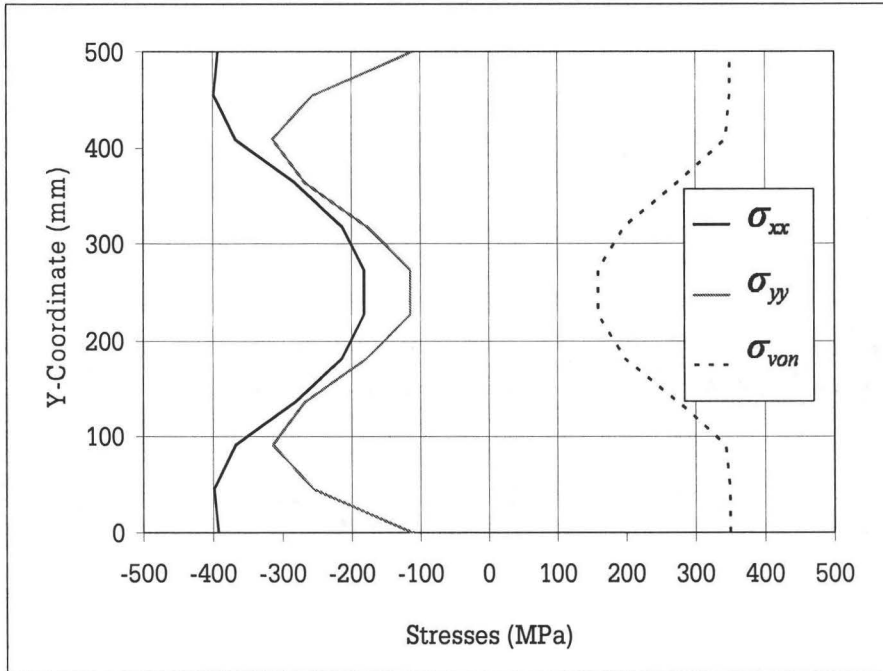


Figure 5.5: Stresses variation along A-A on the inner surface (concave face)of the plate at the peak load level

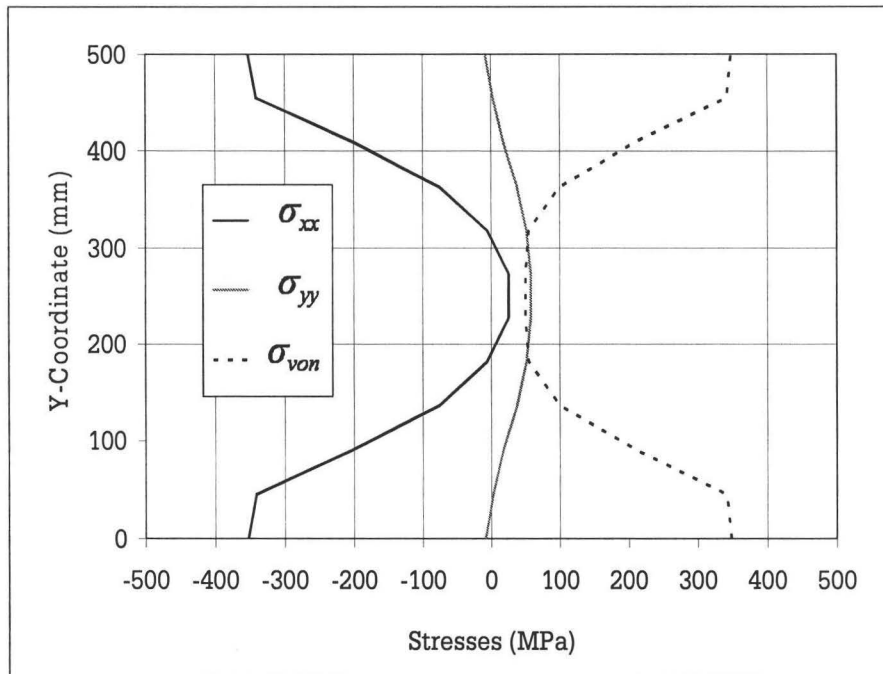


Figure 5.6: Stresses variation along A-A on the mid-surface (mid-thickness)of the plate at the peak load level

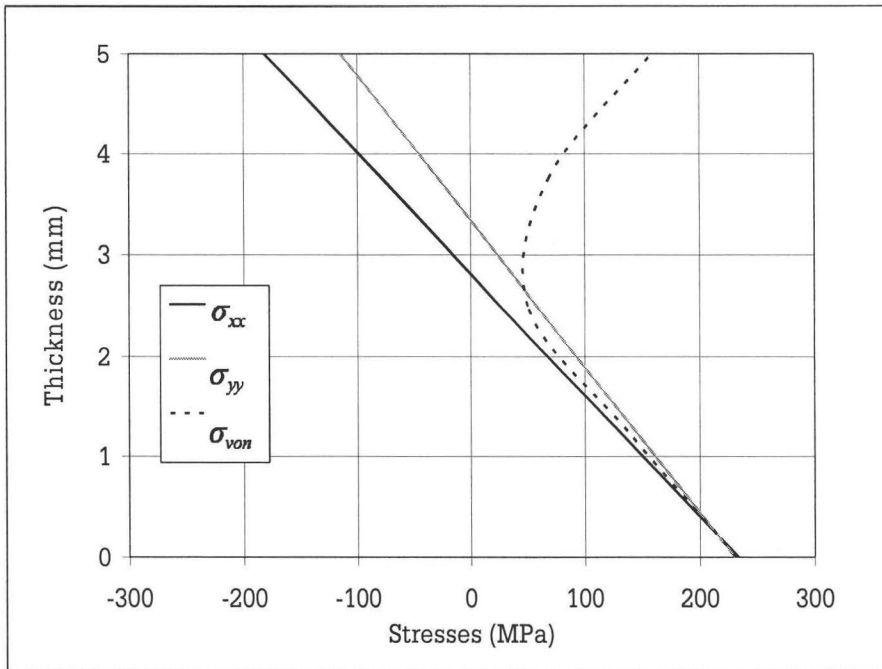


Figure 5.7: Stresses through the thickness at the center of the plate

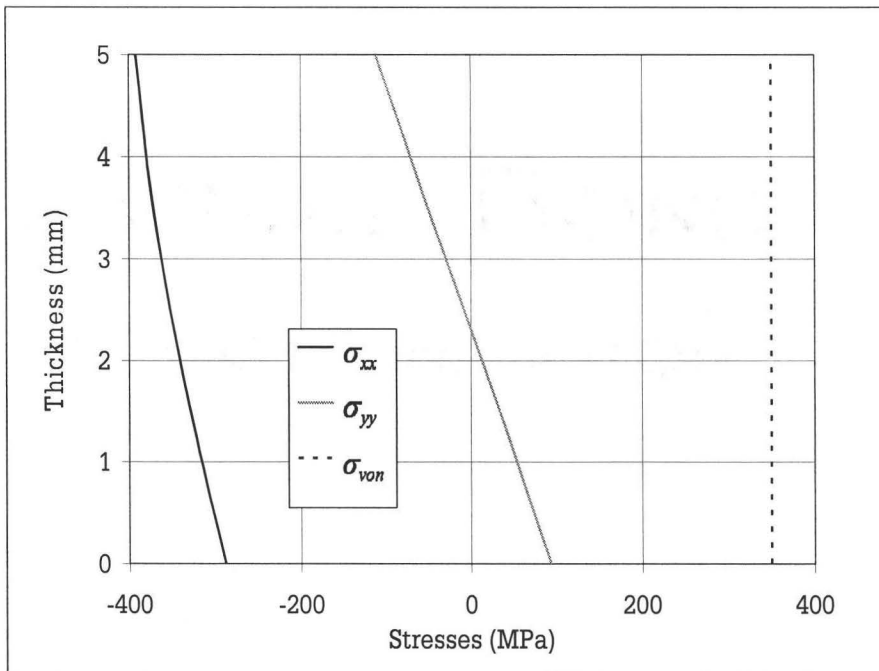


Figure 5.8: Stresses through the thickness at the side-edge of the plate

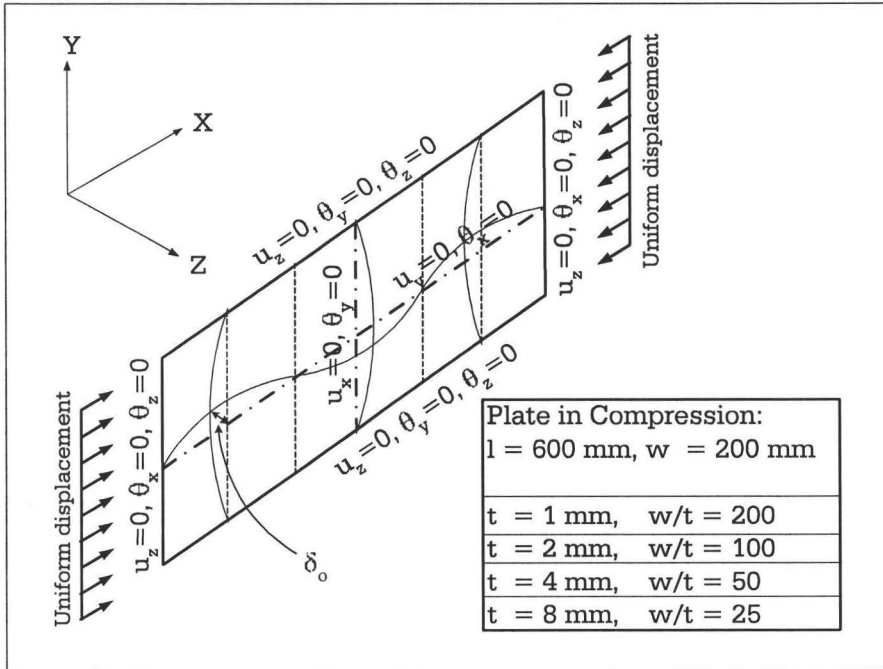


Figure 5.9: Finite element boundary conditions for the long plate in compression

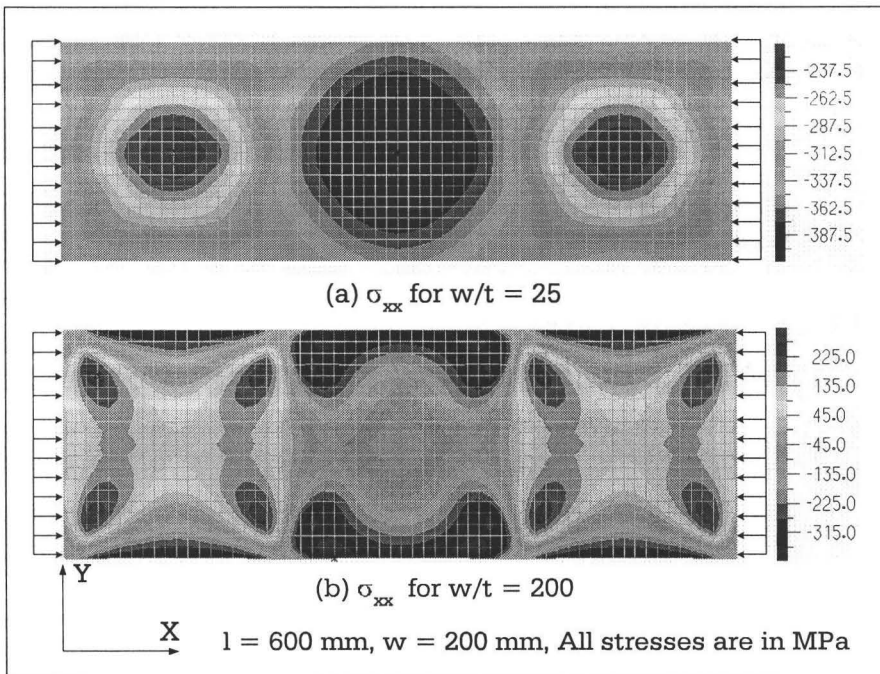


Figure 5.10: Band plots of axial stress for the plate in compression (a) thick plate (b) thin plate

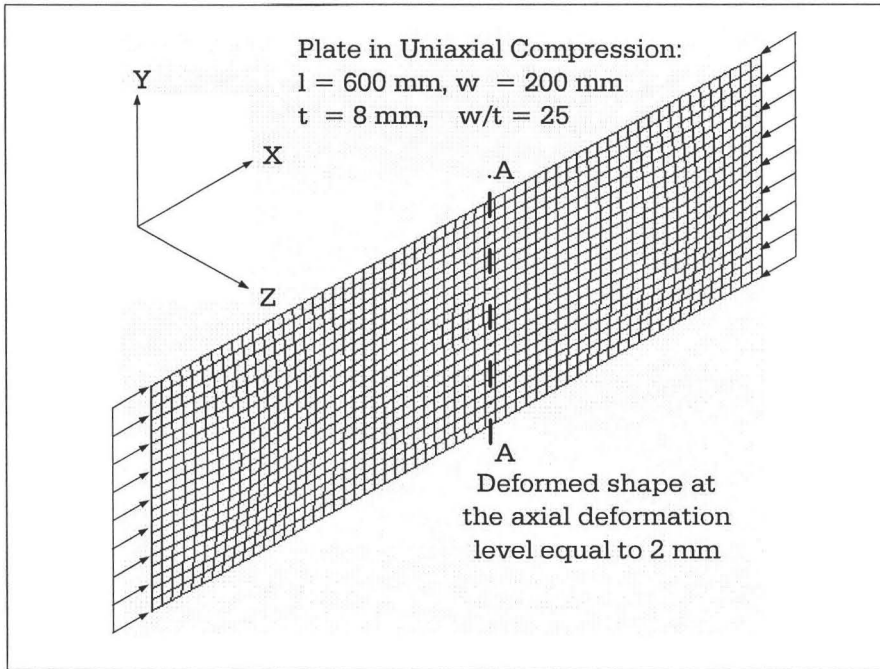


Figure 5.11: Deformed shape of thick plate in compression

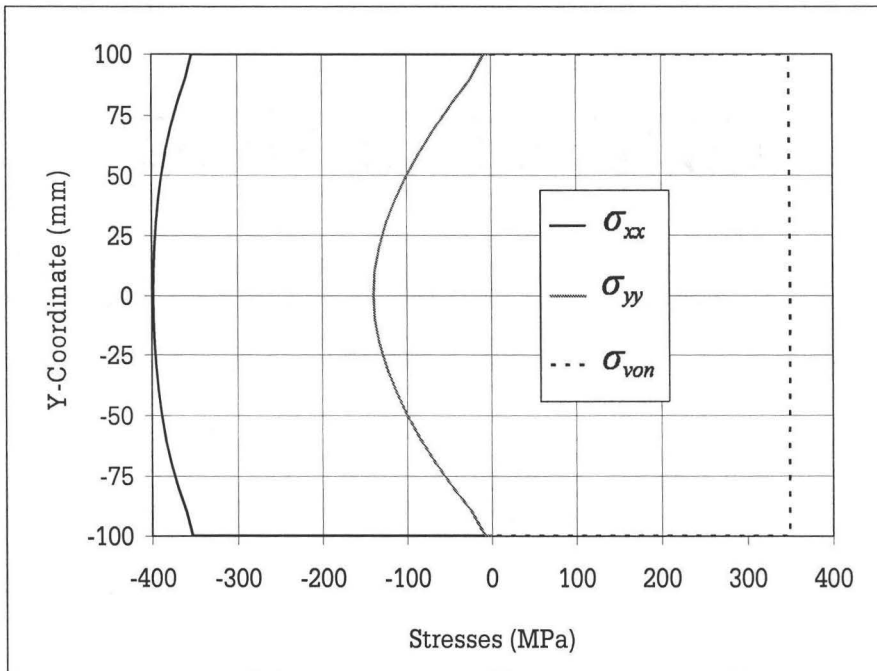


Figure 5.12: Stresses along A-A mid-length of thick plate in compression

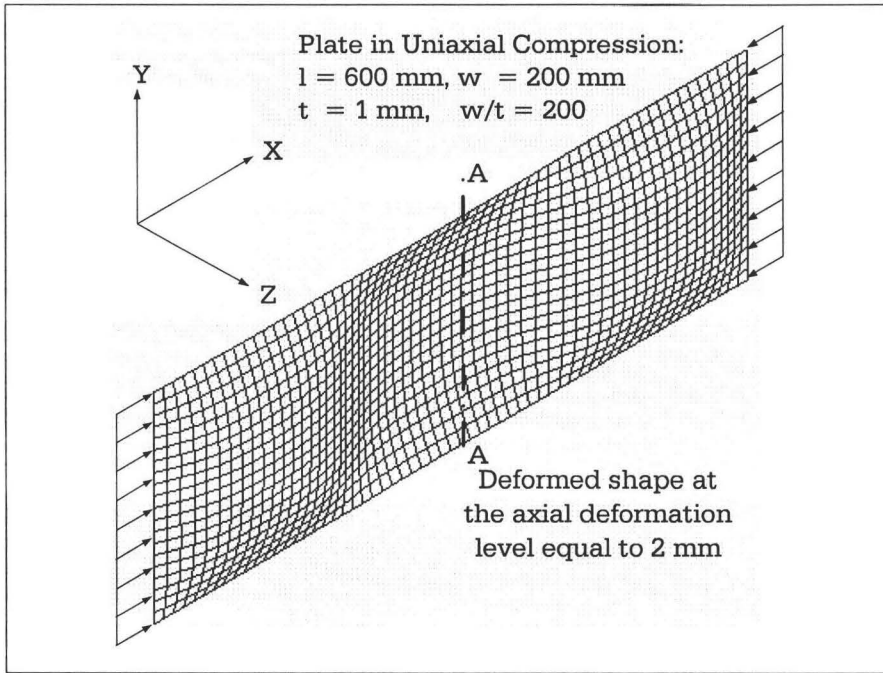


Figure 5.13: Deformed shape of thin plate in compression

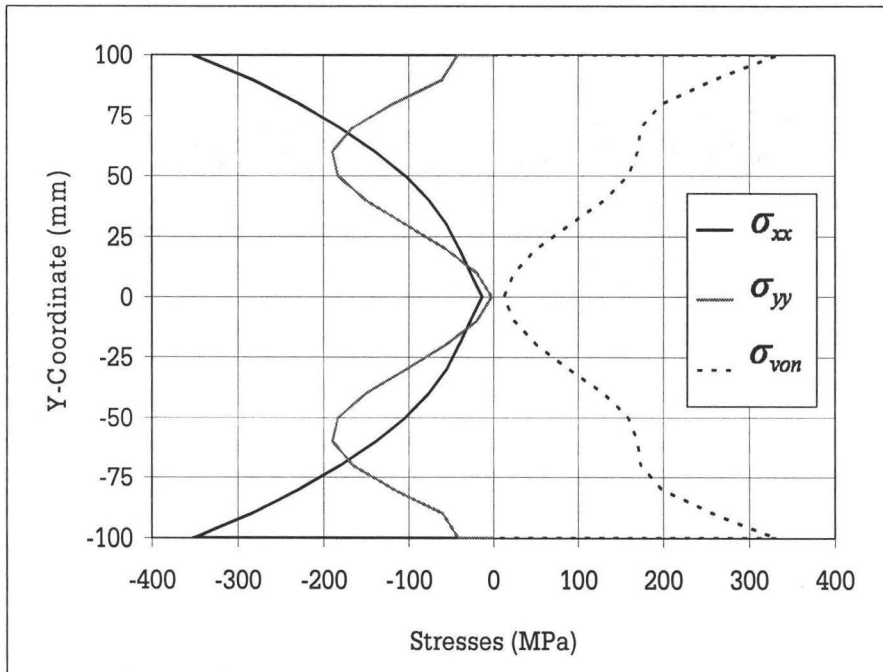


Figure 5.14: Stresses along A-A of thin plate in compression

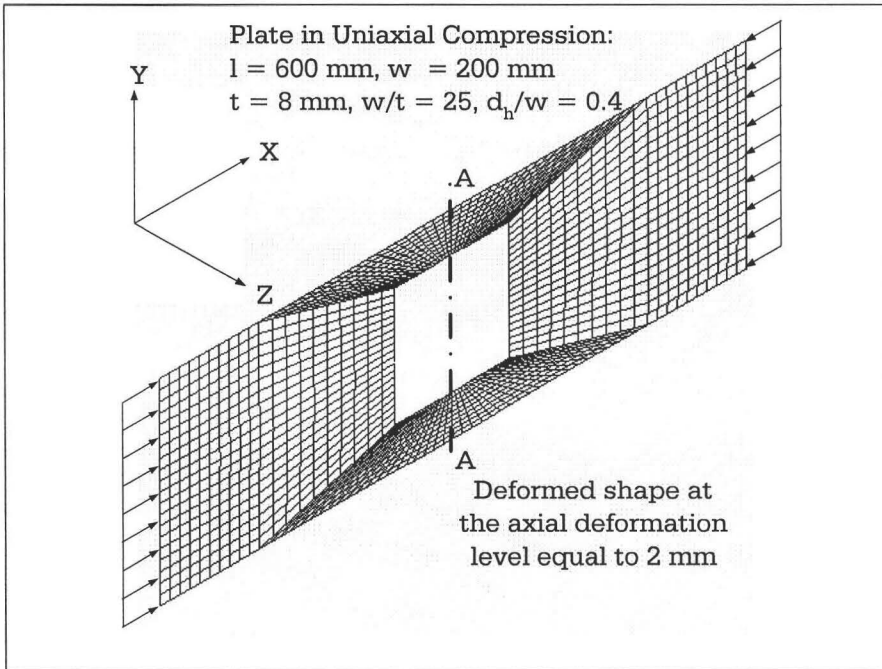


Figure 5.15: Deformed shape of thick plate having square openings in compression

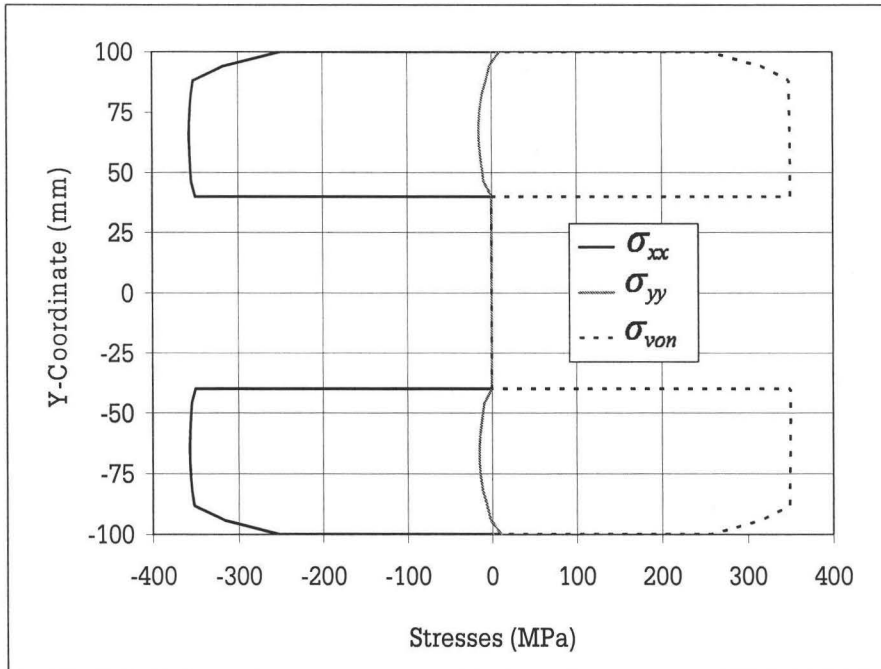


Figure 5.16: Stresses along A-A of thick plate having square openings in compression

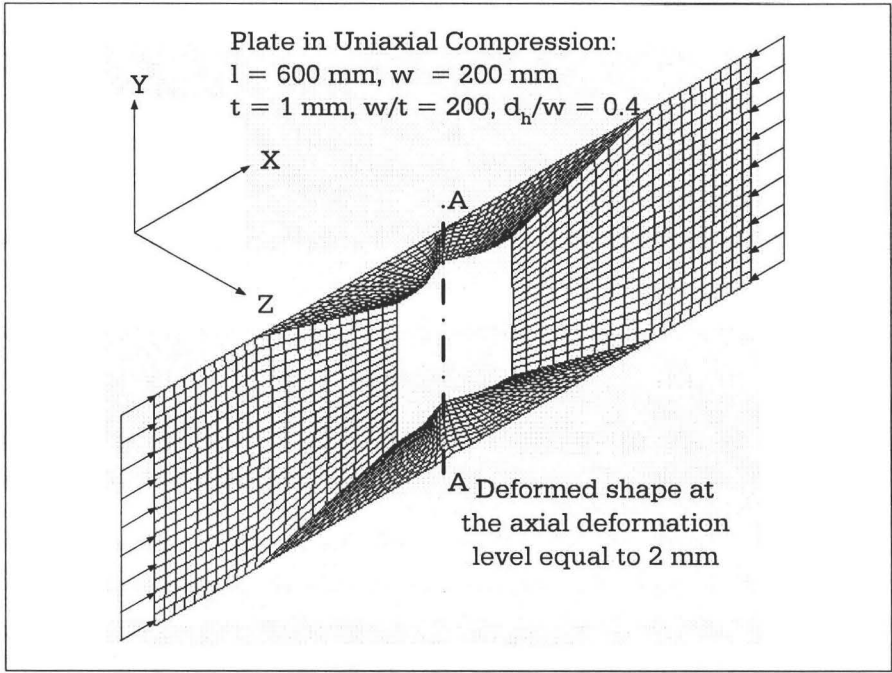


Figure 5.17: Deformed shape of thin plate having square openings in compression

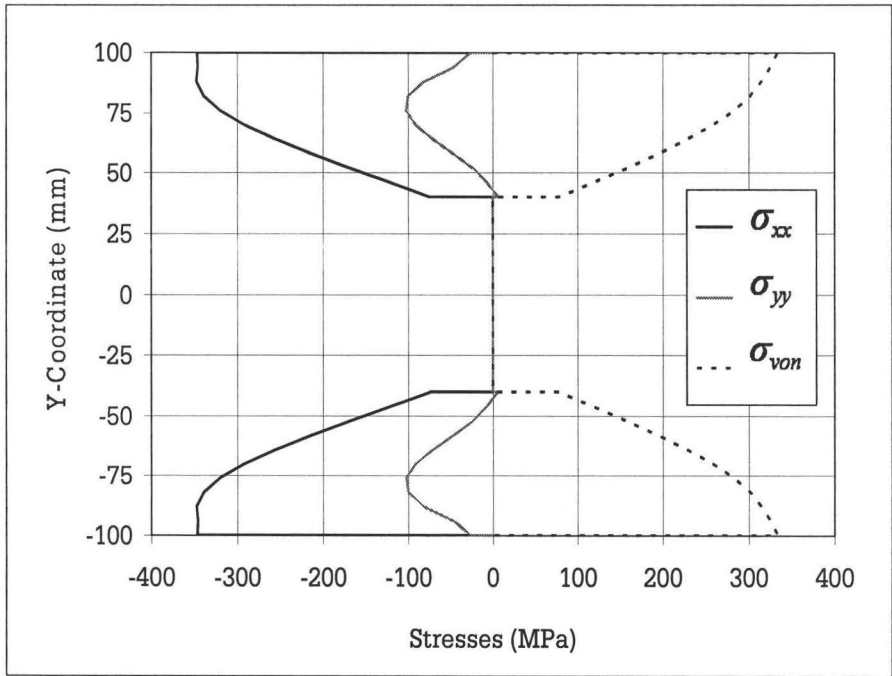


Figure 5.18: Stresses along A-A of thin plate having square openings in compression

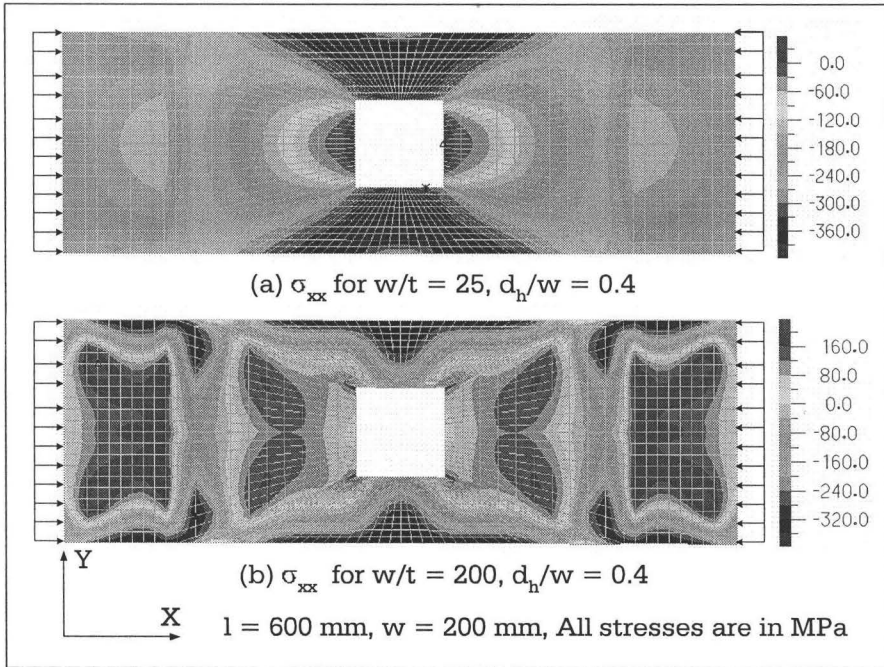


Figure 5.19: Band plots of stress for the plate having square opening in compression (a) thick plate (b) thin plate

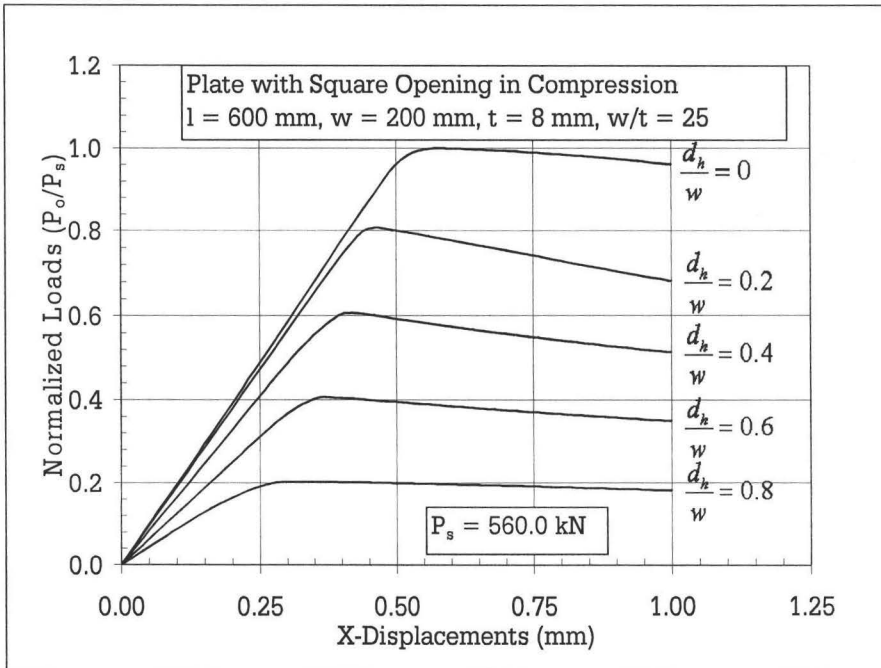


Figure 5.20: Load deformation curves for the thick plate having square openings in compression

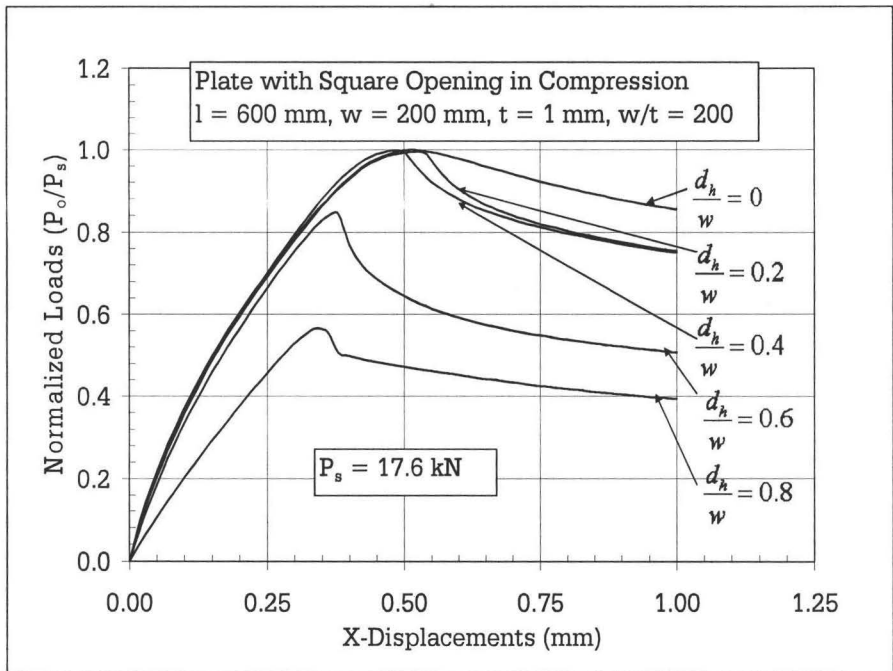


Figure 5.21: Load deformation curves for the thin plate having square openings in compression

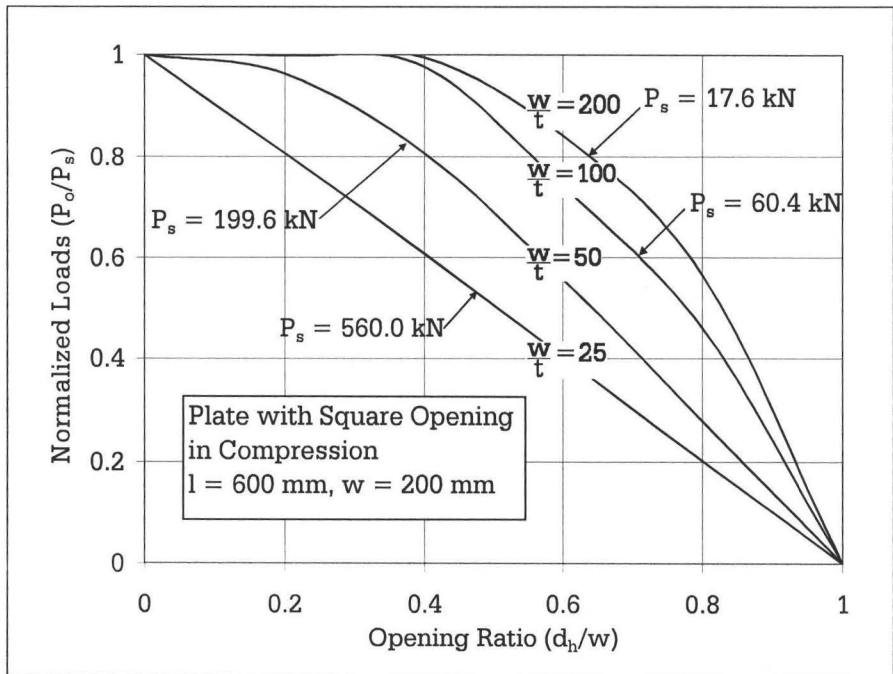


Figure 5.22: Load reduction curves for the plates having square openings in compression

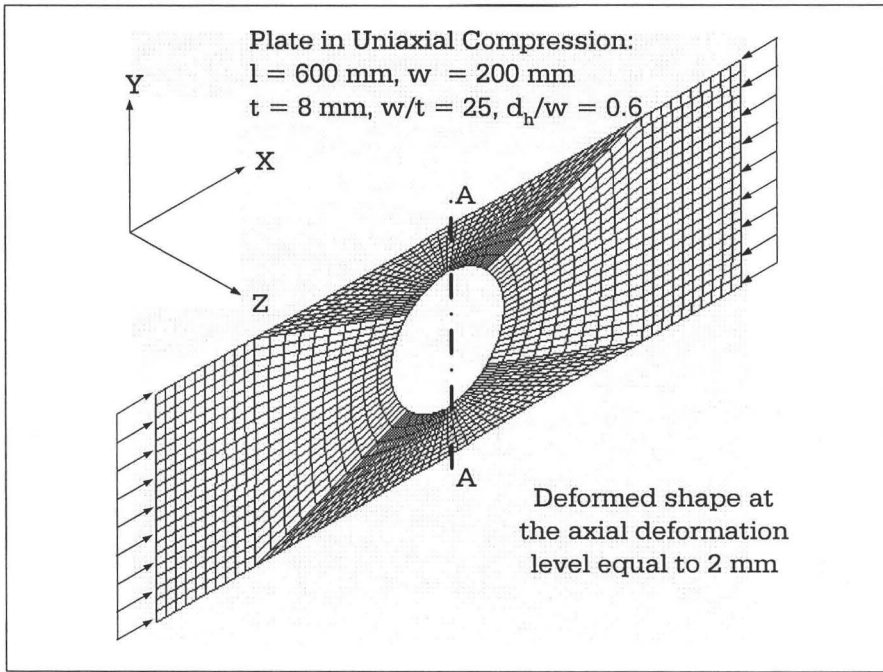


Figure 5.23: Deformed shape of thick plate having circular openings in compression

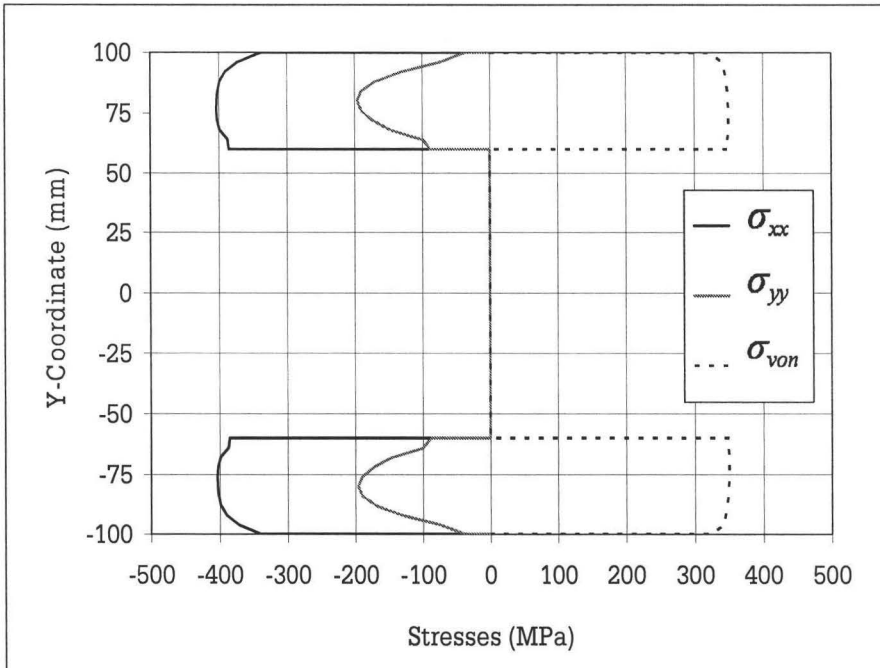


Figure 5.24: Stresses along A-A of thick plate having circular opening in compression

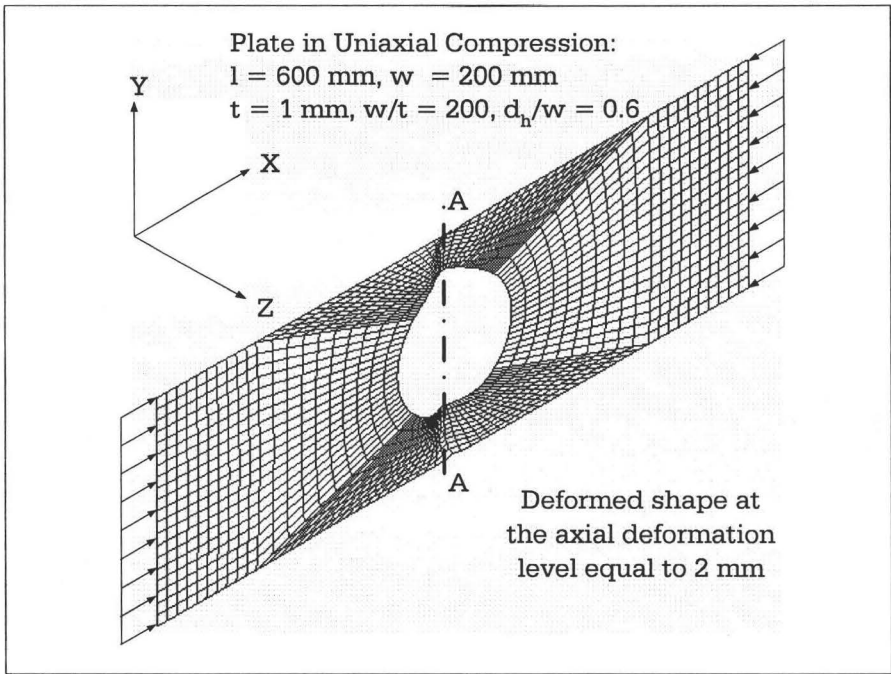


Figure 5.25: Deformed shape of thin plate having circular openings in compression

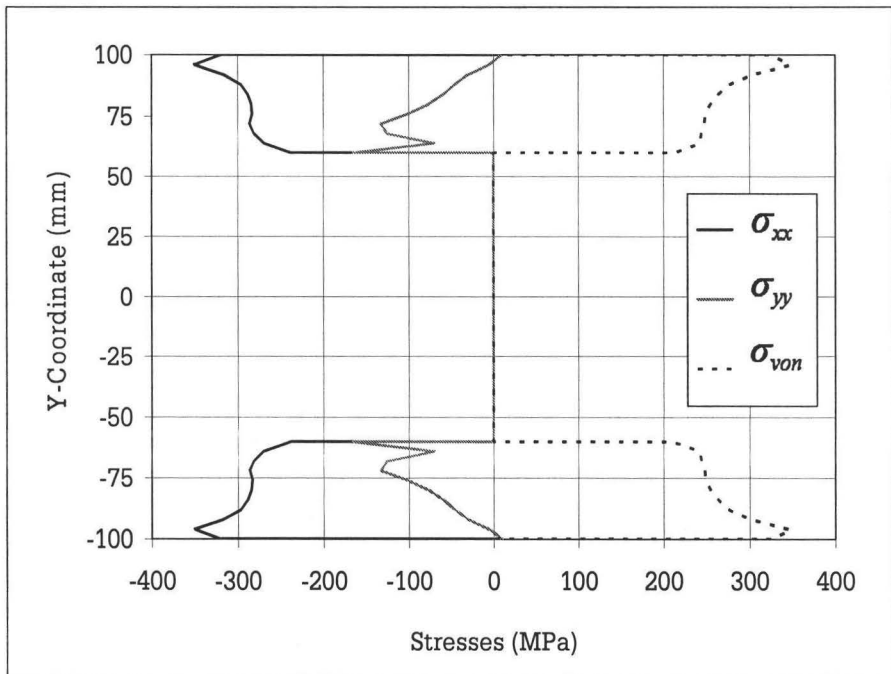


Figure 5.26: Stresses along A-A of thin plate having circular openings in compression

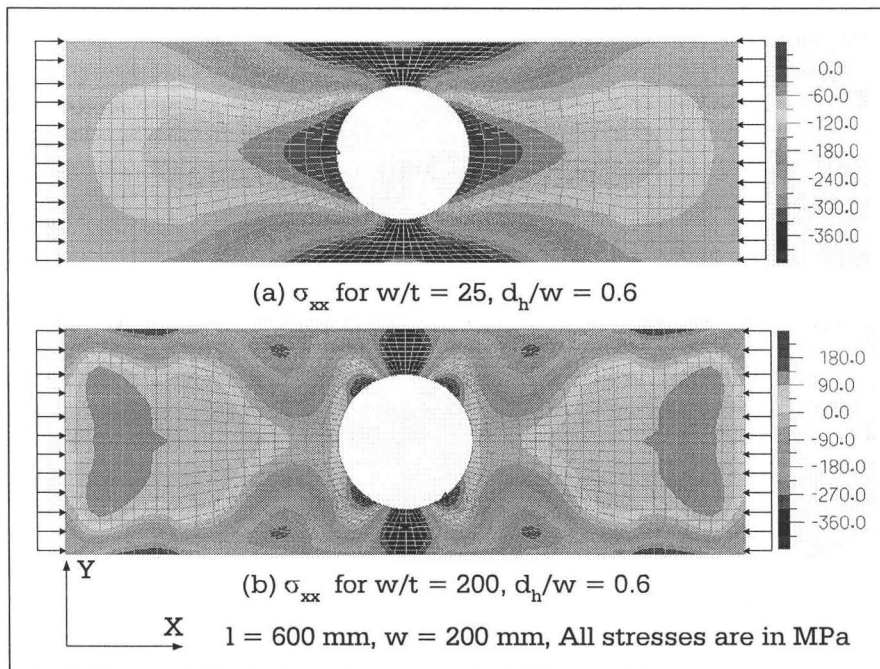


Figure 5.27: Band plot of stress for the plate having circular openings in compression (a) thick plate (b) thin plate

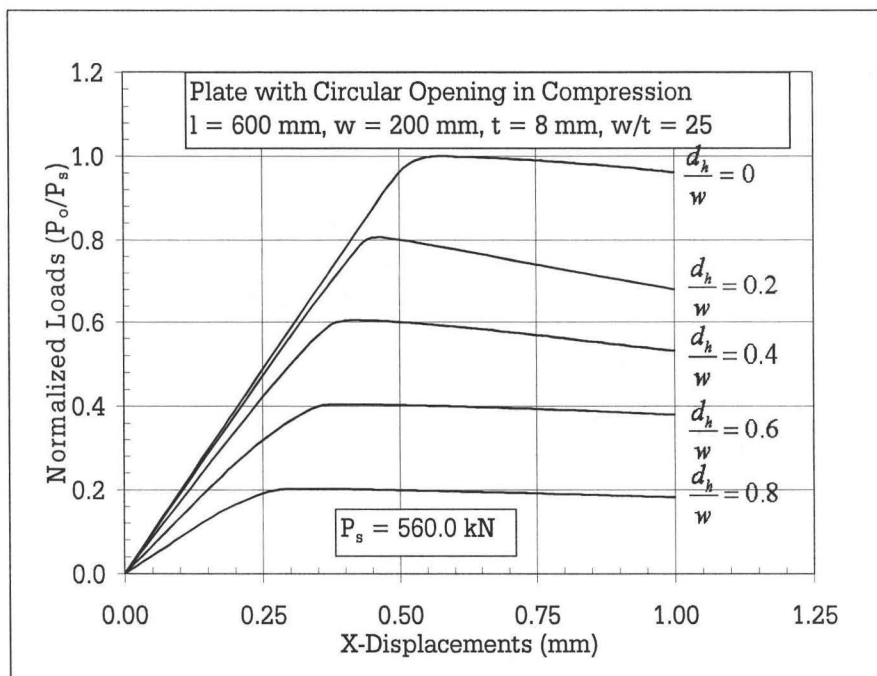


Figure 5.28: Load deformation curves for the thick plate having circular openings of various sizes in compression

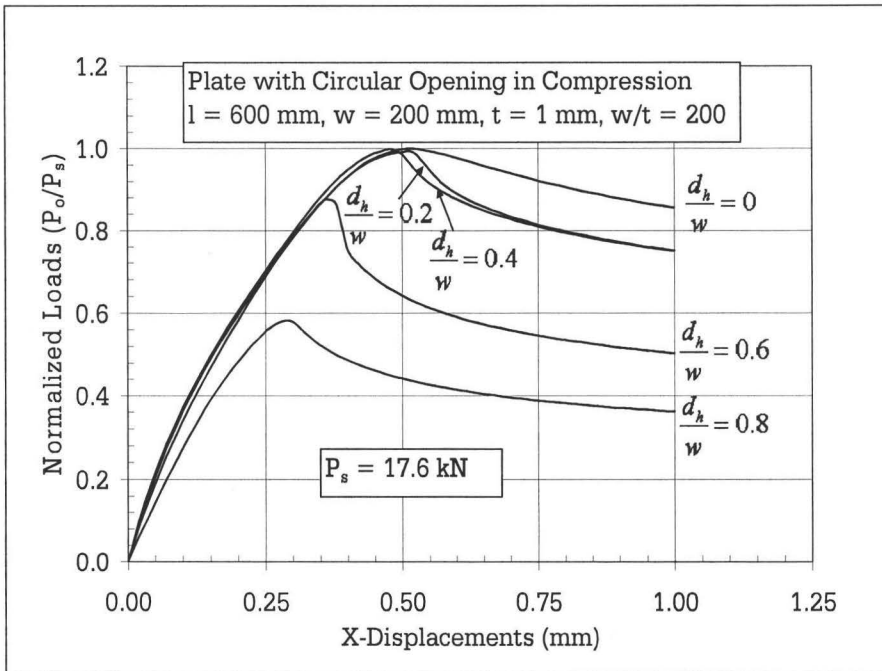


Figure 5.29: Load deformation curves for the thin plate having circular openings of various sizes in compression

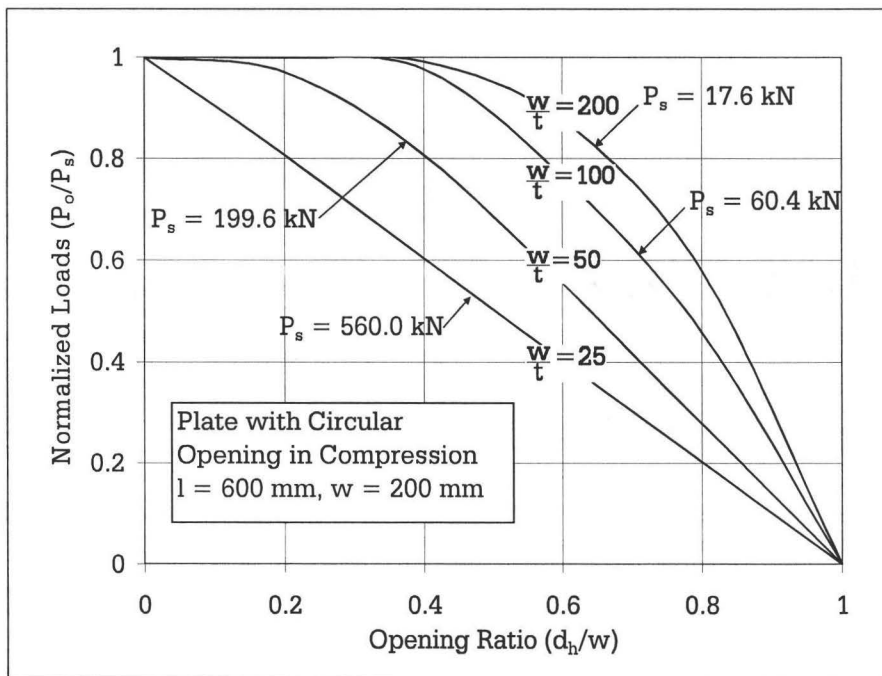


Figure 5.30: Load reduction curves for the plates having circular openings in compression

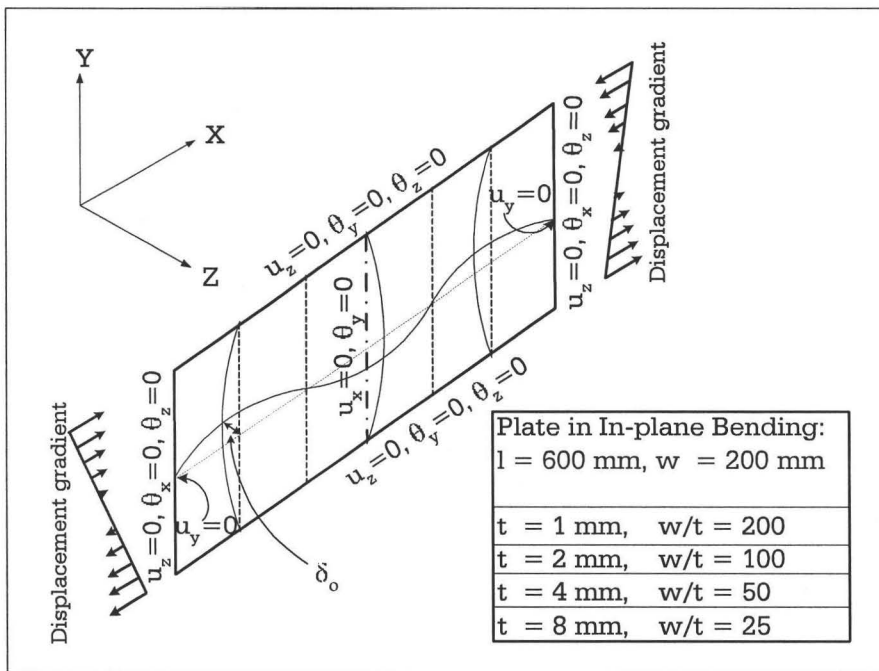


Figure 5.31: Finite element boundary conditions for the plate in in-plane bending

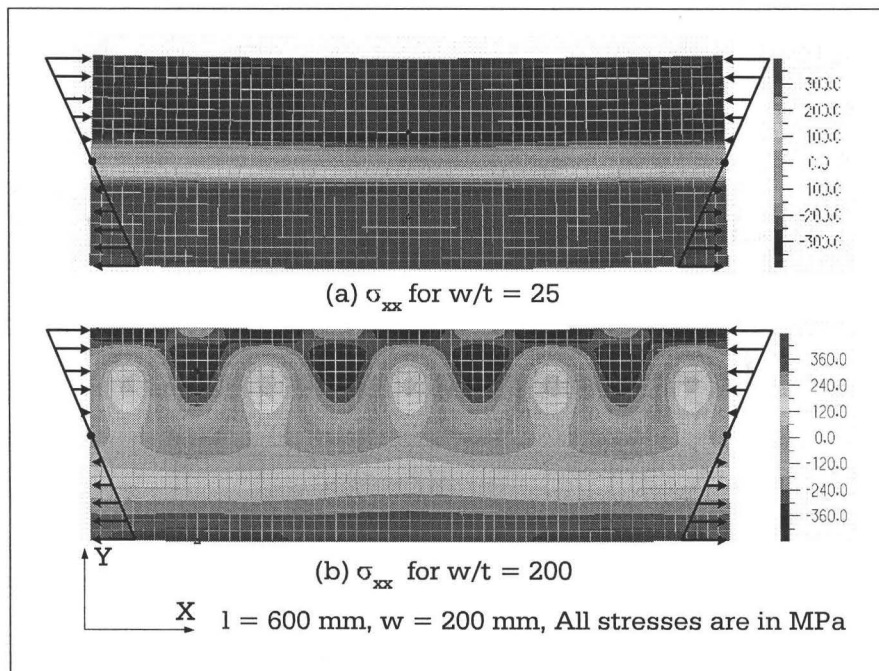


Figure 5.32: Band plot of stress for the plate in bending (a) thick plate (b) thin plate

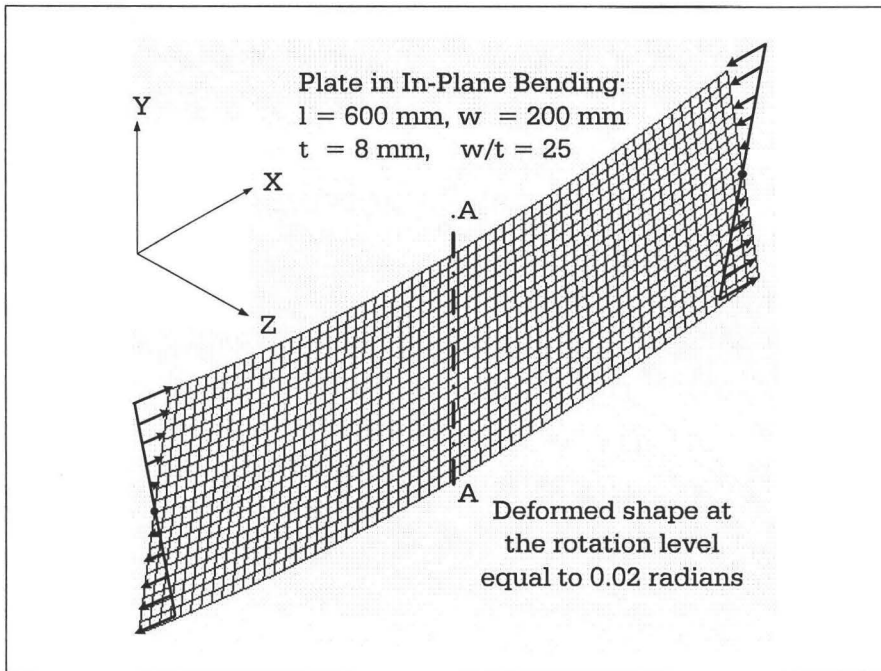


Figure 5.33: Deformed shape of thick plate in bending

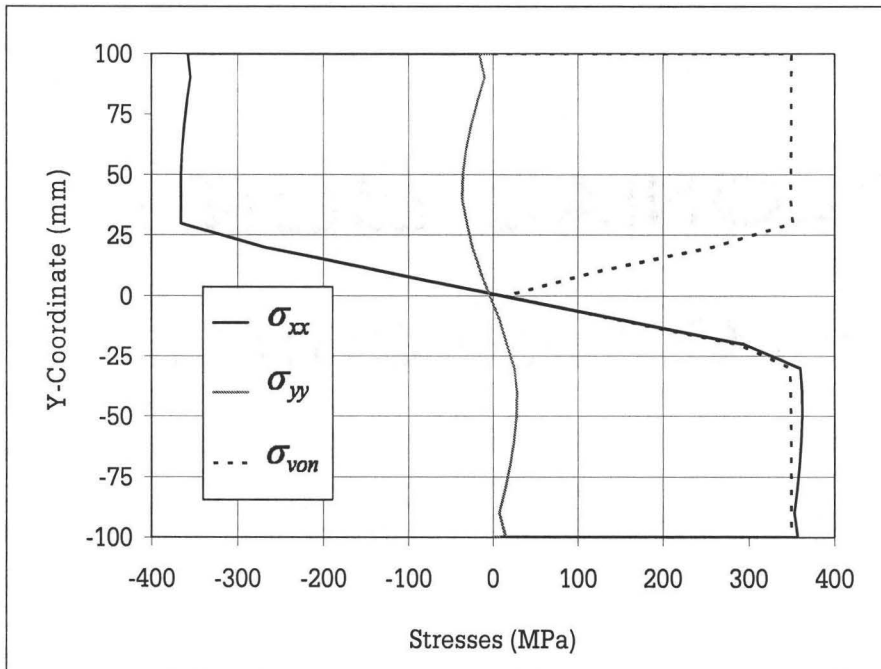


Figure 5.34: Stresses along A-A of thick plate in bending

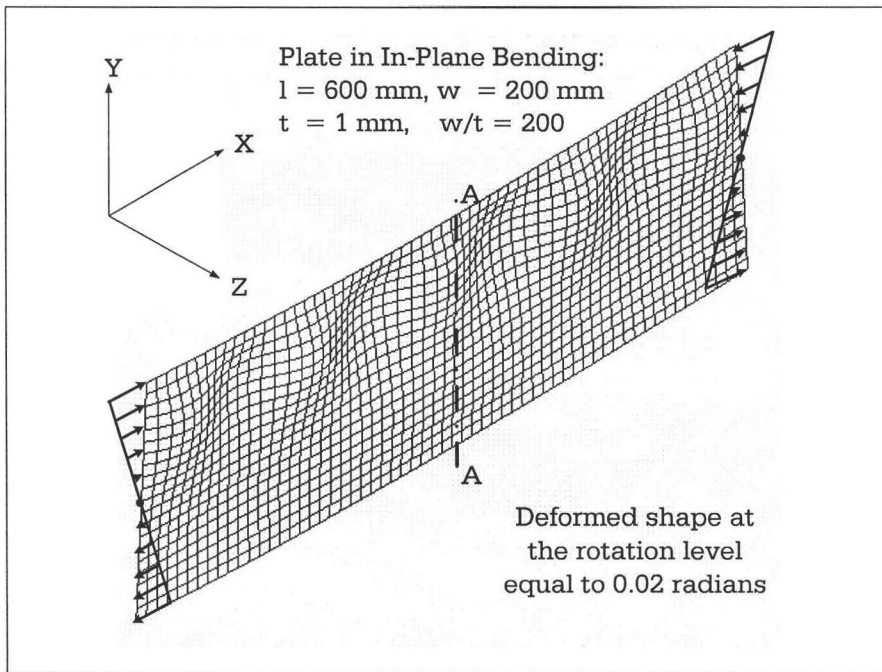


Figure 5.35: Deformed shape of thin plate in bending

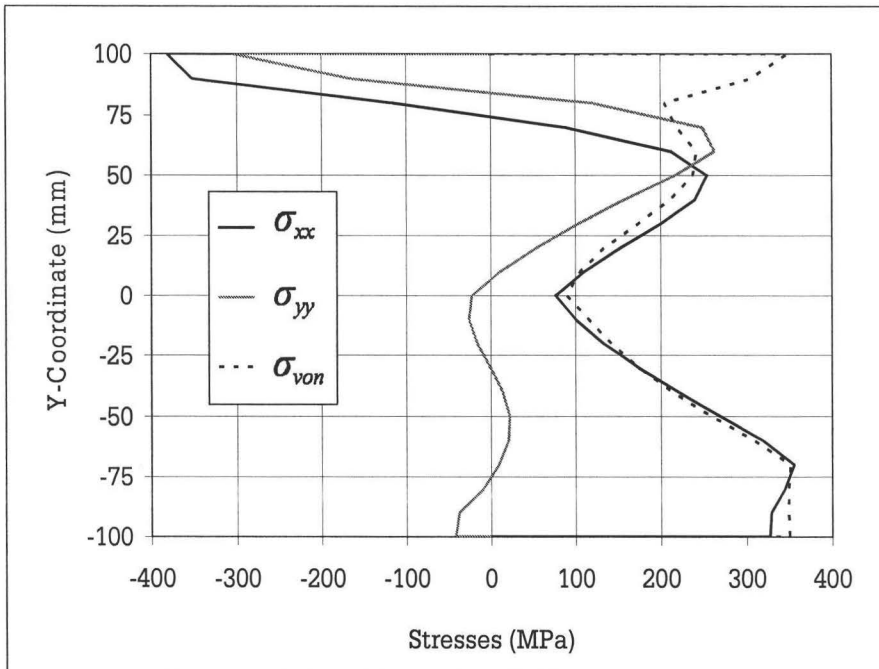


Figure 5.36: Stresses along A-A of thin plate in bending

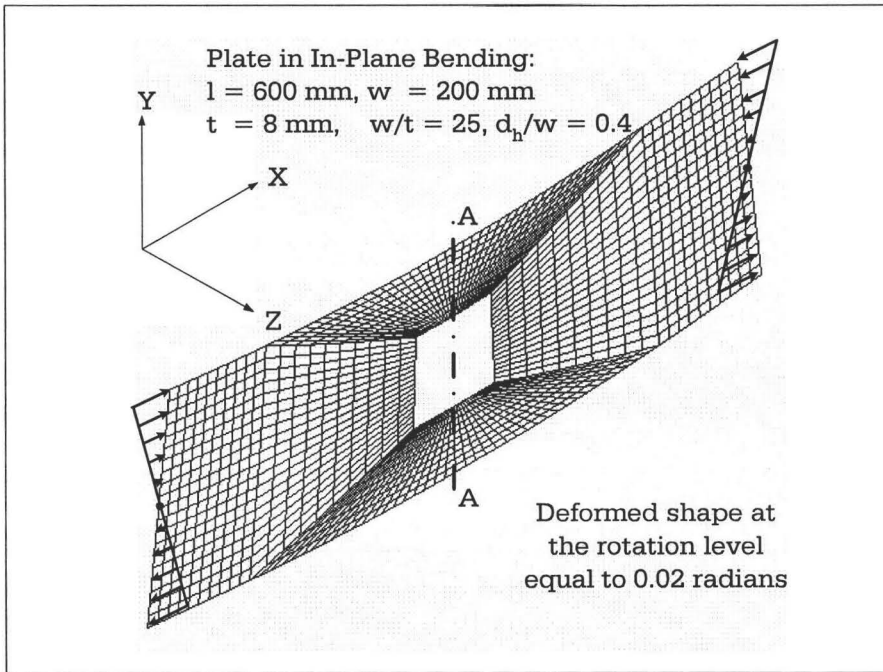


Figure 5.37: Deformed shape of thick plate having square openings in bending

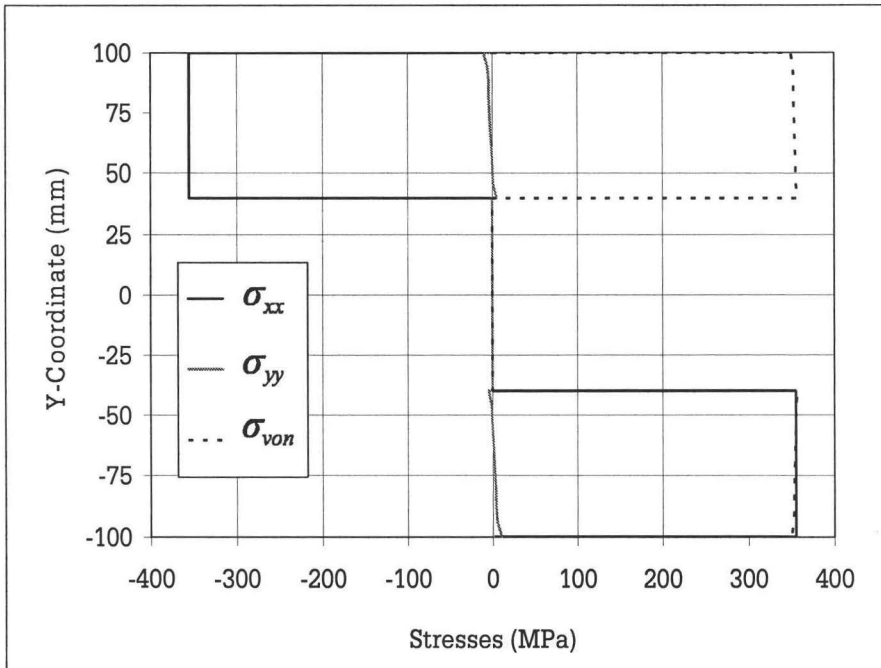


Figure 5.38: Stresses along A-A of thick plate having square openings in bending

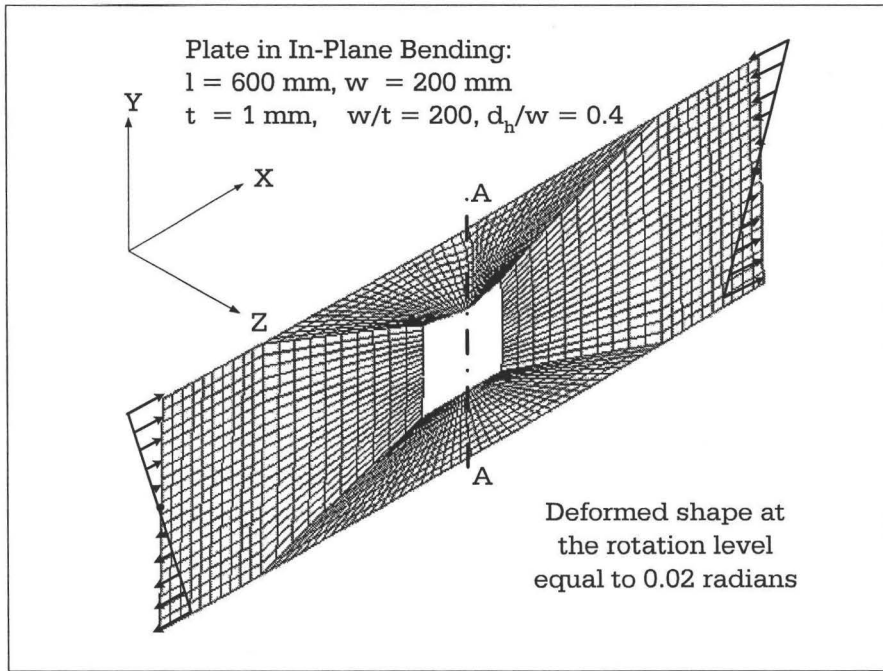


Figure 5.39: Deformed shape of thin plate having square openings in bending

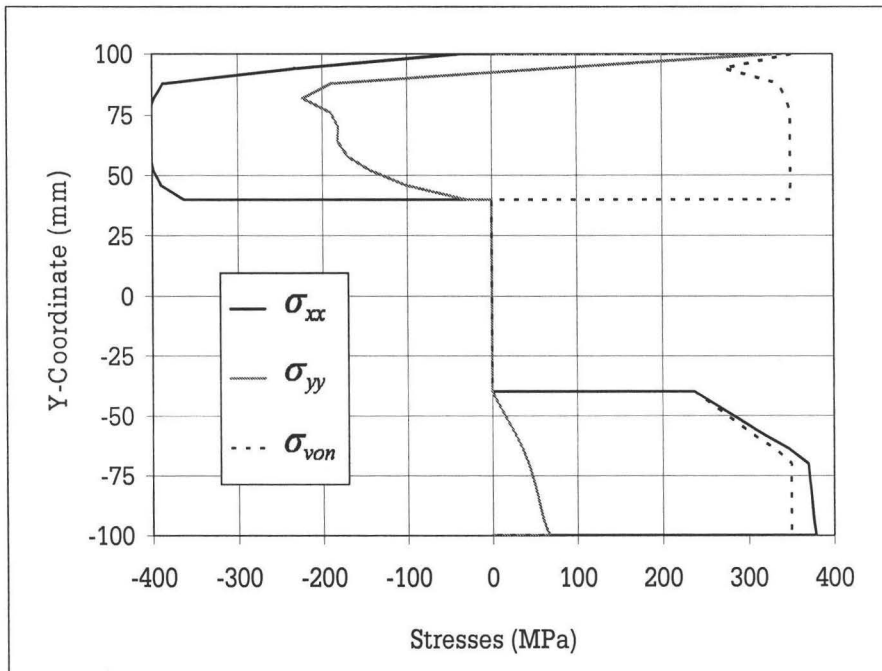


Figure 5.40: Stresses along A-A of thin plate having square openings in bending

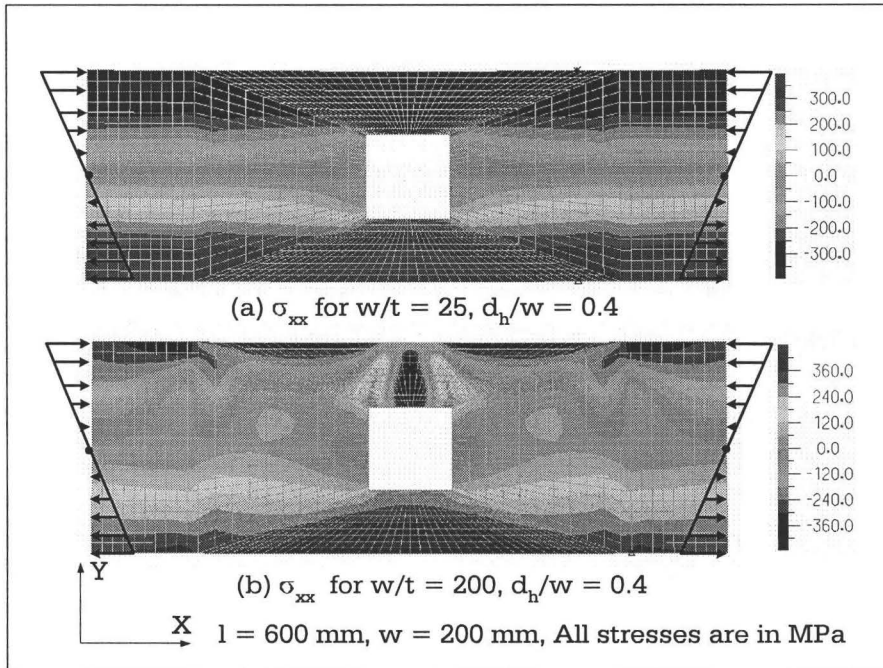


Figure 5.41: Band plots of stress for the plate having square openings in bending (a) thick plate (b) thin plate

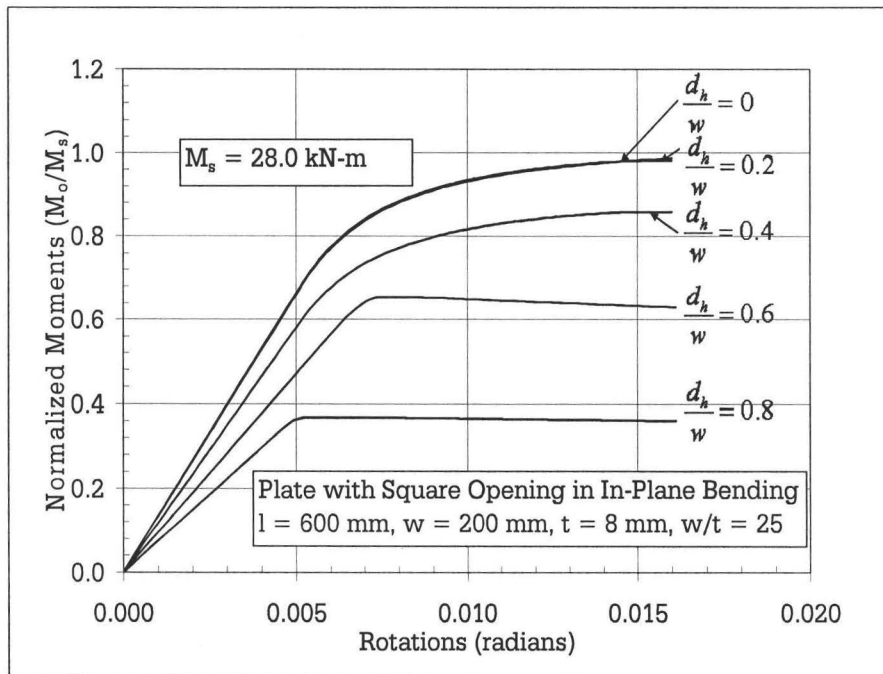


Figure 5.42: Moment rotation curves for the thick plate having square openings in bending

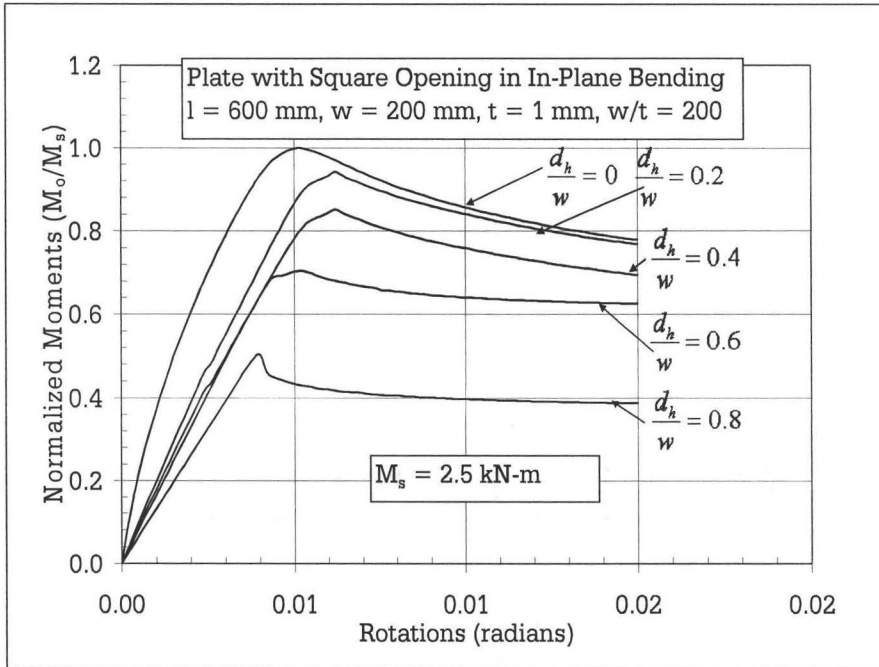


Figure 5.43: Moment rotation curves for the thin plate having square openings in bending

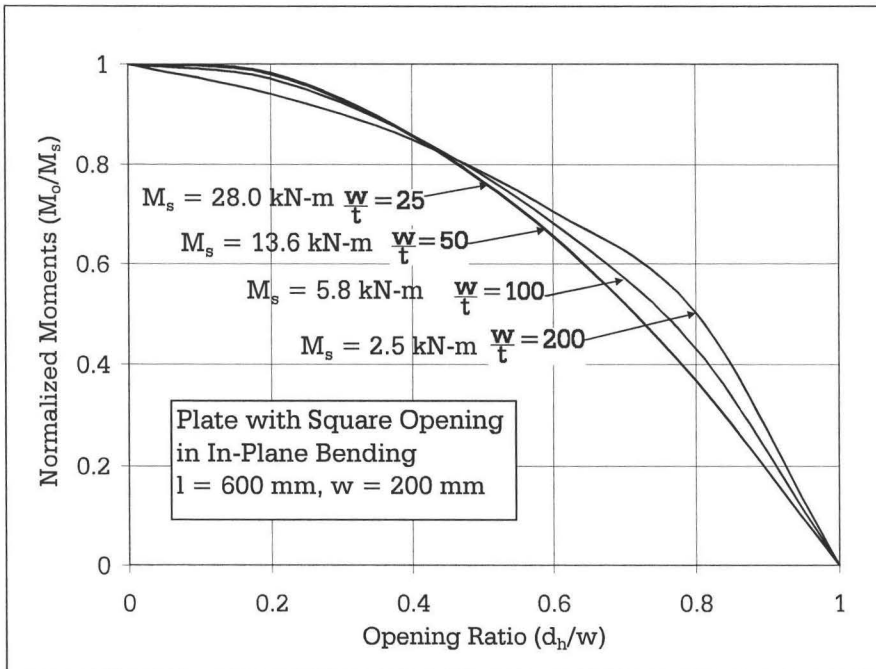


Figure 5.44: Moment reduction curves for the plates having square openings in bending

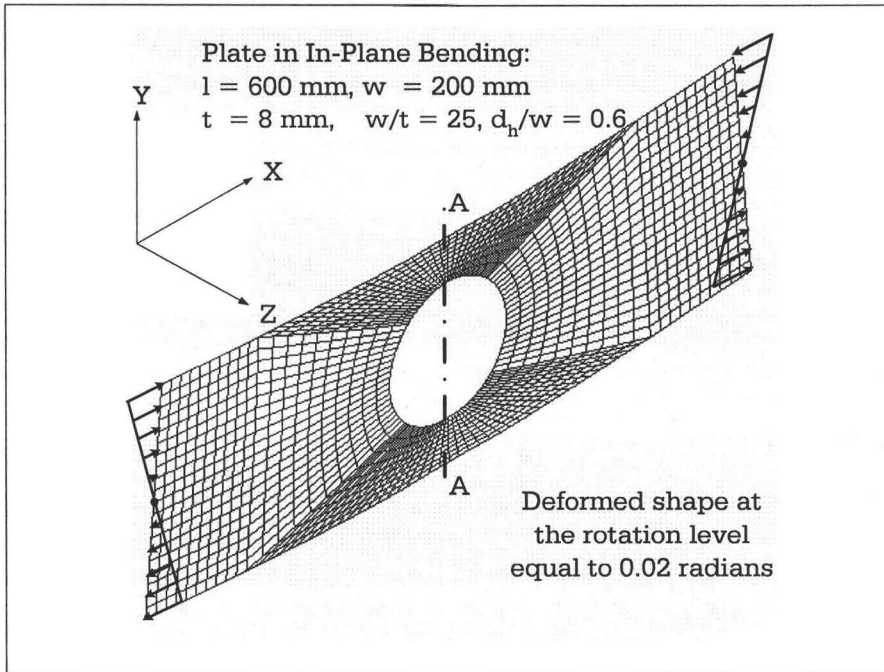


Figure 5.45: Deformed shape of thick plate having circular openings in bending

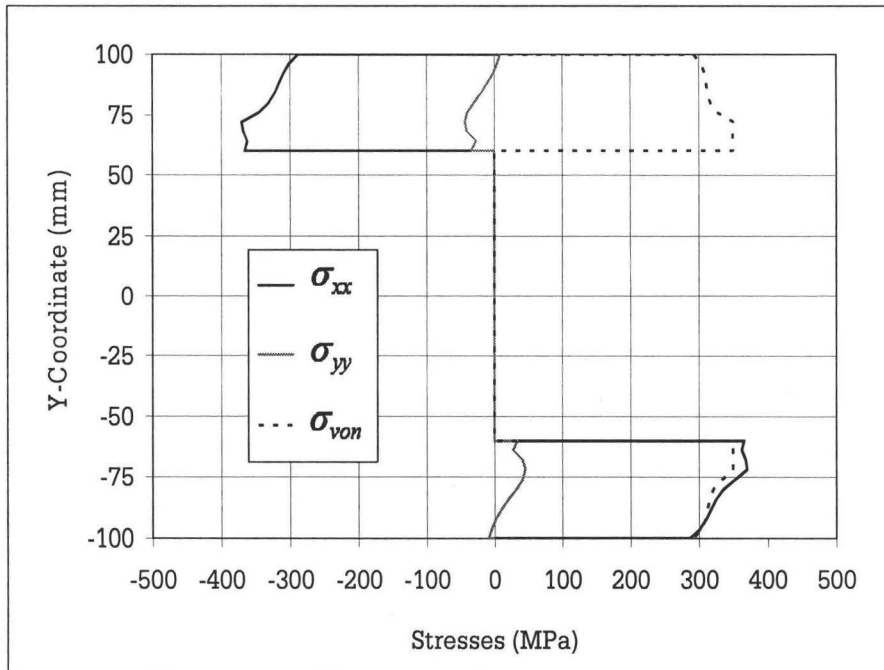


Figure 5.46: Stresses along A-A of thick plate having circular openings in bending

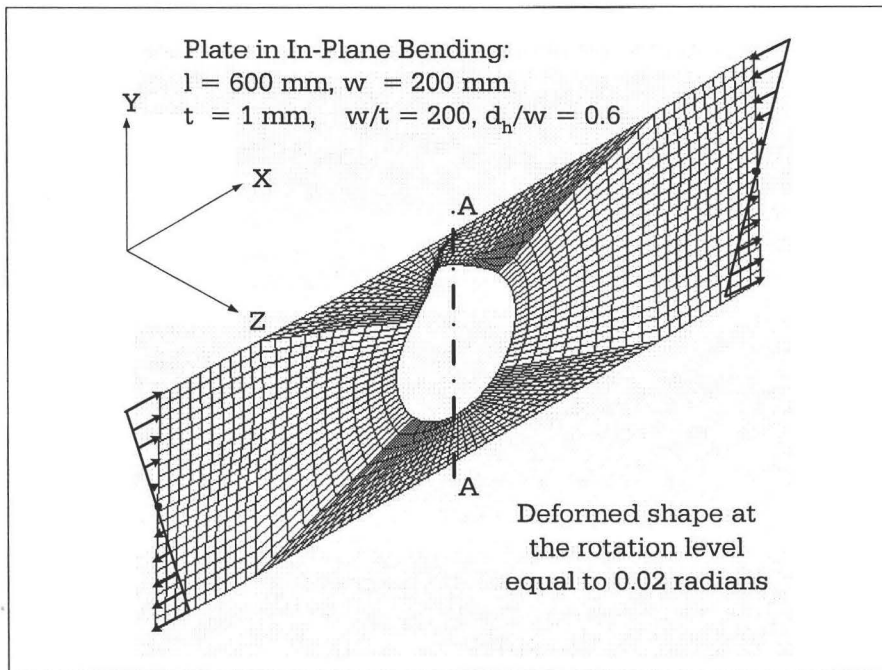


Figure 5.47: Deformed shape of thin plate having circular openings in bending

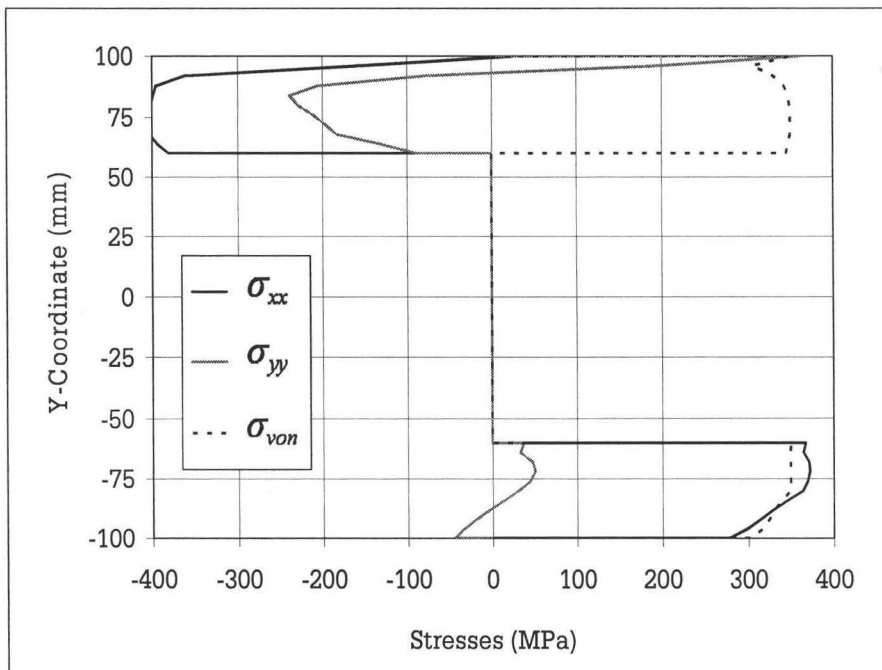


Figure 5.48: Stresses along A-A of thin plate having circular openings in bending

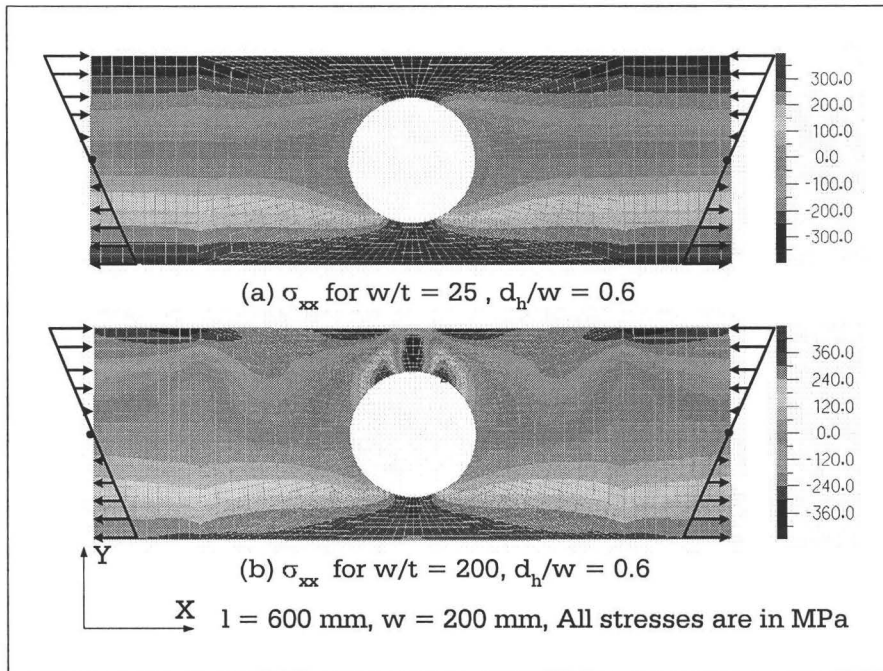


Figure 5.49: Band plots of stress for the plate having circular opening in bending (a) thick plate (b) thin plate

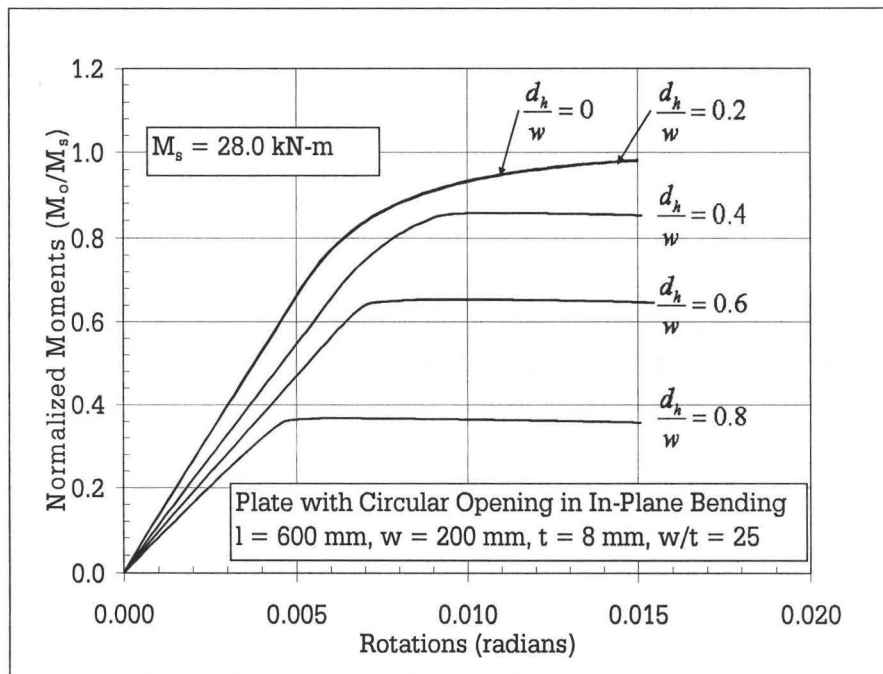


Figure 5.50: Moment rotation curves for the thick plate having circular openings in bending

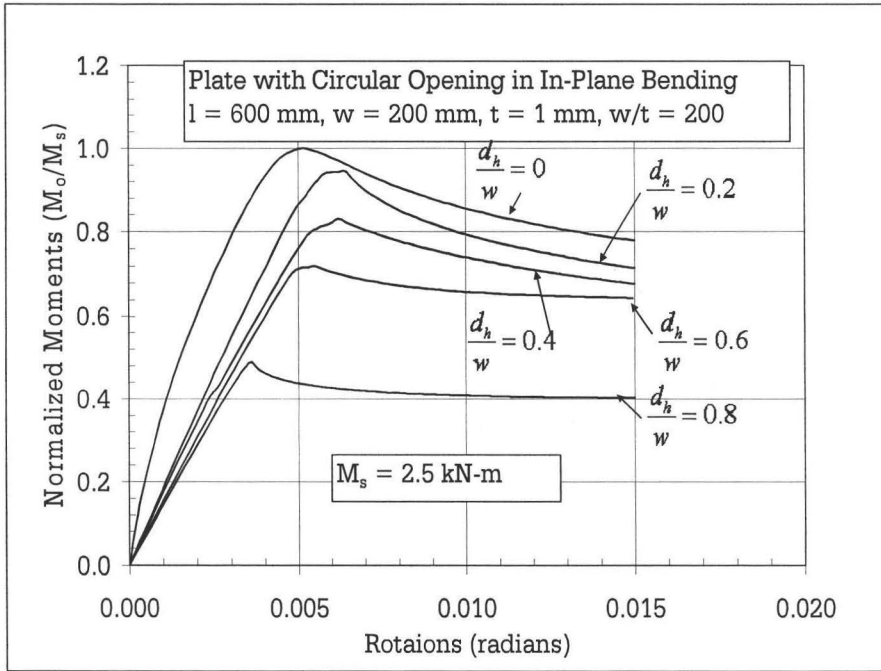


Figure 5.51: Moment rotation curves for the thin plate having circular openings of various sizes in bending

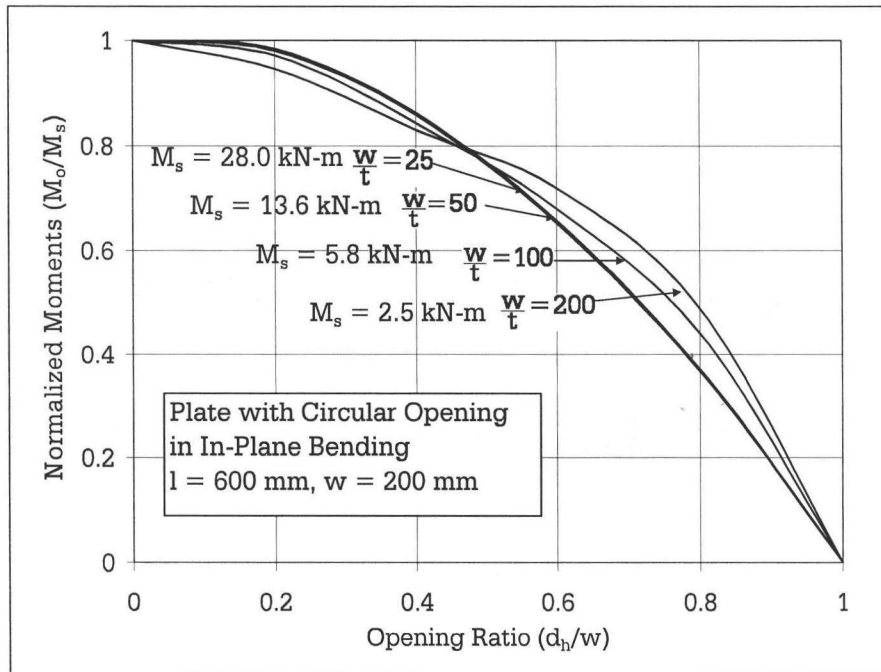


Figure 5.52: Moment reduction curves for the plates having circular openings in bending

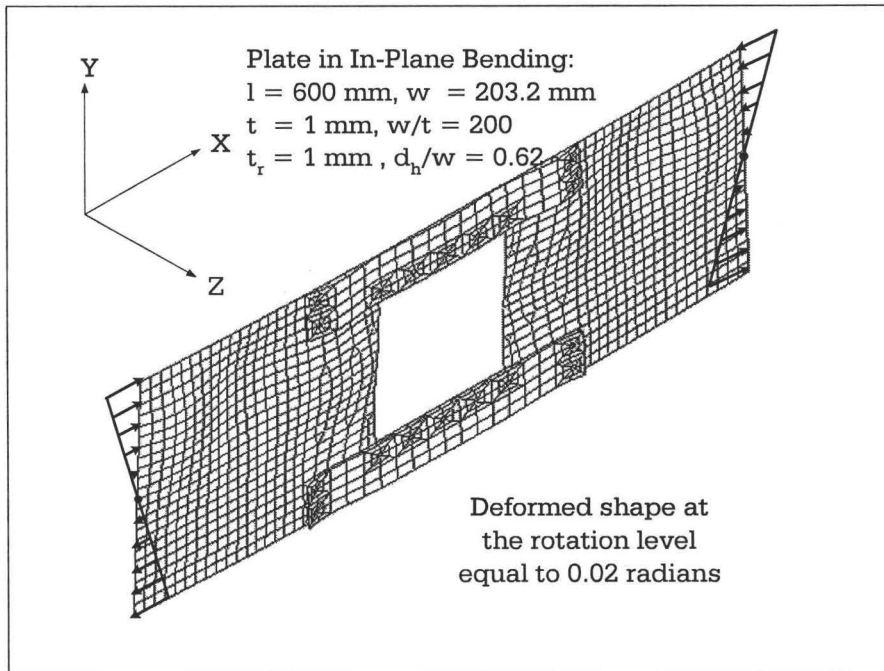


Figure 5.53: Deformed shape of 1 mm thick plate having reinforced square openings in bending

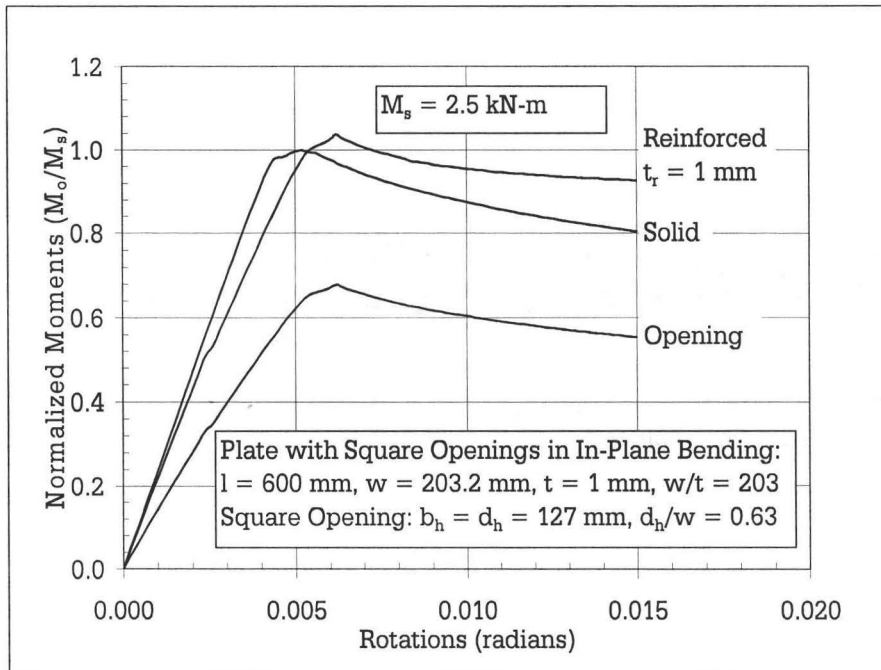


Figure 5.54: Moment rotation curves for 1 mm thick plate having reinforced square openings in bending

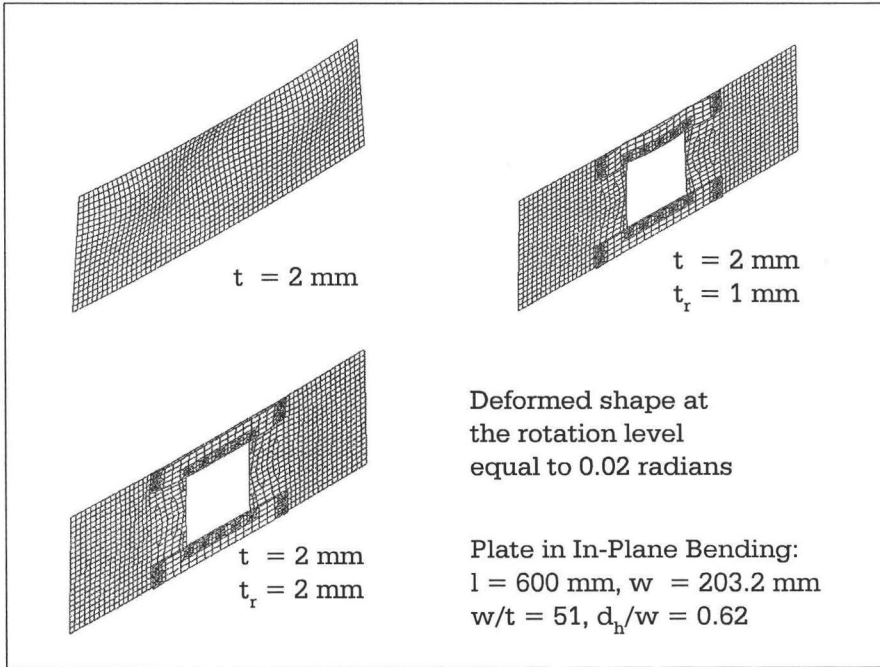


Figure 5.55: Deformed shapes of 2 mm thick plate having reinforced square openings in bending

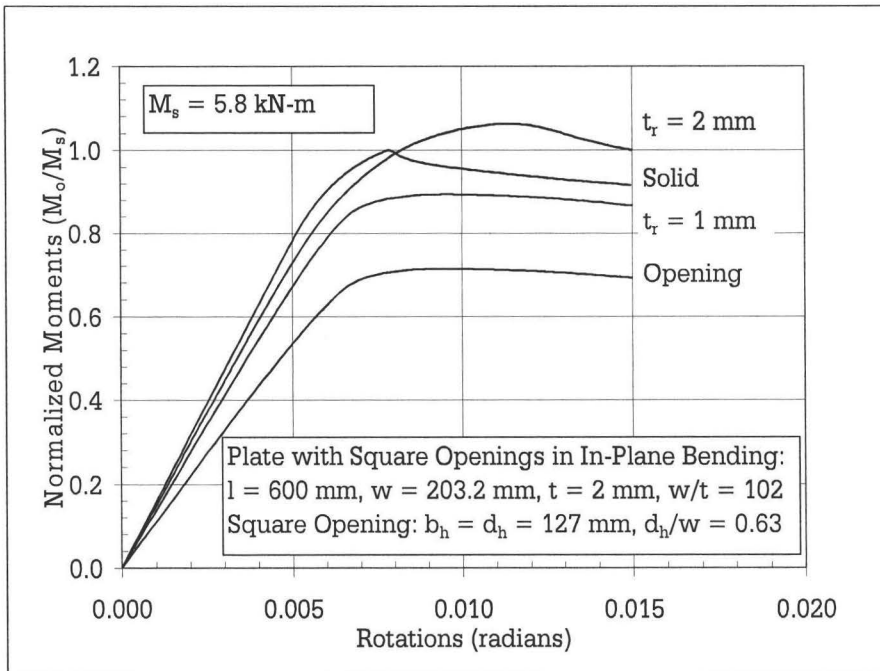


Figure 5.56: Moment rotation curves for 2 mm thick plate having reinforced square openings in bending

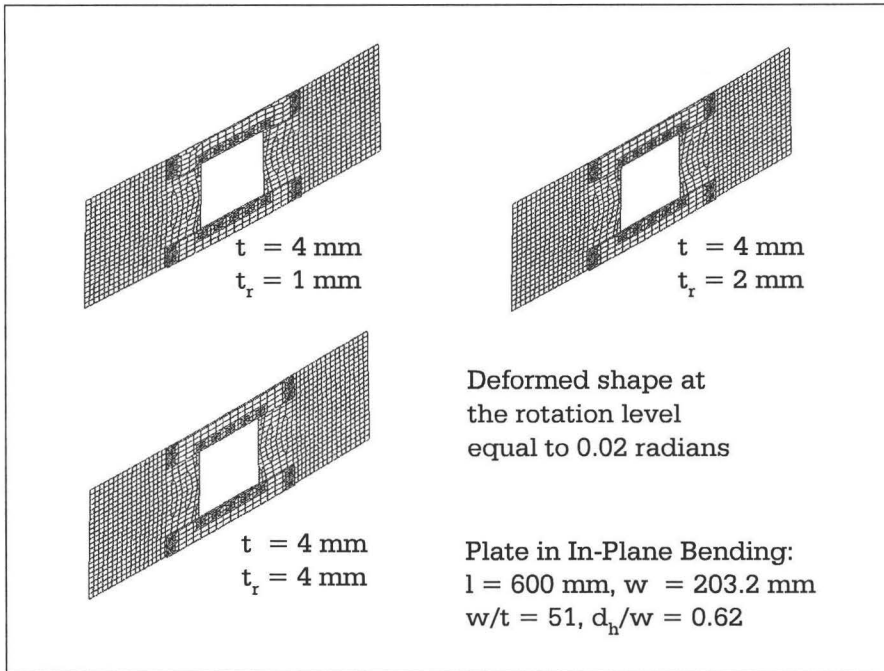


Figure 5.57: Deformed shapes of 4 mm thick plate having reinforced square openings in bending

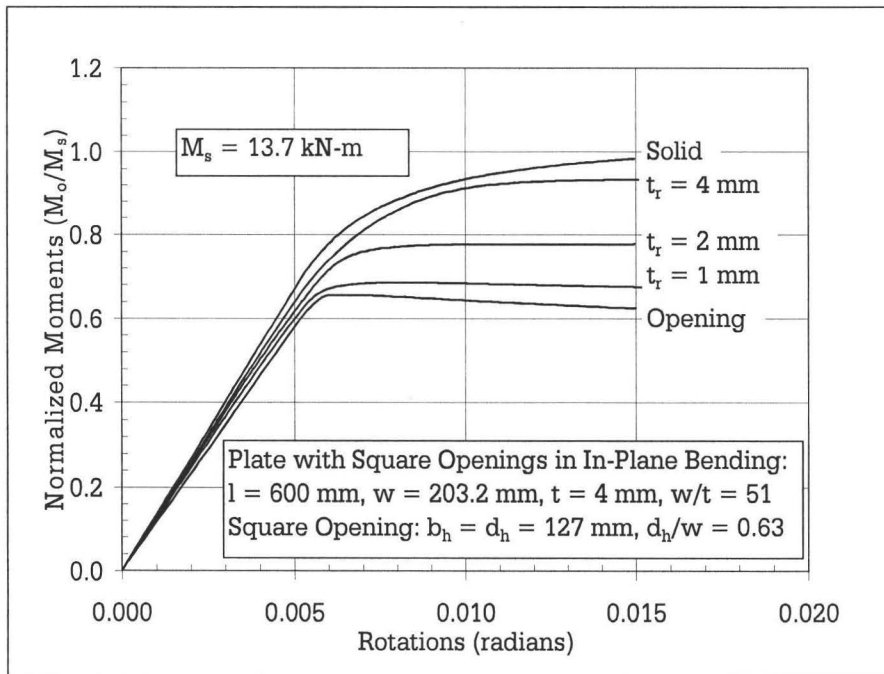


Figure 5.58: Moment rotation curves for 4 mm thick plate having reinforced square openings in bending

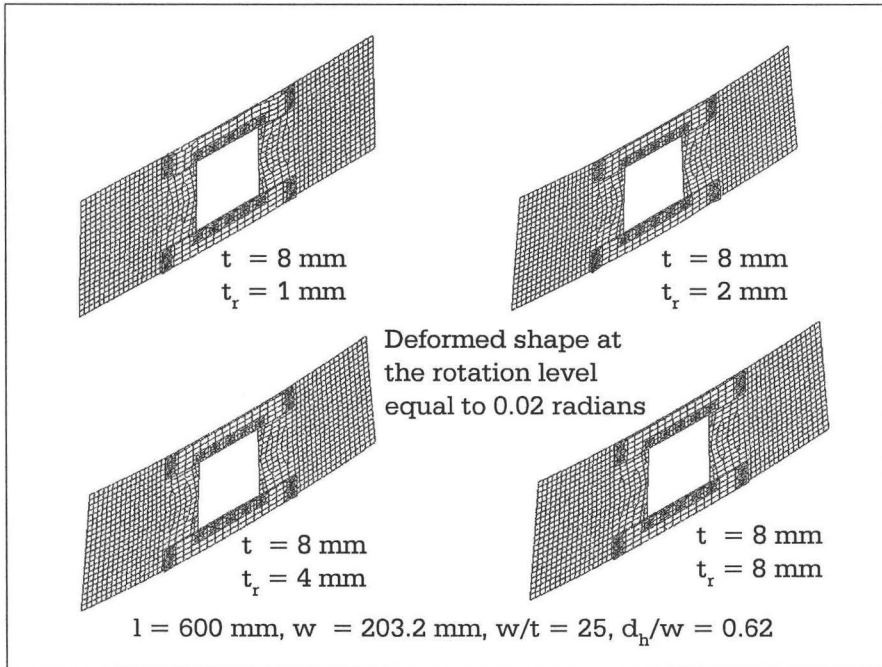


Figure 5.59: Deformed shapes of 8 mm thick plate having reinforced square openings in bending

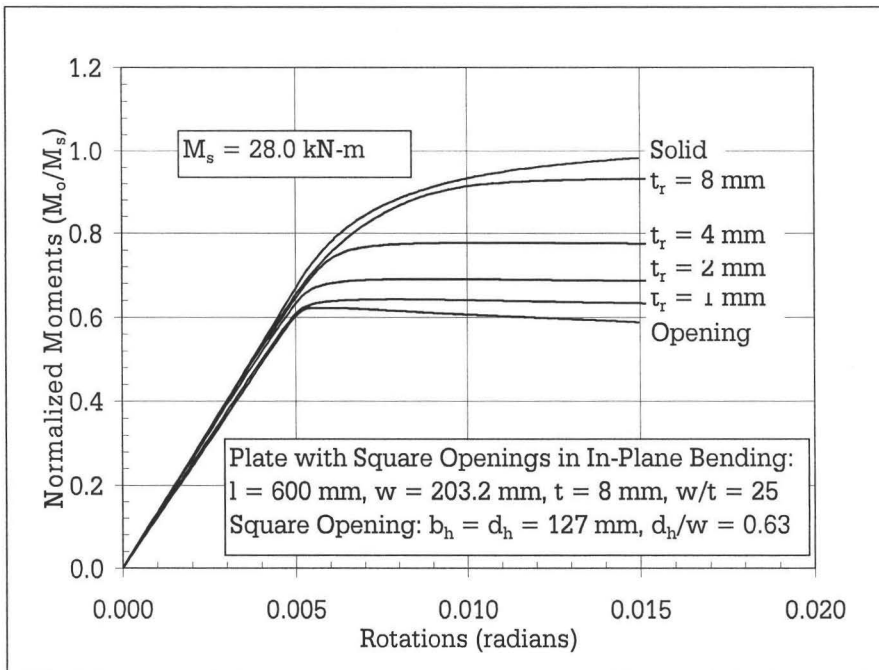


Figure 5.60: Moment rotation curves for 8 mm thick plate having reinforced square openings in bending

Chapter 6

Reinforcement of Cold-Formed Steel Joists with Web Openings in Flexural Zone: Numerical Study

6.1 Introduction

This chapter discusses a finite element based numerical investigation on the flexural resistance of cold-formed steel (CFS) solid joists, joists with unreinforced web openings, and joists with reinforced web openings. The finite element analysis program ADINA (ADINA, 2001), was used for this numerical investigation. The finite element model was verified with the help of experimental results presented in Chapter 2. As a first step, three full scale finite element models were developed for the four point load test setup (flexural test setup-II described in Chapter 2) and the finite element results were compared to the experimental results. Such full scale finite element models can represent the real scenario of the experimental test setup. However, working with the full scale finite element model is a laborious computational job because one has to deal with a large number of elements. To minimize the computational effort, a reduced finite element model was proposed. The reliability of the results from such a reduced model was checked with the results from the experiments and full scale model.

Then a parametric study was carried out using the reduced finite element models. The parameters considered herein include the size of the joists (depth and thickness), the size of the web openings, the type of web openings and the size (thickness) of reinforcements. This investigation considers circular and square web openings. The results and the discussions of the results from the parametric study are presented in this chapter.

6.2 Analysis Consideration for Cold-Formed Steel Joists

6.2.1 Buckling Analysis Techniques

Buckling loads are the critical loads where a structure becomes unstable. For thin walled structures, like cold-formed steel (CFS) joists, the buckling loads influence the flexural strength significantly. The buckling load of CFS joists is very sensitive to web height-to-thickness ratio, h/t . There are two primary methods of performing a buckling analysis viz. eigenvalue buckling analysis and nonlinear buckling analysis. The eigenvalue buckling analysis is capable of predicting the theoretical buckling strength of an ideal elastic structure.

On the other hand, a nonlinear buckling analysis is carried out with initial geometrical imperfections. These initial imperfections are necessary to initiate the desired buckling mode. However, structural imperfections and nonlinearities prevent most real-world structures from reaching their theoretical buckling load. The non-linear buckling analysis thus permits the modeling of geometrical imperfections. A nonlinear buckling analysis was performed in this study.

6.2.2 Geometrical Imperfections

A cold-formed steel joist consists of five plate elements, viz. web, tension flange, compression flange, compression lip and tension lip. These plate elements are susceptible to geometric imperfections which can define the geometric imperfection of the CFS joists. The magnitude and pattern of geometric imperfections play a significant role on the pre-buckling and post-buckling behavior of CFS members. Consideration of the geometric imperfections in an analytical model is necessary in order to consider the effect of the initial imperfection on the member strength and in order to initiate the local buckling mode of individual plate elements of the cross-section. The geometrical imperfections of a single plate described in Section 5.4 were used to define the geometrical imperfections of the web and the flanges of the CFS joists. Figure 6.1 shows the geometrical imperfections of CFS joists considered in this chapter.

6.2.3 Mechanical Properties

Good analytical prediction of behavior and strength of structural members requires full understanding in use of the material properties. The mechanical properties of cold-formed (CFS) joists are significantly changed from virgin sheet steel due to various manufacturing process, such as cold-roll forming, cold bending etc. The cold work of forming causes large changes in the mechanical properties of the corners of cold-formed structural shapes. In fact, the yield strength after cold working may be considerably higher than original ultimate strength of the material (Karren, 1967). The stress-strain behavior also varies across the cross-section.

Various studies have been made to establish the mechanical behavior of CFS sections (Karren, 1967; Karren and Winter, 1967; Coetsee et al., 1990). All of these

studies showed that a significant increase in the yield strength in CFS sections, especially at the corner region and the region around it. Sivakumaran and Abdel-Raheman (1998) have proposed a modified material model for corner region. According to this study it was suggested to divide the cold-formed steel joists into two zones: a flat zone and a corner zone. The yield strength of the flat zone is suggested to be uniform, having a value equal to the specified yield strength, F_y , of the section. The yield strength of the corner zone is increased by ΔF_y defined as,

$$\Delta F_y = 0.6 \left[\frac{B_{co}}{(r/t)^{m_{co}}} - 1 \right] F_y \quad (6.1)$$

where

$$B_{co} = 3.69 \left(\frac{F_u}{F_y} \right) - 0.819 \left(\frac{F_u}{F_y} \right)^2 - 1.79 \quad (6.2)$$

and

$$m_{co} = 0.192 \left(\frac{F_u}{F_y} \right) - 0.068 \quad (6.3)$$

Where, F_u is the ultimate tensile strength of the virgin steel material, r is the inside bending radius of the corner and t is the thickness of the joist. The material model suggested in the analytical study of cold-formed steel joists is shown in Figure 6.2 (Sivakumaran and Abdel-Raheman, 1998).

6.2.4 Residual Stress

Residual stresses are stresses that exist in the member as a result of manufacturing and fabricating processes. Residual stresses reduce the load at which yielding of a

steel member begins. However residual stress has negligible or no effects on ultimate stress, but it lowers the apparent proportional limit of the material.

The flexural strength, according to 1986 AISI Specification was based on residual stresses measured in hot-rolled steel. Due to the difference in manufacturing process, the residual stress pattern in cold-formed steel section may be quite different from that of a hot-rolled section. For a hot-rolled section, the residual stresses are mainly due to variation in the rate of cooling after hot rolling, flame cutting and welding. For a cold-formed steel section, the residual stresses are mainly caused by a cold-bending effect during the forming process.

An experimental investigation (Weng and Pekoz, 1990) found the presence of tension residual stresses on the outside of a channel section and compression residual stresses on the inside surface. Moreover, it was observed that higher residual stresses exist at the corner. However, it was suggested to use uniformly distributed stresses along the perimeter of the section. It was also suggested to use a residual stress equal to 50 percent of the yield stress and with linear variation through the thickness.

Abdel-Rahman and Sivakumaran (1997) proposed to use a residual stress of 40 percent of the yield stress for the corner zones and to use a residual stress of $(0.24 - 0.0006w)F_y$ for the flat zone, where w and F_y represent the width of the flat zone and yield strength of the material. However, these authors suggested that the residual stress should have a linear variation through thickness, with tensile stress on the outside surface and an equal compressive stress on the inside surface at the same location.

Schafer and Pekoz (1998) reported different magnitude of residual stress for two differently manufactured cold-formed steel members. For a roll-formed section, 95 percent of the test results showed that the residual stresses were lower than $0.67F_y$ at a corner, lower than $0.43F_y$ at an edge stiffened element, and lower than $0.71F_y$

at a stiffened element. For a press-braked section the values were $0.56F_y$ at a corner, $0.40F_y$ at an edge stiffened element, and $0.53F_y$ at a stiffened element.

Compression residual stresses cause a direct loss in compressive strength eventually loss in yield moment capacity. All of the studies found that residual stresses are significantly higher at the corner zones. At the same time it should be pointed out that the yield strength is also elevated at corner regions due to significant cold work forming.

6.3 The Finite Element Model

6.3.1 Material Modeling

In the present study, two different tensile coupon test results were considered for the material modeling. The material model for all the finite element models of joists having web depth 203.2 mm (8 inch) were based on the results from tensile coupon taken from a 203.2 mm (8 inch) deep joist. Similarly, j304.8 mm (12 inch) deep joists were analyzed using the material model based on the results from tensile coupon taken from 304.8 mm (12 inch) deep joist. These tensile coupon test results are presented in Table 2.2. As discussed in Section 6.2.3, cold-formed steel (CFS) joists can be divided into two zones: corner zone and flat zone. The corner zone material properties were modified using Equation 6.1.

6.3.2 The Full Scale Model

The full scale finite element model of the test specimens consisted of two joists placed face-to-face. The details of the specimens were described in Section 2.4.4 (test setup-II). The joists considered herein were 304.8 mm (12 inch) deep and 2.464 mm (97

mils) thick channel sections. The objective was to find an appropriate finite element model for the test setup-II and to use it to calibrate a reduced finite element model.

The CFS joists were modeled using four-node shell elements. The thickness of the shell elements used to model the channel section was set equal to the measured average thickness of the joists (2.45 mm) obtained from Table 2.4. The model joist was defined by two types material, described in Section 6.3.1. The flat zone of the section was defined by the flat material properties and the corner zone of the section was defined by corner material properties. The mesh at the corner zone was made finer compared to the mesh in the flat zone. Such fine mesh would define the curvature of the corner zone more accurately. However, mesh quality for both corner and flat zones was controlled by the aspect ratios ($l/w < 5$ and $w/t < 5$).

The presence of steel brackets at the loading and support points were simulated by increasing the thickness of the joist. The geometry (width, height and thickness) of the steel brackets were exactly the same as the geometry of the steel brackets used in the testing program (width = 152.4 mm, height = 304.8 mm, and thickness = 25.4 mm). Furthermore, the top and bottom of the bracket was defined by additional rectangular plate elements placed on the top and bottom of the joists (compression flange side and tension flange side). The mesh of the steel bracket zone was finer than the mesh of the channel section. Such fine mesh for the bracket is necessary to prevent the finite element mesh from high local distortion due to the presence of line load (concentrated load) at the loading points and at the support points.

In the experimental program, a series of steel strips were attached on the top (compression flange) and bottom (tension flange) of the specimen. These strips were screw fastened to the flanges using self-drilling screws. To simulate the presence of such steel strips in the finite element model, steel strips modeled with shell elements were used. The size (length, width and thickness) of these strips were similar to those

used in the experimental program (length = 130 mm, width = 20 mm and thickness = 6.4 mm). The screws were simulated by constraint equations (X, Y and Z translation of the nodes on the flange directly below the steel strips was set equal to the X, Y and Z translation of the nodes of the strips) for four nodes at each end.

The lateral supports were also modeled in the finite element analysis. Such supports were simulated by applying constraints in Z-displacement on the outer-top corner of the middle two steel brackets. The pin-support was simulated by imposing constraints in X-displacement and Y-displacement. Such constraints were applied along the mid-line (across the specimen) of the bottom of the end bracket. Similarly, the roller support was simulated by applying constraint in Y-displacement. Constraints were applied along the mid-line (across the specimen) of the bottom of another end bracket. The point loads were simulated by applying incremental displacements on the top of two middle steel brackets. The displacements were applied along the mid-line of the top plate of the steel bracket across the specimen. The displacements were increased until the clear failure shape of the specimen was obtained.

The applied displacement was divided into 50 incremental steps and the analysis proceeded. Large displacement but small strain formulation was applied during the analysis. An energy convergence criterion was applied at each time step.

Three types specimen were modeled using full scale finite element method. These were: solid joist, joist having circular web opening and joist having square web opening. The depths of the openings were 75 percent of the overall depth of the web. Figure 6.3 and Figure 6.4 show the boundary conditions used in the model and the finite element model of three types.

6.3.3 The Reduced Model

Only the single section at the middle region (between the two mid-brackets) was considered as the reduced finite element model. The full scale model contained 22671 elements but the reduced model contained only 1877 number of elements. The ratio of finite elements between full scale and reduced scale was 12. Such reduction in the number of elements would make the analysis easier and faster. Four-noded shell elements were used. Flat zones were modeled using flat zone material properties and corner zones were modeled using corner zone material properties. Once again, corner zones were meshed in finer pattern to get a fine shape of the curve at the corner region.

As discussed earlier, joists can be considered as a combination of long plates. The boundaries of each plate were treated as simple supports. Overall boundary conditions for this reduced model are shown in Figure 6.5. The Structure was symmetrical about Y-Z plane across middle-length, hence no displacement was allowed in the X direction at the middle of the length.

Since the analysis was displacement controlled, the loading on the reduced finite element model was applied using appropriate displacements at the boundaries. Such displacements were based on the displacement pattern obtained from the full scale finite element model. Figure 6.6 shows the relative X displacements ($u-u_{ave}$) of the web of the joists at three different load levels (within elastic limit, at the peak load level and after failure). The displacements were measured at the loading point of full scale model and measured along the height of the web. The displacement patterns shown in Figure 6.6 show that the displacements along the height of the web at the loading point (along the edge of steel bracket) would remain linear through out the analysis. Therefore a linear displacement along the height of section was applied to

create a constant moment zone over the length of the reduced finite element model. Figure 6.5 also shows the prescribed displacement pattern at the edge of the model.

6.3.4 Reinforcements

Only the reduced models were used to analyze the points with reinforcements. Reinforcements were modeled using four-nodded shell elements. Only one material property (flat material property) was used for the reinforcements. A gap equal to the sum of half of the thickness of joist and half of the thickness of reinforcement channel was provided between the main joist and the reinforcement channels. Such gap is necessary to simulate the eccentricity of the plane of the reinforcement with respect to the plane of web of the joist. The reinforcements were screw fastened to the main plate. The screws were modeled using screw model-II discussed in Chapter 4. Only reinforcement Scheme-C was considered in finite element investigation. The details of the reinforcement schemes were discussed in Section 2.7.2.

6.4 Finite Element Analysis Results

6.4.1 The Full Scale Model

In this section, the results from the experimental program and the results from the full scale finite element analysis are compared and discussed. The cold-formed steel joist considered herein was 304.8 mm (12 inches) deep and 2.464 mm thick (97 mils). The load deflection relation was used for the comparison. The load on the one of the middle steel bracket was plotted against the mid-span deflection. Since the test was two-point load test, the load on one middle steel bracket was expected to be equal to

the support reaction. The load at the end support was compared to the load on the middle steel bracket. These loads were identical as expected.

Figure 6.7 shows the support reaction vs. mid-span deflection curve for solid specimen. The figure shows that the finite element results are close to the experimental results and the joist model was only 4.7 percent stiffer than the tested joist. Such higher stiffness can be explained by the following facts. The connection of the steel bracket to the CFS joists was not modeled in the finite element. Instead, the steel brackets were modeled by increasing the thickness of the joist itself which would increase the stiffness of the specimen. Furthermore, the steel strips on the top of the finite element model of the specimen were connected using nodal constraints in x, y and z displacements. Such nodal constraints would result in a more rigid connection than the actual screw connection. Such rigid connection would ultimately increase the stiffness of the overall specimen. Similarly, the analytical peak support reaction was 4.26 percent lower than the average experimental results.

Figure 6.8 shows the deformed shape of the full scale finite element model. As expected the joists failed at mid-span. Figure 6.8 also shows the enlarged portion of the failure region (mid-span region). The failure was due to localized buckling on the flange and the web accompanied by distortional buckling. The failure mode of the analytical model exactly matches the failure mode observed in testing.

Figure 6.9 and 6.10 show the load displacement curves and deformed shapes for the specimen having circular web openings. The opening size considered was 228.6 mm (9 inches) diameter circular hole at the mid-span of the test specimen. Same size openings were considered in the experimental program. A finer mesh was generated adjacent to the opening region compared to the other flat region of the joists. Such fine mesh was necessary to capture the stress concentrations and high stress variations around the opening region.

Figure 6.9 shows that the finite element results are quite close to the experimental with the modeled joist having slightly higher stiffness. Such higher stiffness might be caused by the modeling technique as discussed in the results for solid specimen earlier. The deformed shape shown in Figure 6.10 resembles the deformed shape observed in the experiment. The failure of the specimen was governed by the localized buckling of the flange and the web at the opening region. A clear picture of the failure mode can be seen in the enlarged figure on the inset.

Similarly, Figure 6.11 and 6.12 show the load displacement curve and deformed shape of the specimen having square web openings. A square opening in each joist equal to 228.6 mm (9 inches) was made at mid-span of the specimen. The analytical model shows higher stiffness compared to the experimental one. Once again, the reason for higher stiffness and ultimate load might be due to the modeling technique. The failure mode shown in Figure 6.12 was local buckling of the flange and buckling of compression element (both web and flange) at the opening region. Similar results were observed during the testing.

In summary, the finite element results were compared to the experimental results in terms of load displacement curves and deformed shapes in this section. The results from all three full scale models (solid specimen, specimen having circular web openings and specimen having square web openings) resemble the results observed from the corresponding experiments. Therefore, it can be concluded that the results from the proposed full scale finite element model would accurately predict the results from the experiments.

6.4.2 The Reduced Finite Element Model

One of the objectives of this chapter was to carry out a parametric study of cold-formed steel joists having web openings. The parameters considered in this chapter are: size of the joist (depth and thickness), size of openings, type of openings and size of reinforcements. Working with a full scale model for the parametric study was both tedious and time consuming. Therefore, a reduced finite element model was developed for the parametric study. Such a reduced finite element model was first validated with the help of experimental results and the results obtained from the full scale finite element models. The modeling techniques for the reduced finite element models were already discussed in Section 6.3.3. This section presents the validation of such reduced finite models.

The reduced finite element models for the cold-formed steel joists were subjected to pure flexural loading. The models were validated with the help of moment-rotation curves and failure modes (deformed shapes). Since no experimental moment-rotation curves were available, the moment-rotation curves from the full scale finite element models were used for the validation of the reduced finite element models.

Figure 6.13 shows the moment rotation curves obtained for a single solid joist from the full scale finite element model and for a reduced finite element model. Only the middle part of the full scale model (having the length of the reduced model) was selected to extract the corresponding moment rotation relation. The figure shows that the curves are identical for both the full scale finite element model and the reduced finite element model until the ultimate moment was reached. However, the reduced model seems stiffer than the full scale model beyond the ultimate moment. This difference might be due to the boundary condition adopted for the reduced finite element model. Provision of edge constraints close to the failure region would also

make the model stiffer especially after failure (at large deformation level). However, the ultimate moment capacity was the major interest in this research.

Figure 6.14 shows the failure modes of the full scale finite element model, the reduced finite element model and the experiment. All three failure modes seem identical. Results from the moment rotation curve and the deformed shape show that the proposed reduced finite element model is equally valid as the full scale finite element model.

Figure 6.15 and 6.16 show the moment rotation curves and the deformed shapes for a joist having circular openings. It can be seen from the figure that the moment rotation curves obtained from the full scale finite element model and from the reduced model match each other. The deformed shapes shown in Figure 6.16 also closely match each other. Failure of the section in all three cases (experiment, full scale finite element model and reduced model) was localized buckling at the opening region. Similar results can be observed for the section having square web openings. The results for the section having square web openings are presented in Figures 6.17 and 6.18.

6.5 The Parametric Study: Results and Discussion

6.5.1 Comparative Study of Experimental, FEM and AISI Standard Results

Table 6.1 summarizes the ultimate moment capacity of cold-formed joists having circular web openings. The opening sizes considered here were calculated as the overall depth of the web of the joist minus 76.2 mm (3 inch). In the table are

experimental results, results based on AISI Standard (AISI, 2007) and finite element results. Also included in Table 6.1 are the results from the study by Sivakumaran et al. (2006). Results for only three type of sections were available and are presented in the table. The ultimate moment capacity of all the sections listed in Table 6.1 were calculated using the AISI Standard (AISI 2007) procedure. Finite element analysis was performed only for 203.2mm (8 inch) deep and 304.8 mm (12 inch) deep sections. The finite element results show that thicker sections would cause higher reduction in ultimate moment capacity. This can be explained by the fact that the middle part of the web of thin section has less contribution in ultimate moment capacity, because the middle part of the web experiences less stress due to the buckling of the web. Therefore, cut-outs from area with low stress would have less effect on the ultimate moment capacity of the joists.

Similarly, Table 6.2 gives the ultimate moment capacity of cold-formed steel (CFS) joists having square web openings. The results presented in the table again show that thin sections have less reduction in ultimate moment capacity compared to the thick section having same size of web openings.

6.5.2 Effects of Opening Size

The reduced finite element model presented in Section 6.3.3 was used for the parametric study. The effect of the size of the openings on the flexural strength was examining for five different sizes of openings: 20, 40, 60, 80 and 100 percent of the flat width of the web of the cold-formed steel joists. Figures 6.19 to 6.22 show the normalized moment rotation curves for joists having various sizes of openings. The moment capacity of the joists having openings (M_o) was normalized by the moment capacity of solid joist (M_s). Such normalized moment rotation curve would give a

better picture of the percent reduction in moment capacity due to the presence of openings. The results presented in Figures 6.19 to 6.22 are for thin (1.09 mm) and thick (2.464 mm) joists having two different openings (circular and square).

Figure 6.19 shows the normalized moment rotation curves for 1.092 mm (43 mils) thick joist having a web depth 203.2 mm (8 inches). The curves have a sharp peak at ultimate moment capacity showing that the strength of thin section is controlled by instability (buckling). The curves show that there is always a reduction in flexural resistance and flexural stiffness due to the presence of the web openings. However, openings up to 40 percent of the flat web height showed no significant reduction in either flexural strength or flexural stiffness. The effect of openings higher than 40 percent of flat web height is considerable.

The normalized moment rotation curves for the 2.464 mm (97 mils) thick section having circular openings are presented in Figure 6.20. Compared to the results in Figure 6.19 the curve at the peak moment rotation of 2.464 mm (97 mils) thick sections are flat. This shows that a portion of the joists started yielding before the moment reached the ultimate level. However, the descending part of the curves after the peak seems sharp which would indicate that the failure of the section was controlled by buckling. Contrary to thin (1.092 mm thick) sections, thick (2.464 mm thick) sections have a higher reduction in ultimate moment capacity due to the presence of web openings. However, openings less than 20 percent of the flat web depth had no significant reduction in the strength.

Figure 6.21 and Figure 6.22 show the normalized moment reduction curves for the thin and thick joists having square web openings. The curves show that the effect of square opening less than 40 percent of flat web height is negligible for thin sections (1.092 mm). However, the presence of square openings cause comparably higher reduction in strength of thick joists (2.464 mm). Once again, thin sections exhibited

a sharp peak moment rotation curve and thick sections had flatter peaks. This shows that some portions of the thick sections reached yielding before the moment reached its ultimate level.

6.5.3 Effects of h/t Ratio

The strength of thin-walled structures, like CFS structures, is governed by the h/t ratio of the plate elements of the structures. Therefore, the effect of h/t was one of the parameter selected for the investigation, where h is the flat height of the web and t is the thickness of the web. In this study, the four different cold-formed steel joists are commonly used in the steel construction were investigated. The thicknesses considered were: 1.092 mm (43 mils), 1.372 mm (54 mils), 1.727 mm (68 mils), and 2.464 mm (97 mils) which would produce four different h/t ratio (180, 142, 112, 76), respectively, for a joist having 203.2 mm overall web depth. The results presented in Figure 6.23 and 6.24 are the moment reduction curves for joists having web depth equal to 203.2 mm (8 inches) and h/t ratios of 180, 142, 112 and 76.

Figure 6.23 shows the moment reduction curves for the joists having circular web openings. The curves show that low h/t ratios cause higher reduction in ultimate moment capacity. The joists having h/t ratio 180, 142 and 112 had negligible moment reduction if the circular opening size was less than 40 percent of the flat height of the web. However, joist having h/t equal to 76 has considerable moment reduction when the size of web opening was 40 percent.

The moment reduction for the joists having square web openings and various h/t ratios are showing in Figure 6.24. Once again, the curves show that sections having low h/t ratio would suffer a higher reduction in moment capacity due to the presence of square web openings.

Figures 6.25 and 6.26 show the failure mode of CFS solid joists having low h/t ratios and high h/t ratios. Figure 6.25 show that the failure of the joists having high h/t ratio (thin joists) would be governed by the localized buckling of the flange and the web. On the other hand, Figure 6.26 shows that the failure mode of the joists having low h/t ratio (thick joists) would be governed by distortional buckling (rotation of the flange toward or outwards from the web).

6.5.4 Effects of Shape of Opening

Two types of web openings were considered in this study: circular and square. These are the common shapes of openings usually made on the web of CFS floor joists. Figures 6.27 and 6.28 show the moment reduction curves for the CFS joists having circular and square web openings. The curves clearly show that the reduction in ultimate moment capacity of CFS joists having square web openings is higher than the reduction of the ultimate moment capacity of CFS joists having circular web openings. In other words, the presence of square web openings is more severe than the presence of circular web openings on the flexural strength of CFS joists. This can be explained by the fact that square openings would have longer unsupported edge (opening edge) than those of circular openings. Even though the net cross-section of the joists having the same size of square and circular opening would be equal, longer unsupported edges of square openings could buckle at lower load levels. Thus, the effect of square web openings is more severe than that of circular web openings on the flexural strength of CFS joists.

6.5.5 Effects of Web Depth

The commonly used CFS joists have depth of 203.2 mm (8 inches) and 304.8 mm (12 inches). This study also considers CFS joists having these two depths. Figures 6.27 and 6.28 show the moment reduction curves for 304.8 mm (12 inches) deep joists having circular and square openings. Only two thicknesses, 2.464 mm (97 mils) and 1.727 mm (68 mils), were considered in this case because 304.8 mm (12 inches) deep CFS joists are only available in these two thicknesses. Figures 6.27 and 6.28 show that the presence of large openings (larger than 80 percent of flat web) in deeper sections (304.8 mm deep) cause higher reduction in the ultimate strength compared to shallow sections (203.2 mm, see Figure 6.23 and 6.24). In other words, the reduction in the moment capacity of a 203.2 mm (8 inches) deep section due to the presence of 100 percent openings (100 percent of depth of flat web) was less than 48 percent. But, the reduction in the moment capacity of a 304.8 mm (12 inches) deep section due to the presence of 100 percent openings (100 percent of depth of flat web) was about 70 percent.

6.5.6 Reinforcements

A 203.2 mm deep (8 inches) joist having four different thicknesses (1.092 mm, 1.372 mm, 1.727 mm, and 2.464 mm) and having square web openings of 127 mm size was considered for investigation. The opening was reinforced using 38.1 mm deep (1.5 inches) bridging channels. The details of this reinforcement scheme (Scheme-C) are described in Section 2.7.2.

6.5.7 Effects of Reinforcement Size

Four different commonly available thicknesses of bridging channels were considered as reinforcements. The available thicknesses were: 1.092 mm (43 mils), 1.372 mm (54 mils), 1.727 mm (68 mils), and 2.464 mm (97 mils). Figure 6.29 shows the normalized moment rotation curve for a 2.464 mm (97 mils) thick section with various sizes of reinforcements. The moment rotation curves were normalized by the ultimate moment capacity of solid joist (M_s). The moment rotation curves show that reinforcements having thickness less than the thickness of joist (2.464 mm) are not capable of restoring the moment capacity to the full moment capacity of solid joist. However, the 2.464 mm thick reinforcement was able to restore the moment capacity.

Figure 6.30 shows the deformed shapes of the joists having various sizes of reinforcements. The deformed shapes show that joists having small sizes of reinforcements (reinforcements having thickness less than the thickness of the joist) failed in distortional buckling within the opening region. Figures 6.31 to 6.34 show the normalized moment rotation curves and deformed shapes of joists having various thicknesses. In summary, the results show that the thickness of the flexural reinforcements (bridging channel) should be equal to at least the thickness of the joist.

6.6 Conclusion

In this chapter result from the finite element investigation on the CFS joists having web openings with and without reinforcements subjected to flexural load were presented. A full scale finite element model was first developed and validated with experimental results. Then a reduced finite element model was introduced and validated with the full scale finite element model and experimental results. The reduced finite element model was then used for various parametric studies. The parameters

considered included: the size of the joist (depth and thickness), the size of openings, the type of openings and the size of reinforcements. The study showed that circular web openings up to 40 percent of the flat web height had no significant reduction on the flexural strength of the joists. However, square web openings had more severe effect than the circular web openings. It was found that square web openings with sizes greater than 20 percent of the flat web height caused significant reduction on the flexural resistance of the CFS joists. The failure of joists having high h/t ratios (thin joists) would be governed by localized buckling of the flange and the web. But, the failure of the joists having low h/t ratio (thick joists) would be governed by distortional buckling of the flange (rotation of the flange toward or outwards from the web). Furthermore, sections having low h/t ratio would suffer higher reduction in moment capacity due to the presence of web openings. Joists having high depth had a higher reduction in the moment capacity compared to joists having low depth due to the presence of web openings. The study showed that the moment capacity of the CFS joists having web openings could be restore by providing appropriate reinforcement schemes. It was observed that the thickness of the flexural reinforcements (bridging channel) should be at least equal to the thickness of the joist.

Table 6.1: Moment capacity of CFS joists with large circular web openings: Opening size = (h-76.2 mm)

Designation	h/t	Solid (kN-m)			Circular Opening (kN-m)			Percentage Reduction		
		Experiment	AISI	FEM	Experiment	AISI	FEM	Experiment	AISI	FEM
550S162-33	161		2.39			1.97			17.68	
550S162-43	122		3.33			2.70			18.98	
550S162-54	96		4.38			3.79			13.53	
550S162-68	75		5.56			5.04			9.39	
550S162-97	51		7.53			7.15			5.03	
800S162-33	236		3.38	3.72		2.96	3.49		12.6	6.04
800S162-43	180	4.40	4.71	5.28	4.13	4.06	4.91	6.10	13.64	6.97
800S162-54	142		6.62	6.77		5.76	6.21		12.98	8.21
800S162-68	112	11.28*	8.91	9.10	9.77*	7.76	8.12	12.30	12.88	10.76
800S162-97	76		12.96	14.52		11.26	12.45		13.12	14.23
1000S162-43	227		6.06			5.16			14.73	
1000S162-54	179		8.57			7.35			14.26	
1000S162-68	141		11.66			9.96			14.58	
1000S162-97	97		17.43			14.58			16.35	
1200S162-43	273		7.43			6.27			15.69	
1200S162-54	216		10.56			8.94			15.36	
1200S162-68	170		14.47	15.13		12.17	11.62		15.89	23.21
1200S162-97	118	23.18	21.86	22.92	19.71	17.93	17.42	14.97	16.25	23.99

*Section 800S162-68 was tested by Sivakumaran et al. (Sivakumaran et al., 2006)

Table 6.2: Moment capacity of CFS joists with large square web openings: Opening size = (h-76.2 mm)

Designation	h/t	Solid (kN-m)			Square Opening (kN-m)			Percentage Reduction		
		Experiment	AISI	FEM	Experiment	AISI	FEM	Experiment	AISI	FEM
550S162-33	161		2.39			1.97			17.68	
550S162-43	122		3.33			2.70			18.98	
550S162-54	96		4.38			3.79			13.53	
550S162-68	75		5.56			5.04			9.39	
550S162-97	51		7.53			7.15			5.03	
800S162-33	236		3.38	3.72		2.96	3.38		12.6	9.21
800S162-43	180	4.40	4.71	5.28	3.78	4.06	4.66	14.10	13.64	11.65
800S162-54	142		6.62	6.77		5.76	5.73		12.98	15.33
800S162-68	112	11.28*	8.91	9.10	10.07*	7.76	7.51	10.70	12.88	17.44
800S162-97	76		12.96	14.52		11.26	11.78		13.12	18.86
1000S162-43	227		6.06			5.16			14.73	
1000S162-54	179		8.57			7.35			14.26	
1000S162-68	141		11.66			9.96			14.58	
1000S162-97	97		17.43			14.58			16.35	
1200S162-43	273		7.43			6.27			15.69	
1200S162-54	216		10.56			8.94			15.36	
1200S162-68	170		14.47	15.13		12.17	10.94		15.89	27.68
1200S162-97	118	23.18	21.86	22.92	17.77	17.93	16.50	23.34	16.25	28.01

*Section 800S162-68 was tested by Sivakumaran et al. (Sivakumaran et al., 2006)

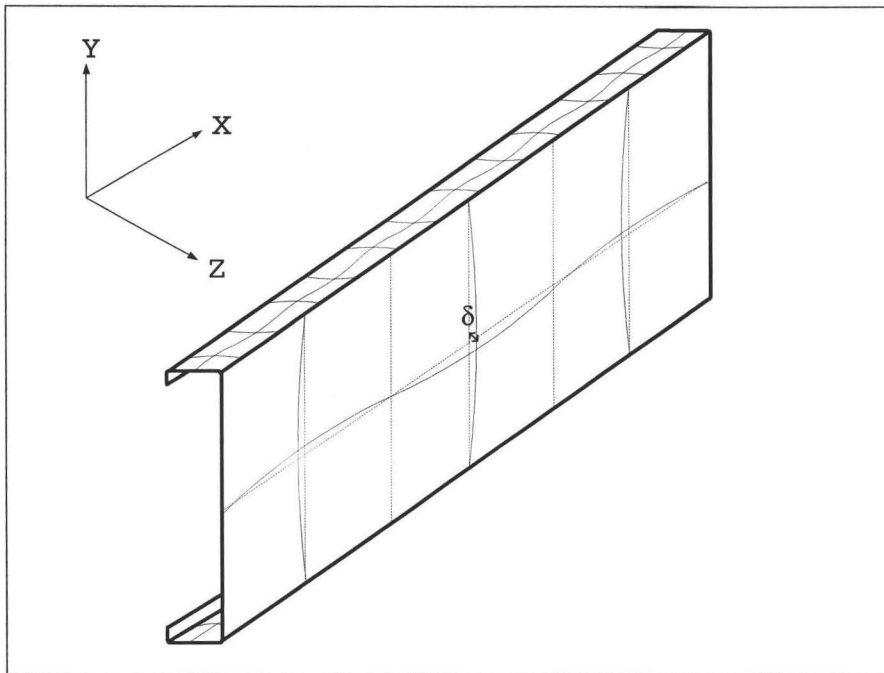


Figure 6.1: Geometrical imperfections (Yu, 2000)

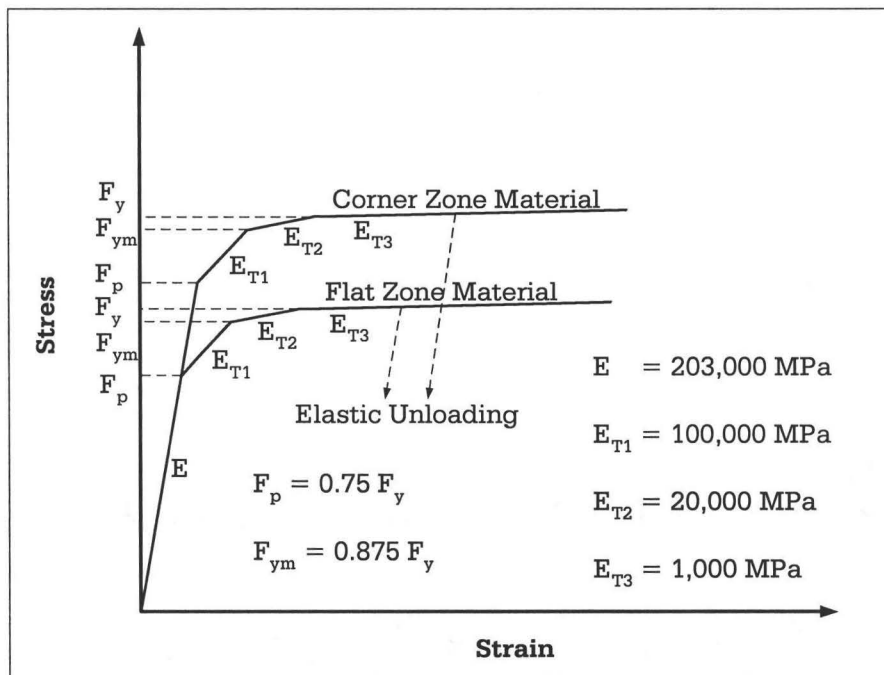


Figure 6.2: Idealized material properties (Abdel-Rahman and Sivakumaran, 1997)

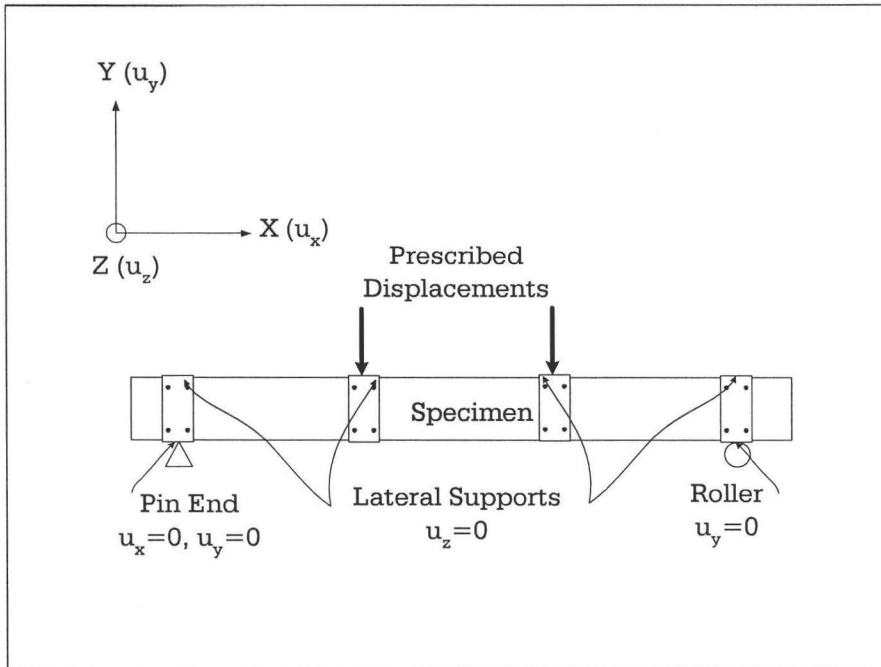


Figure 6.3: Boundary conditions for full scale finite element models

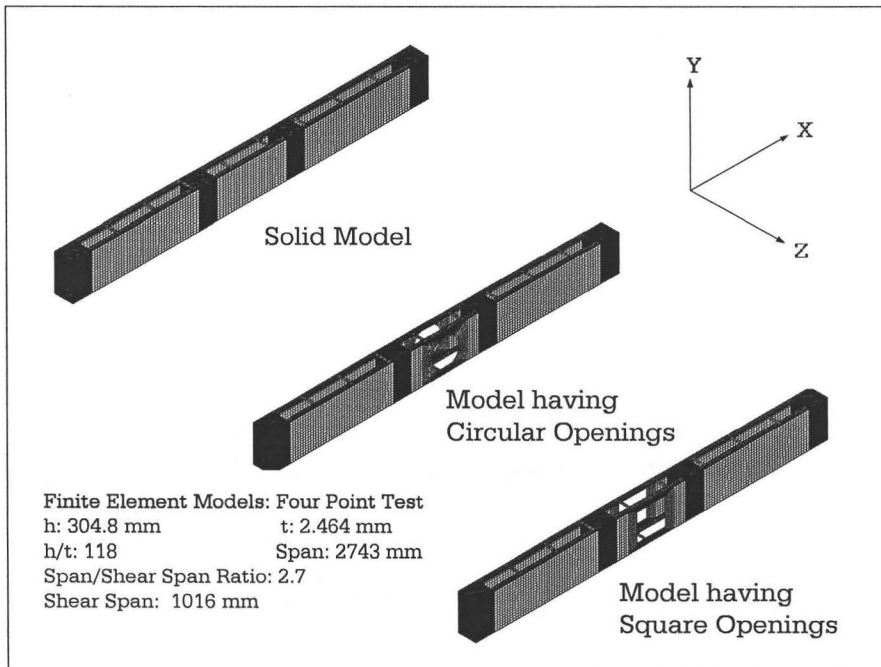


Figure 6.4: Full scale finite element models

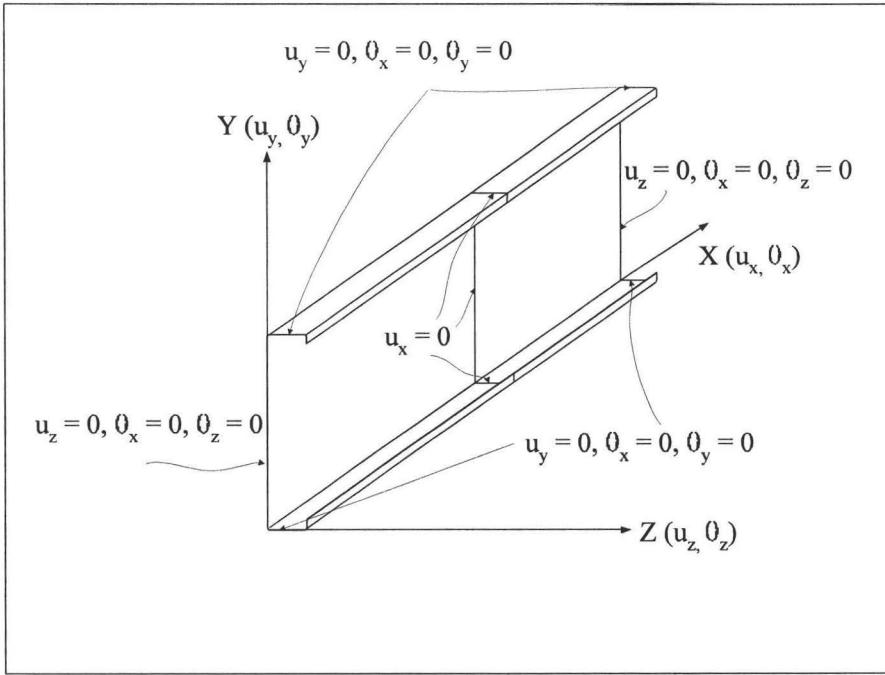


Figure 6.5: Boundary conditions for reduced model

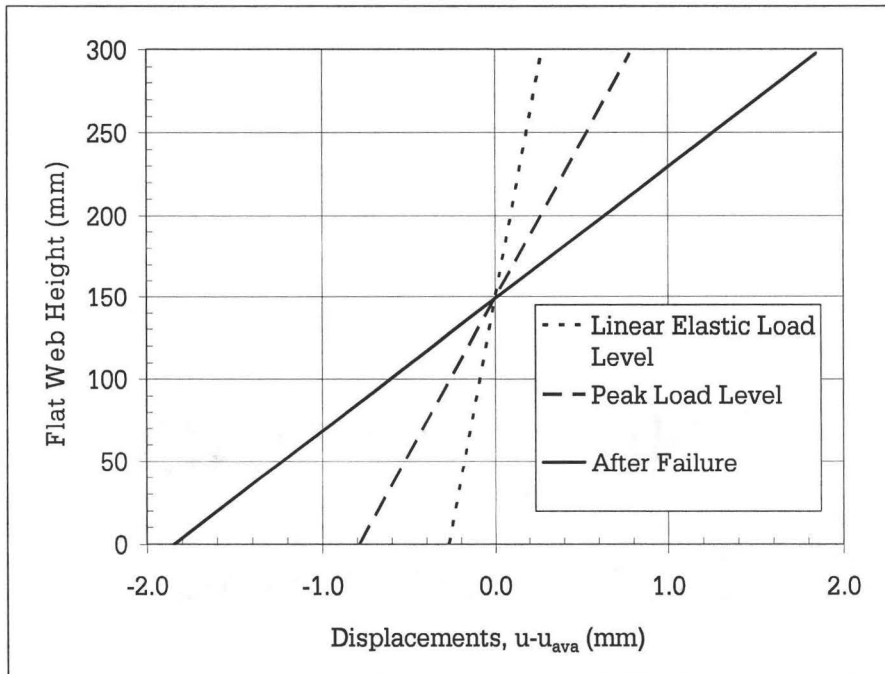


Figure 6.6: X-Displacements of the joist along the height at left loading point

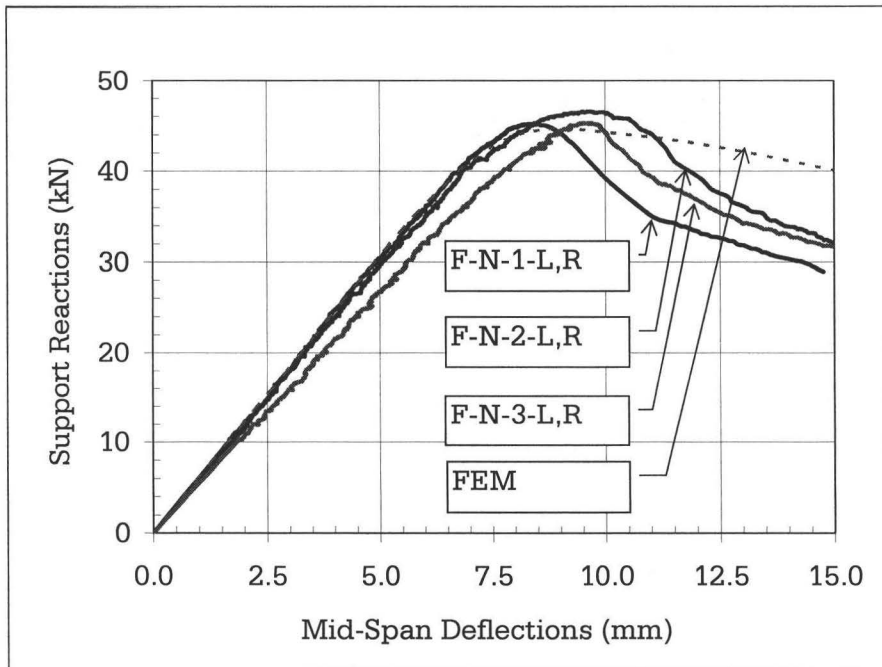


Figure 6.7: Load displacement curve for solid joists

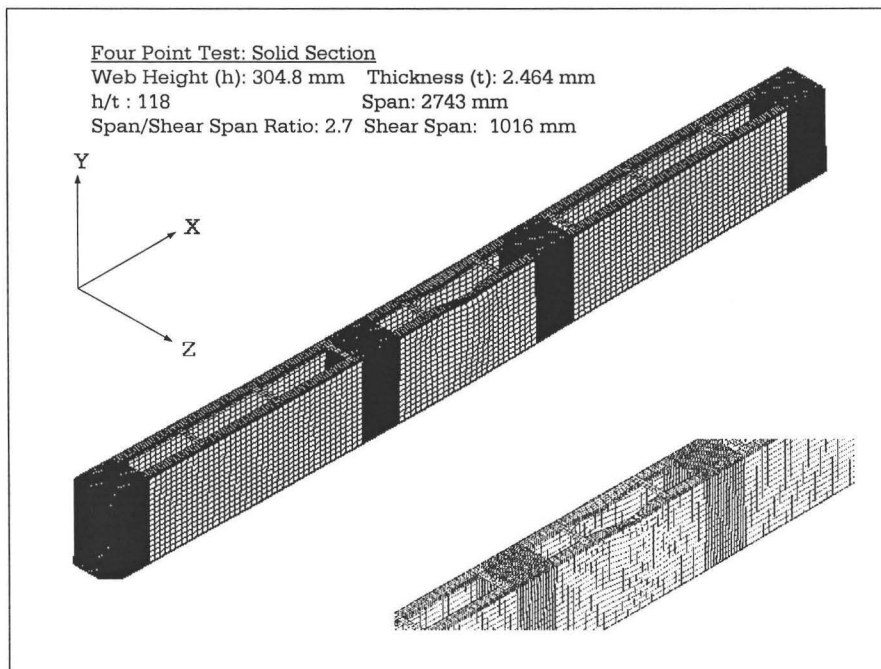


Figure 6.8: Deformed shape of full scale FE model of solid joists

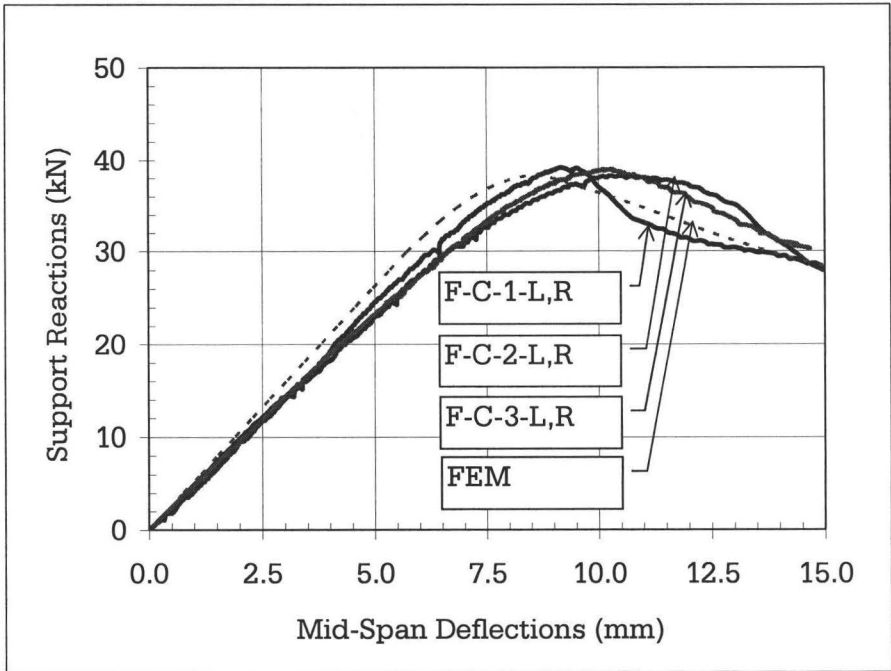


Figure 6.9: Load displacement curve for joists having circular web openings

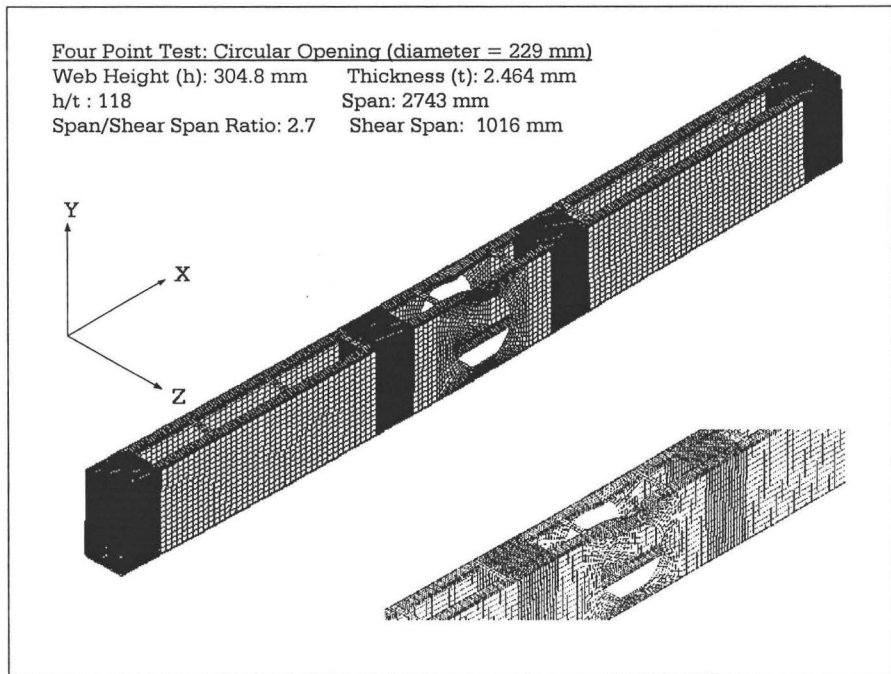


Figure 6.10: Deformed shape of full scale FE model of joists having circular web openings

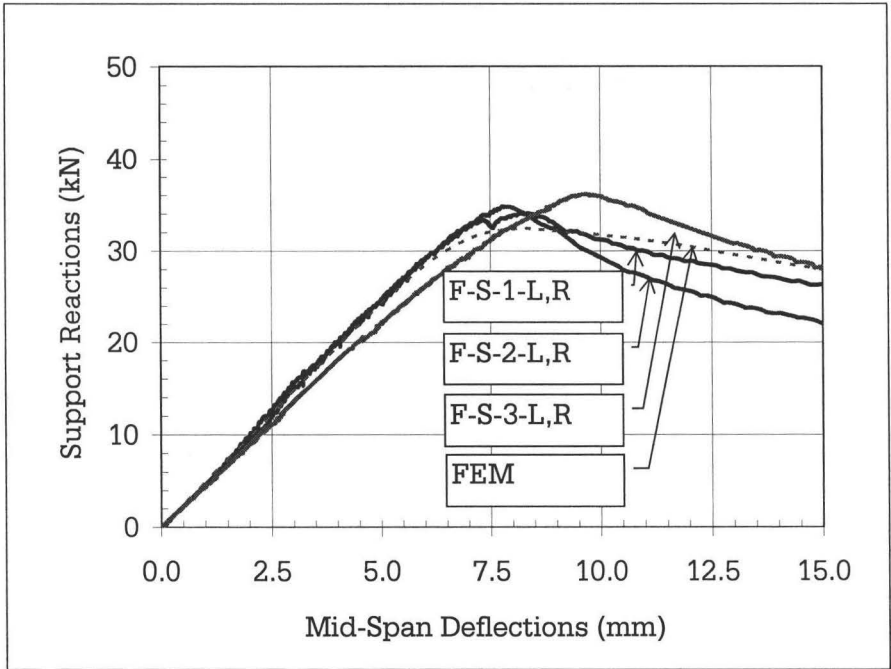


Figure 6.11: Load displacement curve for joists having square web openings

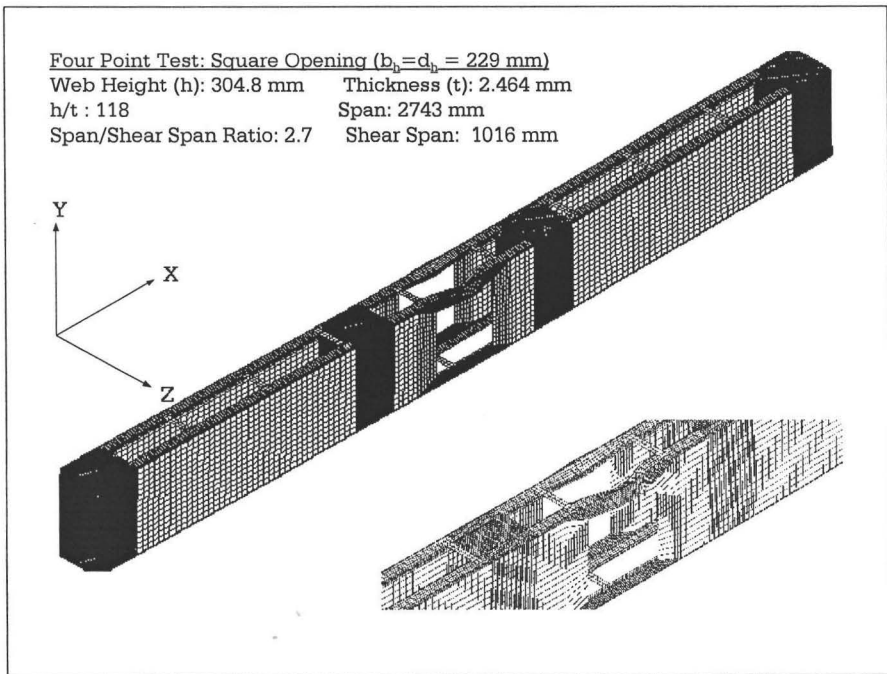


Figure 6.12: Deformed shape of full scale FE model of joists having square web openings

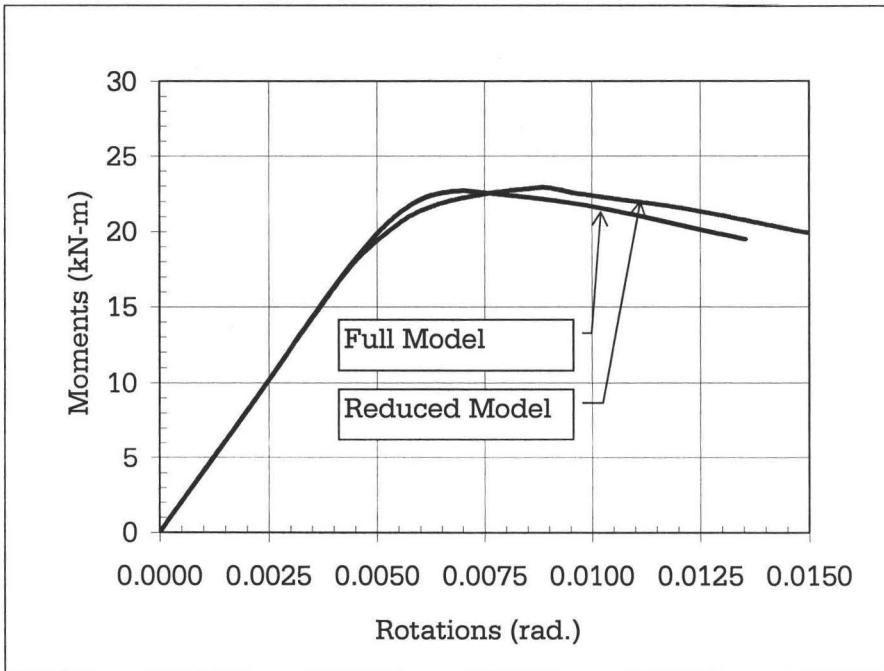


Figure 6.13: Moment rotation curves for solid joists

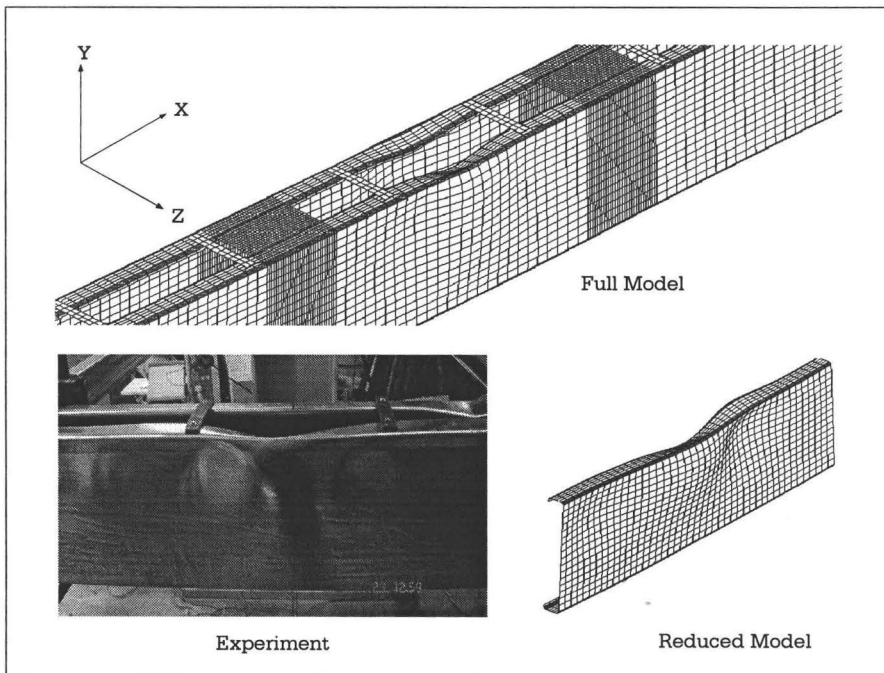


Figure 6.14: Comparison of deformed shapes: Solid joists

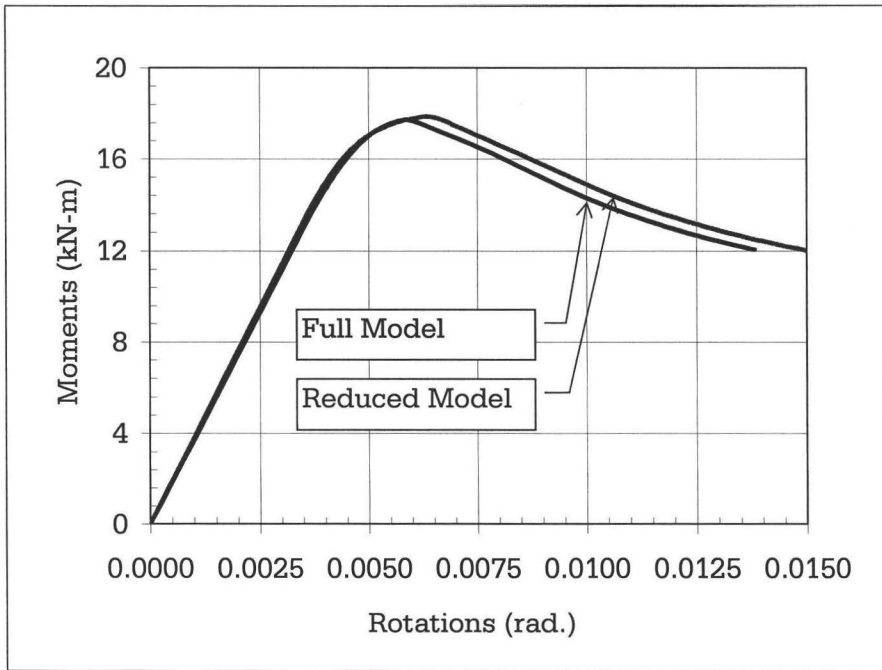


Figure 6.15: Moment rotation curves for joists having circular web openings

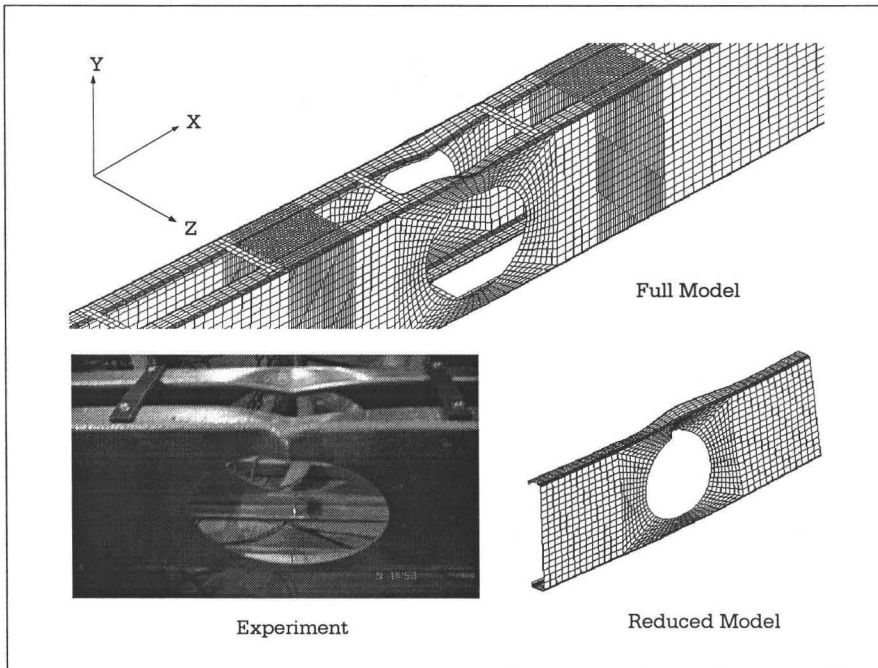


Figure 6.16: Comparison of deformed shapes: Joists having circular web openings

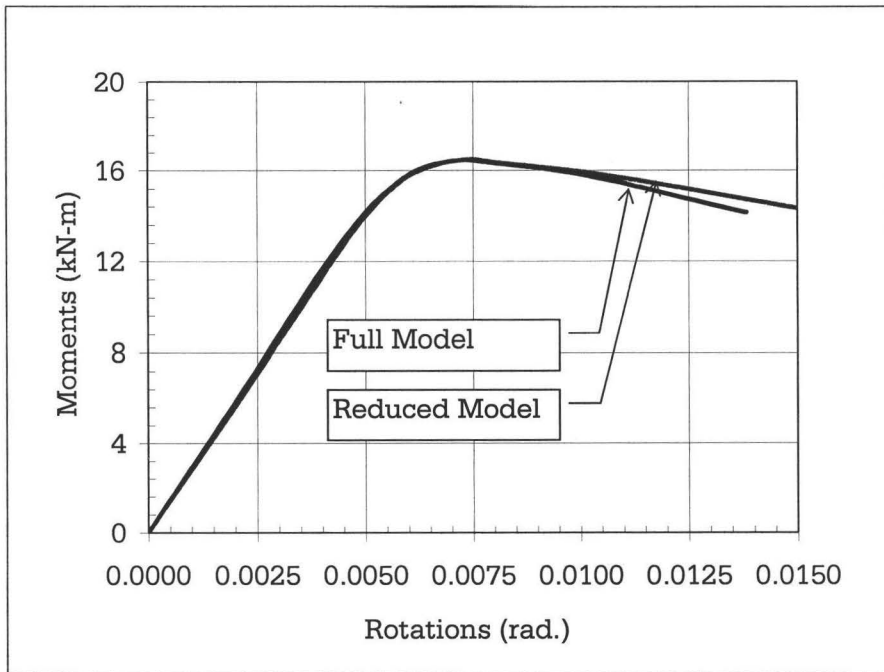


Figure 6.17: Moment rotation curves for joists having square web openings

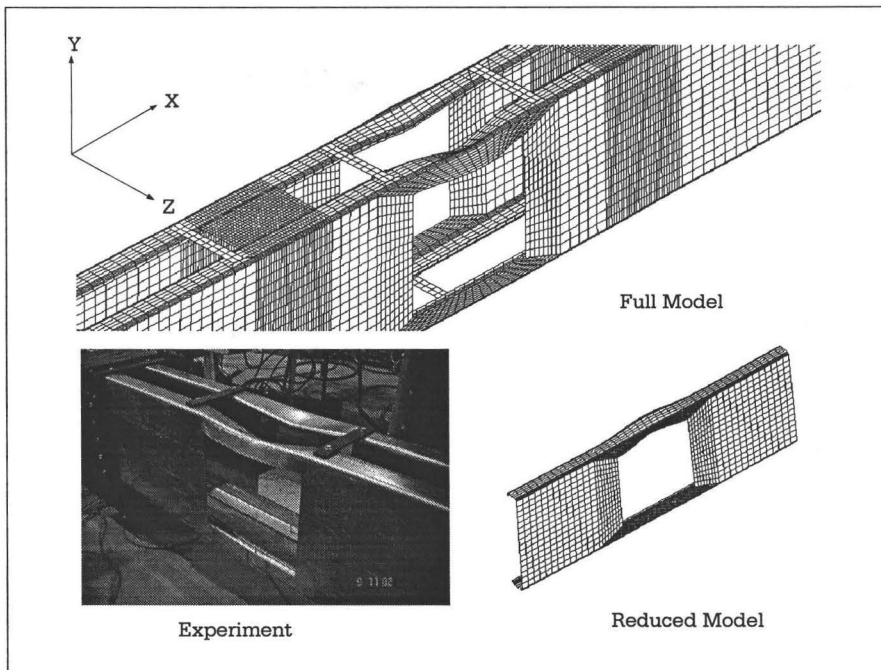


Figure 6.18: Comparison of deformed shapes: Joists having square web openings

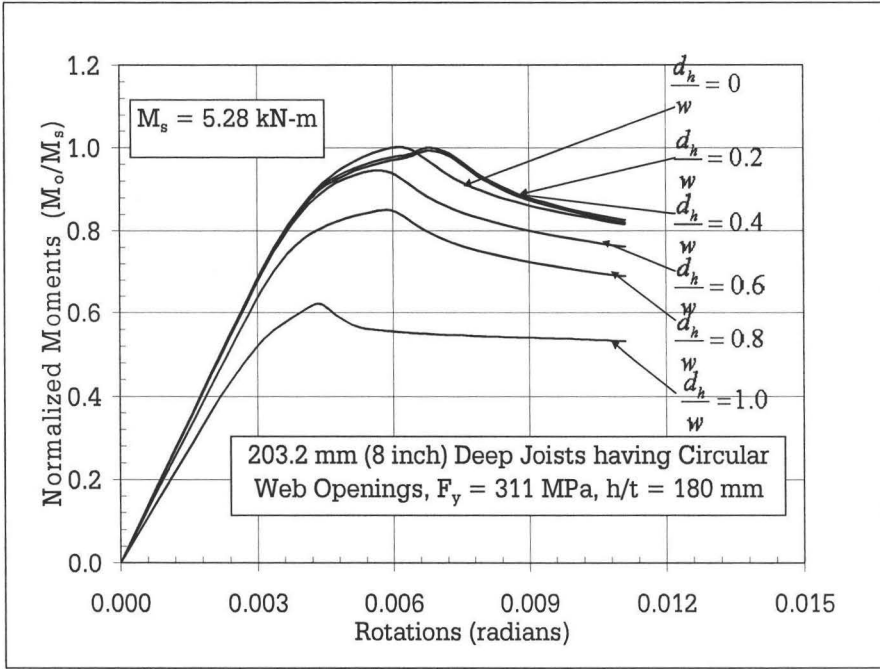


Figure 6.19: Normalized moment rotation curves for the thin joists having circular web openings

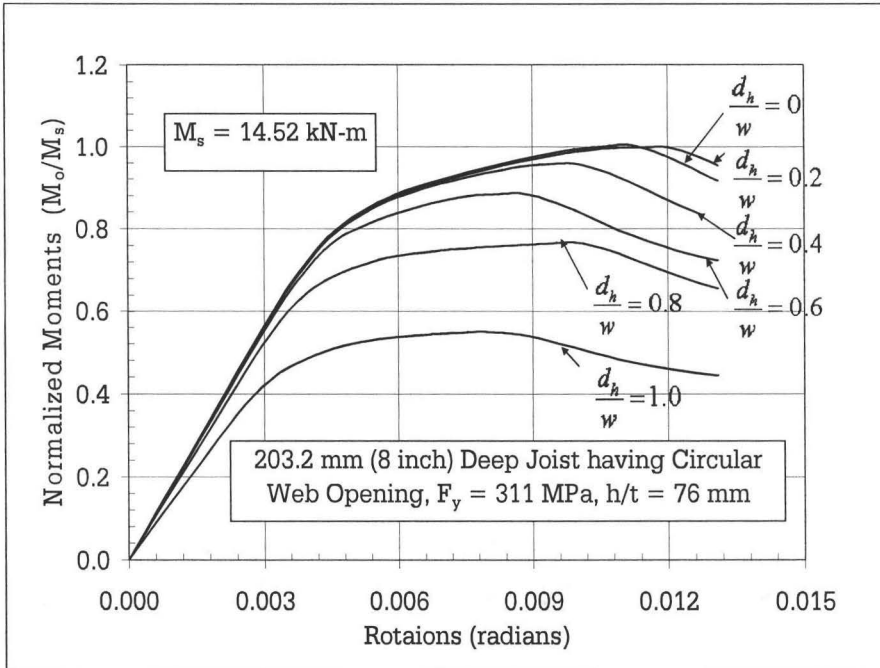


Figure 6.20: Normalized moment rotation curves for the thick joists having circular web openings

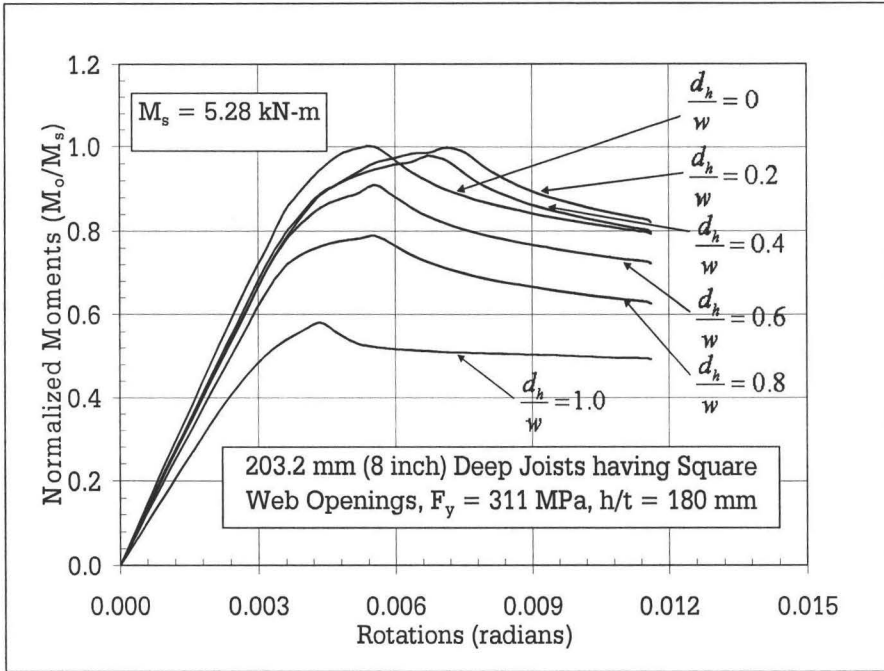


Figure 6.21: Normalized moment rotation curves for the thin joists having square web openings

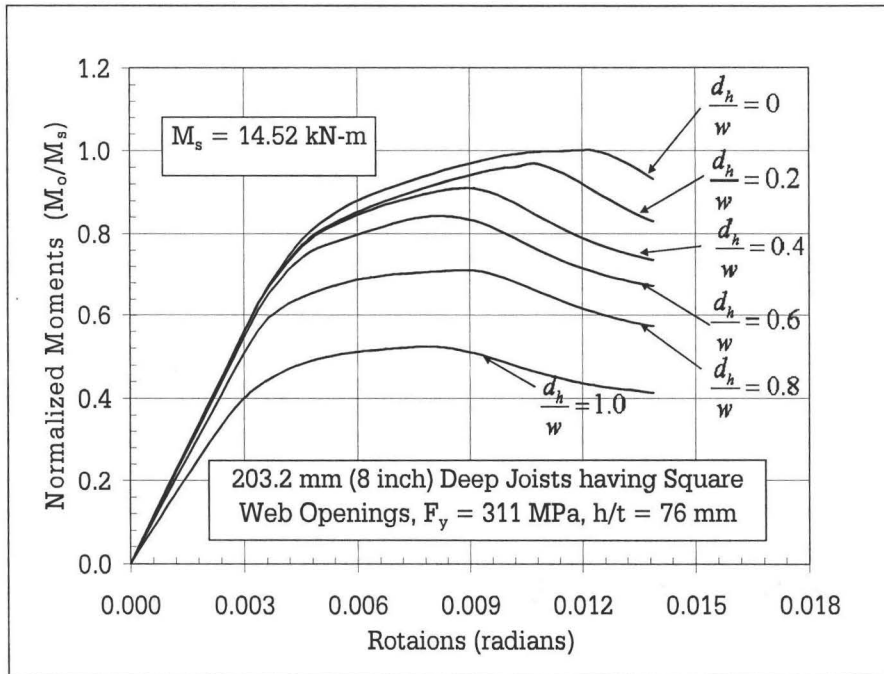


Figure 6.22: Normalized moment rotation curves for the thick joists having square web openings

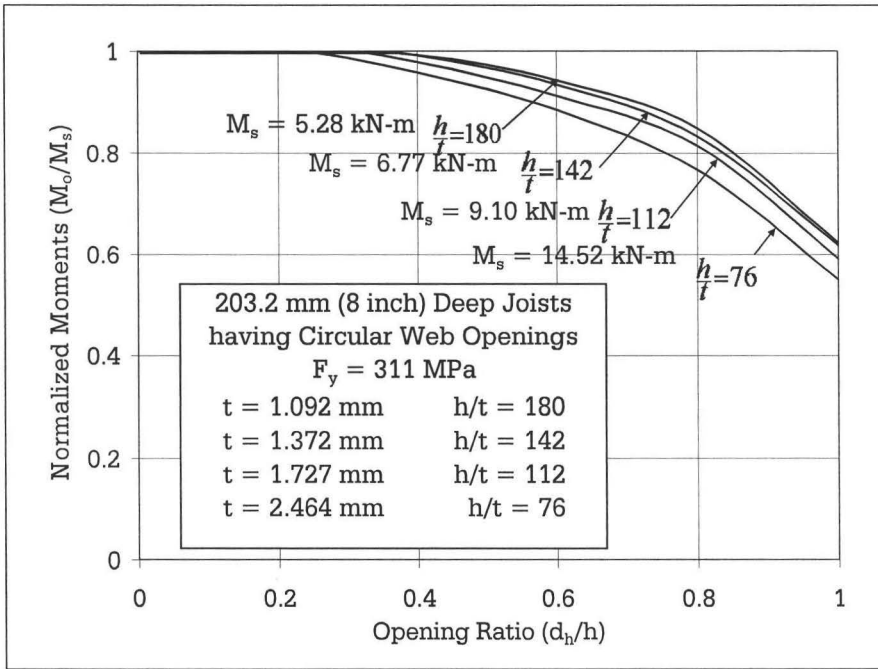


Figure 6.23: Moment reduction curves for the 203.2 mm (8 inch) deep joists having circular web openings

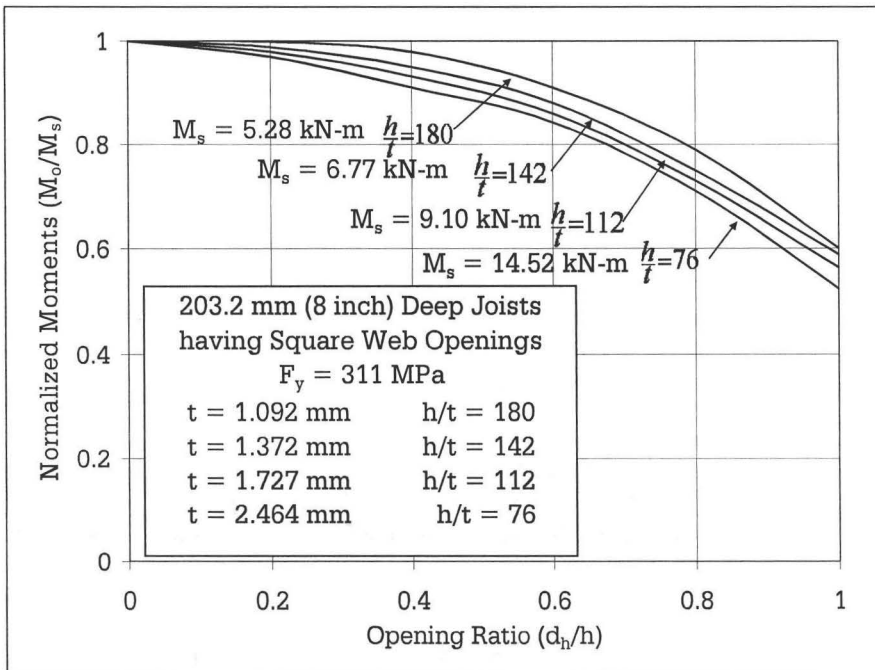


Figure 6.24: Moment reduction curves for the 203.2 mm (8 inch) deep joists having square web openings

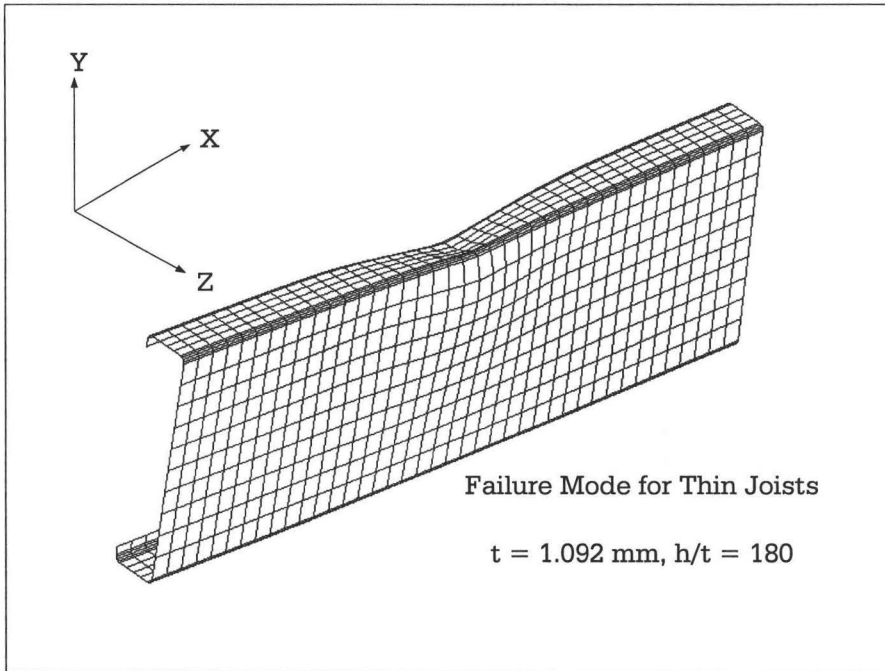


Figure 6.25: Typical failure mode of thin joists

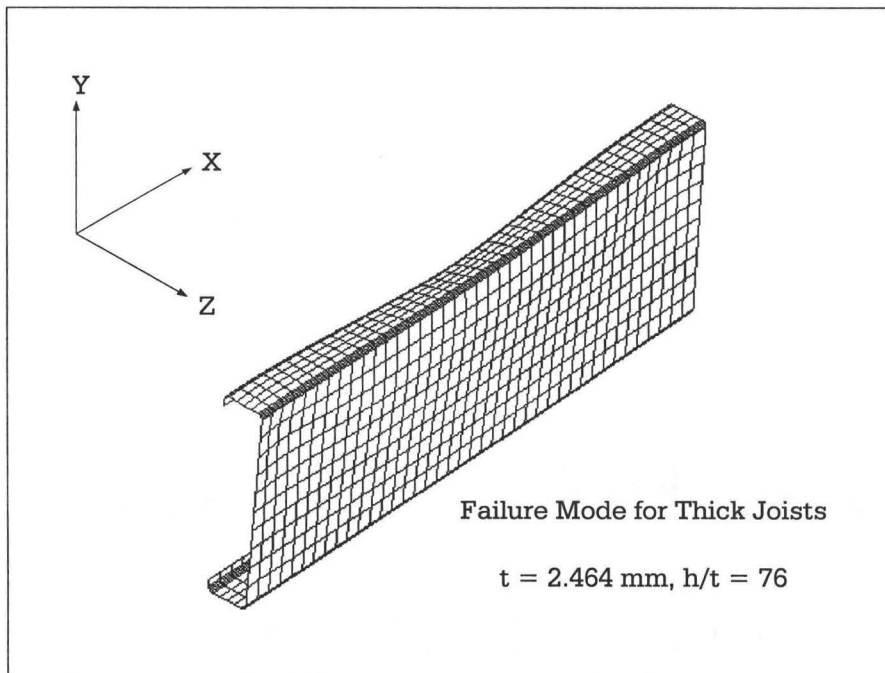


Figure 6.26: Typical failure mode of thick joists

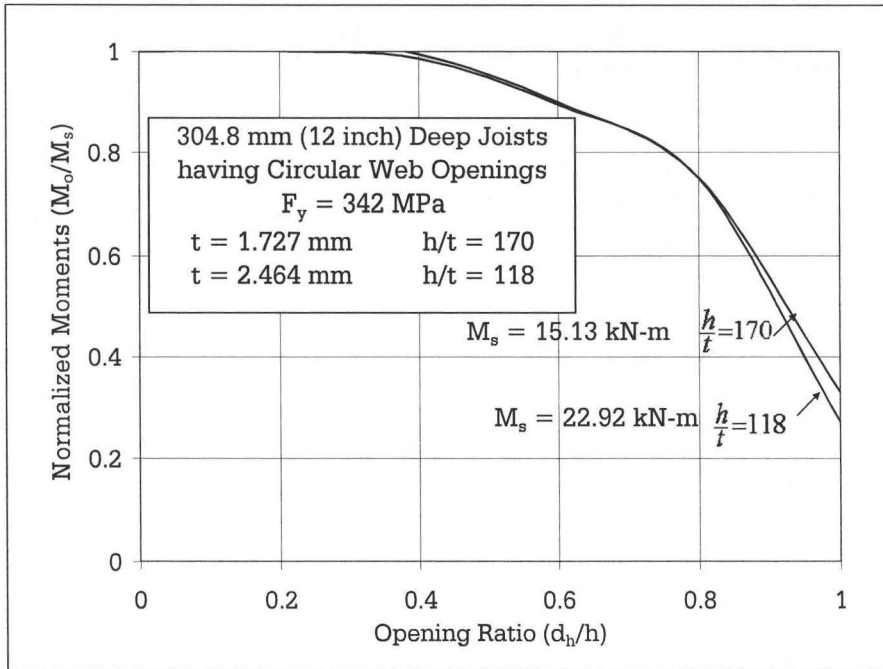


Figure 6.27: Moment reduction curves for the 304.8 mm (12 inch) deep joists having circular web openings

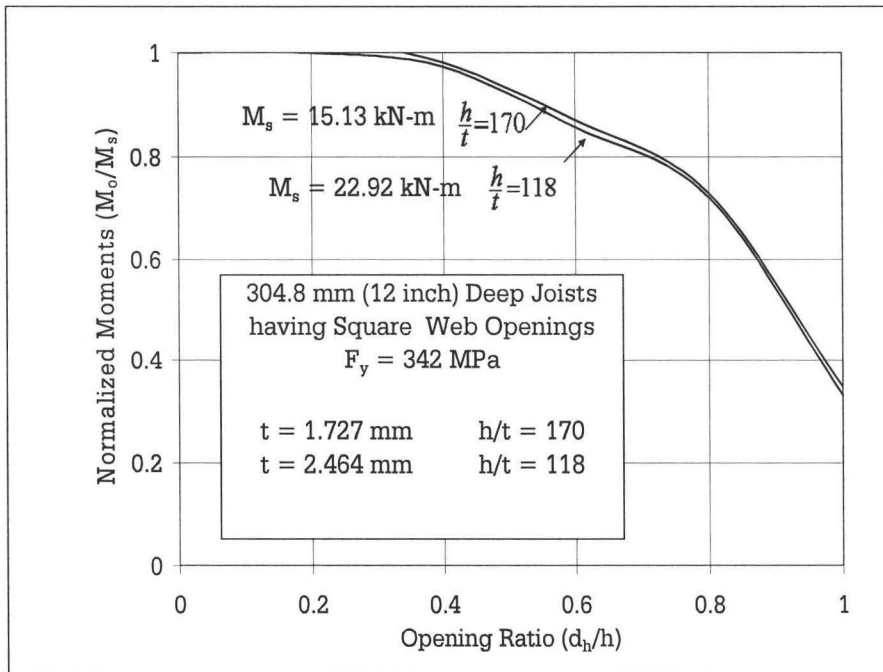


Figure 6.28: Moment reduction curves for the 304.8 mm (12 inch) deep joists having square web openings

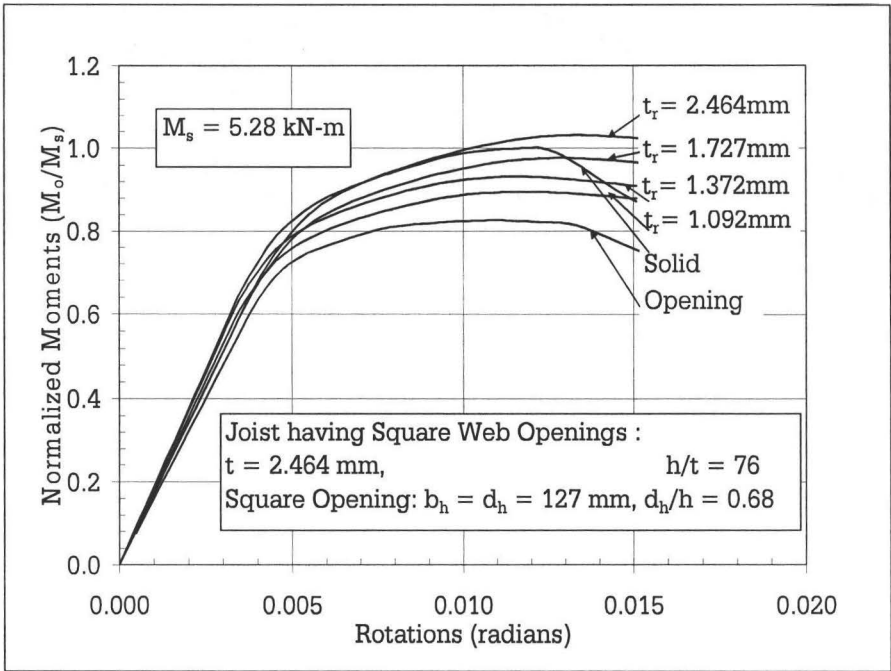


Figure 6.29: Normalized moment rotation curves of reinforced 2.464 mm (97 mils) thick joist

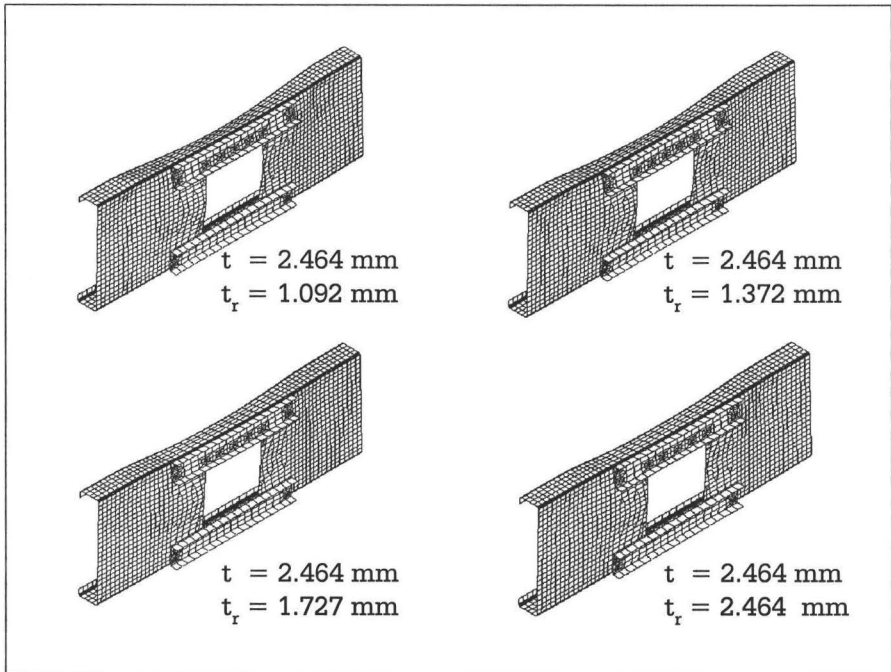


Figure 6.30: Deformed shapes of reinforced 2.464 mm (97 mils) thick joist

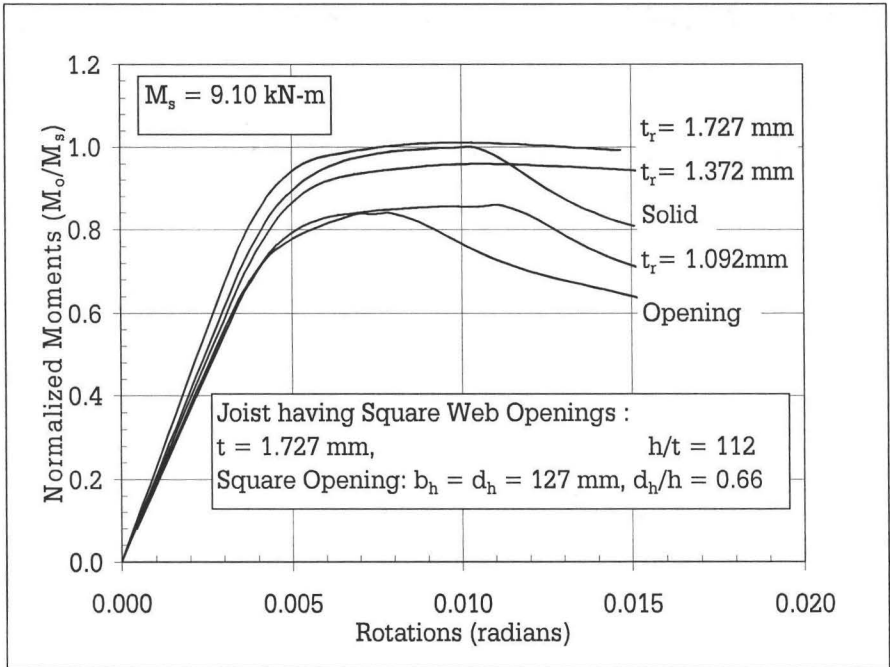


Figure 6.31: Normalized moment rotation curves of reinforced 1.727 mm (68 mils) thick joist

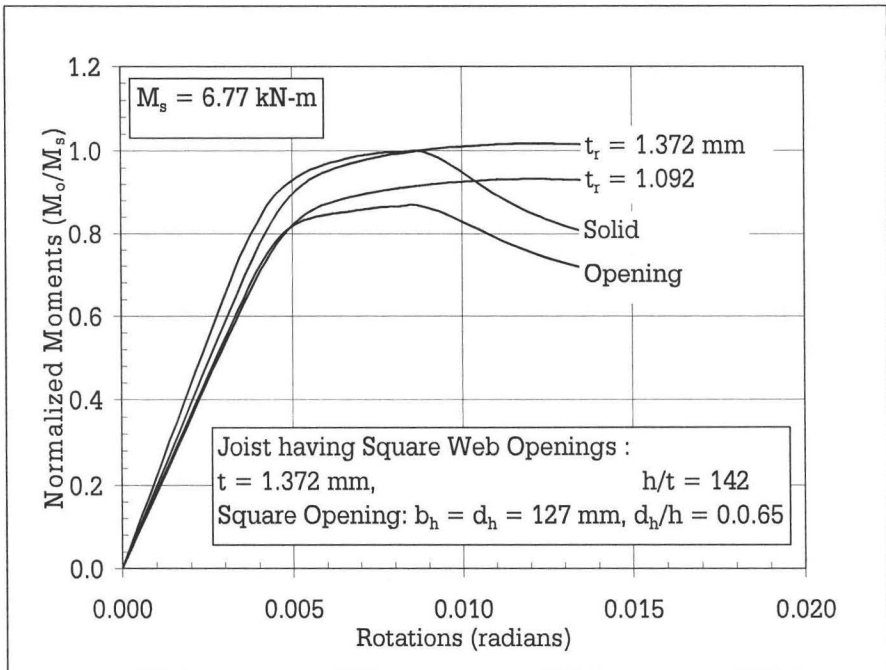


Figure 6.32: Normalized moment rotation curves of reinforced 1.372 mm (54 mils) thick joist

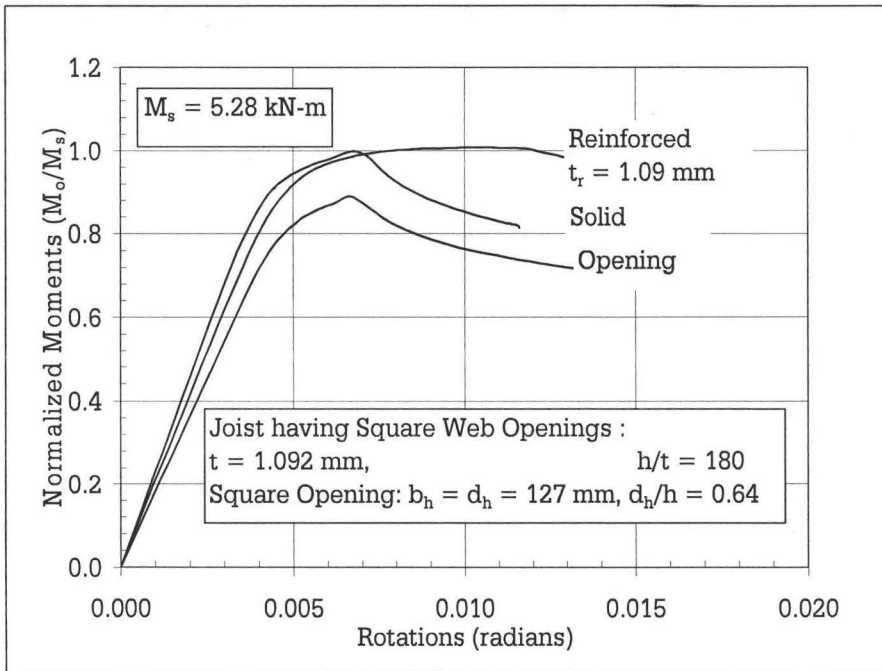


Figure 6.33: Normalized moment rotation curves of reinforced 1.902 mm (43 mils) thick joist

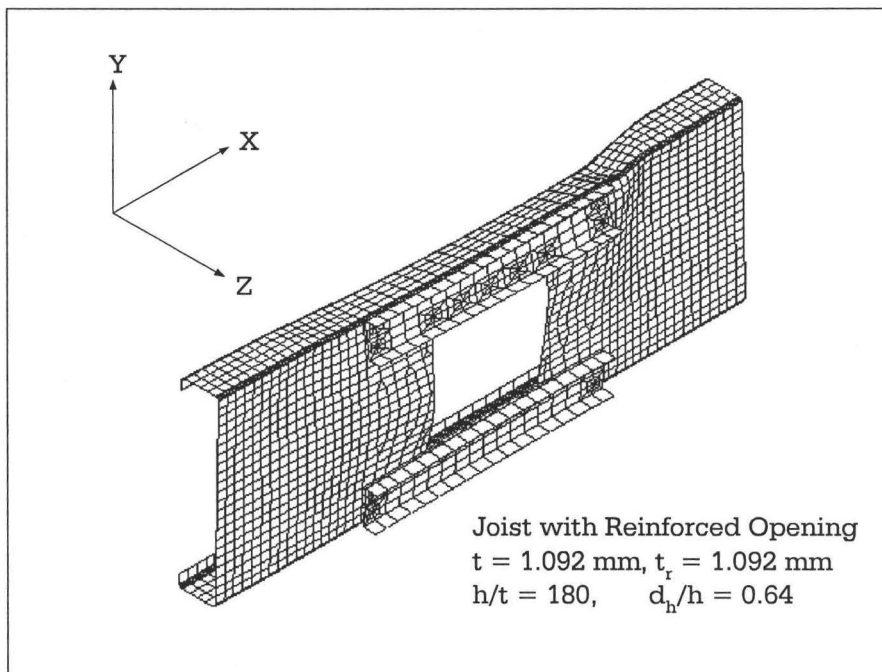


Figure 6.34: Deformed shapes of reinforced 1.092 mm (43 mils) thick joist

Chapter 7

Conclusions and Recommendations

7.1 Summary

The use of cold-formed steel (CFS) structures has become increasingly popular in building construction. For example, small housing systems using cold-formed steel for wall structures, framing systems and roof structures including trusses and shielding materials have been developed during recent years. The reason behind the growing popularity of cold-formed steel products include their ease of fabrication, high strength/weight ratio and suitability for a wide range of applications. These advantages can result in more cost-effective designs, as compared with hot-rolled steel, especially in short-span applications. Cold-formed steel offers very flexible design using different cross-sectional shapes.

As the floor joists of CFS structures frequently require large web openings. Such web openings can provide the necessary passage through space for ductwork, piping and other systems. Appropriate use of web openings can enhance the aesthetic appeal and improve the constructional efficiency of CFS floor systems. However, the presence of a large web opening could cause problems as a result of localized redistribution of stresses at the opening region. The openings also affect the flexural stiffness resulting

in poor serviceability performance. Providing appropriate reinforcements for such openings may mitigate the detrimental effects of such large web openings.

In this study, experimental and analytical (Finite Element Analysis) investigation of cold-formed steel sections having circular and square large web openings were carried out. The research considered three reinforcement schemes for such openings. The test specimens were simply supported at their ends, and were subjected to two type loadings (uniformly distributed load and point loads). Web openings were first reinforced using two reinforcement schemes (plate and stud reinforcements) as prescribed by the current AISI Specification. It was observed that these reinforcement schemes are ineffective in both shear and flexure. A new reinforcement scheme (bridging channel) was developed and experimentally studied. The new reinforcement scheme was also analytically verified. It was observed that the new reinforcement scheme is effective for joists having various web depth. Overall, the test and analytical results showed that it is possible to establish a cost-effective reinforcement scheme for cold-formed steel sections having large web openings.

7.2 Limitations

The flexural and shear reinforcement schemes discussed in this dissertation are based on the experimental and analytical study of cold-formed steel (CFS) lipped channel sections. The study has the following limitations; Section Type: Lipped channel sections; Web Depth: 203.2 mm (8 inch) - 304.8 mm (12 inch); Thickness: 1.09 mm (43 mils) - 2.46 mm (97 mils); Opening Type: Circular and square; Opening Location: Centered on the web; Opening Depth: ≤ 75 percent of web depth.

7.3 Conclusions

The main conclusions drawn from the research program are as follows.

Flexural Resistance of CFS Joists: Experimental Study

- The flexural strength of CFS joists can be estimated using current AISI Standard (AISI, 2007) procedure. The experimental values were higher than the calculated nominal values by up to 8 percent.
- The reduction in flexural strength of a cold formed steel joist section due to a web opening up to 75 percent of the web height was less than 25 percent.
- Circular web openings up to 40 percent of the flat web height had no significant effect on the flexural strength of CFS joists.
- Square web openings had a more severe effects on the flexural strength of CFS joists than circular web openings. Square web openings with size greater than 20 percent of flat web height caused significant reduction on the flexural strength of the CFS joists.
- The failure of the CFS joists having high h/t ratio (thin joists) was governed by the local buckling of the flange and the web. However, the failure of CFS joists having low h/t ratio (thick joists) was governed by the distortional buckling of the flange (rotation of the flange toward or outwards from the web).
- Openings in CFS joist with low h/t ratio caused large reduction in moment capacity.
- Web openings in joists having high depth caused higher reduction in the moment capacity compared to joists having low depth.

- The reinforcement schemes (designated as Scheme-A and B) recommended by current AISI Standard (AISI, 2007a) are ineffective in sections having low w/t ratios.
- Reinforcement Scheme-C can restore the flexural strength of cold formed steel joist sections having web openings up to 75 percent of web height.

Shear Resistance of CFS Joists: Experimental Study

- The shear strength of CFS joists according to current AISI Standard (AISI, 2007) procedure was very conservative. The experimental values were higher than the calculated values by 41 percent.
- The reduction in shear strength of a CFS joist section due to the web opening up to 65 percent of web height, was as high as 60 percent.
- Reinforcement Schemes -A and B, established by AISI Standard (AISI, 2001), are not adequate to restore the shear strength of joists with web openings.
- Reinforcement Scheme-C, which is a Vierendeel type reinforcement system for web openings is capable of restoring the original shear strength of a CFS joist.

Recommendation for Flexural and Shear Reinforcement

- The region $0.30L$ from the end-support and $0.375L$ from the intermediate-support of CFS floor joist is defined as "Shear Zone".
- When there is a opening at "Shear Zone" such opening needs shear reinforcement as shown in Figures 3.18 and 3.21.
- Presence of opening in the remaining region can be defined as "Flexural Zone" hence needs only flexural reinforcement (see Figure 2.23).

Lap Connections for Thin-Walled Members:

- The behaviors of screw connections and bolt connections associated with cold-formed steel members are influenced by the low plate stiffness. The tilting of screws in the connection is governed by the plate stiffness around the screws and the end conditions at the connected end.
- Experimental and analytical work provided evidence of curling in lap connections of thin plates. Prevention in curling would make the connection stiffer by up to 4.6 percent. Moreover, it was observed that screw tilting might be decreased by up to 32.6 percent by preventing the occurrence of curling.

Plates with Openings:

- Considering plates subjected to in-plane compression and flexure, failure would be governed by cross sectional yielding of plates having low slenderness ratio and by plate buckling for plates having high slenderness ratio.
- Plates having slenderness ratios, w/t , equal to 100, and 200, there was no significant reduction in the ultimate compressive strength when the size of the central openings was less than 40 percent of the plate width.
- Small central openings caused higher reduction in moment capacity in plates having high slenderness ratios compared to plates having low slenderness ratios.
- Large central openings caused less reduction in moment capacity of thin plates compared to the thick plates.
- It is possible to reinforce plates having openings using plates. Such reinforcements are capable of restoring the in-plane flexural strength of plates having

openings. The strength of a reinforced plate could be as high as the strength of solid plates.

Flexural Resistance of CFS Joists: Numerical Study

- Circular web openings up to 40 percent of the flat web height had no significant reduction in the flexural strength of CFS joists.
- Square web openings had more severe effects on the flexural strength of CFS joists than circular web openings. It was found that square web openings with a size greater than 20 percent of flat web height caused significant reduction on the flexural strength of the CFS joists.
- Failure of CFS joists having high h/t ratio (thin joists) would be governed by the localized buckling of the flange and web. But, failure of CFS joists having low h/t ratio (thick joists) would be governed by the distortional buckling of the flange (rotation of the flange toward or outwards from the web).
- Low h/t ratios caused higher reduction in moment capacity of CFS joists with web openings.
- Joists having high depth caused higher reduction in the moment capacity compared to joists having lower depth due to the presence of web openings.

7.4 Recommendations for Future Research

The following recommendations may be considered in any future research involving the reinforcement schemes for CFS joists having web openings.

- Only one shape and two sizes of cold-formed joists were tested in this study. Further verification tests should be carried out using other available shapes and sizes of CFS joists with multiple openings.
- This study considered the reinforcement schemes only for the flexural and shear zone. Further studies could be carried out to examine reinforcement schemes for combined flexure and shear.
- The finite element investigation could be extended to include the shear load and combination of flexure and shear.

References

- Abdel-Rahman, N. and Sivakumaran, K. S. (1997). Material properties models for analysis of cold-formed steel members. *Journal of Structural Engineering*, 123(9):1135–1143.
- Abdel-Rahman, N. and Sivakumaran, K. S. (1998). Effective design width for perforated cold-formed steel compression members. *Canadian Journal of Civil Engineering*, 25:319–330.
- Aceti, R., Ballio, G., Capsoni, A., and Corradi, L. (2004). A limit analysis study to interpret the ultimate behaviour of bolted joints. *Journal of Construction Steel Research*, 60:1333–1351.
- Acharya, S. R., Heerema, P., and Sivakumaran, K. S. (2007). Testing of cold-formed steel members with reinforced web openings in high shear zones. In *6th International Conference on Steel and Aluminium Structures*, Oxford, UK.
- Acharya, S. R. and Sivakumaran, K. S. (2006). Flexural strength of steel plates with reinforced opening. In *Proceedings of the Tenth Asia-Pacific Conference on Structural Engineering and Construction (EASEC-10)*, Thailand, Bangkok.
- Acharya, S. R. and Sivakumaran, K. S. (2008a). Bending strength of cfs members with reinforced openings. In *Proceeding of the 2nd Canadian Conference on Effective Design of Structures*, Hamilton, Canada.
- Acharya, S. R. and Sivakumaran, K. S. (2008b). Finite element models for connections in thin walled members. In *Proceeding of the 2nd Canadian Conference on Effective Design of Structures*, Hamilton, Canada.
- ADINA (2001). *Theory and Modeling Guide*. ADINA R and D, Inc., USA.
- AISI (2007). *North American Specification for the Design of Cold-Formed Steel Structural Members*. American Iron and Steel Institute, USA.
- AISI (2007a). *Standard for Cold-Formed Steel Framing- Prescriptive Method for One and Two Family Dwellings*. American Iron and Steel Institute, USA.

- ASTM (2003). *Standard Test Methods and Definitions for Mechanical Testing of Steel Products*, volume A 370-03a. American Society of Testing and Materials, Philadelphia, USA.
- Bakker, M. C. M. and Pekoz, T. (2003). The finite element methods for thin-walled members-basic principles. *Thin-Walled Structures*, 41:179–189.
- Basler, K. (1961). Strength of plate girders in shear. *Journal of Structural Division*, 87(ST7, Oct):151–180.
- Bathe, K. (1996). *Finite Element Procedures*. Printice Hall, New Jersey, USA.
- Bathe, K. and Chaudhary, A. (1984). On finite element analysis of large deformation frictional contact problems. In *Unification of Finite Element Methods*, North-Holland, Amsterdam.
- Bathe, K. and Chaudhary, A. (1986). A solution method for planer and axisymmetric contact problems. *International Journal of Numerical Methods in Engineering*, 21:65–88.
- Biskin, L. (1944). Strengthening of circular holes in plates under edge forces. *Journal of Applied Mechanics*, pages A–140.
- Bower, J. E. (1966a). Elastic stresses around holes in wide-flange beams. *Journal of Structural Division*, 92(ST2, Apr):85–101.
- Bower, J. E. (1966b). Experimental stresses in wide-flange beams with holes. *Journal of Structural Division*, 92(ST2, Oct):167–185.
- Bower, J. E. (1968). Ultimate strength of beams with rectangular holes. *Journal of Structural Division*, 94(ST6, Jun):1315–1337.
- Chong, K. P. and Matlock, R. B. (1975). Light-gage steel bolted connections without washers. *Journal of Structural Division*, 101(ST7, Jul):1381–1391.
- Chow, F. Y. and Narayanan, R. (1984). Buckling of plates containing openings. In *Proceedings of the Seventh International Specialty Conference on Cold-Formed Steel Structures*, University of Missouri-Rolla.
- CISC-Handbook (2007). *Handbook of Steel Construction*. Canadian Institute of Steel Construction, Markham, Ontario Canada.
- Coetsee, J. S., Van den Berg, G. J., and Van der Merwe, P. (1990). The effect of work hardening and residual stresses due to cold working of forming on the strength of cold-formed stainless steel lipped channel sections. In *10th International Specility Conference on Cold-Formed Steel Structures*, St. Louis, USA.

- Congdon, J. D. and Redwood, R. G. (1968). Plastic behavior of beams with reinforced holes. *Journal of Structural Division*, 93(ST9, Sep):1933–1957.
- Copper, P. B. and Snell, R. R. (1972). Tests on beams with reinforced web openings. *Journal of Structural Division*, 98(ST3, Mar):611–632.
- CSA (2007). *North American Specification for the Design of Cold-Formed Steel Structural Members*, volume S-136-07. Ontario, Canada.
- Davies, J. M., Leach, P., and Taylor, A. (1997). The design of perforated cold-formed steel sections subjected to axial load and bending. *Thin-Walled Structures*, 40:239–262.
- Etrovic, A. and Bathe, K. (1991). On the treatment of inequality constraints arising from contact conditions in finite element analysis. *Computer and Structures*, 40(2):203–209.
- Fan, L., Rondal, J., and Cescotto, S. (1997). Finite element modelling of single lap screw connections in steel sheeting under static shear. *Thin-Walled Structures*, 27(2):165–185.
- Fowler, R. O., Marino, F. J., Palmer, F. J., Redwood, R. G., Snell, R. R., and Bower, J. E. (1971). Suggested design guides for beams with holes. *Journal of Structural Division*, 97(ST11):2707–2077.
- Hancock, G. J. (1985). Distortional buckling of steel storage rack columns. *Journal of Structural Engineering*, 111(12):2771–2783.
- Hoffman, R. M., Dinehart, D. W., Gross, S. P., Yost, J. R., and Hennessey, J. M. (2005). Effects of cope geometry on the strength and behavior of cellular and castellated beams. *Engineering Journal*, Fourth Quarter:261–271.
- Hoglund, T. (1971). Strength of thin plate girders with circular and rectangular web holes without web stiffeners. In *Proceedings of the Colloquium of the International Association of Bridge and Structural Engineering*, London.
- Karren, K. W. (1967a). Corner properties of cold-formed steel shapes. *Journal of Structural Division*, 93(ST1, Feb):401–431.
- Karren, K. W. (1967b). Effects of cold-forming on light-gage steel members. *Journal of Structural Division*, 93(ST1, Feb):433–469.
- Kawai, T. and Ohtsubo, H. (1968). A method of solution for the complicated buckling problems of elastic plates with combined use of rayleigh-ritz's procedure in the finite element method. In *Proceedings of the 2nd Air Force Conference on Matrix Methods in Structural Mechanics*.

- Kim, H. J. and Yura, J. A. (1999). The effect of ultimate-to-yield ratio on the bearing strength of bolted connections. *Journal of Construction Steel Research*, 49:255–269.
- Kim, T. S. and Kuwamura, H. (2007). Finite element modeling of bolted connections in thin-walled stainless steel plates under static shear. *Thin-Walled Structures*, 45:407–421.
- Kroll, W. D. (1949). Instability of simply supported square plates with reinforced and unreinforced holes subjected to shear. *Journal of Research, National Bureau of Standards*, 43:465–478.
- LaBoube, R. A., Yu, W. W., Langan, J. E., and Shan, M. Y. (1997). Cold-formed steel webs with openings: Summary report. *Thin-Walled Structures*, 27(1):79–84.
- Larson, M. A. and Shah, K. N. (1976). Plastic design of web openings. *Journal of Structural Division*, 102(ST5, May):1031–1041.
- Li, L. (2002). *Strength of Cold Formed Steel Beam-Columns*, M. A. Sc. Thesis. McMaster University, Hamilton, Canada.
- Narayanan, R., Al-Amery, R. I. M., and Roberts, T. M. (1989). Shear strength of composite plate girders with rectangular web cut-outs. *Journal of Construction Steel Research*, 12:151–166.
- Narayanan, R. and Der-Avanessian, N. G. V. (1983a). An equilibrium method for assessing the strength of plate girders having reinforced web openings. *Proceedings of the Institute of Civil Engineering*, 75(2).
- Narayanan, R. and Der-Avanessian, N. G. V. (1983b). Equilibrium solutions for predicting the strength of webs with rectangular holes. *Proceedings of the Institute of Civil Engineering*, 75(2).
- Narayanan, R. and Der-Avanessian, N. G. V. (1984). Elastic buckling of perforated plates under shear. *Thin-Walled Structures*, 2:51–73.
- Narayanan, R. and Der-Avanessian, N. G. V. (1985). Design of slender webs having rectangular holes. *Journal of Structural Engineering*, 111(4):777–787.
- Narayanan, R. and Der-Avanessian, N. G. V. (1986). Analysis of plate girders with perforated webs. *Thin-Walled Structures*, 4:363–380.
- Narayanan, R., Der-Avanessian, N. G. V., and Ghannam, M. M. (1983). Small-scale model tests on perforated webs. *The Structural Engineering*, 61B(3).

- Ng, M. Y., Sivakumaran, K. S., and Fox, S. R. (2005). Flexural testing of cold-formed steel members with reinforced web openings. In *33rd Annual General Conference of the Canadian Society of Civil Engineering*, Ontario, Canada.
- Pennock, R. W. (2001). *Strength of Light Gauge Cold Formed Steel Joists with Web Perforation: Senior Report*. University of New Brunswick, New Brunswick, Canada.
- Pu, Y., Godley, M. H. R., Beale, R. G., and Lau, H. H. (1999). Prediction of ultimate capacity of perforated lipped channels. *Journal of Structural Engineering*, 125(5):510–514.
- Put, M. B., Pi, Y., and Trahair, N. S. (1999). Lateral buckling tests on cold-formed channel beams. *Journal of Structural Engineering*, 125(5):532–539.
- Redwood, R. G. (1967). Discussion on elastic stresses around holes in wide-flange beams. *Journal of Structural Division*, 93(ST1, Feb):609–610.
- Redwood, R. G., Baranda, H., and Daly, M. J. (1978). Tests of thin-webbed beams with un-reinforced holes. *Journal of Structural Division*, 104(ST3, Mar):577–595.
- Redwood, R. G. and McCutcheon, J. O. (1968). Beam tests with unreinforced web openings. *Journal of Structural Division*, 94(ST1, Jan):1–17.
- Redwood, R. G. and Uenoya, M. (1979). Critical loads for webs with hole. *Journal of Structural Division*, 105(ST10, Oct):2053–2067.
- Roberts, T. M. and Azizian, Z. G. (1984). Strength of perforated plates subjected to in-plane loading. *Thin-Walled Structures*, 2:153–164.
- Rockey, K. C., Anderson, R. G., and Cheung, Y. K. (1969). The behavior of square shear webs having a circular hole. *Thin-Walled Structures*. K. C. Rockey and H. V. Hill, eds., Gordon and Breach Science Publishers.
- Sabir, A. B. and Chow, F. Y. (1986). Elastic buckling of plates containing eccentrically located circular holes. *Thin-Walled Structures*, 4:135–149.
- Sarawit, A. T., Kim, Y., Bakker, M. C. M., and Pekoz, T. (2003). The finite element methods for thin-walled members-applications. *Thin-Walled Structures*, 41:191–206.
- Schafer, B. W. and Pekoz, T. (1998). Computational modeling of cold-formed steel: Characterizing geometric imperfections and residual stresses. *Journal of Construction Steel Research*, 47:193–210.

- Schuster, R. M., Rogers, C. A., and Celli, A. (1995). *Perforated C-Sections in Shear-Research into Cold-Formed Steel: Progress Report-1*. University of Waterloo, Waterloo, Ontario, Canada.
- Segner, E. P. (1964). Reinforcement requirements for girder web openings. *Journal of Structural Division*, 90(ST3, Jun):147–164.
- Shan, M. Y. and LaBoube, R. A. (1994). *Behaviour of Web Elements with Openings Subjected to Bending, Shear and the Combination of Bending and Shear*. University of Missouri-Rolla, Rolla, Missouri.
- Shan, M. Y., LaBoube, R. A., and Yu, W. W. (1996). Bending and shear behavior of web elements with openings. *Journal of Structural Engineering*, 122(8):854–859.
- Shanmugam, N., Lian, V. T., and Thevendran, V. (2002). Finite element modeling of plate girders with web openings. *Thin-Walled Structures*, 40:443–464.
- Shanmugam, N. E. (1997). Openings in thin-walled steel structures. *Thin-Walled Structures*, 28(3/4):355–372.
- Shanmugam, N. E. and Thevendran, V. (1992). Critical loads of thin-walled beams containing web openings. *Thin-Walled Structures*, 14:219–305.
- Shrivastava, S. C. and Redwood, R. G. (1979). Shear carried by flanges at unreinforced web holes. *Journal of Structural Division*, 105(ST8, Aug):1706–1711.
- Sivakumaran, K. S. (1987). Analysis for local buckling capacity of cold-formed steel sections with web opening. *Computer and Structures*, 26(1/2):275–282.
- Sivakumaran, K. S. and Abdel-Rahman, N. (1998). A finite element analysis model for the behavior of cold-formed steel members. *Thin-Walled Structures*, 31:305–324.
- Sivakumaran, K. S., Ng, M. Y., and Fox, S. R. (2006). Flexural strength of cold-formed steel joists with reinforced web openings. *Canadian Journal of Civil Engineering*, 33:1195–1208.
- Sivakumaran, K. S. and Zielonka, K. M. (1989). Web crippling strength of thin-walled steel members with web openings. *Thin-Walled Structures*, 8(3/4):295–319.
- Tomà, A., Sedlacek, G., and Weynand, K. (1993). Connections in cold-formed steel. *Thin-Walled Structures*, 16:219–237.
- von Karman, T., Sechler, E. E., and Donnell, L. H. (1932). The strength of thin plate in compression. *Transaction ASME*, 54:APM 54–5.
- Wand, T. M. and Snell, R. R. (1975). Strength of beams with eccentric reinforced holes. *Journal of Structural Division*, 101(ST9, Sept):1783–1800.

- Wang, C. K. (1946). Theoretical analysis of perforated shear webs. *Journal of Applied Mechanics*, B2:A77–A84.
- Wang, T. M., Snell, R. R., and Cooper, P. B. (1975). Strength of beams with eccentric reinforced holes. *Journal of Structural Division*, 101(ST9, Sep):1783–1800.
- Weng, C. C. and Peköz, T. (1990). Residual stresses in cold-formed steel members. *Journal of Structural Engineering*, 116(6):1611–1625.
- Weng, C. C. and White, R. N. (1990). Residual stresses in cold-bent thick steel plates. *Journal of Structural Engineering*, 116(1):24–39.
- Winter, G. (1956). Tests on bolted connections in light gage steel. *Journal of Structural Division*, 82(ST2, Mar):920/1–920/25.
- Yu, W. W. (2000). *Cold Formed Steel Design*. John Wiley and Sons, Inc., New York, USA.
- Yu, W. W. and Davis, C. S. (1973). Cold-formed steel members with perforated elements. *Journal of Structural Division*, 99(ST10, Oct):2061–2077.
- Zaras, J., Rhodes, J., and Krolak, M. (1992). Buckling and post-buckling of rectangular plates under linearly varying compression and shear: Part 2 - experimental investigations. *Thin-Walled Structures*, 14:59–87.

Appendices

Appendix A

Mechanical Properties of the CFS Joists

A.1 General

In order to establish the performance of cold-formed steel (CFS) joists, it is required to first establish the magnitudes and variations of material properties through tensile coupon tests. The material properties that are of interest include: proportional limit, yield strength, ultimate strength, and strain at rupture.

The mechanical properties of the flat zones of the flanges and web of the cold-formed steel (CFS) joists were established in accordance with the tensile testing procedures conforming to ASTM Standard Test A370 (ASTM, 2003). Accordingly, three tensile coupons were taken from the flat portions of three randomly selected test joists of each type (203.2 mm deep and 304.8 mm deep). For each such joist, two coupons were taken from the web and one coupon was taken from one of the flanges, resulting in a total of nine tensile coupons for each type of joists. The locations of these tensile coupons with respect to the joists are shown in Figure A.1. Altogether, eighteen tensile coupons were tested.

A.2 Tensile Coupons

The tensile coupons were cut along the longitudinal direction. This direction was parallel to the direction of rolling for such steel joists. Each of coupons was identified as follows. The first three letter sets in coupons identification code represent a part of identification code of corresponding parent joists; fourth and fifth letter-set represent the coupon number and location of the coupon on parent section. For example, "8F-N-2-1-f" means: "8F-N-2"-corresponding the parent joist, "1"- 1st coupon and "f" indicates flange. The tensile coupons were then machined to a shape to the dimensions required by ASTM Standard Test A370 (ASTM, 2003) for sheet-type material. The required dimensions of the tensile coupons were as shown in Figure A.1. Actual width, overall thickness and base metal thickness were measured. The base metal thickness was measured after removing the galvanized layer on the metal surface. The galvanized surface was removed by dipping one end of tensile coupons into the hydrochloric acid for a while. The identification for coupons and corresponding parent sections, measured width and base metal thickness are listed in Table A.1 and Table A.2.

A.3 Test Procedure

An INSTRON5566 testing machine with a calibrated load cell with 10 kN capacity was used for these tensile coupon tests (see Figure A.2). The machine has a load accuracy of 0.5 percent of indicated load. The coupons were mounted in the testing machine using the gripping devices and aligned with respect to the vertical axis of the machine. According to ASTM Standard Test A370 (ASTM, 2003) any loading rate can be applied up to yield strength. A constant loading rate of 0.1 mm/min was

applied up to yielding of the specimen. The loading rate was then increased to 1-2 mm/min (ASTM suggestion for such coupons: 0.36-3.57 mm/min) until yielding of the specimen. The loading rate was further increased to 5 mm/min (ASTM suggestion for such coupons: 2.8-28.5 mm/min) until the ultimate strength. Moreover, the rates of stressing from yielding to ultimate strength were observed as 91-560 MPa/minute (ASTM suggestion: 70-690 MPa/minute). The extensometer based extensions and the separation between cross heads of the test machine were monitored. A calibrated extensometer, INSTRON-2620-601 with 12.5 mm extender, was attached to the center of the tensile coupons to measure the axial elongation of the coupons during the test. This extensometer can measure a maximum of 20 percent strain. The extensometer was initially compressed to about 15 percent strain in order to increase the range of maximum strain that can be measured. Therefore, the extensometer was capable of measuring up to 35 percent strain from the initial compression.

A.4 Test Results

Figure A.3 and Figure A.4 show the coupons under consideration before and after testing. Figure A.5 to Figure A.10 show the measured stress-strain (σ - ϵ) relations. The stress value for each load was established based on the measured width at the reduced section, and the measured base metal thickness. Considering all nine tensile coupons for each type of joists (203.2 mm deep and 304.8 mm deep), in general, consistent stress-strain relationships were observed. The stress-strain curves for these coupons showed yield plateau and strain hardening characteristics prior to rupture. A gradual yielding was observed for all coupons of 203.2 mm (8 inch) deep joists and sharp yielding was observed for all coupons of 304.8 mm (12 inch) deep joists. The

0.01 percent offset, and 0.2 percent offset methods with an initial slope of 203,000 MPa were used to establish the proportional limit and the yield strength, respectively.

Table A.3 presents the results for 203.2 mm (8 inch) deep joists. The proportional limit values ranged between 266 and 298 MPa, the yield strength values ranged between 304 and 316 MPa, whereas the ultimate strength values ranged between 394 and 407 MPa. The average proportionality limit, yield strength and ultimate strength were 288, 311 and 401 MPa with standard deviation 10, 4 and 4 MPa, respectively. Further, as shown in Table A.3, the steel used in this investigation exhibited the following mechanical characteristics; average ultimate tensile strength to yield strength ratio of 1.29 with standard deviation 0.01, and the average strain at rupture, which reflects the ductility of the steel, of 0.21 with standard deviation 0.04.

Similarly, the results for 304.8 mm (12 inch) deep joists are presented in Table A.4. The average proportional limit for 304.8 mm (12 inch) deep joists was established as 340 MPa. The average values of yield strength and ultimate strength were 343 MPa and 469 MPa. The table also shows that 304.8 mm (12 inch) deep joists had ultimate tensile strength to yield strength ratio equal to 1.29 and strain at rupture equal to 0.33. The standard deviations for corresponding measured values are also presented in the table.

These average values were derived from the nine tests for each type of joists presented in Table A.4 and Table A.5. The values in Table A.4 were based on the test results plotted in Figure A.5 to Figure A.7. Similarly, Table A.5 was obtained from the test results presented in Figure A.8 to Figure A.10.

Table A.1: Measured gauge width and thickness for tensile coupons from 203.2 mm (8 inch) deep joists

Parent Section	Specimen	Gauge Width (mm)	Base Metal Thickness (mm)
8F-N-2-R	8F-N-2-1-f	13.00	1.12
	8F-N-2-2-w	12.99	1.12
	8F-N-2-3-w	12.99	1.13
8F-C-2-R	8F-C-2-1-f	12.85	1.13
	8F-C-2-2-w	12.85	1.12
	8F-C-2-3-w	12.87	1.13
8F-S-2-L	8F-S-2-1-f	12.92	1.10
	8F-S-2-2-w	12.88	1.10
	8F-S-2-3-w	12.94	1.09
	Average	12.92	1.12
	Standard Deviation	0.06	0.01

Table A.2: Measured gauge width and thickness for tensile coupons from 304.8 mm (12 inch) deep joists

Parent Section	Specimen	Gauge Width (mm)	Base Metal Thickness (mm)
12F-N-2-R	12F-N-2-1-f	12.98	2.45
	12F-N-2-2-w	12.86	2.46
	12F-N-2-3-w	12.97	2.46
12F-C-2-R	12F-C-2-1-f	12.89	2.45
	12F-C-2-2-w	12.96	2.47
	12F-C-2-3-w	12.94	2.46
12F-S-2-L	12F-S-2-1-f	12.91	2.44
	12F-S-2-2-w	12.99	2.46
	12F-S-2-3-w	12.94	2.46
	Average	12.94	2.46
	Standard Deviation	0.04	0.01

Table A.3: Material properties based on tensile coupons from 203.2 mm (8 inch) deep joists

Specimen	Proportional Yield Limit, F_p (MPa)	Yield Strength, F_y (MPa)	Ultimate Strength F_u (MPa)	F_u/F_y	Percent Elongation
8F-N-2-1-f	292	313	400	1.28	0.26
8F-N-2-2-w	298	312	406	1.30	0.20
8F-N-2-3-w	284	304	394	1.30	0.19
8F-C-2-1-f	284	316	407	1.29	0.27
8F-C-2-2-w	298	315	404	1.28	0.17
8F-C-2-3-w	292	309	402	1.30	0.18
8F-S-2-1-f	266	312	400	1.28	0.24
8F-S-2-2-w	295	309	398	1.29	0.18
8F-S-2-3-w	286	310	397	1.28	0.16
Average	288	311	401	1.29	0.21
Std. Dev.	10	4	4	0.01	0.04

Table A.4: Material properties based on tensile coupons from 304.8 mm (12 inch) deep joists

Specimen	Proportional Yield Limit, F_p (MPa)	Yield Strength, F_y (MPa)	Ultimate Strength F_u (MPa)	F_u/F_y	Percent Elongation
12F-N-2-1-f	303	347	470	1.35	0.35
12F-N-2-2-w	353	342	470	1.37	0.36
12F-N-2-3-w	347	343	467	1.36	0.27
12F-C-2-1-f	351	347	472	1.36	0.31
12F-C-2-2-w	350	351	472	1.34	0.32
12F-C-2-3-w	335	334	461	1.38	0.35
12F-S-2-1-f	338	342	466	1.36	0.35
12F-S-2-2-w	342	334	469	1.40	0.33
12F-S-2-3-w	342	343	473	1.38	0.31
Average	340	343	469	1.37	0.33
Std. Dev.	15	6	4	0.02	0.03

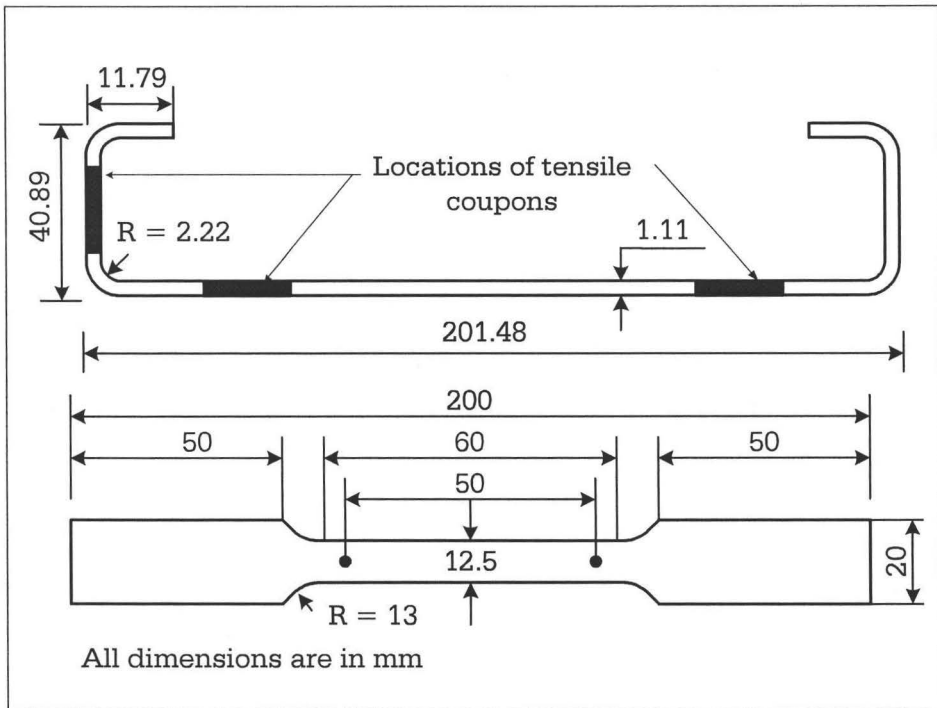


Figure A.1: Locations and dimensions of tensile coupons

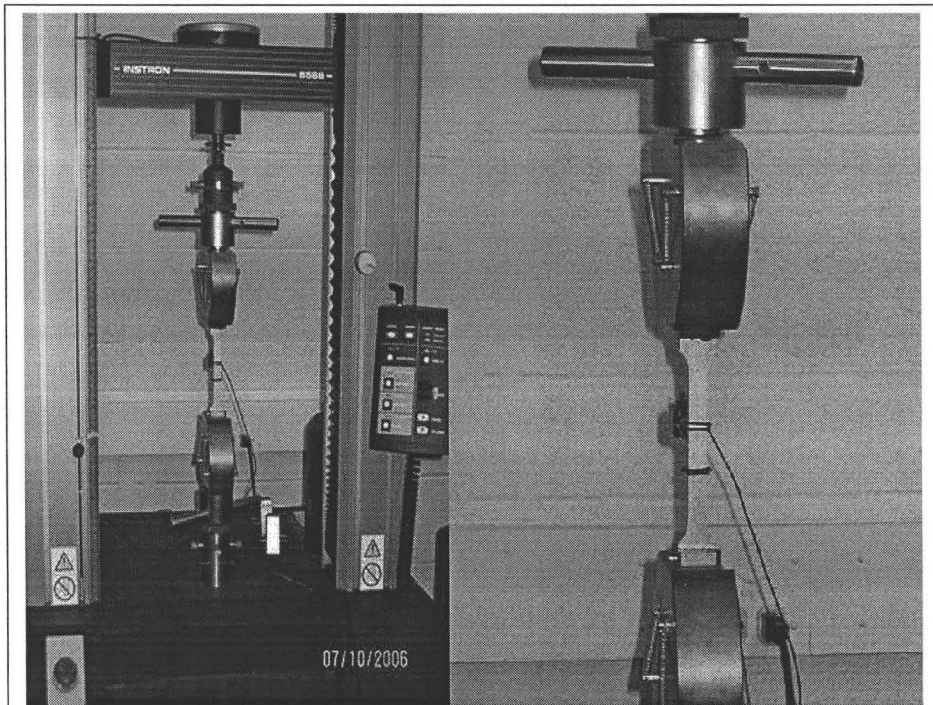


Figure A.2: Tensile coupons testing on INSTRON-5566 machine

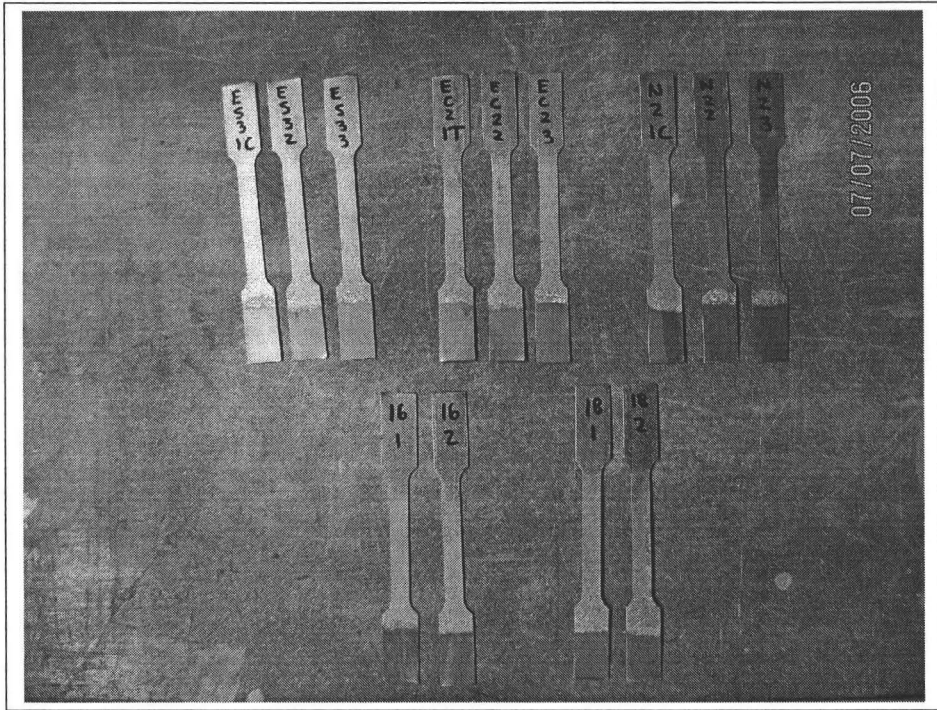


Figure A.3: Tensile coupons before testing

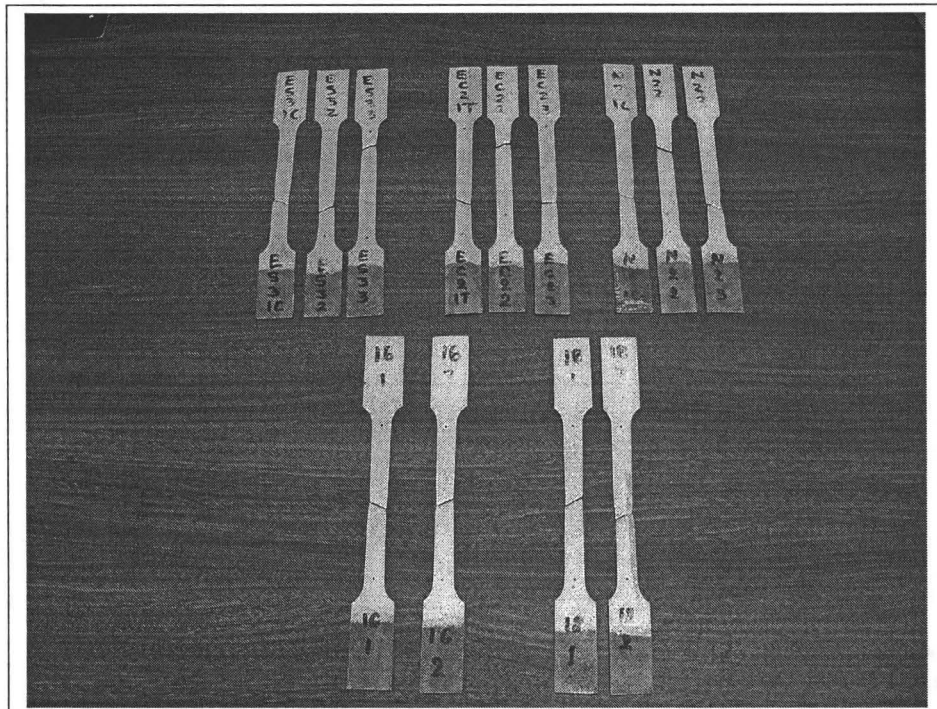
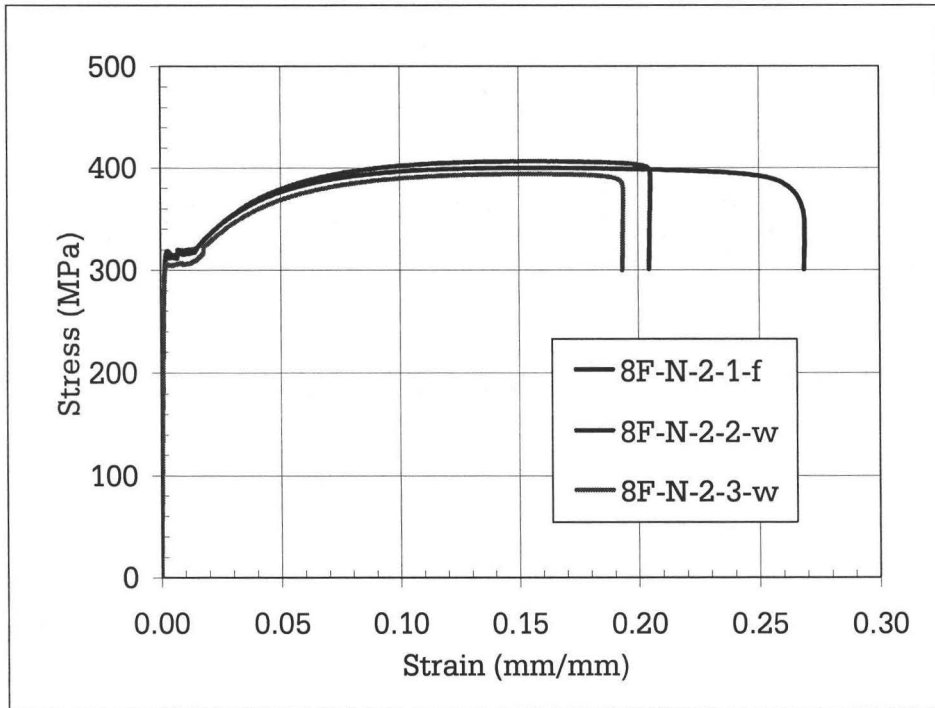
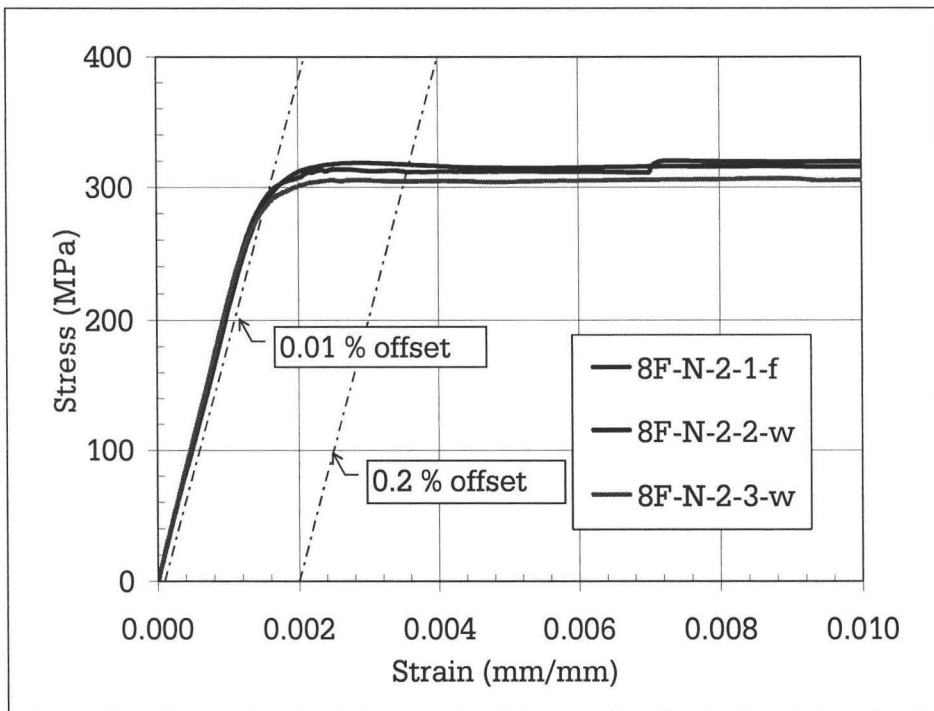


Figure A.4: Tensile coupons after testing

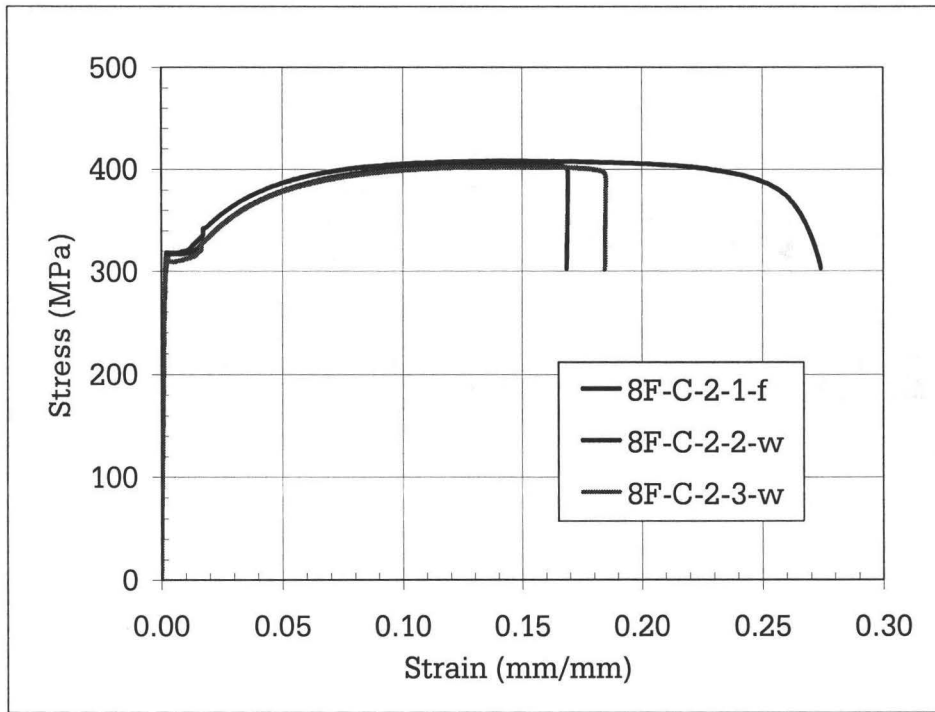


(a)

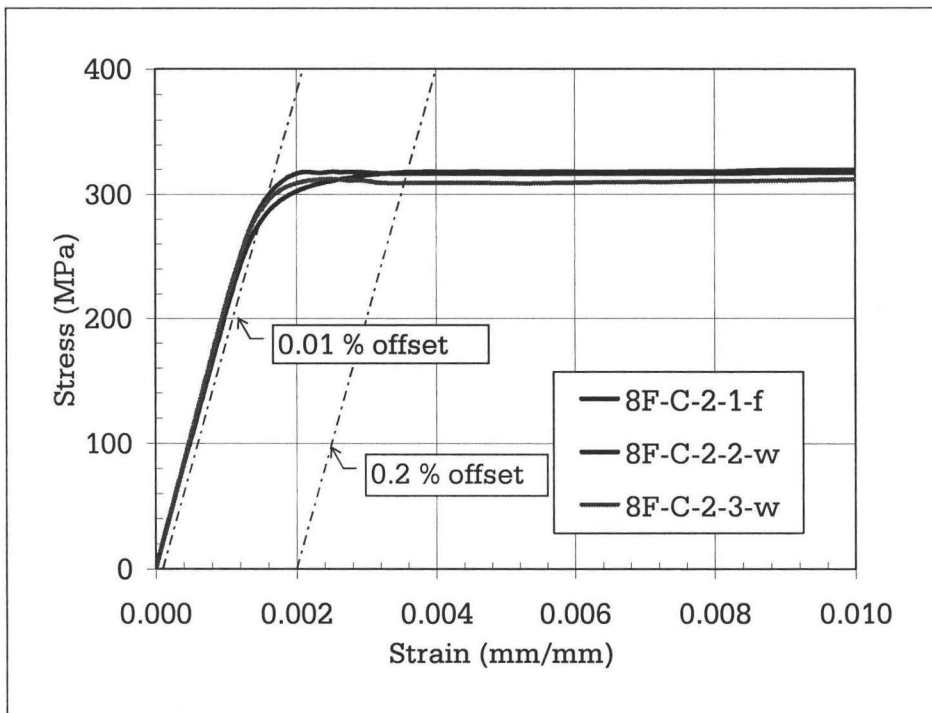


(b)

Figure A.5: Stress-strain relationships of tensile coupons for 43-mils thick section-1
(a) overall σ - ϵ relation (b) initial σ - ϵ relation

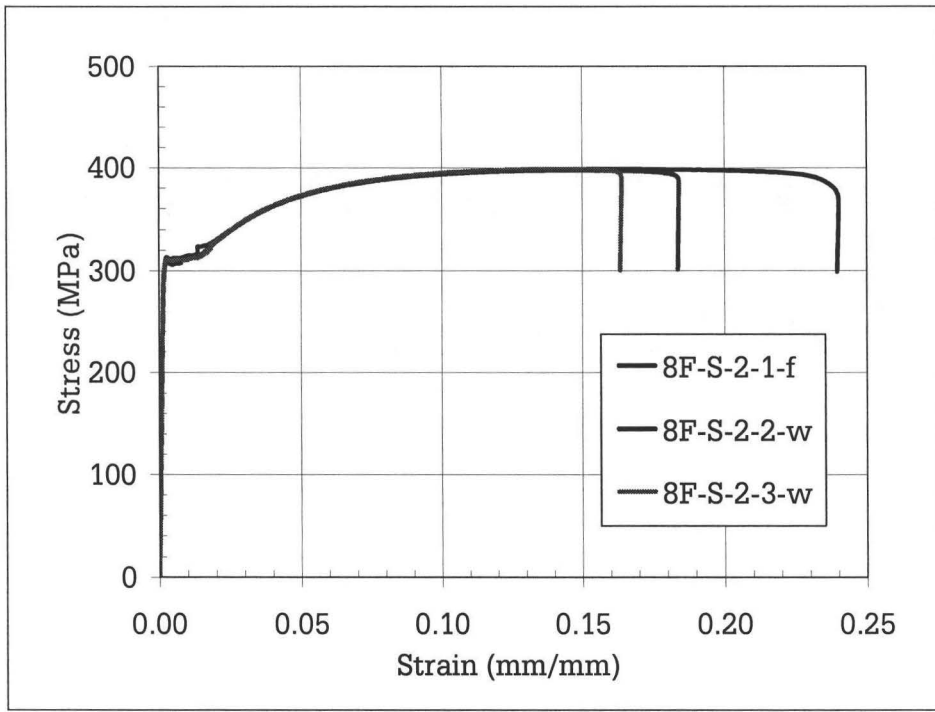


(a)

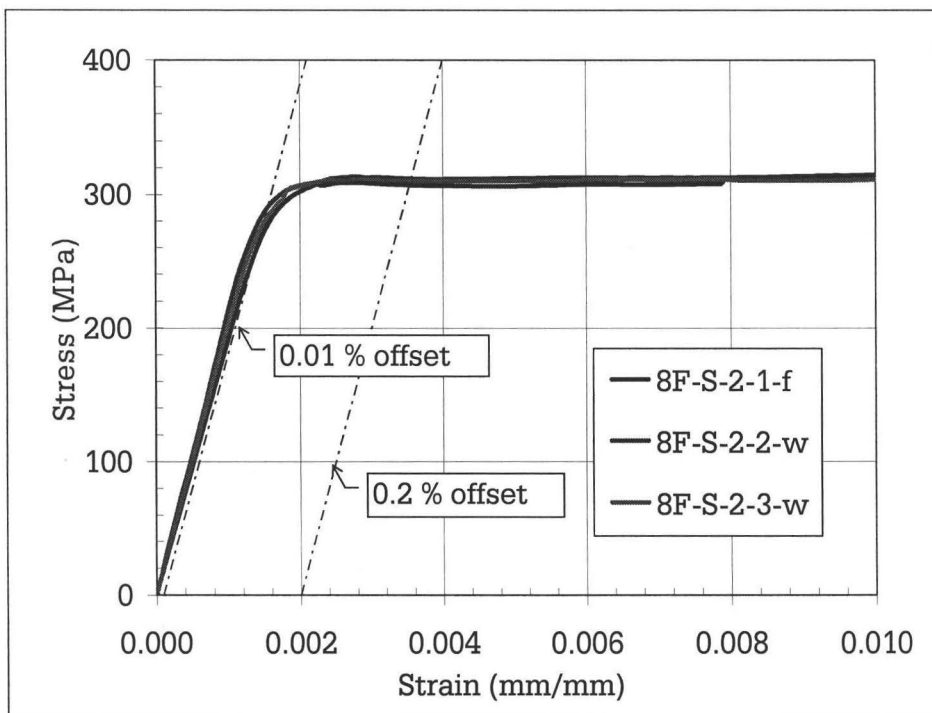


(b)

Figure A.6: Stress-strain relationships of tensile coupons for 43-mils thick section-2
(a) overall σ - ϵ relation (b) initial σ - ϵ relation

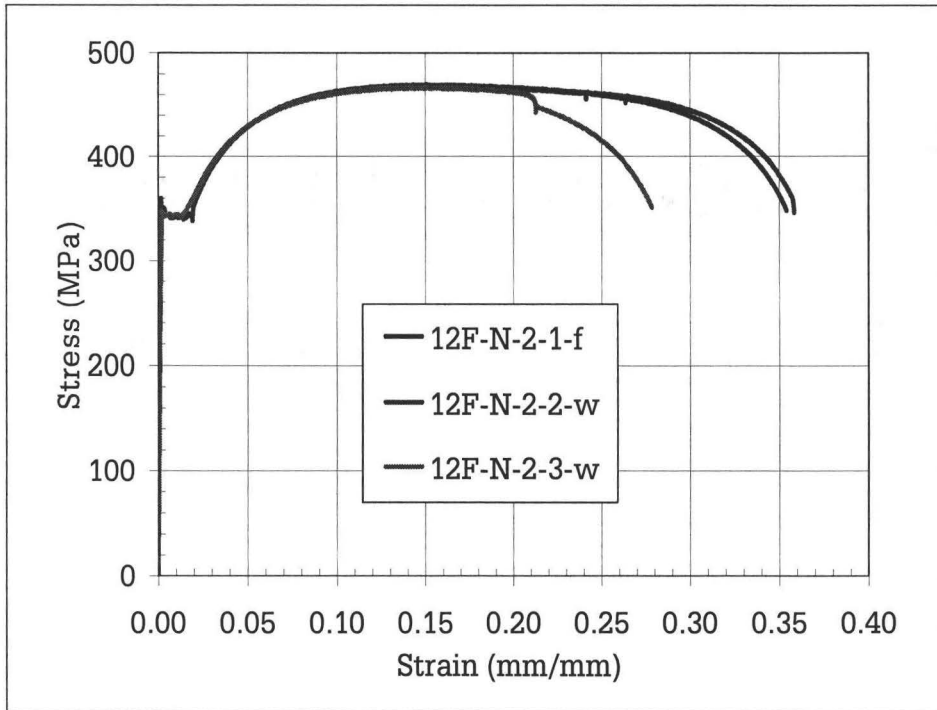


(a)

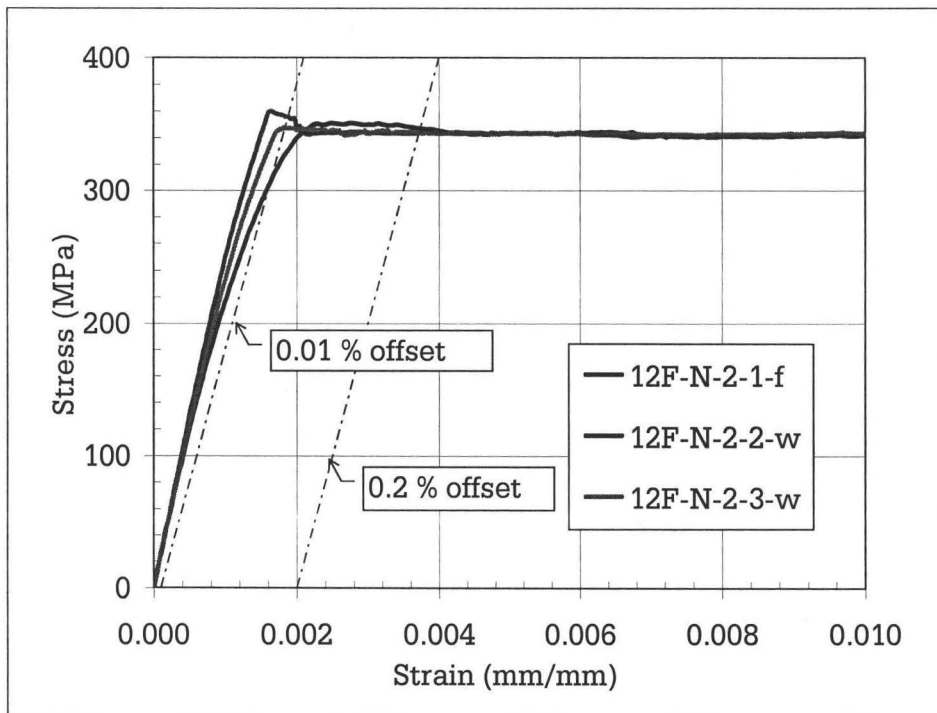


(b)

Figure A.7: Stress-strain relationships of tensile coupons for 43-mils thick section-3
(a) overall σ - ϵ relation (b) initial σ - ϵ relation

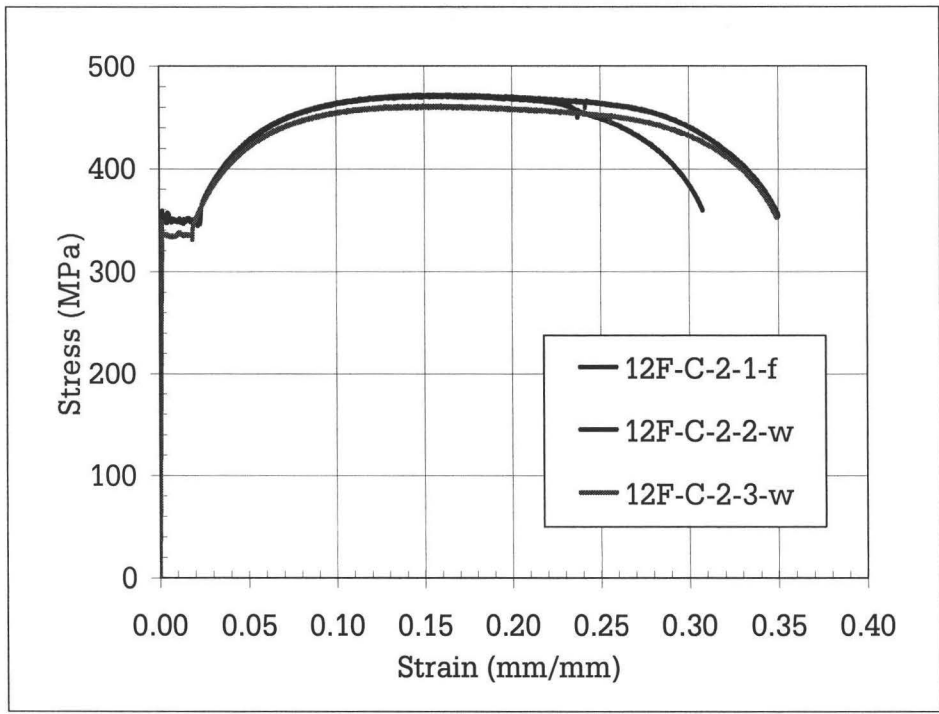


(a)

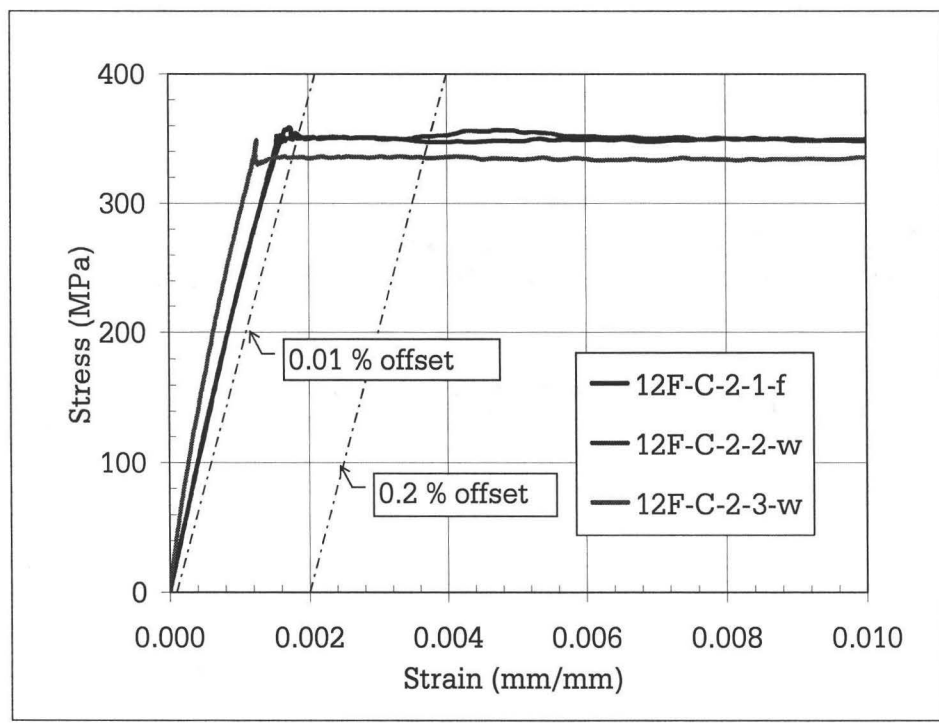


(b)

Figure A.8: Stress-strain relationships of tensile coupons for 97-mils thick section-1
(a) overall σ - ϵ relation (b) initial σ - ϵ relation

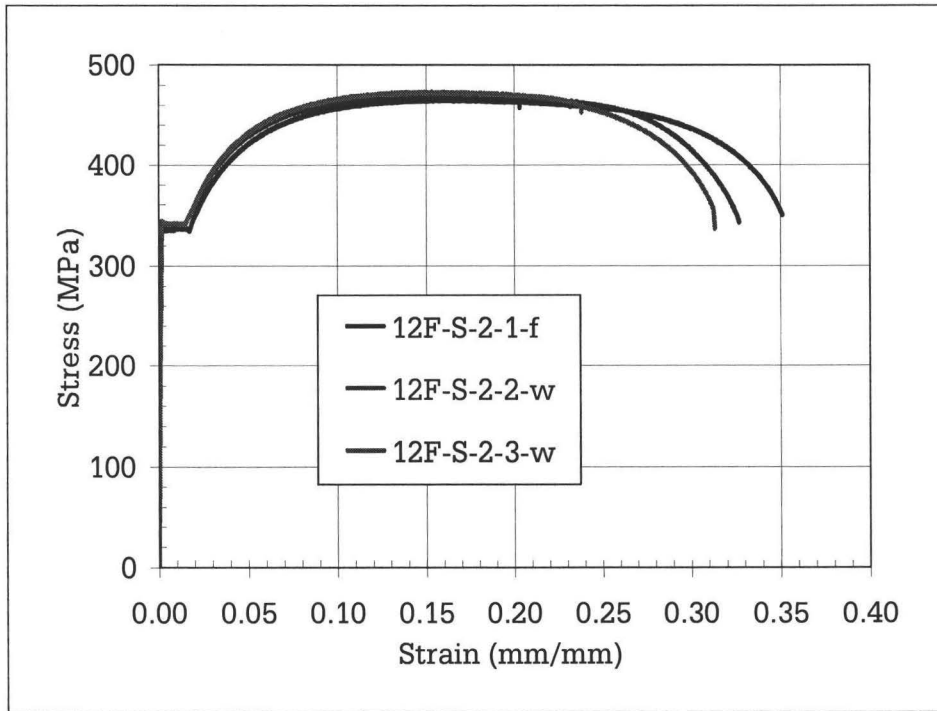


(a)

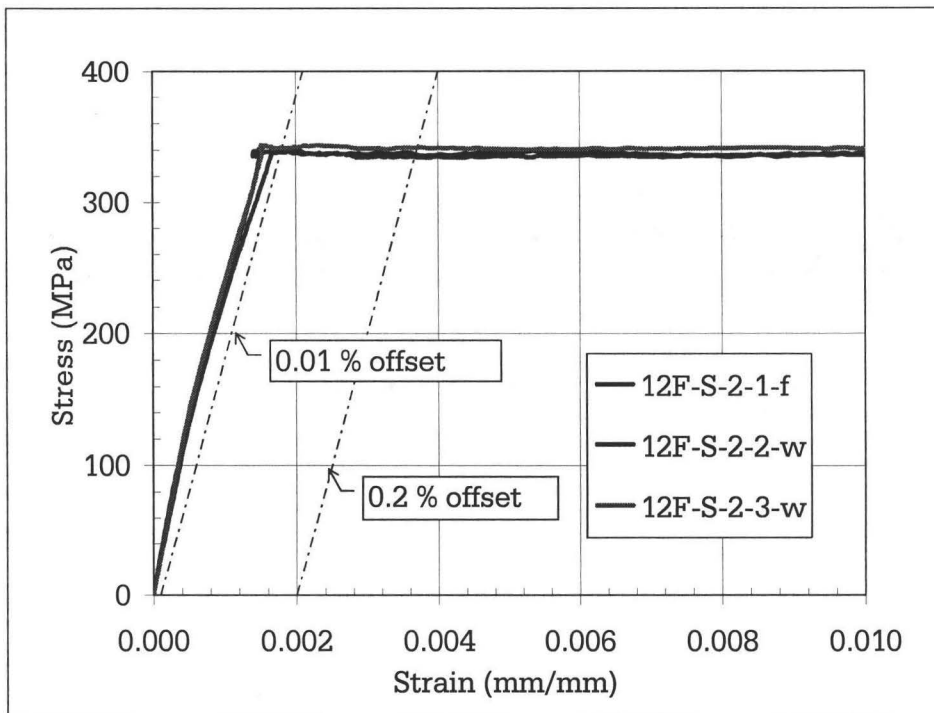


(b)

Figure A.9: Stress-strain relationships of tensile coupons for 97-mils thick section-2 (a) overall σ - ϵ relation (b) initial σ - ϵ relation



(a)



(b)

Figure A.10: Stress-strain relationships of tensile coupons for 97-mils thick section-3
(a) overall σ - ϵ relation (b) initial σ - ϵ relation

Appendix B

Cold-Formed Steel Joists with Large Web Openings Flexural Tests: Section 800S162-43

B.1 General

A total of twenty three cold-formed steel (CFS) joists having w/t ratio 180 were subjected to flexural tests, which established the moment resistances of such joists having unreinforced web openings, and having reinforced web openings. This part considered 203.2 mm (8 inch) deep, 1.092 mm (43 mils) thick [800S162-43] joists.

B.2 Flexural Tests: Solid Sections, Circular Openings and Square Openings

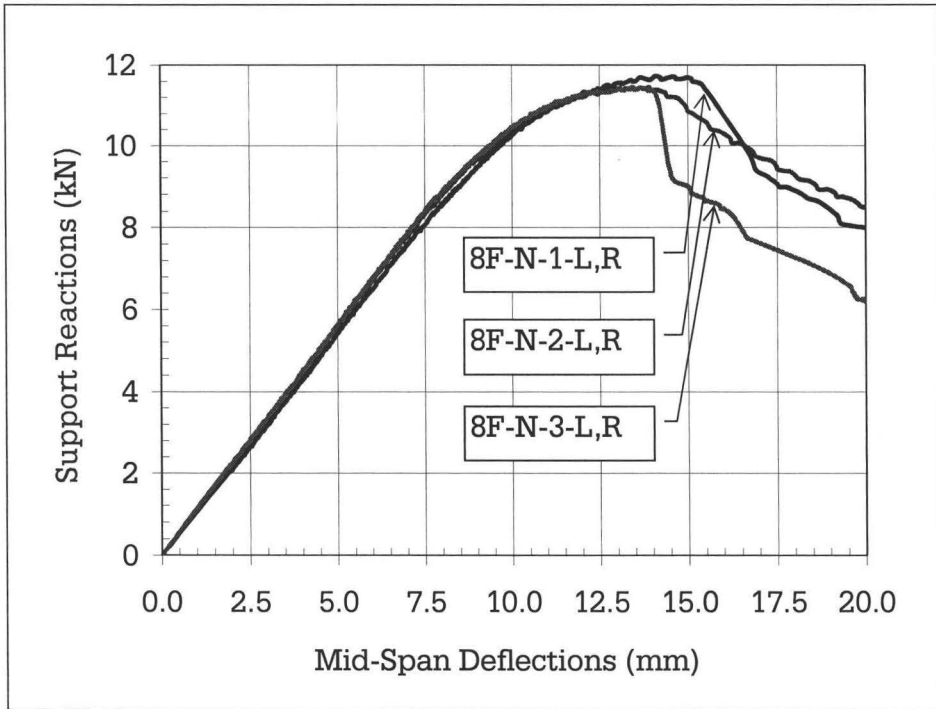
The first part of the investigation considered the flexural resistance of (a) joists with no openings, (b) joists with circular openings and (c) joists with square openings. Three identical tests were done for each case, thus, this part included nine tests. The load-displacement relations and sample photographs of failed specimens are given in Figures B.1 through B.3.

B.3 Flexural Tests: Reinforced Circular Openings (Schemes-A, B and C)

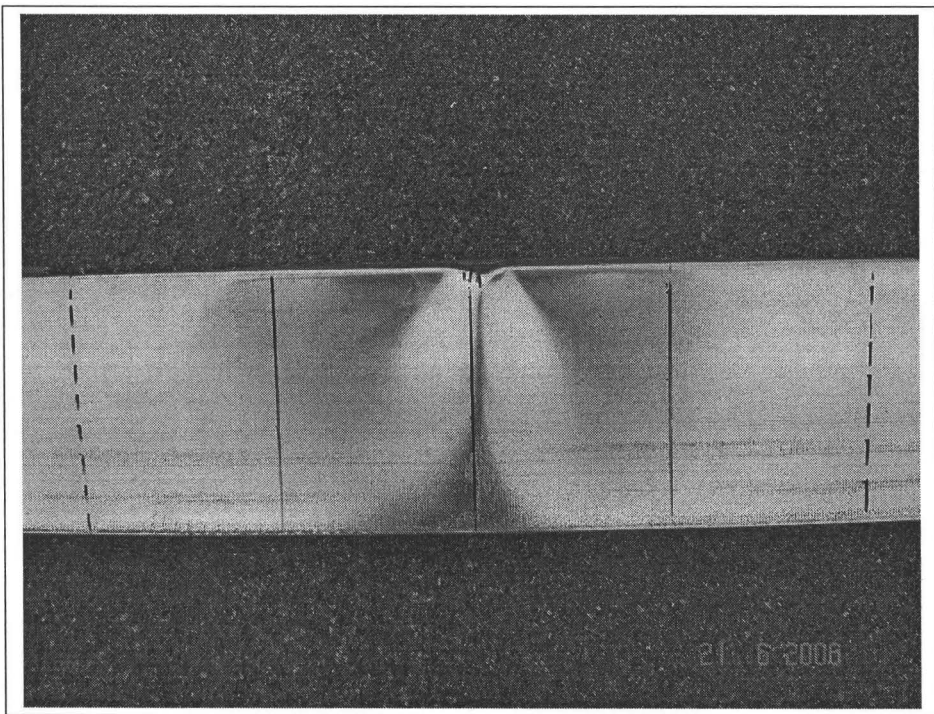
The second part of the investigation includes five tests, which considered the flexural resistance of joists with reinforced circular openings. Three different reinforcement schemes were considered; (a) Scheme A: solid steel plate of 1.09 mm (43 mils) thick, (b) Scheme B: joist section [203.2 mm (8 inch) deep and 1.092 mm (43 mils) thick], and (c) Scheme C: 1.09 mm (43 mils) thick bridging channels along the top and bottom edges of the openings. The load-displacement relations and sample photographs of failed specimens are given in Figures B.4 through B.6.

B.4 Flexural Tests: Reinforced Square Openings (Schemes- A, B and C)

This part of the investigation considered the joists with reinforced square openings. Three different reinforcement schemes, similar to the circular openings (previous section) were considered. The load-displacement relations associated with the nine tests and sample photographs of failed specimens are given in Figures B.7 through B.9.

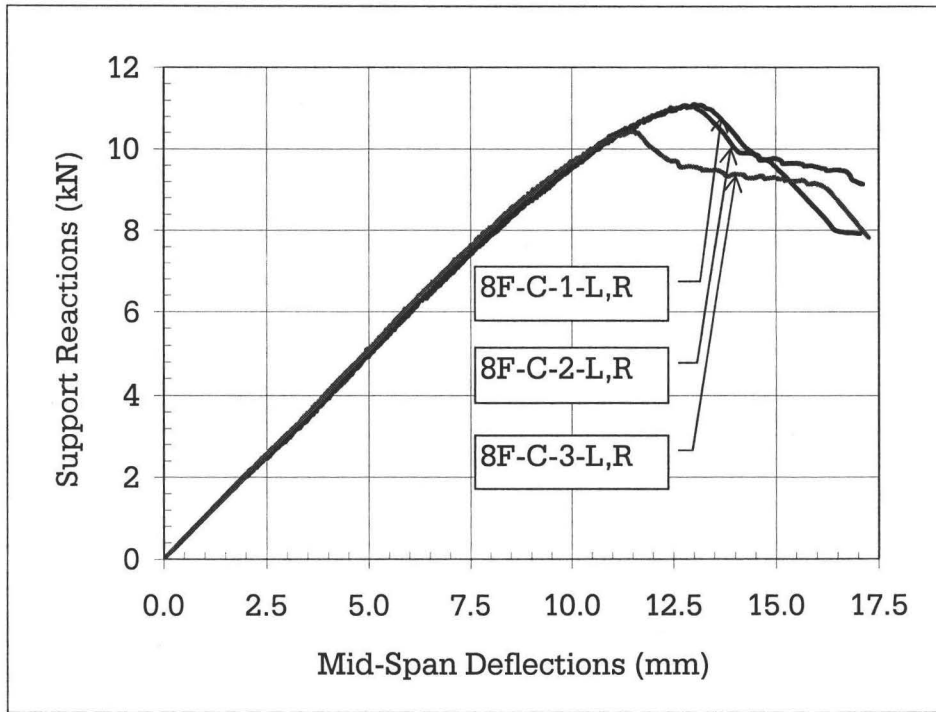


(a)

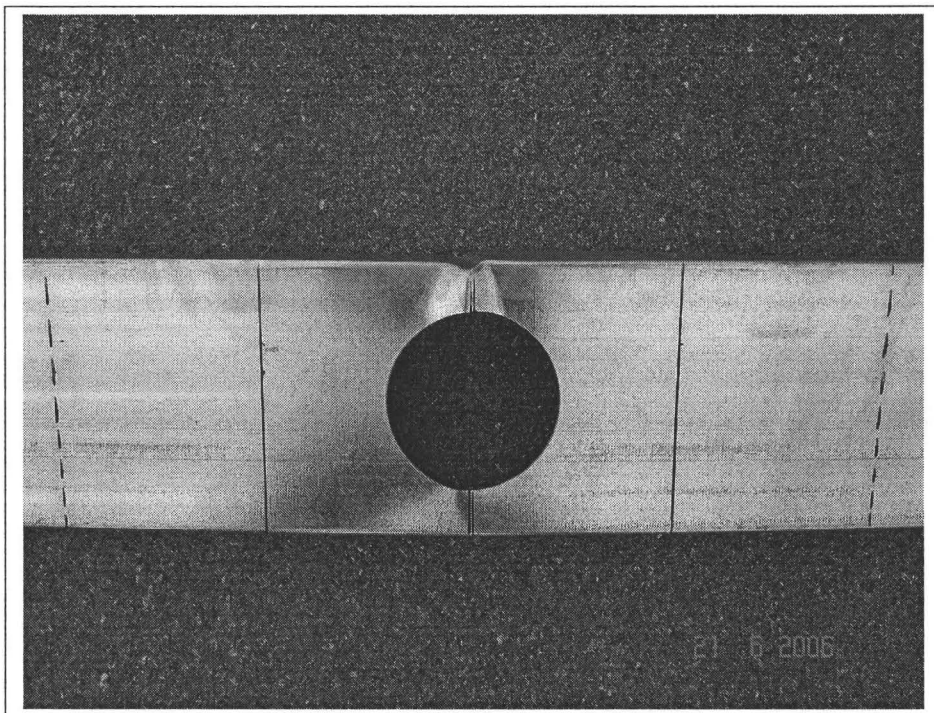


(b)

Figure B.1: Test results for solid specimens (a) load-displacement relations (b) typical flexural failure

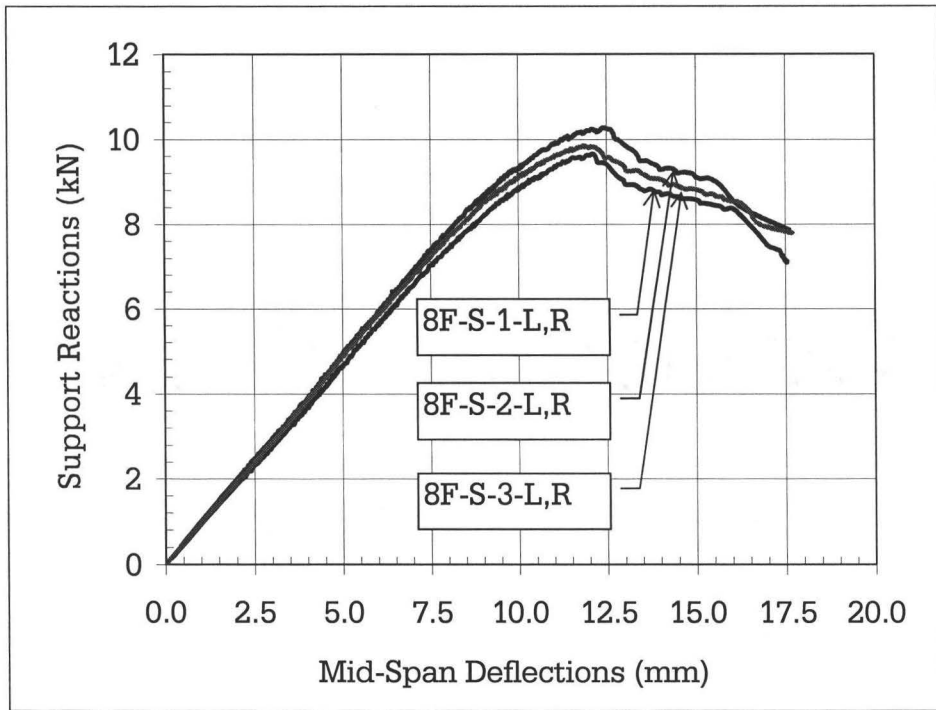


(a)

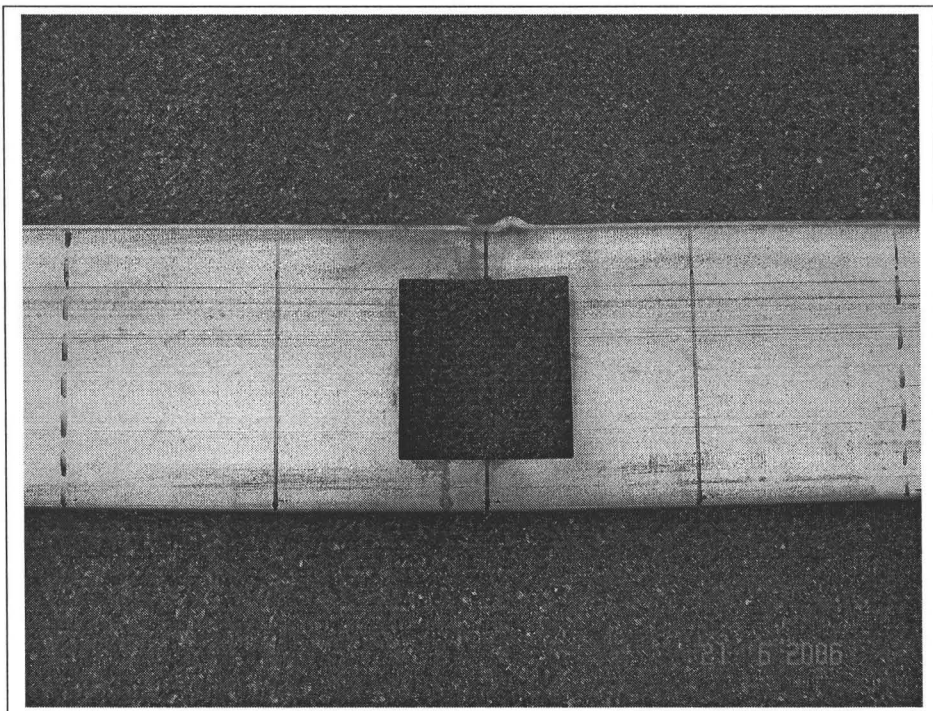


(b)

Figure B.2: Test results for specimens having circular web openings (a) load-displacement relations (b) typical flexural failure

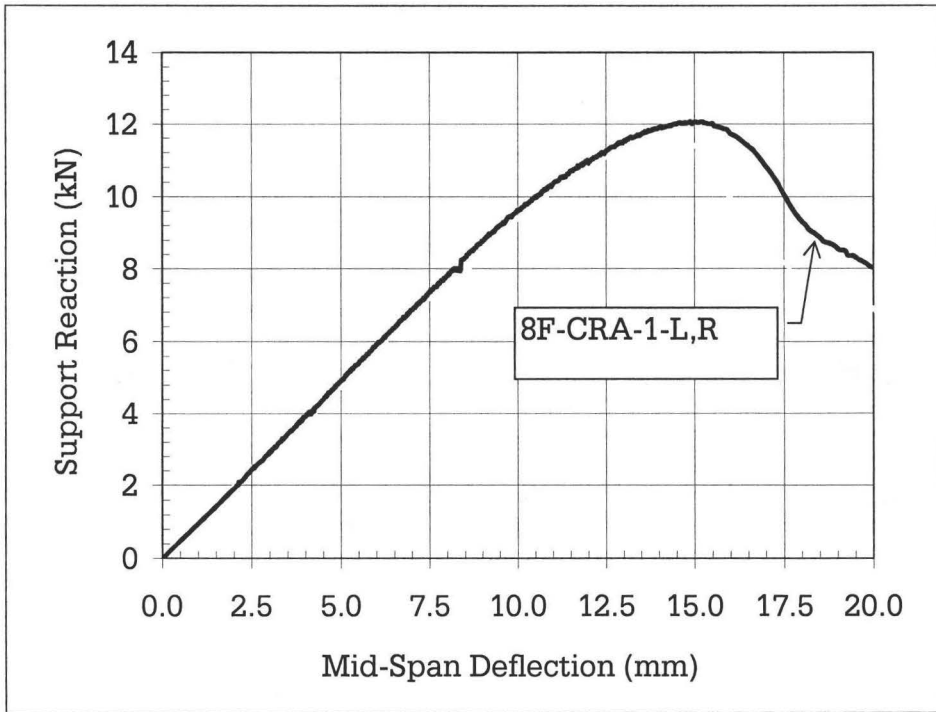


(a)

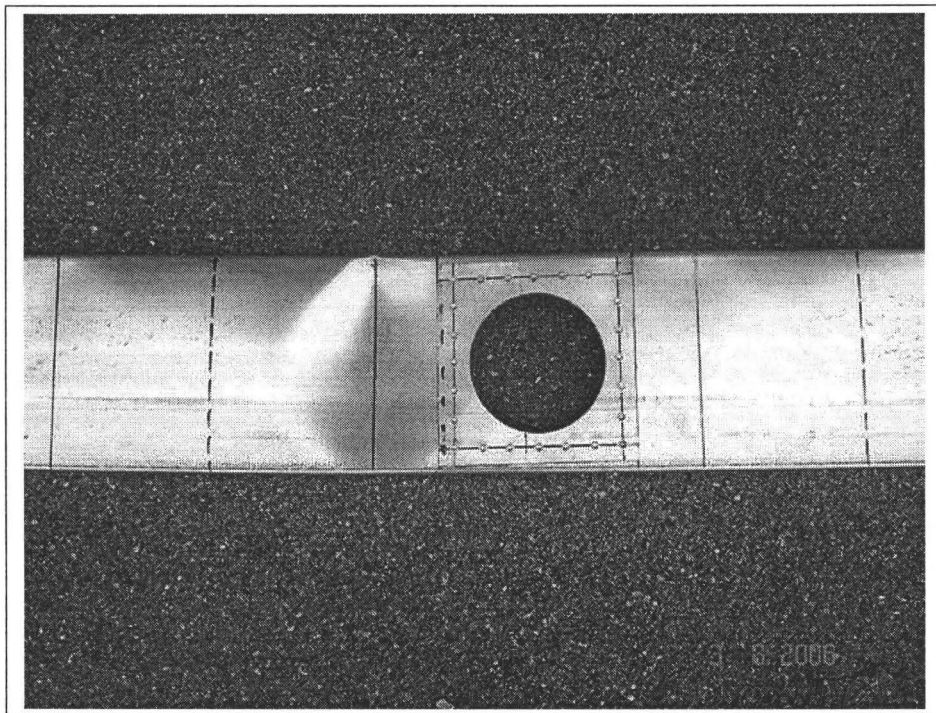


(b)

Figure B.3: Test results for specimens having square web openings (a) load-displacement relations (b) typical flexural failure

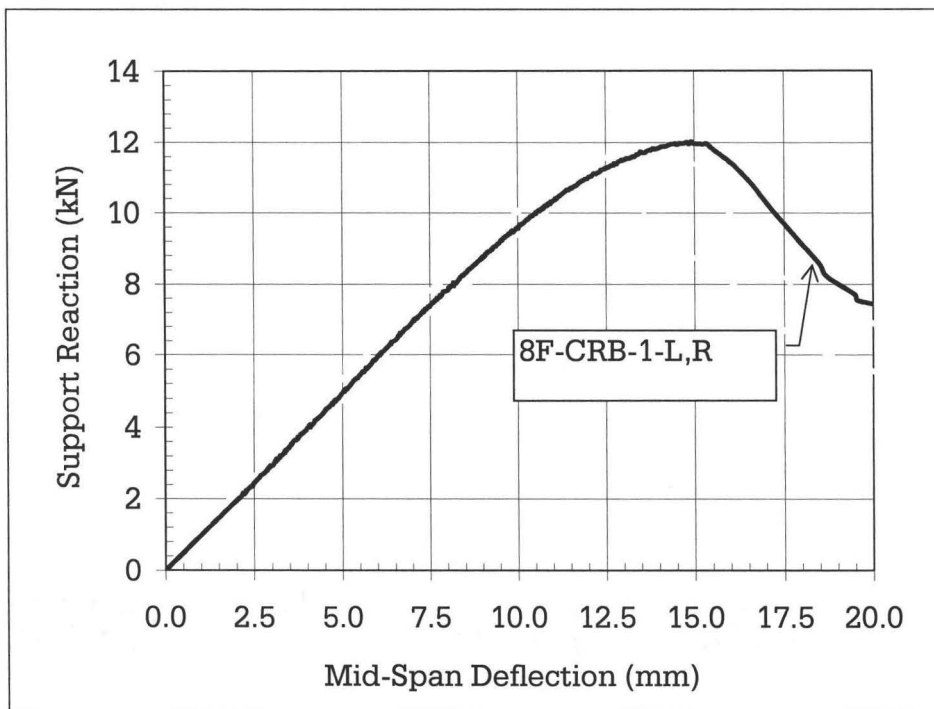


(a)

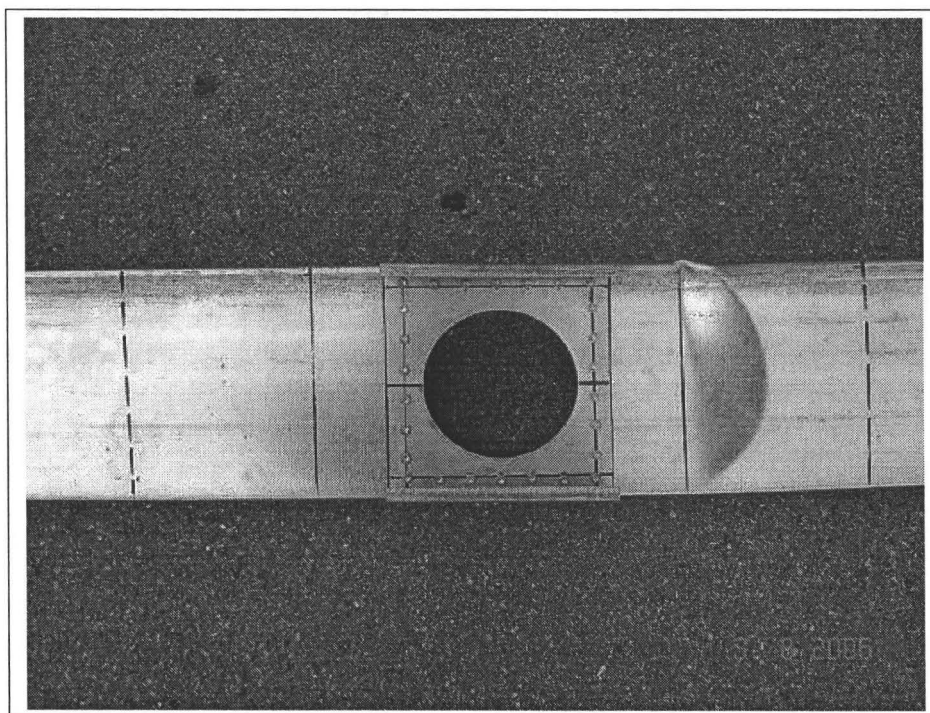


(b)

Figure B.4: Test results for specimens having reinforced (Scheme-A) circular web openings (a) load-displacement relations (b) typical flexural failure

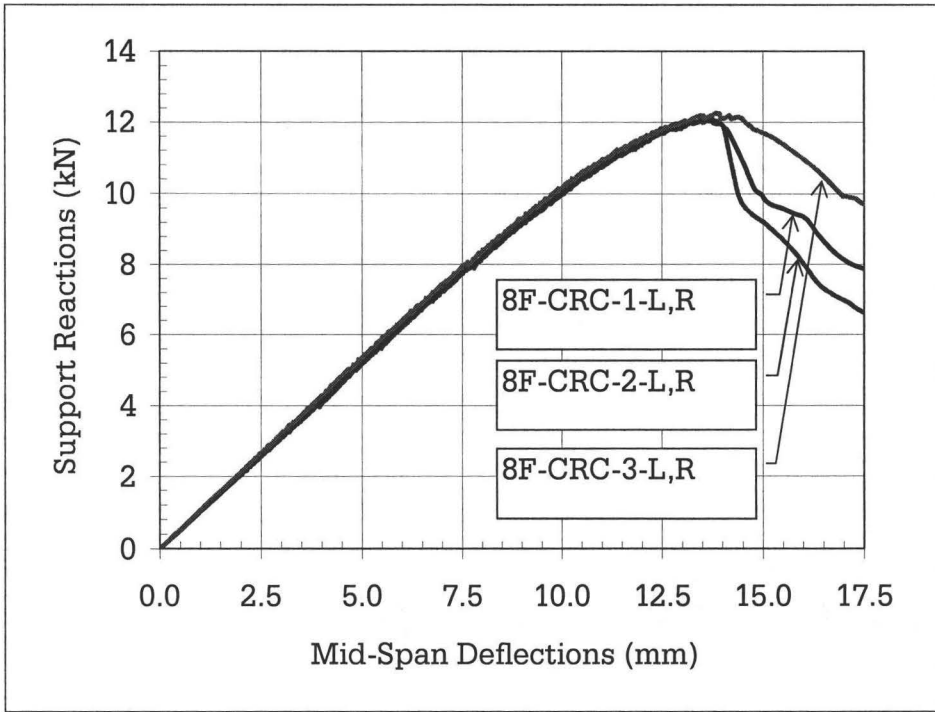


(a)

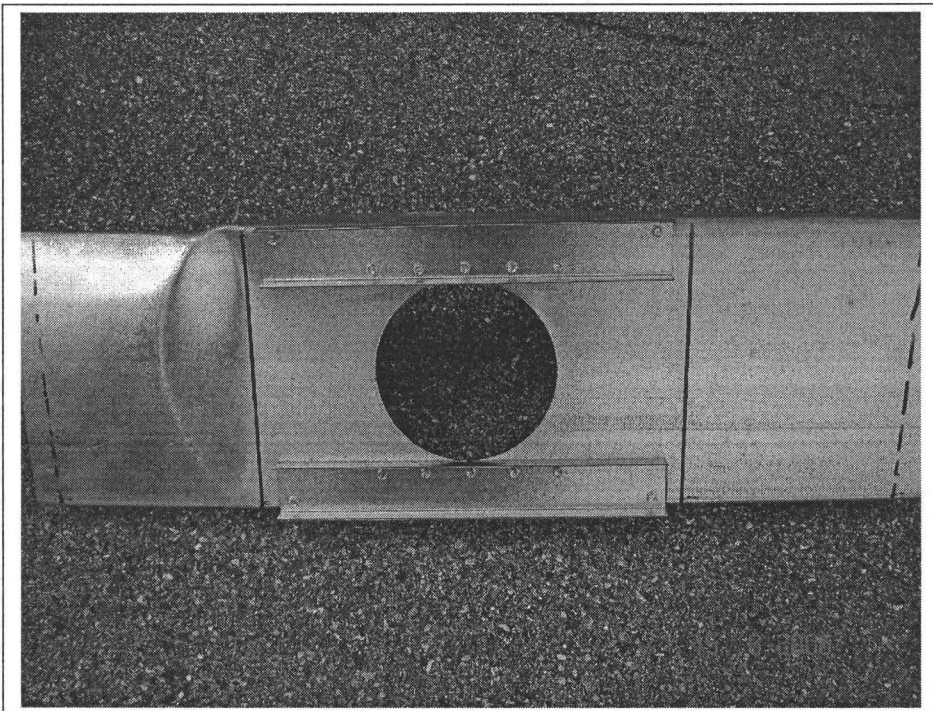


(b)

Figure B.5: Test results for specimens having reinforced (Scheme-B) circular web openings (a) load-displacement relations (b) typical flexural failure

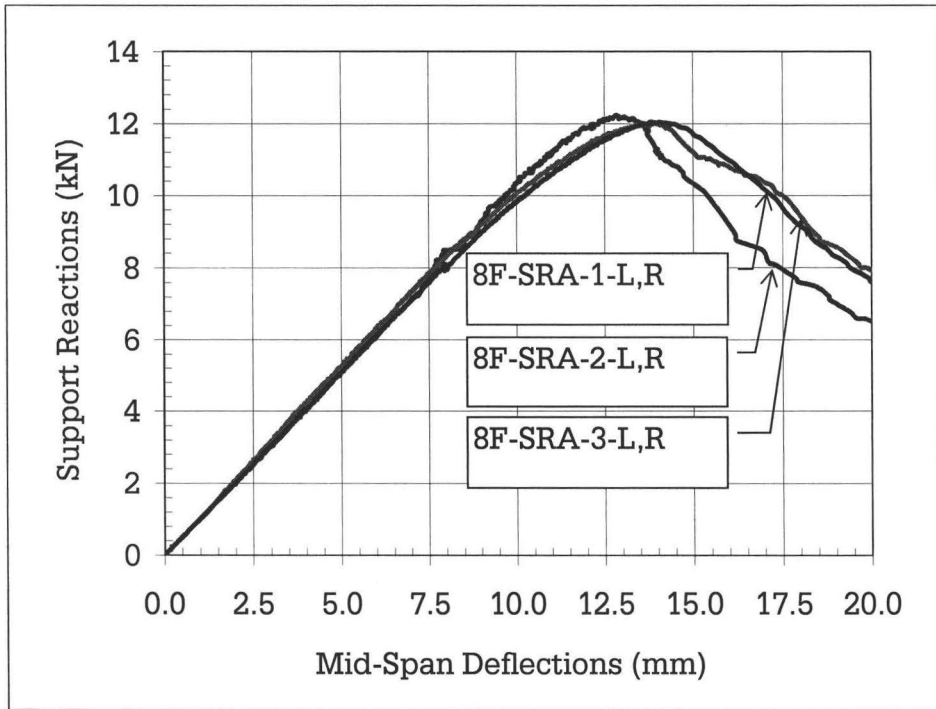


(a)

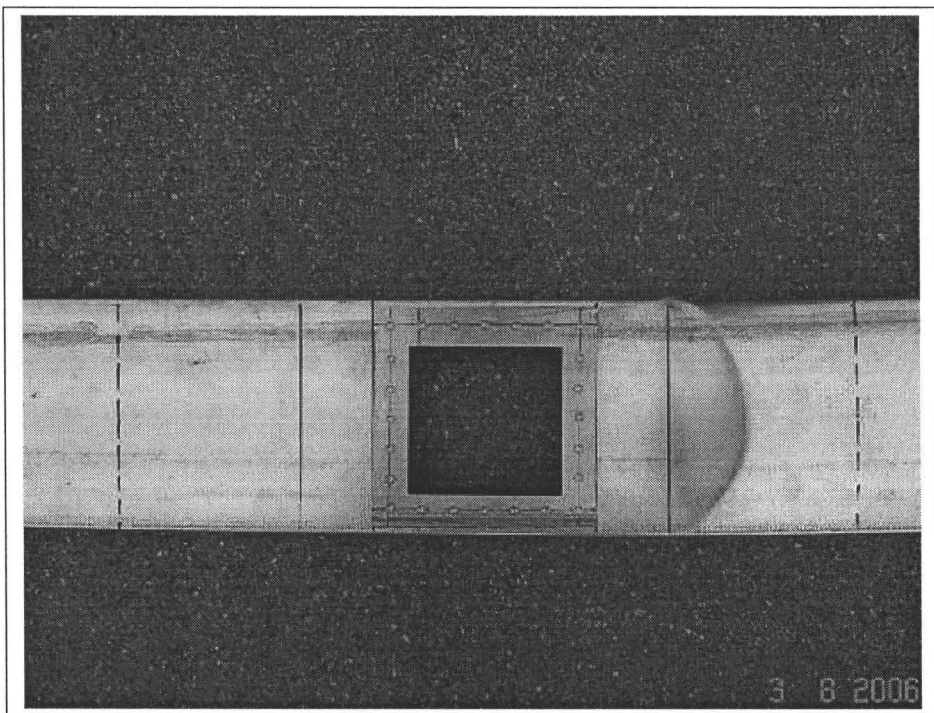


(b)

Figure B.6: Test results for specimens having reinforced (Scheme-C) circular web openings (a) load-displacement relations (b) typical flexural failure

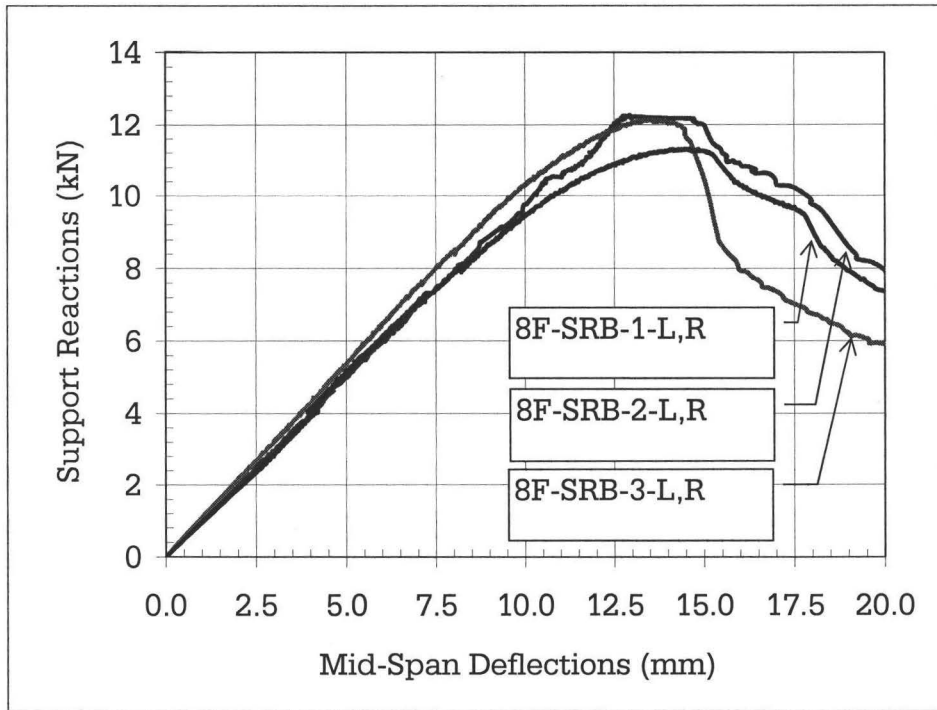


(a)

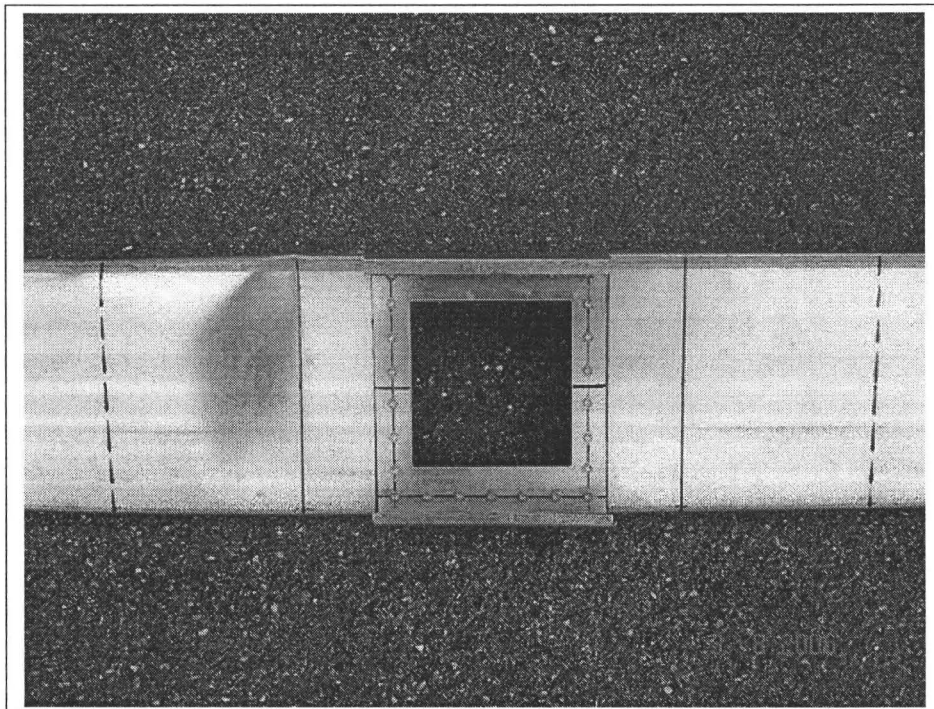


(b)

Figure B.7: Test results for specimens having reinforced (Scheme-A) square web openings (a) load-displacement relations (b) typical flexural failure

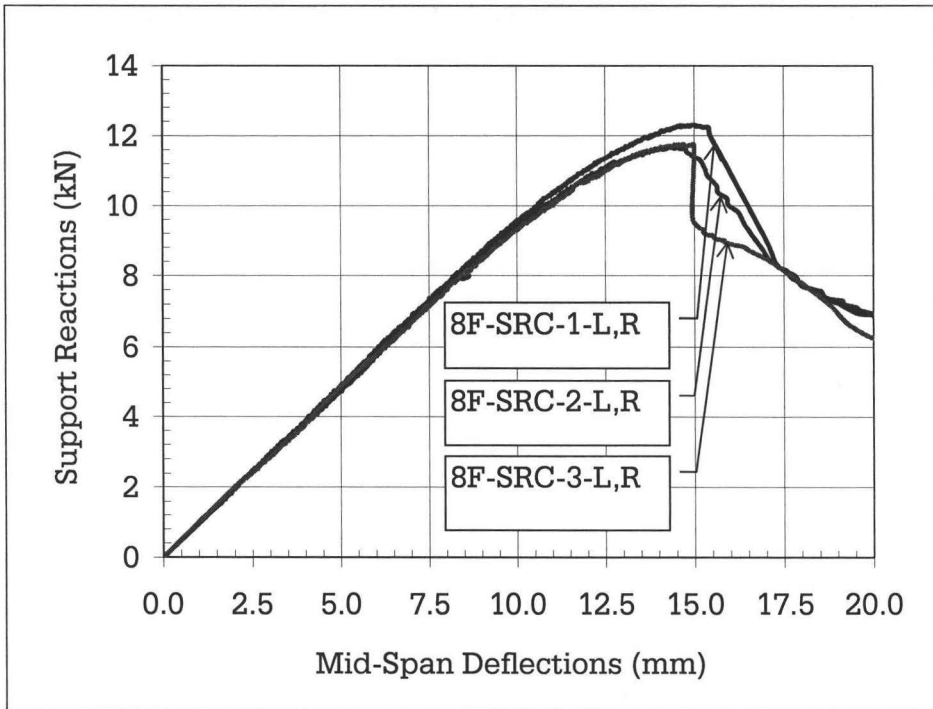


(a)

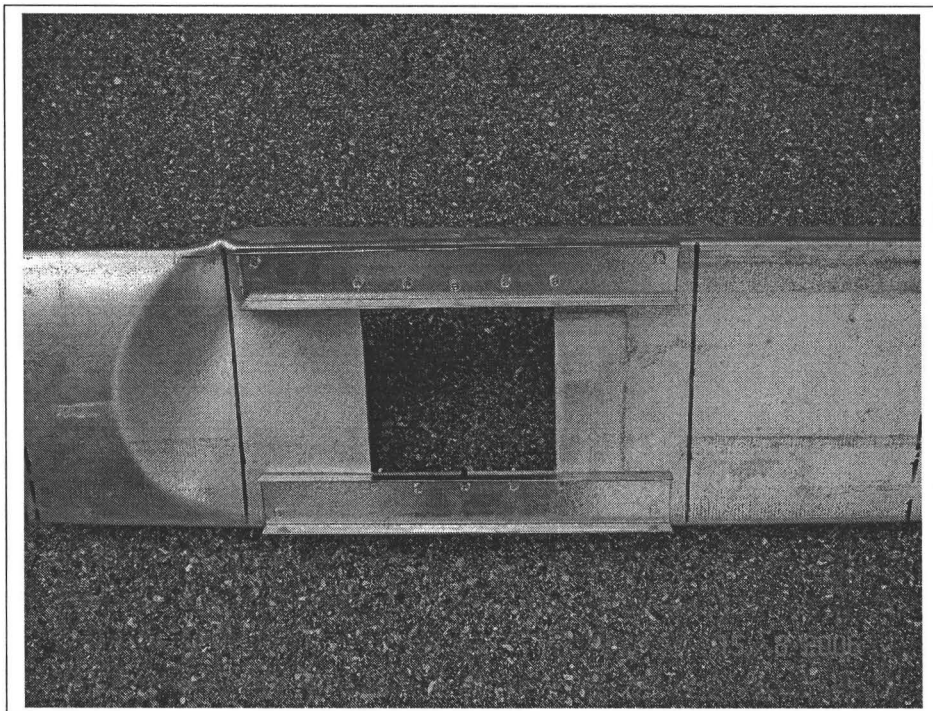


(b)

Figure B.8: Test results for specimens having reinforced (Scheme-B) square web openings (a) load-displacement relations (b) typical flexural failure



(a)



(b)

Figure B.9: Test results for specimens having reinforced (Scheme-C) square web openings (a) load-displacement relations (b) typical flexural failure

Appendix C

Cold-Formed Steel Joists with Large Web Openings Flexural Tests: Section 1200S162-97

C.1 General

A total of nineteen cold-formed steel (CFS) joists having w/t ratio 118 were subjected to flexural tests, which established the moment resistances of such joists having unreinforced web openings, and having reinforced web openings. This part considered 304.8 mm (12 inch) deep, 2.46 mm (97 mils) thick [1200S162-97] joists.

C.2 Flexural Tests: Solid Sections, Circular Openings and Square Openings

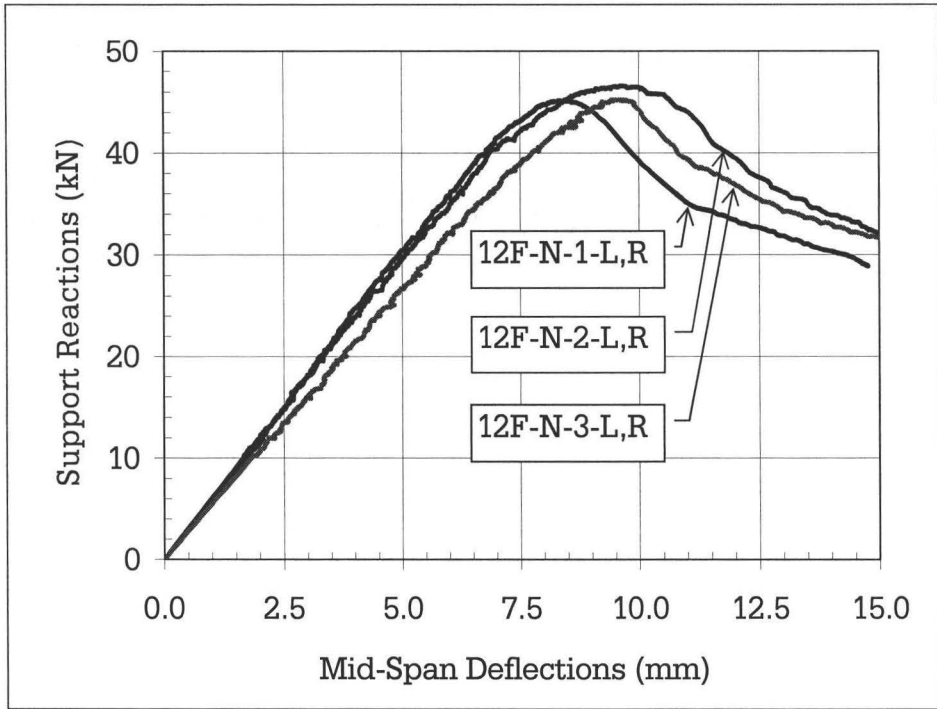
The first part of the investigation considered the flexural resistance of (a) joists with no openings, (b) joists with circular openings and (c) joists with square openings. Three identical tests were done for each case, thus, this part included nine tests. The load-displacement relations and sample photographs of failed specimens are given in Figures C.1 through C.3.

C.3 Flexural Tests: Reinforced Circular Openings (Schemes-A, B and C)

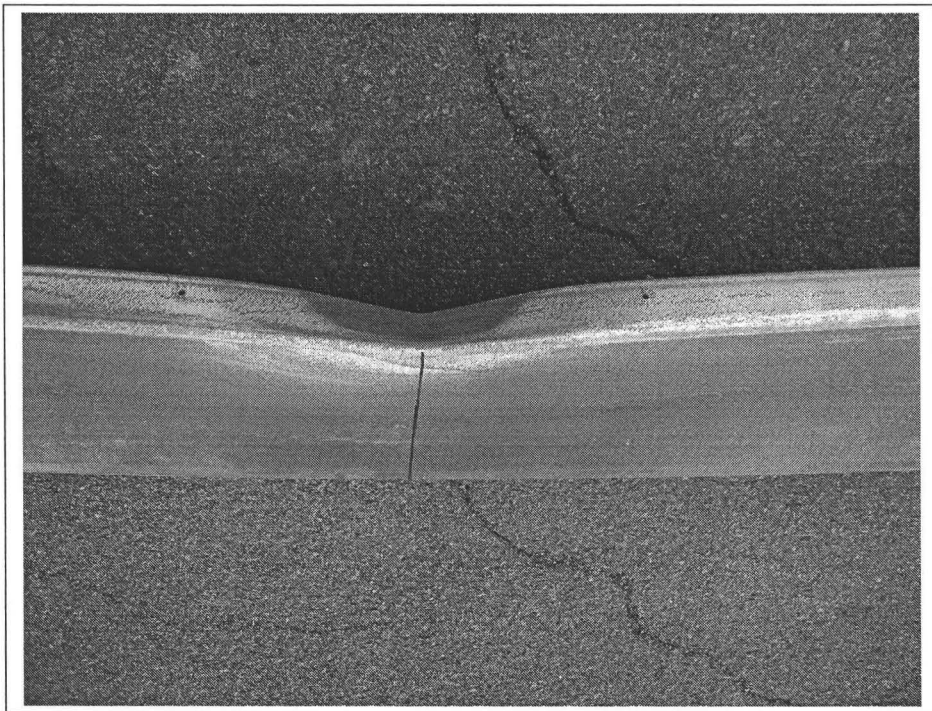
The second part of the investigation includes five tests, which considered the flexural resistance of joists with reinforced circular openings. Three different reinforcement schemes were considered; (a) Scheme A: solid steel plate of 2.46 mm (97 mils) thick, (b) Scheme A: joist section [304.8 mm (12 inch) deep and 2.46 mm (97 mils) thick], and (c) Scheme A: 2.46 mm (97 mils) thick bridging channels along the top and bottom edges of the openings. The load-displacement relations and sample photographs of failed specimens are given in Figures C.4 through C.6.

C.4 Flexural Tests: Reinforced Square Openings (Schemes-A, B and C)

This part of the investigation considered the joists with reinforced square openings. Three different reinforcement schemes, similar to the circular openings (previous section) were considered. The load-displacement relations associated with the five tests and sample photographs of failed specimens are given in Figures C.7 through C.9.

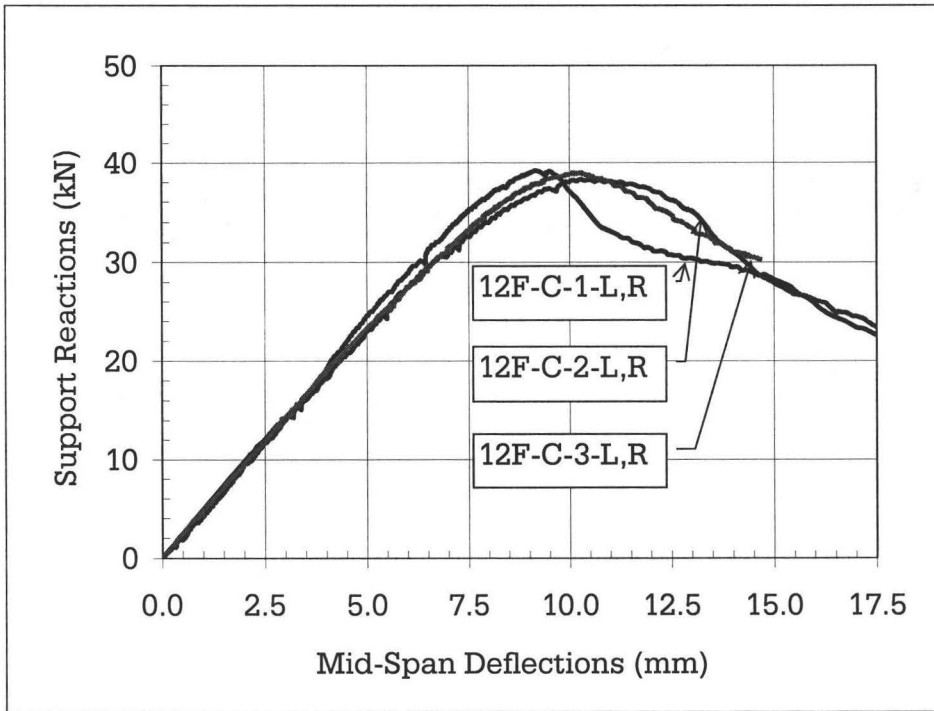


(a)

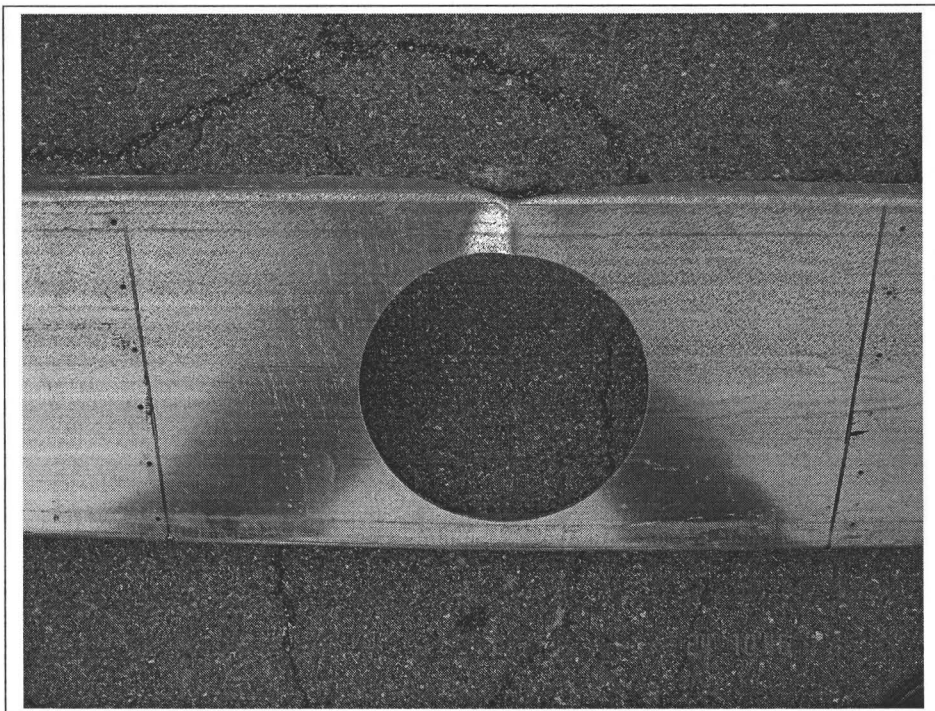


(b)

Figure C.1: Test results for solid specimens (a) load-displacement relations (b) typical flexural failure

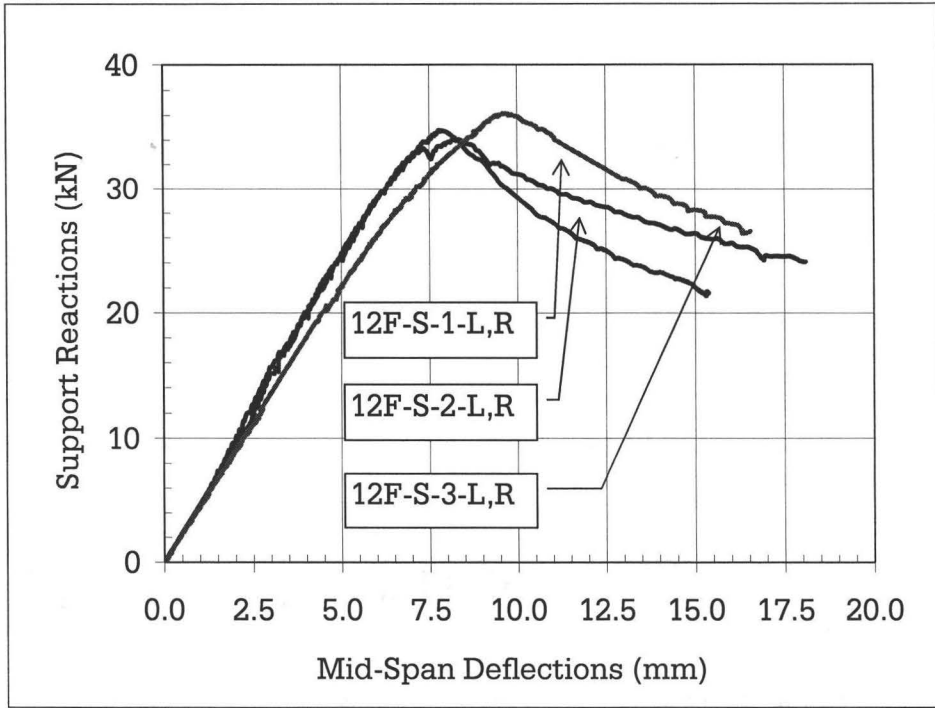


(a)

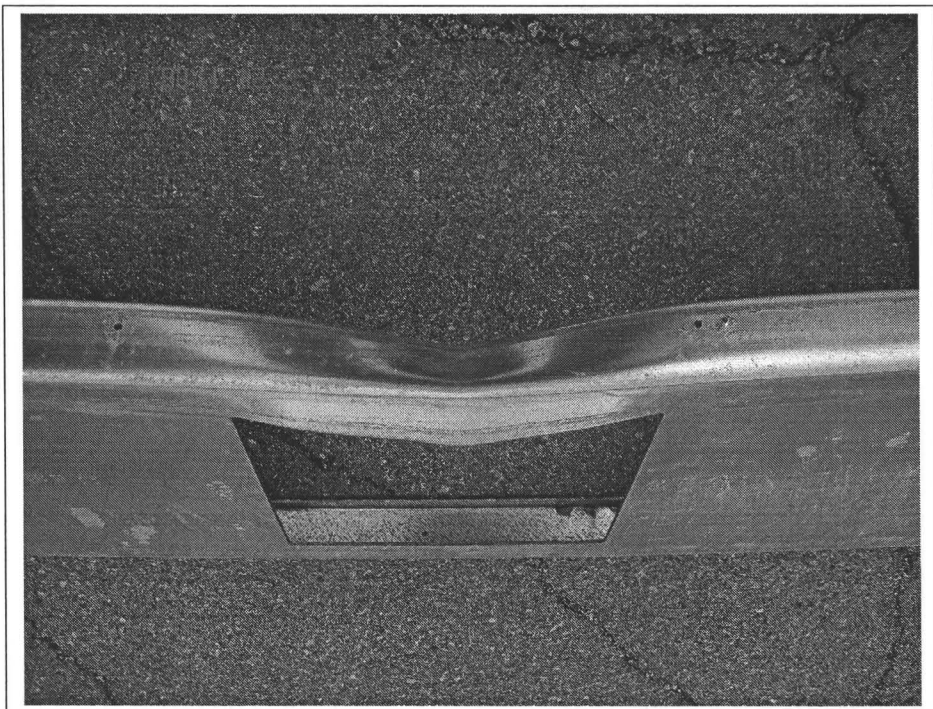


(b)

Figure C.2: Test results for specimens having circular web openings (a) load-displacement relations (b) typical flexural failure

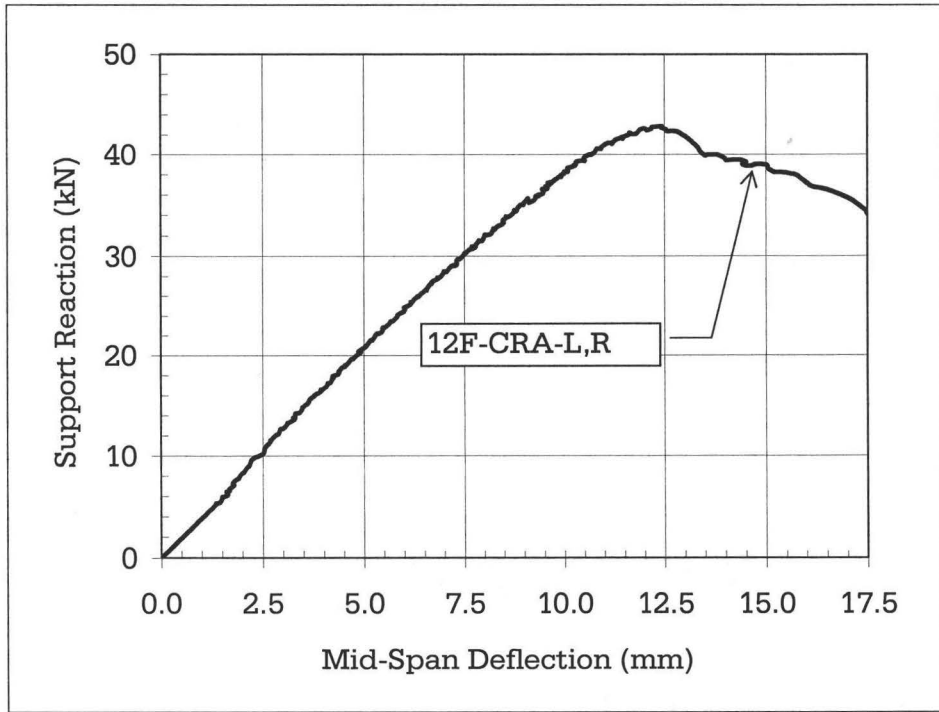


(a)

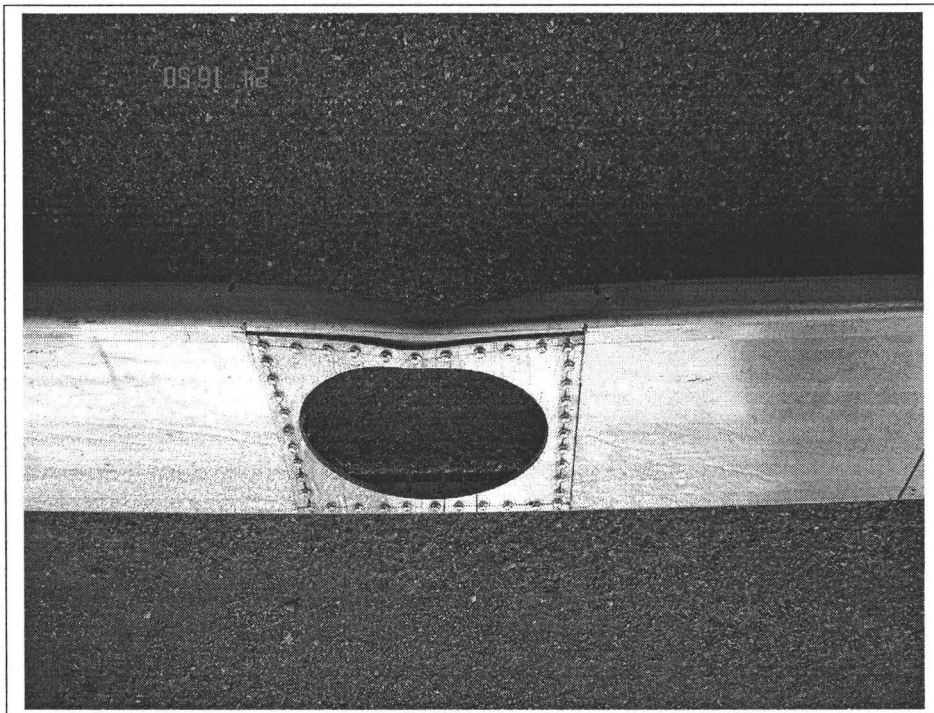


(b)

Figure C.3: Test results for specimens having square web openings (a) load-displacement relations (b) typical flexural failure

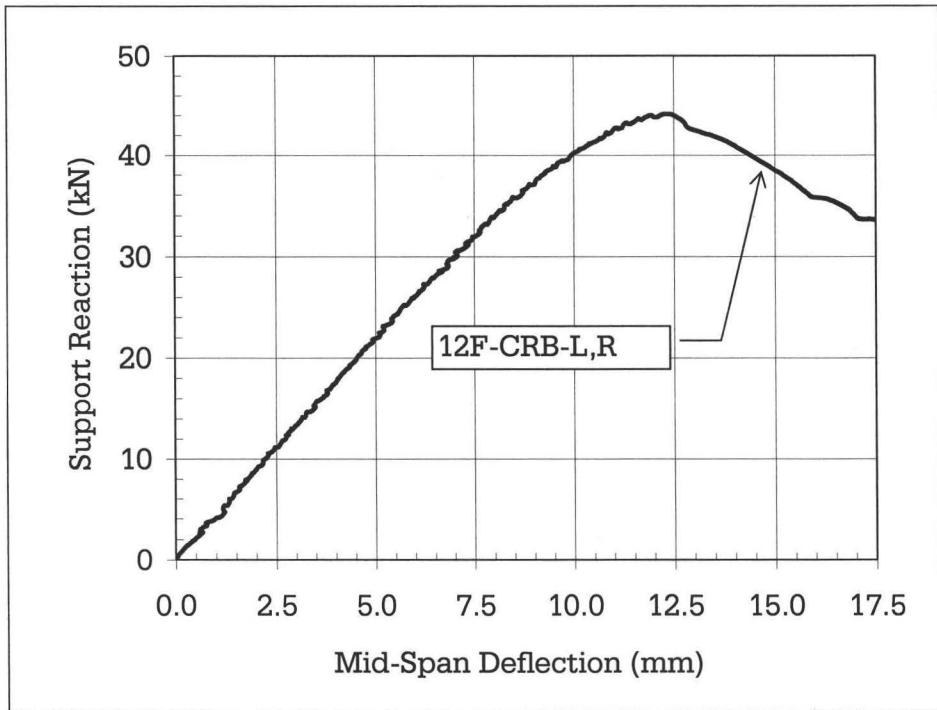


(a)

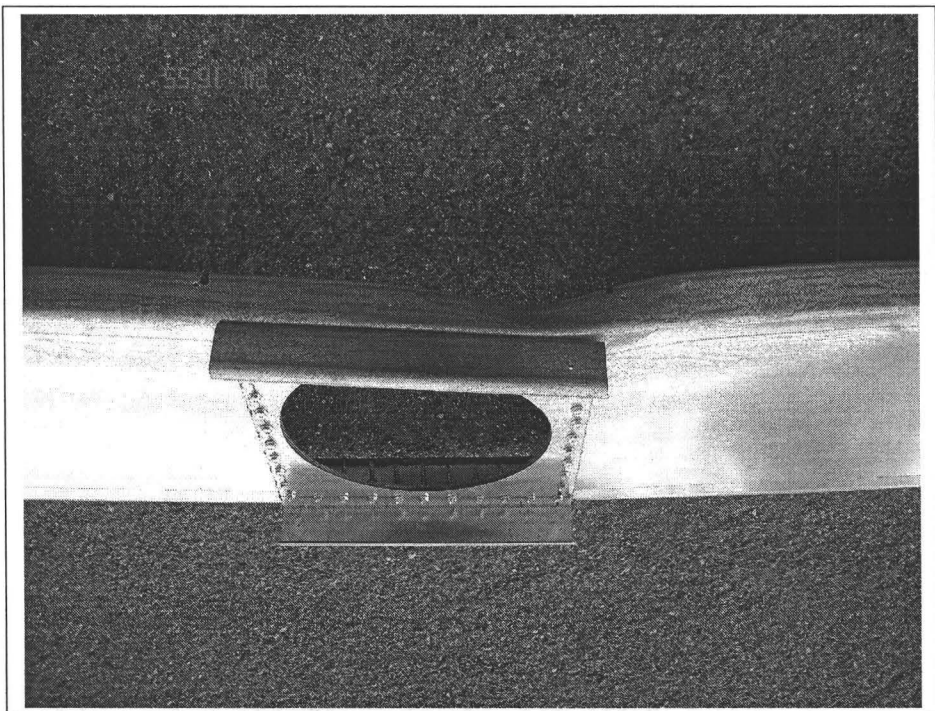


(b)

Figure C.4: Test results for specimens having reinforced (Scheme-A) circular web openings (a) load-displacement relations (b) typical flexural failure

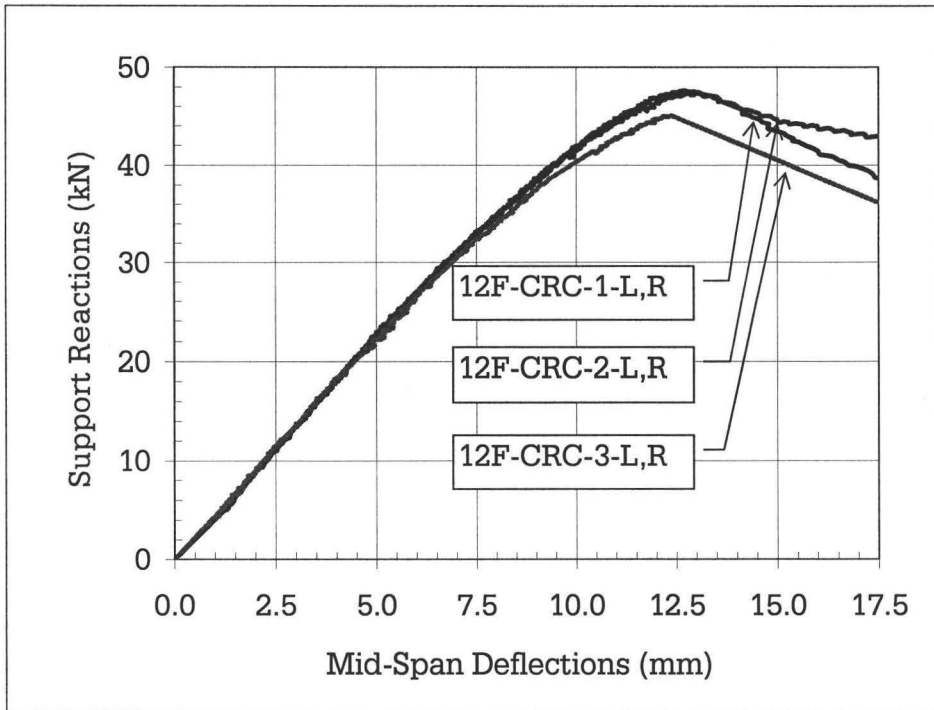


(a)

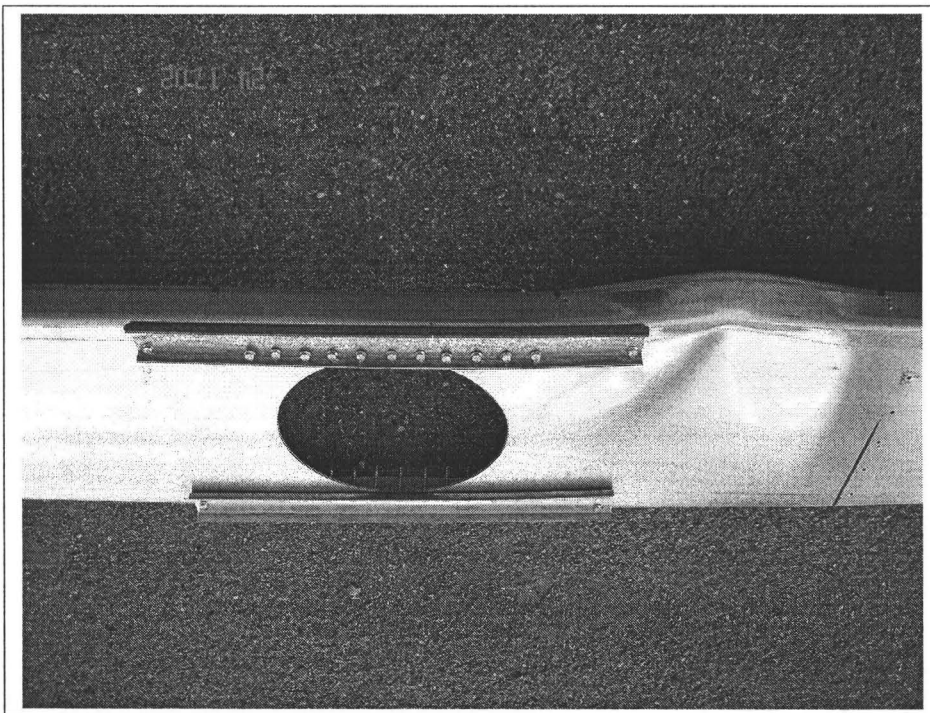


(b)

Figure C.5: Test results for specimens having reinforced (Scheme-B) circular web openings (a) load-displacement relations (b) typical flexural failure

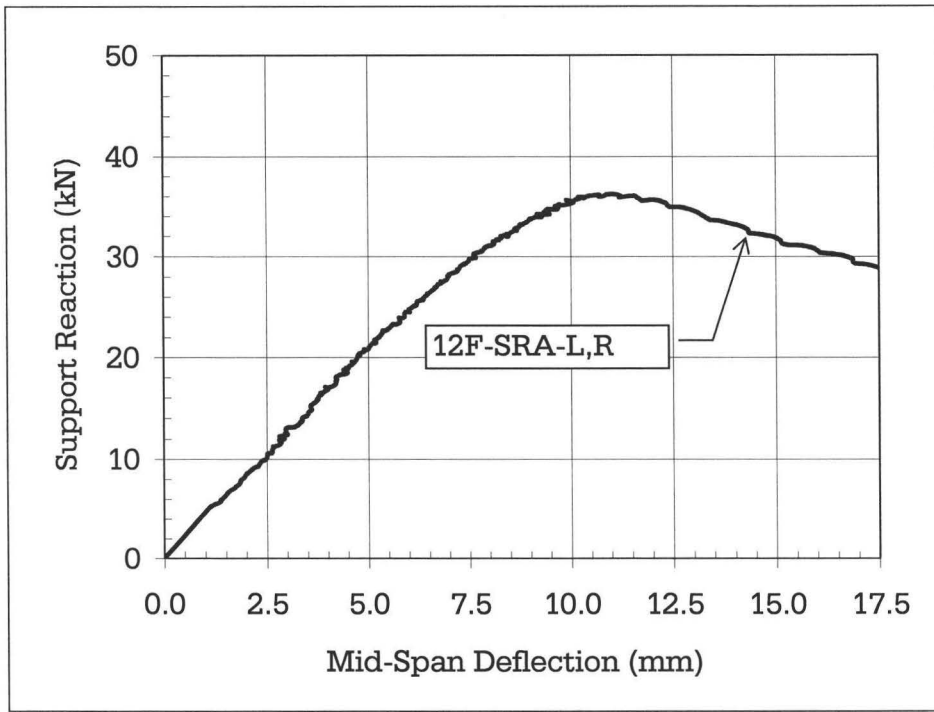


(a)

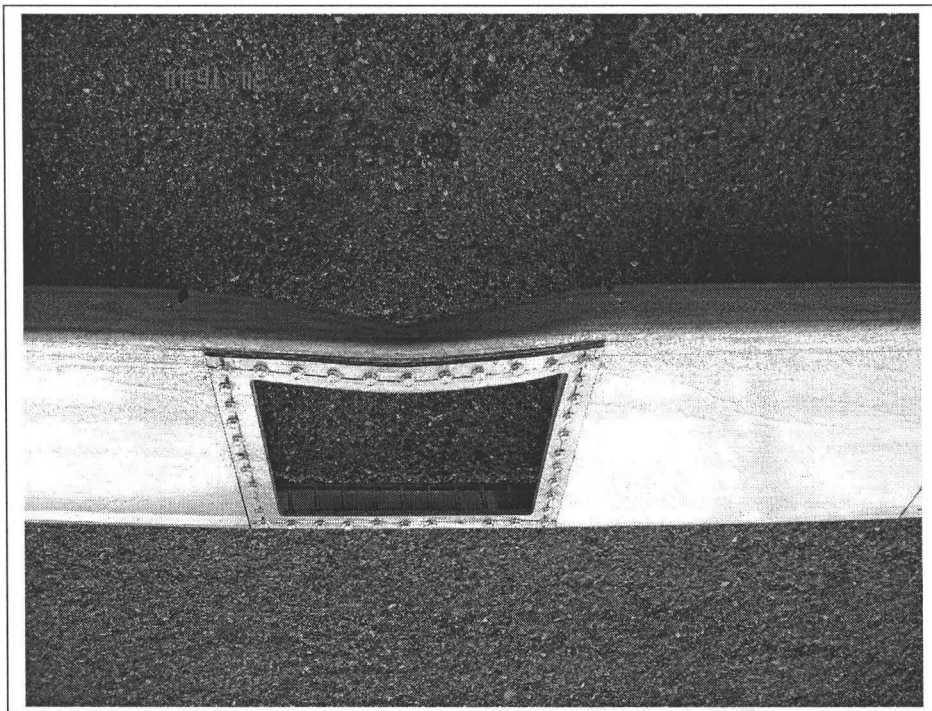


(b)

Figure C.6: Test results for specimens having reinforced (Scheme-C) circular web openings (a) load-displacement relations (b) typical flexural failure

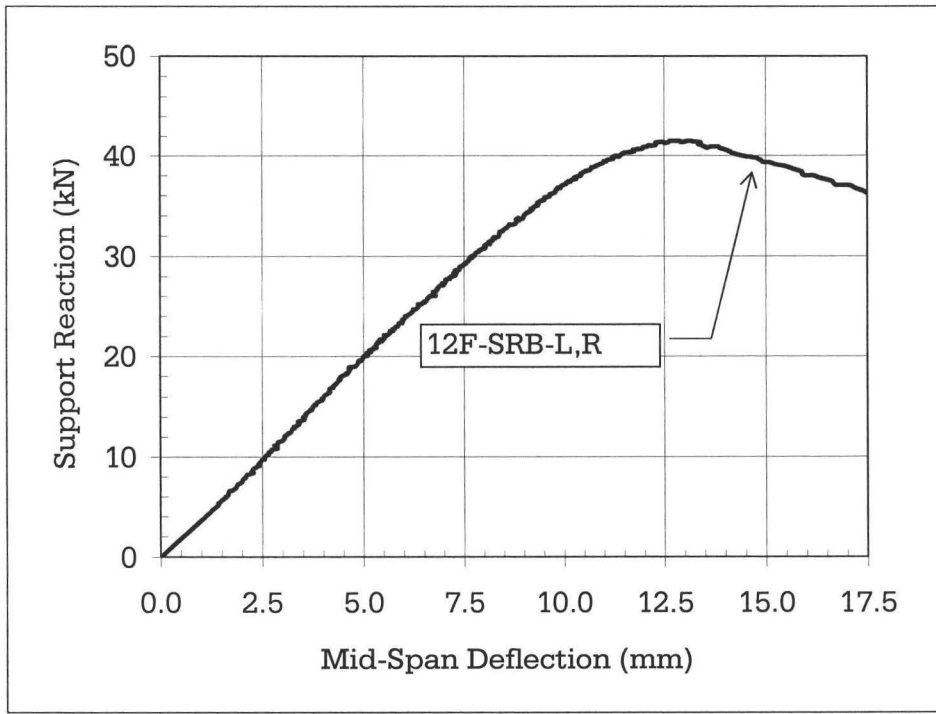


(a)

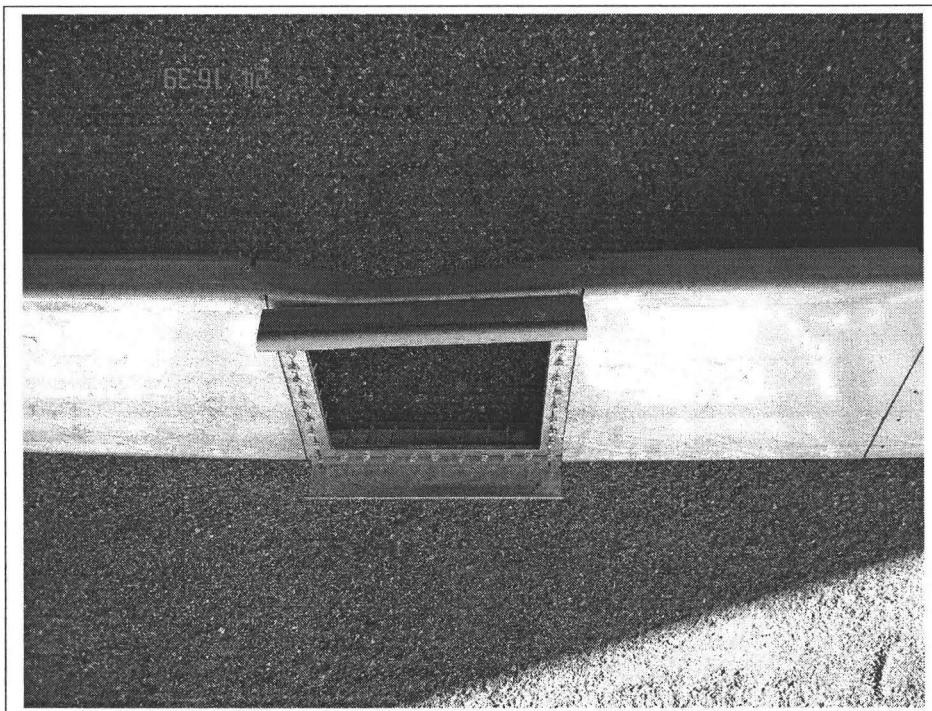


(b)

Figure C.7: Test results for specimens having reinforced (Scheme-A) square web openings (a) load-displacement relations (b) typical flexural failure

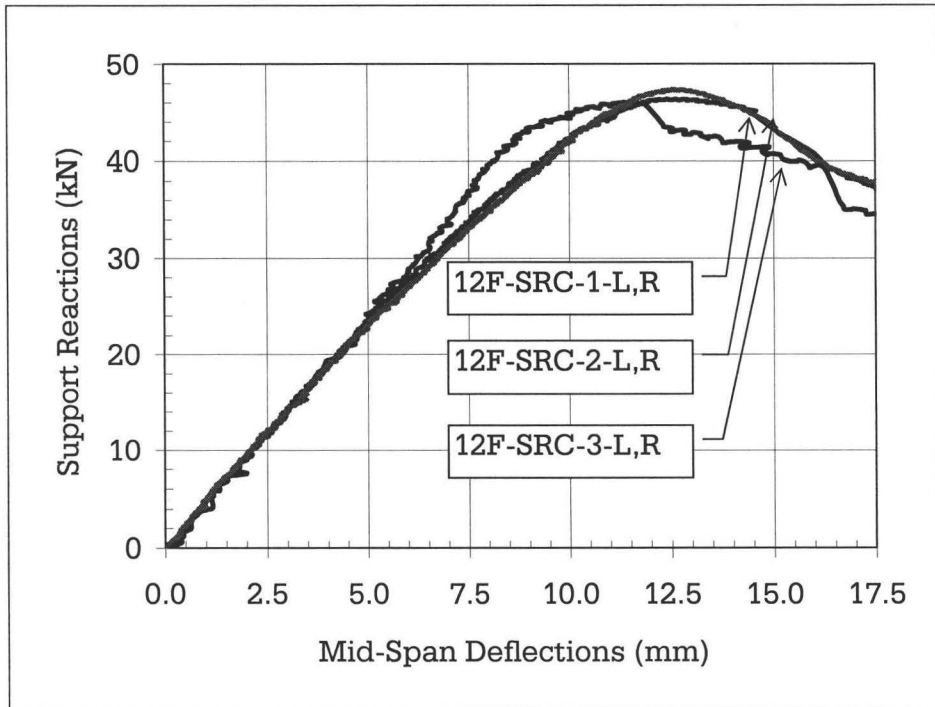


(a)

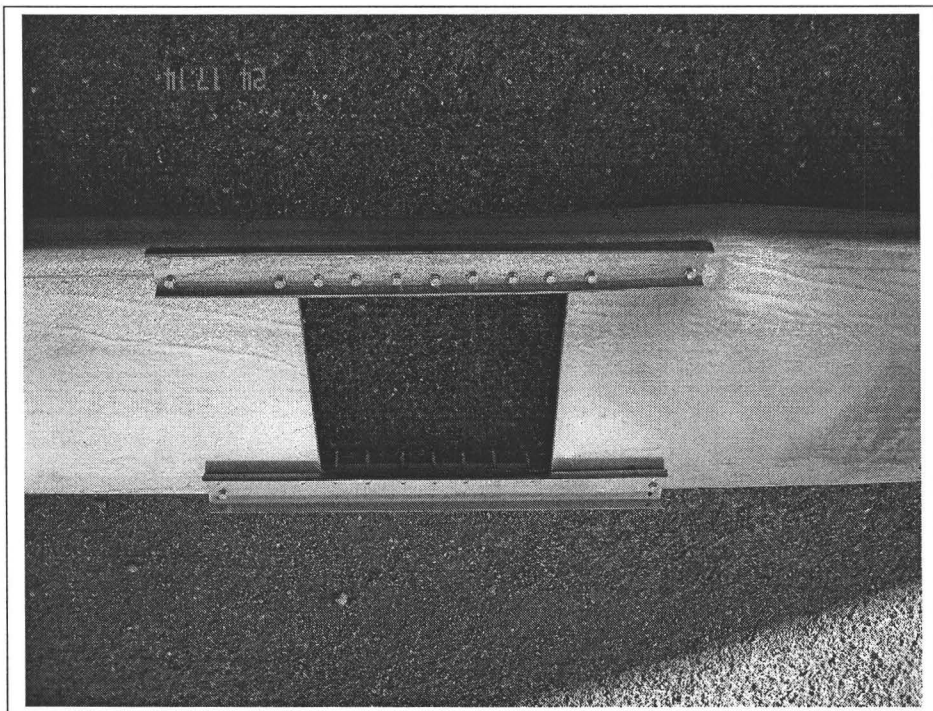


(b)

Figure C.8: Test results for specimens having reinforced (Scheme-B) square web openings (a) load-displacement relations (b) typical flexural failure



(a)



(b)

Figure C.9: Test results for specimens having reinforced (Scheme-C) square web openings (a) load-displacement relations (b) typical flexural failure

Appendix D

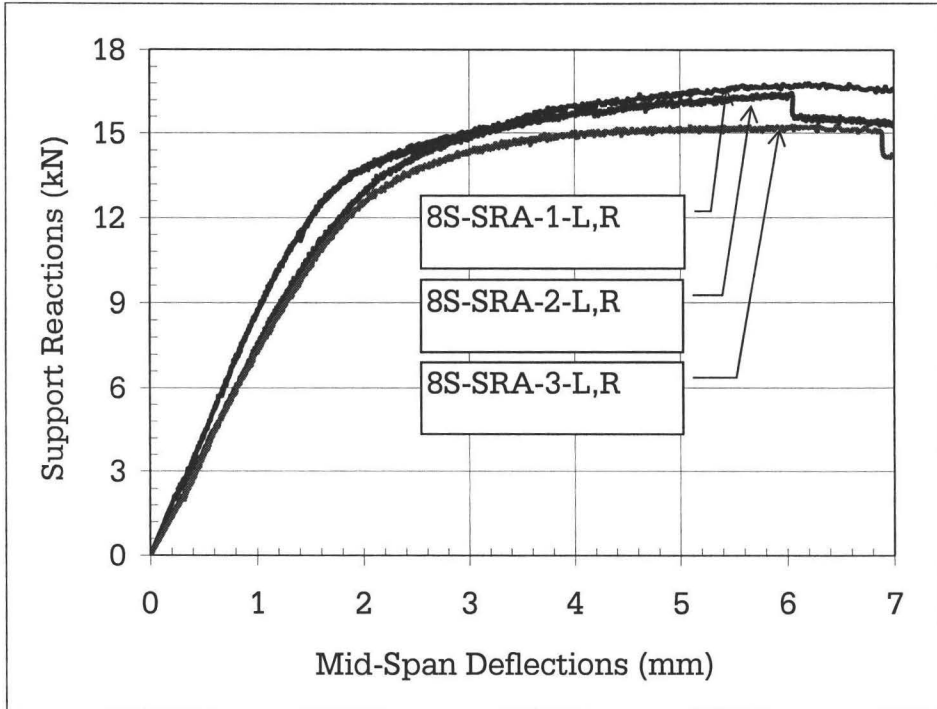
Cold-Formed Steel Joists with Large Web Openings Shear Tests: Section 800S162-43

D.1 General

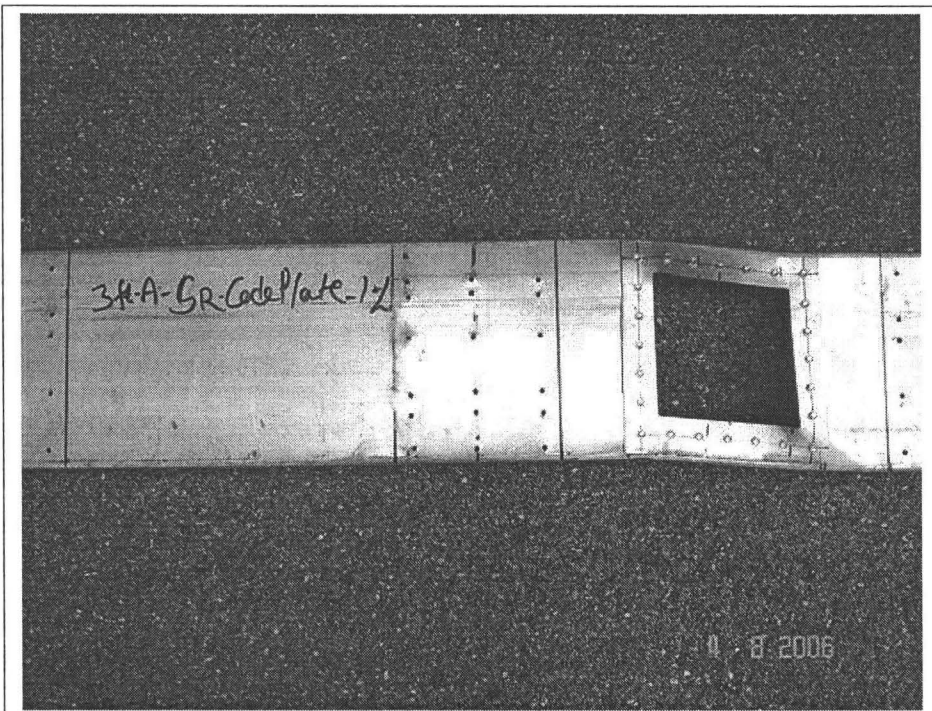
A total of thirty cold-formed steel (CFS) joists having w/t ratio 180 were subjected to shear tests, which established the shear resistances of such joists having unreinforced web openings, and having reinforced web openings. This part considered 203.2 mm (8 inch) deep, 1.092 mm (43 mils) thick [800S162-43] joists.

D.2 Shear Tests: Solid Sections, Circular Openings and Square Openings

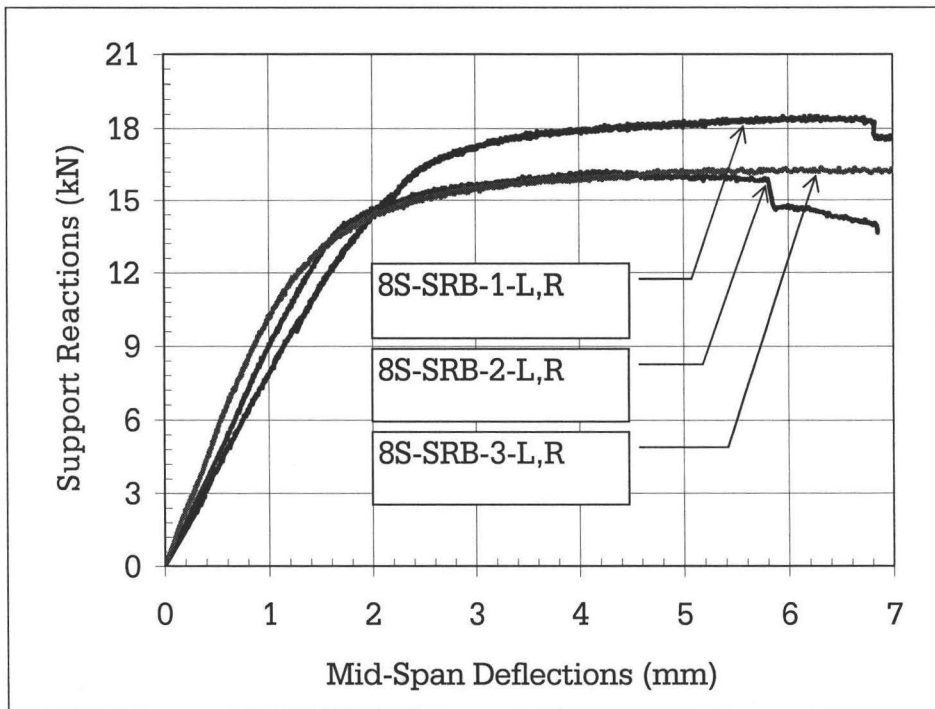
The first part of the investigation considered the shear resistance of (a) joists with no openings, ($a/h = 1.0$ and 1.5) (b) joists with circular openings and (c) joists with square openings. Three identical tests were done for each case, thus, this part included nine tests. The load-displacement relations and sample photographs of failed specimens are given in Figures D.1 through D.4.



(a)



(b)

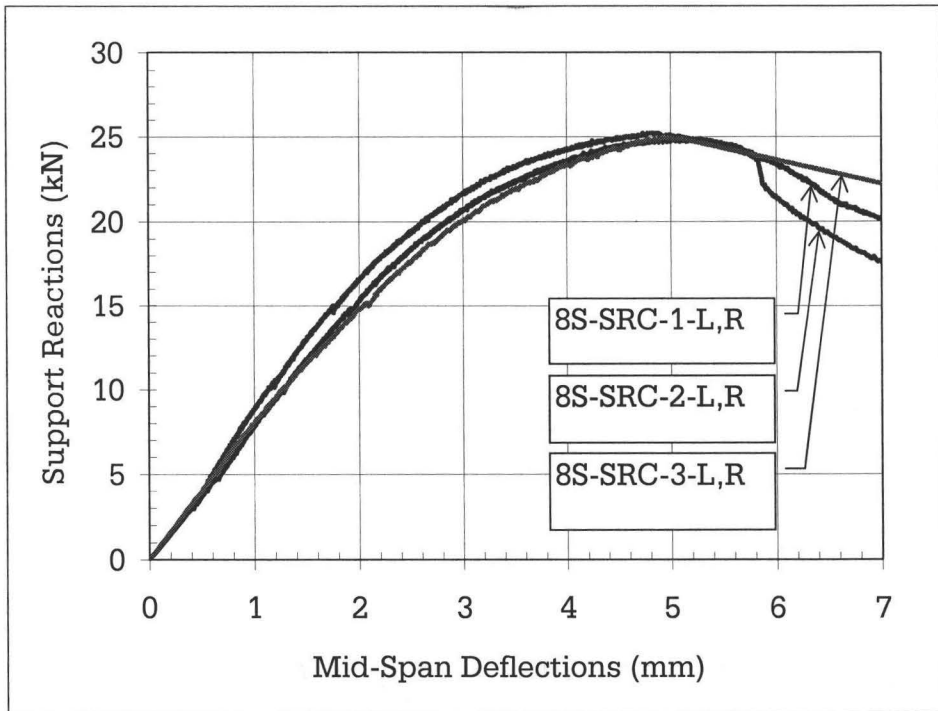


(a)

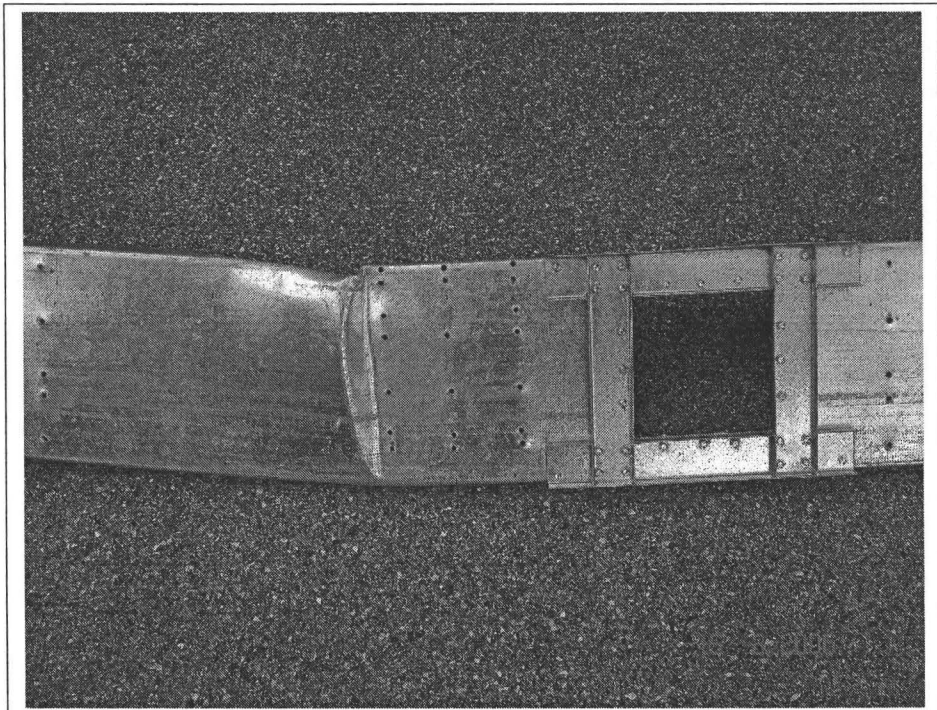


(b)

Figure D.9: Test results for specimens having reinforced (Scheme-B) square web openings (a) load-displacement relations ($a/h = 1.5$) (b) typical shear failure



(a)



(b)

Figure D.10: Test results for specimens having reinforced (Scheme-C) square web openings (a) load-displacement relations ($a/h = 1.5$) (b) typical shear failure